TRANSFER OF CHIRALITY IN NEW SUPRAMOLECULAR COMPLEXES AS DESIGN PRINCIPLE FOR FUTURE ASYMMETRIC CATALYSTS

Helmut Degenbeck

Dipòsit Legal: T. 1354-2011

UNIVERSITAT ROVIRA I VIRGILI
TRANSFER OF CHIRALITY IN NEW SUPRAMOLECULAR COMPLEXES AS DESIGN PRINCIPLE FOR FUTURE ASYMMETRIC CATALYSTS
Helmut Degenbeck
DL: T. 1354-2011

Tarragona 2011

Doctoral Thesis

Helmut Degenbeck

Helmut Degenbeck

Transfer of Chirality in New Supramolecular Complexes as Design Principle for Future Asymmetric Catalysts

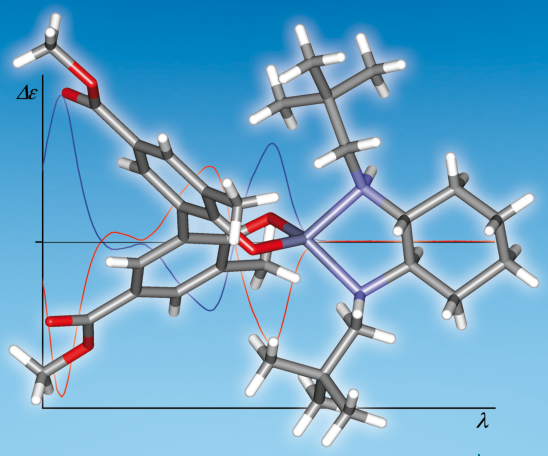

Universitat Rovira i Virgili

ICIQ Institut Català d'Investigació Química

UNIVERSITAT ROVIRA I VIRGILI

TRANSFER OF CHIRALITY IN NEW SUPRAMOLECULAR COMPLEXES AS DESIGN PRINCIPLE FOR FUTURE ASYMMETRIC CATALYSTS

DOCTORAL THESIS PRESENTED BY

HELMUT DEGENBECK

TO RECEIVE THE DEGREE OF DOCTOR
BY THE ROVIRA I VIRGILI UNIVERSITY

Supervisor: Prof. Anton Vidal i Ferran
(Institute of Chemical Research of Catalonia)

Tarragona, July 2011

Institut Català d'Investigació Química

Institute of Chemical Research
of Catalonia (ICIQ)
Av. Països Catalans 16
43007 Tarragona

UNIVERSITAT ROVIRA I VIRGILI

Department of Analytical
and Organic Chemistry
C/ Marcel.lí Domingo s/n
43007 Tarragona

I STATE, that the presented doctoral thesis entitled: "*TRANSFER OF CHIRALITY IN NEW SUPRAMOLECULAR COMPLEXES AS DESIGN PRINCIPLE FOR FUTURE ASYMMETRIC CATALYSTS*", presented by HELMUT DEGENBECK, has been carried out under my supervision at the Institute of Chemical Research of Catalonia (ICIQ) and fulfils all the requirements to be eligible for the European Doctorate Award.

Tarragona, 25th July 2011
Doctoral Thesis Supervisor

Prof. Anton Vidal i Ferran
(ICIQ Group Leader and ICREA Research Professor)

UNIVERSITAT ROVIRA I VIRGILI
TRANSFER OF CHIRALITY IN NEW SUPRAMOLECULAR COMPLEXES AS DESIGN PRINCIPLE FOR FUTURE ASYMMETRIC CATALYSTS
Helmut Degenbeck
DL: T. 1354-2011

We thank *MCYT* and *MICINN* (Grants CTQ2005-02193/BQU and CTQ2008-00950/BQU), DURSI and AGAUR (Grants 2005SGR225 2009GR623), Consolider Ingenio 2010 (Grant CSD2006-0003) and ICIQ Foundation for financial support. I gratefully acknowledge the *"FPU-Program"* for financial support (Grant Number AP2006-04169). Furthermore, I would like to thank Prof. Lorenzo Di Bari of the Università di Pisa for accepting me as a visiting student in his group, for the help and hospitality he has shown me during my research stay in Pisa.

CTQ2005-02193/BQU
CTQ2008-00950/BQU

2005SGR225
2009GR623

***INTECAT* (CSD2006-0003)**

UNIVERSITAT ROVIRA I VIRGILI
TRANSFER OF CHIRALITY IN NEW SUPRAMOLECULAR COMPLEXES AS DESIGN PRINCIPLE FOR FUTURE ASYMMETRIC CATALYSTS
Helmut Degenbeck
DL: T. 1354-2011

Corrections

Page 11, line 8 says:

Electron density is a physical characteristic of every molecule but it is independent of the number of atoms composing the molecule. This allows accurate DFT calculations taking electron correlations (electron-electron repulsion) into account at relatively low computational cost.

Should say:

Electron density is a physical characteristic of every molecule and its determination is independent of the number of atoms composing the molecule. Thus, DFT methods can be very accurate with lower computational cost than other approaches aimed at solving the Schrödinger equation.

Page 11, line 27 says:

…polarisation and/or diffuse ion functions…

Should say:

…polarisation and/or diffuse functions…

Page 44, line 12 says:

Ligand **26b** was identified as being the most efficient…

Should say:

Ligand **26a** was identified as being the most efficient…

Page 84, line 11 says:

Thus, the computed CD data suggested the a*S* sense of rotation for complex **44a**+**45g** by comparison with the experimental data.

Should say:

Thus, the computed CD data suggested the a*S* sense of rotation for complex **44a**+**45c** by comparison with the experimental data.

Page 191, Figure II-37:

In contrast to what is written in the text, Figure II-37 does not show the structure of the complex [$ZnCl_2$((1*R*,2*R*)-**45c**] but instead that of its enantiomer [$ZnCl_2$((1*S*,2*S*)-**45c**].

Table of Contents

List of Abbreviations

BINOL	1,1′-Bi(2-naphthol); synonym: 2,2'-binaphthol
BIPOL	[1,1'-biphenyl]-2,2'-diol; synonym: 2,2'-biphenol, 2,2′-biphenyldiol
^{t}Bu	*tert*-butyl
(±)CAHB	(doubly) charge-assisted hydrogen bond
CD	circular dichroism
CLP	circularly polarised light
COD	1,5-cyclooctadiene
COSY	correlation spectroscopy
d	doublet
DACH	(1,2)-diaminocyclohexane; synonym: cyclohexane-1,2-diamine
dd	doublet of doublet
DIPEA	*N*,*N*-diisopropylethylamine
DMAP	4-(*N*,*N*-dimethylamino)pyridine
DMF	*N*,*N*-dimethylformamide
DMSO	dimethyl sulfoxide
DPEN	diphenylethyl-1,2-diamine; synonym: 1,2-diphenylethane-1,2-diamine
EA	elemental analysis
ee	enantiomeric excess
ECD	electronic circular dichroism
ESI	electrospray ionisation
Et	ethyl
EtOAc	ethyl acetate
EtOH	ethanol
^{c}Hex	cyclohexyl

H-BIPOL	dimethyl 6,6'-dihydroxybiphenyl-3,3'-dicarboxylate
I-BIPOL	dimethyl 6,6'-dihydroxy-5,5'-diiodobiphenyl-3,3'-dicarboxylate
HRMS	high resolution mass spectrometry
IR	infrared
ITC	isothermal calorimetry
m	multiplet
m	medium
MALDI	matrix assisted laser desorption ionisation
Me	methyl
Me-BIPOL	dimethyl 6,6'-dihydroxy-5,5'-dimethylbiphenyl-3,3'-dicarboxylate
MeOH	methanol
Mes	mesitylene
MS	mass spectrometry
NMR	nuclear magnetic resonance
NOESY	nuclear Overhauser enhancement spectroscopy
NO_2-BIPOL	dimethyl 6,6'-dihydroxy-5,5'-dinitrobiphenyl-3,3'-dicarboxylate
Np	neopentyl
OHB	ordinary hydrogen bond
ORD	optical rotatory dispersion
ORTEP	Oak Ridge thermal ellipsoid plot
Piv	pivaloyl; *tert*-butylcarbonyl
^{i}Pr	isopropyl
ROESY	rotating frame Overhauser enhancement spectroscopy
rt	room temperature
s	singlet

s	strong
SAL	self-assembled ligand
SPS	solvent purification system
t	triplet
TBAB	tetra-*n*-butylammonium bromide
td	triplet of doublets
THF	tetrahydrofuran
UV-vis	ultra violet-visible
VCD	vibrational circular dichroism
w	weak

Introduction

The generally accepted definition of chirality (or handedness) was given over one hundred years ago by Lord Kelvin:[1,2] *"I call any geometrical figure, or group of points, chiral, and say it has chirality, if its image in a plane mirror, ideally realized, cannot be brought to coincide with itself."* Although throughout the years there have been arguments about the universal applicability or the need for extensions of the above statement, especially at the macroscopic scale such as with large objects or at the molecular level with supramolecular compounds,[3-5] it is still an amazingly accurate definition. It can also be expressed in a more formal way on the basis of symmetry elements: an object or the spatial arrangement of atoms in a molecule is chiral provided that it does not posses any symmetry elements of the second order, *i.e.* improper (rotation-reflection) axes S_n.* This gives rise to four different types of stereogenic elements, namely axis, helix, plane, and centre.[6] Moreover, there are molecules that are chiral due to their three-dimensional structure but however lack stereogenic elements. Generally, the mirror images of a given molecule are called *enantiomers* (or *enantiomorphs* when talking about macroscopic objects) although one might encounter antiquated or debatable synonyms like (*optical*) *antipodes* and *optical isomers*.[7] A mixture composed in equal parts of two enantiomers is called *racemate* or *racemic* mixture.

* Mirror planes (σ) and inversion centres (i) are included in this statement as they can be considered as S_1 and S_2, respectively, rotation reflection axes.

Introduction

The phenomenon of chirality is omnipresent in nature and everyday life whether someone is putting their gloves on a cold winter day or by chance investigating the reproduction of snails. In the latter case chirality is actually of evolutional consequence.[8-10] The coiling direction of a snails shell (Figure 1) and its whole body organisation is determined in early development. It is generally fixed within a single species since apparently inter-chiral mating is seldom successful. Consequently, unlucky individuals that posses a reversed helical screw sense to that normally associated with their species usually fail to reproduce and thus fall victim to natural selection. Only a few species are known to be capable of maintaining a "racemic" population.[11]

Figure 1. Left panel: helical chirality in snails. Sinistral (left-handed) *Busycon pulleyi* (left) and dextral (right-handed) *Fusinus salisbury* (right) represent species with opposite chirality. Right panel: *Amphidromus perversus* shows chiral dimorphism.[10]

As fateful as the consequences of asymmetry may seem for snails, the impact of chirality on life itself reaches far beyond this one example.[12] In fact it was the existence of certain organic molecules in one dominant enantiomeric form, namely L-amino acids (left-handed, *S* in modern notation) and D-sugars (right-handed, *R*), on prebiotic earth (and possibly anywhere in the universe) that made life possible. This is because of the critical role of amino acids in proteins. Without inherent homochirality, the occasional incorporation of the wrong enantiomer would lead to varying and random protein structures. Although this

factor has been the object of intense research for over one hundred years, the origin of homochirality on earth before the existence of life still remains a matter of lively discussion. Theories include the transport of chiral material in *enantiomeric excesses* (ee) from outer space to earth in meteorites (the famous Murchison meteorite, Australia)[13,14] the chiral amplification of amino acids in certain types of clay,[15-17] and the enantiomeric resolution through spontaneous crystallisation without a chiral dopant.[17,18] The outer space theory assumes the influence of supernovae[19] or a diastereomer-type interaction of circularly polarised light (CPL) with the two possible enantiomers of early organic chiral molecules was responsible for the symmetry breaking.[17,20-24]

Diastereomers are stereoisomers that, in contrast to enantiomers, are not related as non-superimposable mirror images. They differ in their physical and chemical properties, whereas enantiomers show different physical and chemical properties only in chiral environments. The electric field vector of CPL (or more precisely electromagnetic radiation in general) describes a helix along whose axis the electromagnetic radiation is propagated.[6] This helix may possess either left- or right-handed sense of rotation. Consequently, left- and right-handed CPL can be interpreted as being the “enantiomers of chiral photons” which interact differently with the same enantiomer of a given chiral molecule. Ultimately, the observable results are a manifestation of the diastereomeric interaction. These phenomena are broadly utilised in spectroscopic techniques like optical rotation- (OR), optical rotation dispersion- (ORD), and circular dichroism (CD) spectroscopy. In particular the latter has proven to be an extraordinarily useful tool for the investigation of chiral structures.[25-29] Depending on the experimental setup, it can be distinguished between vibrational (VCD) or electronic circular dichroism (ECD). The vibrational spectrum became accessible since the early 1980s owing to advances in instrumentation. Both Raman and infrared techniques are nowadays used and known as

Raman optical activity (ROA)[30-34] and vibrational circular dichroism (VCD).[34-37] However, by far the most commonly used method is ECD[26,27] and indeed it is also the method used in the work presented in this thesis. A simplified description of the fundamental principle of ECD spectroscopy is shown in Figure 2.

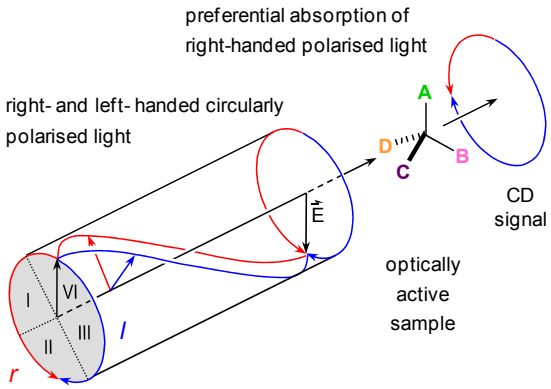

Figure 2. Simplified principle of ECD spectroscopy. In order to clarify the rotational order of the circularly polarised electromagnetic radiation (only the electric field vector is shown here) the mirror-inverted sectors of an imaginary watch (looking through the watch from the bottom) are marked on the lower end of the cylinder.

The detailed background of electronic transition processes and their importance for CD exceeds the scope of this work and therefore only some definitions shall be given here. More in-depth theoretical and phenomenological discussions can be found in the references mentioned above. The definitions and explanations given in the following were taken from the tutorial review written by Pescitelli *et al*.[29] and the textbooks *Circular Dichroism: Principles and Applications*[26] and *Physical Methods in Chemistry*.[38] As depicted in Figure 2, CD is defined as $\Delta A = A_L - A_R$, which indicates the difference between the absorption A of left and right circularly polarised light passing an optically active probe. As with regular UV-vis spectroscopy, the dimensionless (or arbitrarily dimensioned) absorbance A is often

substituted according to the Beer-Lambert law $A = \log(I_0/I) = \varepsilon \cdot c \cdot d$ (where I_0 is the initial light intensity and I the intensity after passing the probe, c = concentration in mol·l^{-1}, and d = pathlength in cm) by the *molar absorptivity* $(\Delta)\varepsilon$ expressed in M^{-1}cm^{-1} (Equation 1). For historic reasons, the measured variable is also often indicated as ellipticity θ in *millidegree* (mdeg) which is related to ΔA through $\Delta A = \theta/32982$.

$$\Delta A = A_L - A_R = \log\frac{I_0}{I_L} - \log\frac{I_0}{I_R} = \log\frac{I_R}{I_L};\ \ \Delta\varepsilon = \varepsilon_L - \varepsilon_R = \frac{\Delta A}{c \cdot d}$$

Equation 1. Definition of CD and $\Delta\varepsilon$.

According to Equation 1, $\Delta\varepsilon$ is defined only in relation to an absorption band and can be either positive or negative. In fact the CD of a given pair of enantiomers in racemic proportions is zero since the curves of the pure enantiomers are exact mirror images if measured under the same conditions. A dichroic peak is also called *Cotton effect* named after the discoverer of the phenomenon. Depending on its sign it can be either positive or negative.

Another parameter particularly useful when concentrations cannot be determined is the *anisotropy* (or *dissymmetry*) *factor g* (Equation 2). It is defined only in relation to an absorption band, *i.e.* when A (or ε) ≠ 0 (which can be ensured over the whole wavelength range by adding a small constant factor to A (or ε) that becomes negligible once the absorbance gets considerable).

$$g = \frac{\Delta\varepsilon}{\varepsilon} = \frac{A_L - A_R}{A}$$

Equation 2. The anisotropy factor *g*.

Generally, in electronic molecular spectroscopy, the quantised absorption of radiation implies the excitation of a (non)bonding electron of the molecule in its ground state (0) into an empty molecular orbital (MO) of higher energy. The result of the electronic transition is an excited state (*a*) that is accompanied by the redistribution of the electron cloud during the transition, *i.e.* the electron distributions in the two states 0 and *a* are different. Allied to this redistribution are the electric ($\vec{\mu}_{0a}$) and the magnetic ($\vec{m}_{0a}$) transition dipoles. A transition is called either electric dipole *allowed* or *forbidden* depending on whether $\vec{\mu}_{0a} \neq 0$ or $\vec{\mu}_{0a} = 0$ applies and naturally the same definition is true for magnetic dipole allowed and forbidden transitions. A measure of the transition probability in the classical interpretation is given by the oscillator strength f_{0a} that constitutes the intensity, or more precisely the integral of a given absorption band. This quantity is also helpful in classifying allowed and forbidden transitions since the physical differentiation is not as clear as might be implied. Transitions showing small values of f_{0a} are referred to as being (more or less) forbidden whereas for values close to 1 a transition becomes allowed.

$$\int \varepsilon \mathrm{d}\nu \propto f_{0a} \approx |\vec{\mu}_{0a}|^2 + |\vec{m}_{0a}|^2$$

Equation 3. Intensity of a given absorption expressed through the oscillator strength f_{0a}.

In the context of absorbance spectroscopy it is enough to consider the electric dipole term only since it is usually much larger than the magnetic one. Using the quantum mechanical expression $\vec{\mu}_{0a} = \int \psi_{\mathrm{el}}^{0} \hat{\mu} \quad \psi_{\mathrm{el}}^{a} \mathrm{d}\nu = \langle 0|\hat{\mu}|a\rangle$ (it has similar form for the magnetic transition dipole), where ψ_{el} denotes the electronic wave functions of the ground and excited states and $\hat{\mu}$ the electric dipole moment operator, the intensity of an absorption may be expressed as:

$$f_{0a} \propto \left| \int_{-\infty}^{+\infty} \psi_{el}^{0} \hat{\mu} \psi_{el}^{a} \, dv \right|^2 = D_{0a}$$

Equation 4. Relationship between the integrated intensity f_{0a} and the dipole strength D_{0a}.

The entire integral in Equation 4 is usually referred to as the transition moment integral which in approximation can be seen to represent the displacement of the electric charge during the transition. In this context it is again spoken of allowed and forbidden transitions depending on whether the integral equals zero or not. Symmetry considerations that take into account the nature of the dipole moment operator $\hat{\mu}$ as a vector quantity, *i.e.* consisting of *x*, *y*, and *z* components, are usually used in order to rationalise whether or not the integrals for each direction in space are zero for a certain transition involving specific MOs. These considerations have led to the so-called *selection rules* that allow predictions about whether or not a transition is allowed.

Equation 3 and Equation 4 are relevant for the absorption of radiation by any given chromophore. In the case of optical activity however, an additional criterion must be taken into account. In contrast to UV-vis spectroscopy, in chiroptical spectroscopy an electronic transition must be both electric and magnetic dipole allowed in order to give rise to CD signals. The scalar product of the two transition dipoles defines the *rotational strength* R_{0a} which is directly proportional to the integral of a given CD band (Equation 5). Consequently, R_{0a} must be of equal value but of opposite sign for a given pair of enantiomers.

$$\int \Delta\varepsilon \, dv \propto R_{0a} \approx \vec{\mu}_{0a} \cdot \vec{m}_{0a}$$

Equation 5. Definition of the rotational strength R_{0a}.

In analogy to Equation 4 this can again be expressed in the quantum chemical formalism:

$$R_{0a} \propto \left[\int \psi_{el}^{0} \hat{\mu} \psi_{el}^{a} \mathrm{d}v\right]\left[\int \psi_{el}^{0} \hat{m} \psi_{el}^{a} \mathrm{d}v\right]$$

Equation 6. Quantum chemical definition of the rotational strength R_{0a}.

Last but not least it should be mentioned that if it were experimentally possible to observe the rotational strength R_{0a} over the complete spectrum of electronic transitions (usually higher energies are not accessible due to instrumentation limits or absorption of radiation by the solvent), the sum of all R_{0a} values (and thus Cotton effects) must be zero (Equation 7).

$$\sum_{0a}^{\text{all transitions}} R_{0a} = 0$$

Equation 7. Summation of R_{0a} over the whole electromagnetic spectrum.

The main application of rotational strengths lies in their utility for non-empirical predictions of CD spectra. To do so the R_{0a} values have to be calculated. The CD spectrum itself can then be generated by running normalised bandshape functions on the calculated rotational strengths in order to broaden them. The calculation of CD properties will be discussed briefly at a later point of this introduction, but first another useful model for the absolute configurational analysis of chiral systems shall be mentioned here; the *exciton coupling method*.[29,39-41] Let us assume a molecule bearing two chromophores (although more than two are possible), both in a chiral environment and located nearby in space. In such molecules the electronic transition moments may become coupled through space and the excited states are no longer degenerated but split into α states of lower (*bathochromic*- or red shift in UV-vis spectra) and β states of higher (*hypsochromic*- or blue shift)

energies (Figure 3). This is of consequence for both the UV-vis and particularly the CD spectrum. In the UV-vis spectrum the resulting absorption band is the result of two component bands of the same sign, which usually add up to a single absorption maximum of up to double intensity (Figure 3c). This absorption maximum may get broadened, or even divided into two maxima if the Davydov splitting $2V_{12}$ (Figure 3b) becomes sufficiently large. The existence of two excited states manifests itself in the CD spectrum in the form of a bisignated curve in which the sequence of signs depends directly on the mutual orientation of the underlying electric dipoles. In order to determine the sign of exciton chirality one must look along the axis connecting the centres of the two dipoles and identify the direction of rotation required to superimpose the dipole in front with that in the back by the shortest way, *i.e.* by following the acute angle. Positive exciton chirality is defined by clockwise rotation and, going from larger to smaller wavelengths, it is generally accompanied by a positive first Cotton effect followed by a negative second one (and *vice versa* if the rotation is anticlockwise). The method is very sensitive and even applicable when only one chromophore is present in the original molecule after chemically introducing a second auxiliary chromophore in close proximity. Furthermore, the chromophores should absorb light of similar energy in order to guarantee efficient coupling. At any rate, the orientation of the dipoles in the (auxiliary) chromophores must be known in order to avoid misleading assumptions. In fact this constitutes the major drawback of this otherwise very practical approach: one must assume a certain structure and have an idea of the intermolecular interactions. Despite the application of emerging *first-principles* or *ab initio* methods that do not require any assumptions, the exciton chirality method is frequently applied for the assignation of absolute configurations, especially in natural products.[42-44]

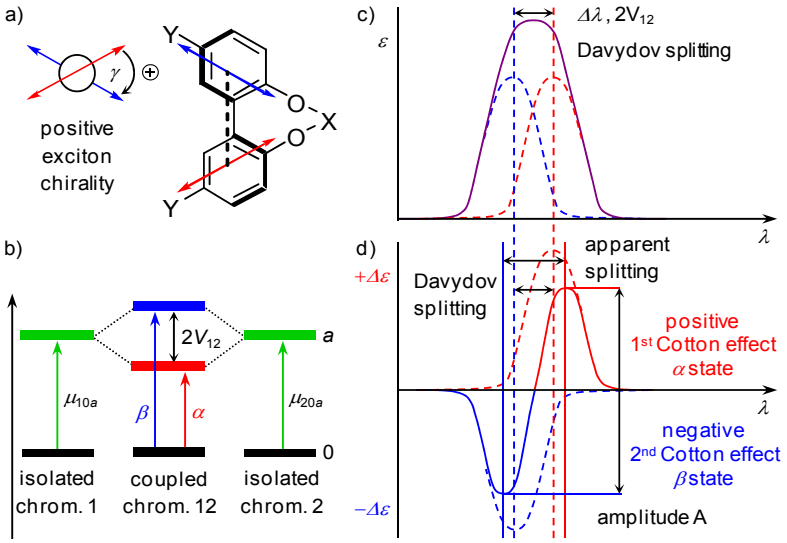

Figure 3. a) Exciton coupling of two identical chromophores 1 and 2 in an imaginary biphenol molecule. Positive chirality is indicated by clockwise rotation following the acute angle γ spanned by the two dipoles; b) splitting of the excited states into α and β states with Davydov split $2V_{12}$, *i.e.* removal of the degeneration in chromophores linked by a chiral relation; c) summation of the idealised partial UV bands corresponding to the two states; d) summation of the idealised partial dichroic peaks giving a bisignated CD curve.

The calculation of CD spectra has dramatically gained in importance in recent years due to advances of the theoretical framework aided by ever improving compute performance. Both semiempirical and first-principle methods are used nowadays with great success.[45-49] Only the latter were applied in the present work and of the various quantum mechanical methods nowadays available for the calculation of excited states,[50] Time-Dependent Density Functional Theory (TD-DFT) methods are probably the most commonly used.[51-55] However, the description of the theoretical background of these methods goes far beyond the scope of this work. Here, only a short account concerning the *modus operandi* shall be given. Moreover, it should be mentioned that the advances of computational methods towards routine applications was not only of fundamental importance for the theoretical

interpretation of electronic spectra but also of great impact on basically every research field that requires deeper understanding of molecular reactivity including catalytic cycles and reaction mechanisms. This importance was acknowledged with the Noble Prize in chemistry for W. Kohn[56] and J. A. Pople[57] in 1998 for their contributions to the elaboration of the density functional theory (DFT)[58, 59] and quantum chemical models. DFT attempts to predict molecular properties from the electron density of the molecule. Electron density is a physical characteristic of every molecule but it is independent of the number of atoms composing the molecule. This allows accurate DFT calculations taking electron correlations (electron-electron repulsion) into account at relatively low computational cost.

To begin with, any calculation of chiroptical properties requires an input structure from which excited states have to be calculated. Input structures are commonly derived from conformational searches carried out at lower levels of theory in order to save computation time, followed by high level geometry optimisation of the relevant conformers. This is a crucial point since CD is sensitive towards conformational variances, *i.e.* it is advisable to model the input structure at the highest level of theory applicable. Currently very popular methods are of the DFT type using standard so-called hybrid functionals like B3LYP,[60-62] MO6,[63] CAMB3LYP,[64] or MPW1PW91,[65] which determine how the exchange and the electron correlation energies are calculated. The basis set on the other hand is required to construct the molecular orbitals (MOs) usually by linear combinations of the atomic orbitals (AOs). The more powerful basis sets are often of split-valence type which include polarisation and/or diffuse ion functions. A good basis set to start with is the standard 6-31G(d).[66-70] More accurate calculations can be achieved with the 6-311G basis set that can also be expanded in order to include polarisation and diffuse functions.[71-78] Last but not least the SVP basis set that has polarisation functions included in its definition and is

applicable to atoms from H to Kr should be mentioned.[79,80] These are only some of the functionals and basis sets available nowadays for DFT calculations. There are no strict rules to predict which method should be applied for a given structure optimisation problem but guidelines can be found in textbooks and the respective scientific journals.[81,82] If required (and feasible), one also might want to model the chemical environment in a given solvent. Once the input structures are obtained and ideally confirmed by experimental data such as X-ray (a single crystal structure may also serve as input) or NMR, the excited states and rotational strengths can be calculated at discrete energies for each conformer as is done today predominantly by TD-DFT methods. The rotational strengths must then be transformed into spectra. As mentioned before this is done by applying normalised bandshape functions, usually Gaussians, but others are also feasible from case to case,[83] on the rotational strengths with suitable software. Before comparing these with the experimental CD, the input structures should be weighed on the basis of their computed relative energies. Usually this can be done by applying the Boltzmann distribution and depending on the result an averaged CD spectrum can be calculated. A recent review article written by Autschbach outlines the theoretical basics and course of action of the computation of chiroptical properties in much more detail.[53]

Finally, a few more words about the significance of chirality for modern chemistry should be said. Nowadays chiral compounds are of tremendous importance to various sectors of the chemical industry. Amongst them are drug development and pharmacology,[84-87] agrochemical research,[88-90] and advanced materials science.[91-93] Consequently, high enantiomeric purities are widely sought for, especially in today's life-science products whose unquestioned usefulness has led to their broad application but has also raised the problem of chiral toxicity.[94] In order to ensure the regulated preparation, use and selling of active pharmaceutical ingredients (APIs), agencies

like the U.S. Food and Drug Administration (FDA) now outline and enforce respective guidelines.[95]

In fact, many of the drugs in use today are chiral and usually the biological or pharmacological properties of these drugs are restricted to only one of the enantiomers while the other one may show no or far different activity, including positive, and in the worst case scenario undesirable (toxic, teratogenic, *etc*.) effects.[96] Not knowing the metabolism of even one of the two enantiomers of a given drug may have fatal consequences. This was probably most obviously demonstrated by the infamous thalidomide incident. Whilst the (*R*)-isomer is an effective sedative, the (*S*)-isomer caused numerous birth defects in countries all around the world during the late 50s and early 60s of the last century.[97] However, in recent years the interest in thalidomide and its analogues as APIs for example, in the treatment of multiple myeloma[98-101] has grown anew thanks to its undeniable potential. There also exist examples of different activities under physiological conditions of two enantiomers of the same drug where both isomers were found to have independent therapeutic value. For instance, α-dextropropoxyphene (DARVON) is an analgesic marketed by Eli Lilly whereas its enantiomer α-levopropoxyphene (NOVRAD) was used as an antitussive drug without showing any analgesic properties. It should be mentioned however, that DARVON has been gradually withdrawn from the market due to its, amongst other things, elevated overdose lethality.[102,103] Interestingly, the trade names of both enantiomers also have a mirror-image relationship.

Apart from pharmaceutical products, agrochemicals like chiral pesticides, fungicides, herbicides, and insecticides are another class of compounds that will have to meet increased demands regarding enantiopurity.[104] Consequently, obtaining the different classes of life-science products in the highest enantiopurities, ideally by controlling their stereochemistry during preparation, will be an ongoing challenge for the chemical industry. Strategies to prepare enantiopure compounds can be divided into three groups depending on the kind of starting materials used (Figure 4).[105]

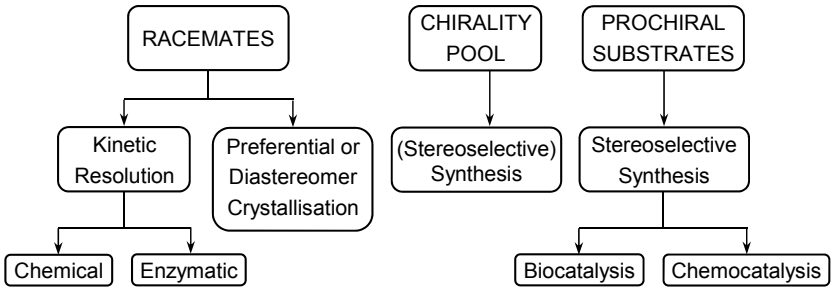

Figure 4. Methodologies for the preparation of enantiopure compounds.[105]

The resolution of racemates into their enantiomers by either preferential or diastereomer crystallisation was one of the first methods to be used and it still is probably the most important method for the industrial preparation of pure enantiomers. Theoretical yields of 100% of the pure enantiomer are achievable for both crystallisation types under certain conditions like spontaneous *in situ* racemisation (for preferential crystallisation) and spontaneous diastereomer interconversion (for diastereomer crystallisation). However, the more common cases result in theoretical yields of 50%. The success of kinetic resolutions on the other hand depends on the fact that the two enantiomers of a given starting material may react at different rates with a chiral reagent or interact differently with a chiral catalyst. Ideally, one of the enantiomers is transformed whereas the other remains un-reacted. Again the

theoretical yield is 50% but can be increased if the unwanted enantiomer can be readily racemised and recycled. Furthermore, diastereomer crystallisation and non-catalytic kinetic resolution require stoichiometric amounts of a chiral reagent or resolving agent, which in industrial processes calls for recycling of the chiral resolving agent with the corresponding operative expenses. The chiral pool approach relies on inexpensive and readily available enantiomerically pure natural products or their derivatives that can be transformed into the desired products through chemical means. One inherent weakness of this method results from the limited starting materials of the chiral pool that cannot nearly cover all of the required optically pure compounds. Last but not least the transformation of substrates that contain a prostereogenic element into enantiomerically pure compounds by reaction in the presence of a chiral species is referred to as stereoselective synthesis. The use of chiral reagents or chiral auxiliaries (a chemical compound that is reversibly incorporated into an organic substrate so that the required reaction can be carried out asymmetrically under selective formation of one of the two enantiomers) was tantamount to a revolution as these reagents allowed the preparation of complex enantiopure organic molecules. However, both approaches come with substantial drawbacks. Chiral reagents must be applied in stoichiometric amounts whereas chiral auxiliaries require additional syntheses steps (attachment and removal of the chiral auxiliary plus its recycling). Furthermore, the availability of these chiral entities is again limited.

Asymmetric catalysis, in which each equivalent of chiral catalyst, by virtue of being generated perpetually, yields a multiple equivalent of enantiomerically pure product is *a priori* the more elegant approach compared to the ones mentioned above. During the past few decades, asymmetric transformations catalysed by different classes of artificial catalysts have become highly versatile tools in asymmetric

organic synthesis, thus providing efficient solutions for a growing number of asymmetric transformations.[106,107] Economic considerations, the increase in competitiveness, and a reduction of waste and by-products are some of the additional advantages associated with asymmetric catalysis.[108]

It is immediately understandable that in such a variety of reactions different mechanisms must be at work and indeed, taking only homogeneous catalytic transformations into account, they can be roughly divided into several classes as is shown in Table 1.[109]

Table 1. Classification of homogenously catalysed reactions.[109]

catalyst	catalyst role[a]	substrate activation	description
Brønsted acid/base	PD/PA	protonation/ deprotonation	Brønsted-acid-base catalysis
Lewis acid/base	EPA/EPD	formation of a Lewis-acid-base adduct	electro-/nucleo-philic catalysis
metal complex	ED/EA	electron transfer	redox catalysis
metal complex	EPA[b]	coordinative interaction	complex catalysis
metal complex	EPA[b] (EPD)[c]	coordinative inter-action; organome-tallic intermediates	organometallic complex catalysis

[a]PD/PA = proton donor/acceptor, EPD/EPA = electron pair donor/acceptor, ED/EA = electron donor/acceptor; [b]the formation of a metal-ligand interaction is usually described as EPA-EPD interaction; [c]the substrate activation through π- and σ-complex formation also depends on the back-donation ability of the metal, thus, the metal is also acting as EPD.

Based on this classification one might postulate a catalytic cycle that is traversed in the formation of the desired product from the substrate. Such a cycle is shown in very general form for a reaction catalysed by a metal complex in Scheme 1. Similar cycles can be formulated for organocatalytic reactions which are usually of one of the first three classes in Table 1. Enantioselective process control generally requires complexes constituted from chiral ligands in order to favour the desired reaction outcome *via* diastereomeric discrimination in the transition state. Chiral catalysts are capable of doing so by preferential recognition of an enantiotopic atom, group or face in the substrate. Additionally, the chiral catalyst provides a low energy pathway to the preferred product.

I→II) formation of the chiral catalyst [*M] from the precatalyst [*M'].
II→III) activation of the substrate S by complexation [*M]-S.
III→IV) formation of the metal-intermediate-complex [*M]-I.
IV→II) elimination of the product P and re-generation of the catalyst [*M].
III→V) reversible formation of a catalytically inactive complex [*M]-S'.
IV→VI) irreversible degradation of the metal-intermediate-complex.

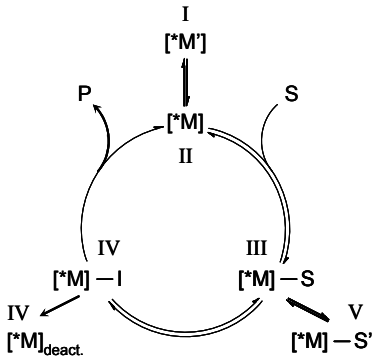

Scheme 1. Typical elemental steps of a reaction carried out under complex-catalysis.[109]

Accordingly, the chiral ligand design is decisive for the enantioselectivity of the catalyst. This includes the definition of the absolute configuration of the stereogenic elements in the ligand as well as its binding mode to the active metal centre. Although by now it has been shown with several examples that monodentate ligands may perform just as well[110-115] as their c*helating* (from Greek *Chelat* = crab's claw) bidentate competitors, the latter currently dominate the field of enantioselective catalysis as is reflected in the vast amounts recent

publications present in the literature.[116-128] This is due to several obvious reasons: i) bidentate ligands allow the formation of defined and highly stable complexes aided by the chelate effect, ii) heterobidentate ligands give rise to sterically and electronically asymmetric ligands, and iii) flexible ligand backbones provide the catalysts with high adaptability to various substrates yet maintain the chiral environment shaped around the active centre. However, there are several disadvantages associated with the use of bidentate ligands in enantioselective catalysis such as the often more complicated synthesis that must be considered. Though computational methods are becoming more and more feasible in both mechanistic studies[129-131] and catalyst design,[132-134] the goal of preparing catalysts based purely on predictions is still far from being accomplished. Whilst this may be realised to some extent in the enzyme approach[135,136] the inherently different strategy of using metal complex catalysts still strongly depends on the screening of large libraries of potential catalysts. Although these methodologies are elaborated to astonishing levels in high-throughput[137] and computer assisted screening[138] the laboratory route is still defined by time consuming syntheses of catalyst libraries.

The lion's share of this effort is often due to the necessity to form covalent bonds in order to realise the desired bidentate structures. In recent years however, supramolecular chemistry has been utilised in the preparation of a growing number of highly efficient bidentate ligands (examples are given in the literature sections of the following chapters). In contrast to covalent bonds, supramolecular linkages are usually reversible. The underlying forces include solvatophobic effects, dispersion and induction (van der Waals, induced dipole-dipole), electrostatics (ion pairing, ion-dipole, and permanent dipole-dipole), π–π-stacking, hydrogen bonding, and metal-ligand interactions.[139-141] Although the latter may not be regarded as being fully non-covalent, their reversible character has made them very useful for the assembly of

supramolecular architectures. Several of these reversible forces can be utilised efficiently to create new ligands. In some ways supramolecular assemblies have closed the gap between strictly monodentate and typical bidentate ligands (Scheme 2). Depending on the interaction and environmental influences (*e.g.* solvent polarity, temperature, *etc.*) the resulting supramolecular binding strengths may give rise to ligands of more or less bidentate character.

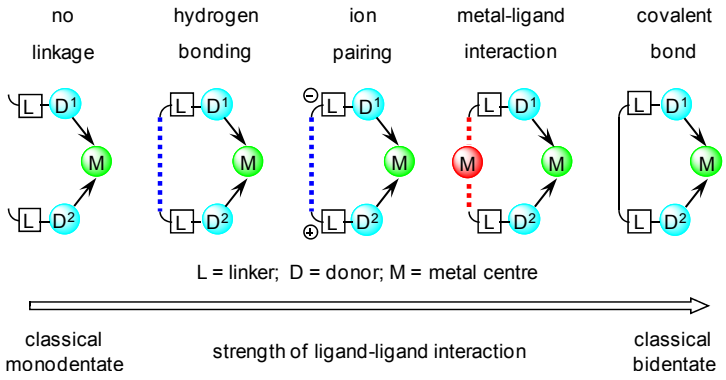

Scheme 2. Continuum of attractive ligand-ligand interactions going from the unbound to the covalently bound state. The ligand character is changing from monodentate to bidentate in an MD_2 complex.

Aims

In enantioselective catalysis research, a key challenge and, moreover, aim of this thesis work, is to use supramolecular chemistry to control the chirality of the catalytic ligand itself, by dynamically inducing a stereogenic element through a low-cost and widely available chiral inducer. The often high-yielding supramolecularly directed assembly processes could thus be exploited in a final *in situ* generation of the chiral environment around the catalytic centre. Based on this idea a concept for the induction of chirality into prochiral compounds has to be devised. Consequently, the aims of this thesis can be summarised as follows:

- Selection of the supramolecular interactions that should be responsible for the assembly process.
- Identification and synthesis of suitable building blocks for the (catalytic) ligand. Two families of building blocks are required: a prochiral one and an easily accessible chiral one. These building blocks should fulfil the prerequisite of modifiability (both sterical and electronic) at minimum preparative effort in order to optimise their interaction.
- Development of methodologies for the *in situ* preparation of the new supramolecular complexes and their characterisation.
- Elucidation of the configurational properties of the induced chirality of the prochiral building blocks.
- Determination of the stability of the supramolecular complexes using suitable methods.

Depending on the progress of the project with respect to the aims outlined in the previous page, possible transformations of the model ligands to potential catalytically active entities should be pursued and realised. This premises the identification of catalytic reactions of interest with preference for those already under investigation in our group.

References

[1] L. Kelvin, *Baltimore Lectures*, **1884**.
[2] L. L. Whyte, *Nature* **1958**, *182*, 198.
[3] O. Katzenelson, H. Z. Hel-Or, D. Avnir, *Chem. Eur. J.* **1996**, *2*, 174.
[4] L. D. Barron, *Chem. Eur. J.* **1996**, *2*, 743.
[5] D. Avnir, O. Katzenelson, H. Z. Hel-Or, *Chem. Eur. J.* **1996**, *2*, 744.
[6] E. L. Eliel, S. H. Wilen, L. N. Mander, *Stereochemistry of Organic Compounds*, WILEY, New York, **1994**.
[7] K. Mislow, *Chirality* **2002**, *14*, 126.
[8] M. Schilthuizen, A. Davison, *Naturwissenschaften* **2005**, *92*, 504.
[9] M. Schilthuizen, P. G. Craze, A. S. Cabanban, A. Davison, J. Stone, E. Gittenberger, B. J. Scott, *J Evol Biol* **2007**, *20*, 1941.
[10] C. Grande, N. H. Patel, *Nature* **2009**, *457*, 1007.
[11] R. Ueshima, T. Asami, *Nature* **2003**, *425*, 679.
[12] L. D. Barron, *Space Sci. Rev.* **2008**, *135*, 187.
[13] K. A. Kvenvolden, J. Lawless, K. Pering, E. Peterson, J. Flores, C. Ponnamperuma, I. R. Kaplan, C. Moore, *Nature* **1970**, *228*, 923.
[14] R. Breslow, *Tetrahedron Lett.* **2010**, *52*, 2028.
[15] D. G. Fraser, D. Fitz, T. Jakschitz, B. M. Rode, *Phys. Chem. Chem. Phys.* **2011**, *13*, 831.
[16] R. M. Hazen, *Sci Am* **2001**, *284*, 76.
[17] W. A. Bonner, *Origins Life Evol. Biosphere* **1991**, *21*, 59.
[18] S. Kojo, *Symmetry* **2010**, *2*, 1022.
[19] R. N. Boyd, T. Kajino, T. Onaka, *Astrobiology* **2010**, *10*, 561.
[20] W. L. Noorduin, A. A. C. Bode, M. van der Meijden, H. Meekes, A. F. van Etteger, W. J. P. van Enckevort, P. C. M. Christianen, B. Kaptein, R. M. Kellogg, T. Rasing, E. Vlieg, *Nat. Chem.* **2009**, *1*, 729.
[21] C. Meinert, J.-J. Filippi, L. Nahon, S. V. Hoffmann, L. d'Hendecourt, P. de Marcellus, J. H. Bredehoft, W. H. P. Thiemann, U. J. Meierhenrich, *Symmetry* **2010**, *2*, 1055.
[22] S. P. Fletcher, *Nat. Chem.* **2009**, *1*, 692.
[23] J. Bailey, *Origins Life Evol. Biosphere* **2001**, *31*, 167.
[24] C. Cerf, A. Jorissen, *Space Sci. Rev.* **2000**, *92*, 603.
[25] S. F. Mason, *Molecular Optical Activity and the Chiral Discriminations*, Cambridge University Press, Cambridge, **1982**.
[26] N. Berova, K. Nakanishi, R. W. Woody, *Circular Dichroism: Principles and Applications*, 2nd ed., Wiley-VCH, New York, **2000**.
[27] D. A. Lightner, J. E. Gurst, *Organic Conformational Analysis and Stereochemistry from Circular Dichroism Spectroscopy*, John Wiley & Sons, New York, **2000**.

References

[28] *Chirality* **2009**, *21*, 1E.
[29] N. Berova, L. Di Bari, G. Pescitelli, *Chem. Soc. Rev.* **2007**, *36*, 914.
[30] L. D. Barron, F. Zhu, L. Hecht, G. E. Tranter, N. W. Isaacs, *J. Mol. Struct.* **2007**, *834-836*, 7.
[31] L. D. Barron, *Nature* **2007**, *446*, 505.
[32] L. D. Barron, F. Zhu, L. Hecht, *Vib. Spectrosc.* **2006**, *42*, 15.
[33] C. Merten, H. Li, X. Lu, A. Hartwig, L. A. Nafie, *J. Raman Spectrosc.* **2010**, *41*, 1273.
[34] L. A. Nafie, *Annu. Rev. Phys. Chem.* **1997**, *48*, 357.
[35] L. D. Barron, A. D. Buckingham, *Chem. Phys. Lett.* **2010**, *492*, 199.
[36] R. A. Lombardi, L. A. Nafie, *Chirality* **2009**, *21*, e277.
[37] T. B. Freedman, X. Cao, R. K. Dukor, L. A. Nafie, *Chirality* **2003**, *15*, 743.
[38] R. S. Drago, *Physical Methods in Chemistry*, Saunders College Publishing, Philadelphia, **1977**.
[39] N. Harada, S.-M. L. Chen, K. Nakanishi, *J. Am. Chem. Soc.* **1975**, *97*, 5345.
[40] N. Harada, K. Nakanishi, *J. Amer. Chem. Soc.* **1969**, *91*, 3989.
[41] N. Berova, K. Nakanishi, in *Circular Dichroism: Principles and Applications*, 2nd ed. (Eds.: N. Berova, K. Nakanishi, R. W. Woody), Wiley-VCH, New York, **2000**, pp. 337.
[42] X.-F. He, S. Zhang, R.-X. Zhu, S.-P. Yang, T. Yuan, J.-M. Yue, *Tetrahedron* **2011**, *67*, 3170.
[43] J. Luo, J.-S. Wang, X.-B. Wang, J.-G. Luo, L.-Y. Kong, *J. Nat. Prod.* **2010**, *73*, 835.
[44] N. Ousaka, Y. Inai, *J. Org. Chem.* **2009**, *74*, 1429.
[45] J. Sandström, in *Circular Dichroism: Principles and Applications*, 2 ed. (Eds.: N. Berova, K. Nakanishi, R. W. Woody), Wiley-VCH, New York, **2000**, pp. 459.
[46] A. Koslowski, N. Sreerama, R. W. Woody, in *Circular Dichroism: Principles and Applications*, 2 ed. (Eds.: N. Berova, K. Nakanishi, R. W. Woody), Wiley-VCH, New York, **2000**, pp. 55.
[47] T. D. Crawford, M. C. Tam, M. L. Abrams, *J. Phys. Chem. A* **2007**, *111*, 12057.
[48] T. D. Crawford, *Theor. Chem. Acc.* **2006**, *115*, 227.
[49] G. Pescitelli, N. Sreerama, P. Salvadori, K. Nakanishi, N. Berova, W. Woody Robert, *J. Am. Chem. Soc.* **2008**, *130*, 6170.
[50] A. Dreuw, M. Head-Gordon, *Chem. Rev.* **2005**, *105*, 4009.
[51] G. Pescitelli, L. Di Bari, A. M. Caporusso, P. Salvadori, *Chirality* **2008**, *20*, 393.
[52] M. Rudolph, J. Autschbach, *J. Phys. Chem. A* **2011**, *115*, 2635.
[53] J. Autschbach, *Chirality* **2009**, *21*, e116.
[54] Y. Si, G. Yang, M. Hu, M. Wang, *Chem. Phys. Lett.* **2011**, *502*, 266.

[55] P. Przybylski, M. Kwit, K. Pyta, R. Pankiewicz, G. Schroeder, J. Gawronski, B. Brzezinski, *Tetrahedron: Asymmetry* **2010**, *21*, 973.
[56] W. Kohn, *Rev. Mod. Phys.* **1999**, *71*, 1253.
[57] J. A. Pople, *Rev. Mod. Phys.* **1999**, *71*, 1267.
[58] W. Kohn, L. J. Sham, *Phys. Rev.* **1965**, *140*, A1133.
[59] R. G. Parr, W. Yang, *Density-functional Theory of Atoms and Molecules*, Oxford Univ. Press, Oxford, **1989**.
[60] C. Lee, W. Yang, R. G. Parr, *Phys. Rev. B* **1988**, *37*, 785.
[61] B. Miehlich, A. Savin, H. Stoll, H. Preuss, *Chem. Phys. Lett.* **1989**, *157*, 200.
[62] A. D. Becke, *J. Chem. Phys.* **1993**, *98*, 5648.
[63] Y. Zhao, D. G. Truhlar, *Theor. Chem. Acc.* **2008**, *120*, 215.
[64] T. Yanai, D. P. Tew, N. C. Handy, *Chem. Phys. Lett.* **2004**, *393*, 51.
[65] C. Adamo, V. Barone, *J. Chem. Phys.* **1998**, *108*, 664.
[66] R. Ditchfield, W. J. Hehre, J. A. Pople, *J. Chem. Phys.* **1971**, *54*, 724.
[67] W. J. Hehre, R. Ditchfield, J. A. Pople, *J. Chem. Phys.* **1972**, *56*, 2257.
[68] M. M. Francl, W. J. Pietro, W. J. Hehre, J. S. Binkley, M. S. Gordon, D. J. DeFrees, J. A. Pople, *J. Chem. Phys.* **1982**, *77*, 3654.
[69] V. A. Rassolov, J. A. Pople, M. A. Ratner, T. L. Windus, *J. Chem. Phys.* **1998**, *109*, 1223.
[70] V. A. Rassolov, M. A. Ratner, J. A. Pople, P. C. Redfern, L. A. Curtiss, *J. Comput. Chem.* **2001**, *22*, 976.
[71] A. D. McLean, G. S. Chandler, *J. Chem. Phys.* **1980**, *72*, 5639.
[72] R. Krishnan, J. S. Binkley, R. Seeger, J. A. Pople, *J. Chem. Phys.* **1980**, *72*, 650.
[73] J.-P. Blaudeau, M. P. McGrath, L. A. Curtiss, L. Radom, *J. Chem. Phys.* **1997**, *107*, 5016.
[74] A. J. H. Wachters, *J. Chem. Phys.* **1970**, *52*, 1033.
[75] P. J. Hay, *J. Chem. Phys.* **1977**, *66*, 4377.
[76] K. Raghavachari, G. W. Trucks, *J. Chem. Phys.* **1989**, *91*, 2457.
[77] M. P. McGrath, L. Radom, *J. Chem. Phys.* **1991**, *94*, 511.
[78] L. A. Curtiss, M. P. McGrath, J.-P. Blaudeau, N. E. Davis, r. C. Binning, Jr., L. Radom, *J. Chem. Phys.* **1995**, *103*, 6104.
[79] A. Schaefer, H. Horn, R. Ahlrichs, *J. Chem. Phys.* **1992**, *97*, 2571.
[80] A. Schaefer, C. Huber, R. Ahlrichs, *J. Chem. Phys.* **1994**, *100*, 5829.
[81] C. J. Cramer, *Essentials of Computational Chemistry, 2nd Edition*, **2004**.
[82] K. I. Ramachandran, G. Deepa, K. Namboori, *Computational Chemistry and Molecular Modeling: Principles and Applications*, Springer, Berlin, **2008**.

References

[83] P. J. Stephens, N. Harada, *Chirality* **2010**, *22*, 229.
[84] J. Clayden, W. J. Moran, P. J. Edwards, S. R. LaPlante, *Angew. Chem., Int. Ed.* **2009**, *48*, 6398.
[85] S. R. LaPlante, P. J. Edwards, L. D. Fader, A. Jakalian, O. Hucke, *ChemMedChem* **2011**, *6*, 505.
[86] C. Bun Ching, J. Zhang, J. Sui, W. Ning Chen, *Proteomics* **2010**, *10*, 888.
[87] A. K. Peepliwal, S. B. Bagade, C. G. Bonde, *J. Biomed. Sci. Res.* **2010**, *2*, 29.
[88] F. Spindler, B. Pugin, H. Buser, H.-P. Jalett, U. Pittelkow, H.-U. Blaser, *Pestic. Sci.* **1998**, *54*, 302.
[89] A. Williams, *Pestic. Sci.* **1996**, *46*, 3.
[90] B. S. Sekhon, *J. Pestic. Sci. (Tokyo, Jpn.)* **2009**, *34*, 1.
[91] A. Bosco, M. G. M. Jongejan, R. Eelkema, N. Katsonis, E. Lacaze, A. Ferrarini, B. L. Feringa, *J. Am. Chem. Soc.* **2008**, *130*, 14615.
[92] O. Trushkevych, P. Ackerman, W. A. Crossland, I. I. Smalyukh, *Appl. Phys. Lett.* **2010**, *97*, 201906/1.
[93] G. Carbone, P. Salter, S. J. Elston, P. Raynes, L. De Sio, S. Ferjani, G. Strangi, C. Umeton, R. Bartolino, *Mol. Cryst. Liq. Cryst.* **2010**, *525*, 41.
[94] S. W. Smith, *Toxicol. Sci.* **2009**, *110*, 4.
[95] FDA Policy Statement for the Development of New Stereoisomeric Drugs, Washington DC, **1992**: http://www.fda.gov/Drugs/GuidanceComplianceRegulatoryInformation/Guidances/ucm122883.htm
[96] D. E. Drayer, *Clin. Pharmacol. Ther. (St. Louis)* **1986**, *40*, 125.
[97] S. V. Rajkumar, *Mayo Clin. Proc.* **2004**, *79*, 899.
[98] A. Palumbo, *Nat. Rev. Clin. Oncol.* **2010**, *7*, 425.
[99] A. Palumbo, F. Davies, M. Kropff, J. Blade, M. Delforge, F. Leal da Costa, R. Garcia Sanz, S. Schey, T. Facon, G. Morgan, P. Moreau, *Ann. Hematol.* **2010**, *89*, 803.
[100] M. Engelhardt, M. Kleber, J. Udi, R. Waesch, A. Spencer, F. Patriarca, S. Knop, B. Bruno, M. Gramatzki, F. Morabito, M. Kropff, A. Neri, O. Sezer, R. Hajek, D. Bunjes, M. Boccadoro, C. Straka, M. Cavo, A. Polliack, H. Einsele, A. Palumbo, *Leuk. Lymphoma* **2010**, *51*, 1424.
[101] J. Laubach, P. Richardson, K. Anderson, *Annu. Rev. Med.* **2011**, *62*, 249.
[102] S. Gaubert, M. Vie, C. Damase-Michel, A. Pathak, J.-L. Montastruc, *Fundam. Clin. Pharmacol.* **2009**, *23*, 247.
[103] P. Corcoran, U. Reulbach, H. S. Keeley, I. J. Perry, K. Hawton, E. Arensman, *BMC Clin. Pharmacol.* **2010**, *10*, 1.
[104] N. Kurihara, J. Miyamoto, G. D. Paulson, B. Zeeh, M. W. Skidmore, R. M. Hollingworth, H. A. Kuiper, *Pure Appl. Chem.* **1997**, *69*, 2007.

[105] R. A. Sheldon, *Chirotechnology: Industrial Synthesis of Optically Active Compounds*, Dekker, New York, **1993**.
[106] I. Ojima, Editor, *Catalytic Asymmetric Synthesis*, 3rd ed., Wiley-VCH, **2000**.
[107] E. N. Jacobsen, A. Pfaltz, H. Yamamoto, Editors, *Comprehensive Asymmetric Catalysis, Vol. 1-3*, Springer, Berlin, **1999**.
[108] P. Anastas, J. Warner, *Green Chemistry: Theory and Practice*, Oxford University Press, Oxford, UK, **1998**.
[109] D. Steinborn, *Grundlagen der Komplexkatalyse*, Teubner, Wiesbaden, **2007**.
[110] A. Grabulosa, G. Muller, R. Ceder, M. A. Maestro, *Eur. J. Inorg. Chem.* **2010**, 3372.
[111] A. Gillon, K. Heslop, D. J. Hyett, A. Martorell, A. G. Orpen, P. G. Pringle, C. Claver, E. Fernandez, *Chem. Commun.* **2000**, 961.
[112] M. T. Reetz, T. Sell, *Tetrahedron Lett.* **2000**, *41*, 6333.
[113] D. W. Norman, C. A. Carraz, D. J. Hyett, P. G. Pringle, J. B. Sweeney, A. G. Orpen, H. Phetmung, R. L. Wingad, *J. Am. Chem. Soc.* **2008**, *130*, 6840.
[114] M. T. Reetz, G. Mehler, *Angew. Chem., Int. Ed.* **2000**, *39*, 3889.
[115] M. van den Berg, A. J. Minnaard, E. P. Schudde, J. van Esch, A. H. M. de Vries, J. G. de Vries, B. L. Feringa, *J. Am. Chem. Soc.* **2000**, *122*, 11539.
[116] P. E. Goudriaan, P. W. N. M. van Leeuwen, M.-N. Birkholz, J. N. H. Reek, *Eur. J. Inorg. Chem.* **2008**, 2939.
[117] K. N. Gavrilov, S. V. Zheglov, E. B. Benetsky, A. S. Safronov, E. A. Rastorguev, N. N. Groshkin, V. A. Davankov, B. Schaeffner, A. Boerner, *Tetrahedron: Asymmetry* **2009**, *20*, 2490.
[118] H. Landert, F. Spindler, A. Wyss, H.-U. Blaser, B. Pugin, Y. Ribourduoille, B. Gschwend, B. Ramalingam, A. Pfaltz, *Angew. Chem., Int. Ed.* **2010**, *49*, 6873.
[119] J. Meeuwissen, R. Detz, A. J. Sandee, B. de Bruin, M. A. Siegler, A. L. Spek, J. N. H. Reek, *Eur. J. Inorg. Chem.* **2010**, 2992.
[120] K. N. Gavrilov, S. V. Zheglov, A. A. Shiryaev, N. N. Groshkin, E. A. Rastorguev, E. B. Benetskiy, V. A. Davankov, *Tetrahedron Lett.* **2011**, *52*, 964.
[121] P. Daka, Z. Xu, A. Alexa, H. Wang, *Chem. Commun.* **2011**, *47*, 224.
[122] J. Wassenaar, J. N. H. Reek, *Org. Biomol. Chem.* **2011**, *9*, 1704.
[123] H. Fernandez-Perez, P. Etayo, A. Panossian, A. Vidal-Ferran, *Chem. Rev.* **2011**, *111*, 2119.
[124] K. Ding, Z. Han, Z. Wang, *Chem. Asian J.* **2009**, *4*, 32.
[125] Q. Tan, M. Hayashi, *Adv. Synth. Catal.* **2008**, *350*, 2639.
[126] I. Arribas, S. Vargas, M. Rubio, A. Suarez, C. Domene, E. Alvarez, A. Pizzano, *Organometallics* **2010**, *29*, 5791.
[127] F. Fernandez, A. Gual, C. Claver, S. Castillon, G. Muller, M. Gomez, *Eur. J. Inorg. Chem.* **2010**, 758.

References

[128] M. Lotz, R. Schuecker, K. Mereiter, P. Knochel, *Organometallics* **2010**, *29*, 6503.
[129] L. M. Pratt, S. Voit, F. N. Okeke, N. Kambe, *J. Phys. Chem. A* **2011**, *115*, 2281.
[130] G. Barone, G. Li Manni, A. Prestianni, D. Duca, H. Bernas, D. Y. Murzin, *J. Mol. Catal. A: Chem.* **2010**, *333*, 136.
[131] M.-H. Baik, S. Mazumder, P. Ricci, J. R. Sawyer, Y.-G. Song, H. Wang, P. A. Evans, *J. Am. Chem. Soc.* **2011**, *133*, 7621.
[132] M. Hoelscher, W. Leitner, *Chem. Eur. J.* **2010**, *16*, 14266.
[133] K. N. Houk, P. H.-Y. Cheong, *Nature* **2008**, *455*, 309.
[134] T. Wondimagegn, D. Wang, A. Razavi, T. Ziegler, *Organometallics* **2008**, *27*, 6434.
[135] S. Marti, J. Andres, V. Moliner, E. Silla, I. Tunon, J. Bertran, *Chem. Soc. Rev.* **2008**, *37*, 2634.
[136] J. B. Siegel, A. Zanghellini, H. M. Lovick, G. Kiss, A. R. Lambert, J. L. St. Clair, J. L. Gallaher, D. Hilvert, M. H. Gelb, B. L. Stoddard, K. N. Houk, F. E. Michael, D. Baker, *Science* **2010**, *329*, 309.
[137] S. Monfette, J. M. Blacquiere, D. E. Fogg, *Organometallics* **2011**, *30*, 36.
[138] C. R. Corbeil, N. Moitessier, *J. Mol. Catal. A: Chem.* **2010**, *324*, 146.
[139] K. Ariga, T. Kunitake, *Supramolecular Chemistry - Fundamentals and Applications*, Springer, Heidelberg, **2006**.
[140] J. W. Steed, J. L. Atwood, Ed., *Supramolecular Chemistry*, 2nd ed., WILEY, **2009**.
[141] C. P. Pradeep, L. Cronin, *Annu. Rep. Prog. Chem., Sect. A: Inorg. Chem.* **2007**, *103*, 287.

I Design and Preparation of New Chiral Ligands by Chiral Induction Using Hydrogen Bonding as the Mediating Force

1 Literature Precedents

Hydrogen bonding has long been taken advantage of for chiral recognition and sensing. Nowadays, a large number of excellent examples of chiral supramolecular complexes that have been formed by hydrogen bonding can be found in the literature. These include complexes formed using chiral induction,[1-14] allosteric control,[15-17] and chiral amplification.[6,18-25] Concerning the work in this thesis, the induction of chirality *via* hydrogen bonding, especially into dynamic axially racemic biaryl compounds, was of particular interest.

In an early study Mizutani *et al*. showed that a preferential axial sense of rotation can be induced into flexible biphenols **1** by steric interactions upon hydrogen bonding with enantiopure *trans*-1,2-diaminocyclohexane (DACH) derivatives **2** (Scheme I-1).[1] Cotton effects that could be assigned to the biphenol chromophore indicating the presence of axial chirality, *i.e.* a preferential axial sense of rotation in the biaryl compound, were only observable after the addition of the chiral inducer (DACH). Furthermore, dependence of the chiral induction on the steric bulk of the DACHs N-substituents and solvent polarity was reported. The use of more polar solvents apparently resulted in smaller CD amplitudes, although the binding strength was not necessarily affected by the change in solvent.

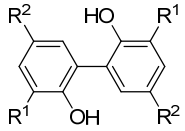

1a: R^1 = Br, R^2 = NO_2
1b: R^1 = H, R^2 = NO_2
1c: R^1 = Me, R^2 = H

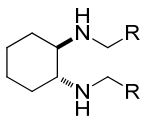

(1*R*,2*R*)-**2a**: R = Np
(1*R*,2*R*)-**2b**: R = Me
(1*R*,2*R*)-**2c**: R = H

Scheme I-1. Complementary hosts and guests for the induction of chirality by hydrogen bonding.[1]

In continuation of this work, Mizutani and co-workers investigated the proton transfer in the binding event between biphenols and chiral amines and its consequences on the axial chirality induction process (Scheme I-2).[2]

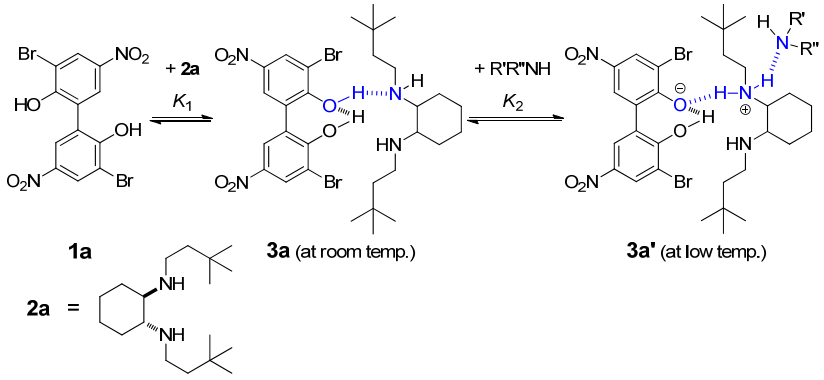

Scheme I-2. Binding of diamine **2a** to biphenol **1a** and formation of the ternary complex **3a'** with excess amine.[2]

The authors showed by NMR studies that at room temperature the degree of proton transfer is small and relatively independent from the amount of amine present. At low temperatures however, the complexation of two molecules of excess diamine with biphenol resulted in elevated proton transfer and gave rise to ternary hydrogen bonded complexes, presumably of type **3a'**. Axial chirality was also observed in 1:1 complexes of type **3a** at room temperature. But the appearance of an intense Cotton effect and UV-vis absorbance in the phenolate band upon lowering the temperature clearly indicated the formation of a well-ordered chiral supramolecular system that was accompanied by enhanced chiral induction.

A nice example for the potential application of induced atropisomerism in chiroptical probes was reported by Kubo *et al.* (Scheme I-3).[4]

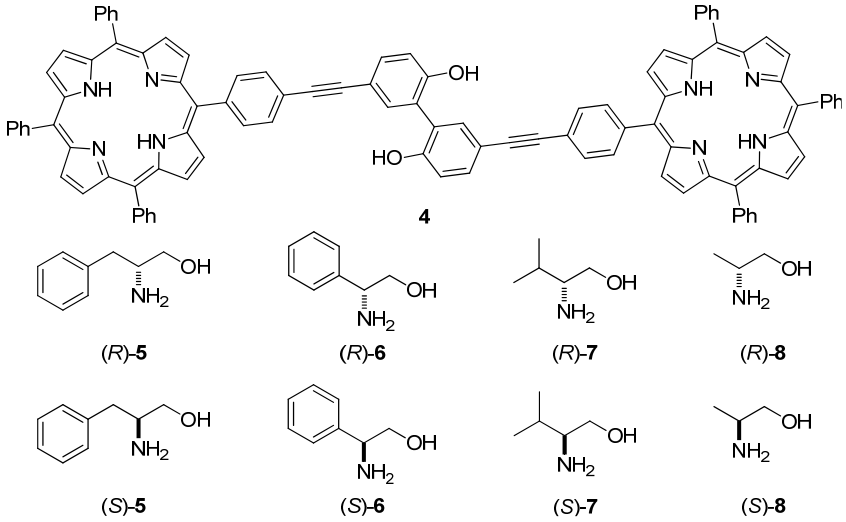

Scheme I-3. 2,2'-Biphenol-bridged bis(free base porphyrin) **4** and enantiopure amino alcohols **5**-**8**.[4]

The 2,2'-biphenol-bridged bis(free base porphyrin) **4** was used as a chiral sensor for optically pure amino alcohols **5**-**8**. These amino alcohols appeared to interact with the C_2 symmetric biphenol linker *via* hydrogen bonding. Steric hindrance generated by these aliphatic or aromatic substrates resulted in the preferential formation of diastereomers of either a*R* or a*S* preferential sense of axial rotation in the biphenol unit. The use of amino alcohols **8** that contained the smallest substituents of this series resulted in CD silent spectra. The shifting of the conformational equilibrium itself was detected by the appearance of exciton-coupled Cotton effects in the CD curve that were assignable to the intense Soret transition band of the two porphyrin units. The authors declared that employing the amino alcohols in higher concentrations (in the order of 10^{-2} M) allowed them to determine the absolute configuration of the respective guests, with *R* configurations leading to negative, and *S* configurations leading to positive exciton-coupled CD spectra. Table I-1 shows selected CD spectral data for the hydrogen bonded complexes resulting from self-assembly of **4** with

(*R*)- and (*S*)-phenylalaninol **5** (see the original article for the remaining substrates) in low and high concentrations, respectively. Bisignated Cotton effects were observed and the mirror image form of the CD curves induced by the two enantiomers of **5** becomes most apparent by comparison of the signs and $\Delta\varepsilon$ values of entry 2 with entry 4.

Table I-1. Selected CD spectral data for hydrogen bonded complexes **4**+**5** in CH_2Cl_2 at 25 ºC.[4]

entry	guest	conc.[a]	1st CE[b]		2nd CE[b]	
			sign	$\Delta\varepsilon^c$ $(\lambda)^d$	sign	$\Delta\varepsilon^c$ $(\lambda)^d$
1	(*R*)-**5**	12.6	-	1.98 (425)	+	6.57 (415)
2	(*R*)-**5**	126	-	6.32 (425)	+	9.50 (415)
3	(*S*)-**5**	12.4	+	6.81 (425)	-	1.09 (415)
4	(*S*)-**5**	125	+	9.48 (425)	-	5.19 (415)

[a][amino alcohol], mM. [b]Cotton effect. [c]M^{-1} cm^{-1}. [d]nm.

Maeda *et al*. reported a dynamic axial chirality control of carboxybiphenols **9** through acid-base pairing with enantiomerically pure diamines and amino alcohols.[9] For this purpose they prepared the biphenols **9a**-**d**, bearing an ethynyl substituent for enhancing the effective π–conjugation length, and have combined them with the diamines **10a** and **11**-**12**, the monoamines **13a** and **13b**, and the amino alcohols **13c** and **14** (Scheme I-4). In summary, an induced CD signal was observed for the π–conjugated biaryl **9a** as a result of its complexation with the enantiopure diamines **10**-**12** (used in equimolar and excess amounts) but not with the chiral monoamines and amino alcohols **13** and **14** (used in up to 50-fold excess). In contrast, biphenols **9b** and **9c** did not exhibit CD signals with any of the amines **10**-**14**, indicating that the 2,2'-hydroxy and 3,3'-carboxyl groups were indispensible for strong binding. The observation of a correlation between the absolute configuration of the amine moiety and the sign of

the induced Cotton effects (Table I-2) led the authors to the conclusion that **9a** may serve as chirality sensor in the determination of absolute configurations of enantiopure diamines.

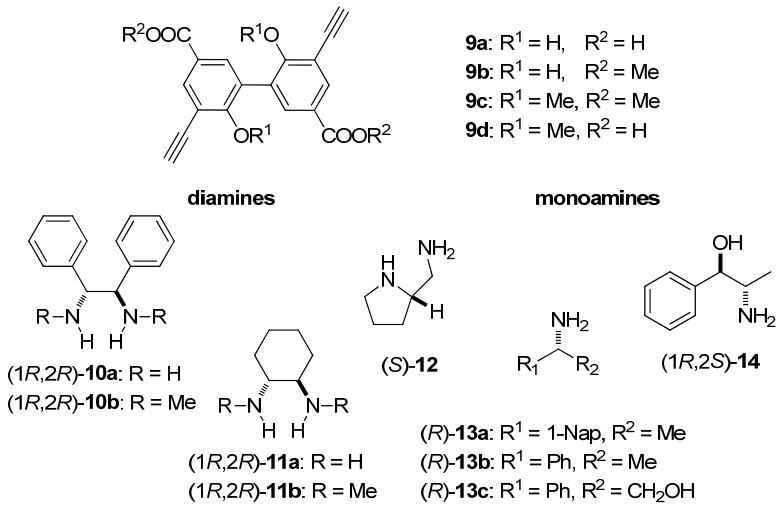

Scheme I-4. Dynamically racemic 2,2'-biphenols and optically active amines.[9]

Table I-2. Selected CD data of complexes of **9a** with diamines **10**-**12** in THF at 25 ºC.[9]

entry	diamine	conc.[a]	1st Cotton effect		2nd Cotton effect	
			sign	$\Delta\varepsilon^d$ (λ)^e	sign	$\Delta\varepsilon^d$ (λ)^e
1	(1*R*,2*R*)-**10a**	9.3	-	1.50 (338)	+	3.44 (316)
2	(1*R*,2*R*)-**10a**	0.12	-	1.98 (338)	+	3.36 (315)
3	(1*S*,2*S*)-**10a**	9.3	+	1.46 (338)	-	3.13 (316)
4	(1*R*,2*R*)-**10b**	9.3	-	1.18 (339)	+	2.58 (316)
5	(1*R*,2*R*)-**10b**	0.12	-	0.30 (340)	+	1.03 (319)
6	(1*R*,2*R*)-**11a**	0.12[b]	-	1.18 (336)	+	0.65 (314)
7	(1*R*,2*R*)-**11b**	7.1	-	0.37 (338)	+	0.37 (314)
8	(1*R*,2*R*)-**11b**	0.12[c]	-	0.52 (339)	+	0.36 (314)
9	(*S*)-**12**	0.12[c]	-	3.48 (341)	+	8.72 (313)

[a][diamine]/**9a** = 1 (entries 1, 3, 4, and 7), [diamine]/**9a** = 4 (entries 2, 5, 6, 8, and 9), in mM. [b]THF/$CHCl_3$ (1:1). [c]THF/$CHCl_3$ (1:9). [d]M^{-1} cm^{-1}. [e]nm.

The above findings together with Job plot analyses and IR titration experiments allowed proposing the formation of 2:2 stoichiometric tetramers as the presumed CD active species (Scheme I-5). Furthermore, it was put forward that these tetramers enabled the formation of the CD active *cisoid* conformation of **9a** by taking advantage of intramolecular hydrogen bonds. Only diamines could form such acid-base complexes, whilst monoamines and amino alcohols were not capable of hindering the rotation along the biaryl axis, and thus were not able to favour the preferential formation of one of the axially twisted conformers.

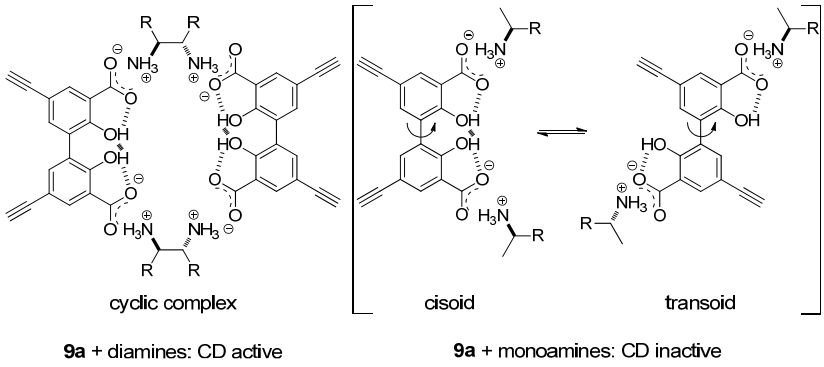

Scheme I-5. Proposed models for the complexation of **9a** with chiral diamines (left) and chiral monoamines and amino alcohols, respectively (right), at [**9a**] = 9.3 mM.[9]

Feringa and Eelkema reported the macroscopic expression of the chirality of amino alcohols by a double amplification mechanism in liquid crystals (LC) (Scheme I-6).[24] The crucial point of their work was the transfer of chirality from the stereogenic centres of amino alcohols **15** to biphenols **16** (Scheme I-6 and Scheme I-7) inducing axial chirality to supramolecular chirality in cholesteric LCs. Liquid crystal mesophases can become chiral due to doping with small amounts of a suitable dopant such as enantiomerically pure biphenols or biphenyls in general.[26,27] The emerging helical organisation usually results in strong

optical rotatory dispersion (ORD) and CD signals.[28-30] However, the chirality of LC material is mainly indicated by the cholesteric pitch *p*, *i.e.* the length of one 360 º cholesteric helix turn. It is dependent on i) the concentration of the chiral dopant, ii) its enantiomeric excess (ee), and most interestingly, iii) the helical twisting power β of the chiral dopant. Deduced from the pitch values, the authors could show the good helical twisting power of their systems. It was also demonstrated that binding of the enantiopure amino alcohols to the biphenol moiety was essential for inducing supramolecular chirality since the amino alcohols alone did not lead to cholesteric LCs.

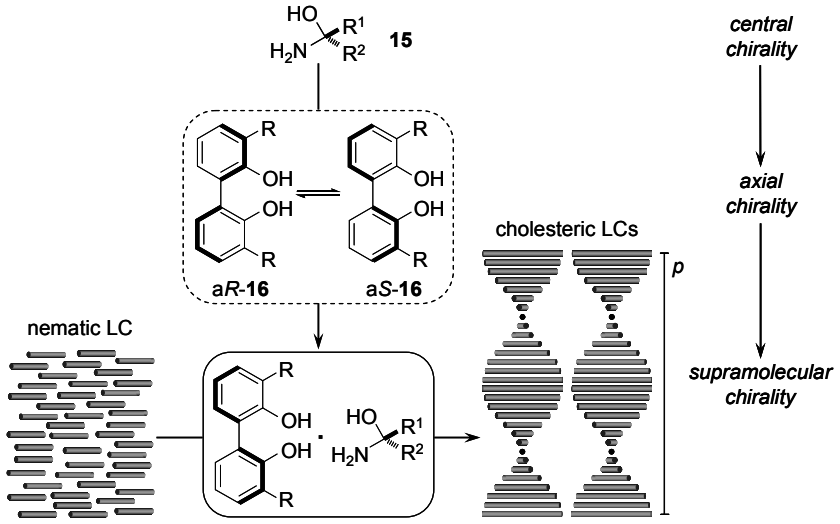

Scheme I-6. Transfer and amplification of chirality.[24]

Regarding the structure of the effective chiral dopant, the authors proposed an assembly of type **17** with the aliphatic part of the amino alcohol entering the pocket that is formed by the 3,3'-substituents of the biaryl (Scheme I-7). This could be demonstrated by the upfield shifts of all aliphatic and some aromatic protons of the enantiomerically pure dopant, implying their situation in the shielding cone of the biaryls aromatic substituents. These findings were confirmed by NOESY

experiments. The hydrogen bonding nature of the interaction between the dynamically racemic biphenol **16** and the chiral inducer **15** was suggested by IR analyses, whereas the 1:1 stoichiometry resulted from Job plot analysis. In continuation of this work, Feringa and Eelkema also reported the expansion of this concept on monoamines as chiral dopants to phosphoric acids derived from biphenol compounds.[25]

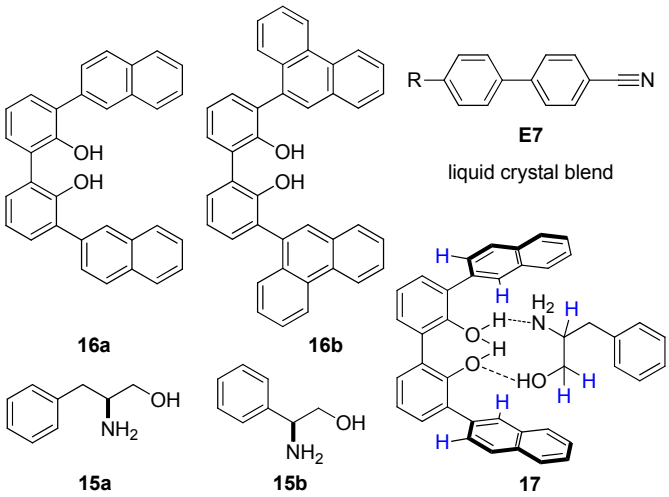

Scheme I-7. 3,3'-Disubstituted biphenols **16**, chiral amino alcohols **15**, and liquid crystal blend **E7** with R = *n*-C_5H_{11}, *n*-$C_8H_{17}O$, 4'-*n*-C_5H_{11}–C_6H_4; **17** shows the proposed binding mode for **15a**+**16a**. The protons with the strongest intermolecular NOEs are depicted in blue.[24]

Based on their previous work on redox switches for chiroptical response systems,[31-33] Suzuki *et al*. developed prototypes for four-way-output molecular response systems based on biphenyl-2,2'-diyldiacridiniums.[12] Essential to these systems was the induction of helicity or axial chirality through intramolecular hydrogen bonding between two amide substituents, which bear chiral fragments and are tethered via a linker to the acridinium nitrogen atoms (Scheme I-8). The systems were sensitive towards redox processes, temperature, and solvent changes. As a whole the authors described their approach as

the realisation of a three-way-input (electrochemical, T-dependency, and solvent polarity) and four-way-output (UV-vis, fluorescence, CD, and fluorescence detected CD (FDCD)) response system. The oxidation/reduction of **18** and **19** was not only responsible for the activation/deactivation of fluorescence and FDCD (only the dications showed fluorescence) but also for the cleavage/formation of a C–C bond. The chiral Aux* groups were said to induce a diastereomeric preference resulting in detectable chiroptical signals due to an exciton coupling mechanism in the helical (**18**, **19**) or axially chiral (**18**$^{2+}$, **19**$^{2+}$) structures.

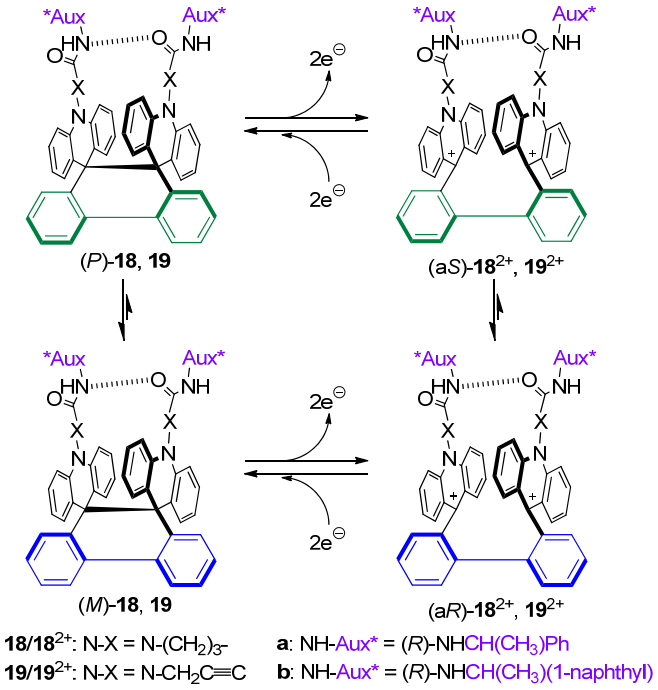

Scheme I-8. Electrochiroptical response systems **18**/**18**$^{2+}$ and **19**/**19**$^{2+}$ and transfer of central chirality into axial chirality.[12]

The diastereomeric excess could be determined for two axially chiral species by ^{1}H NMR analysis in CD_2Cl_2 at -40 ºC. Hence, the preference for one axial sense of rotation was determined to be 70% for **18a**$^{2+}$ and 75% for **18b**$^{2+}$. Deduced from CD intensities and fluorescence activity, system **18a**/**18a**$^{2+}$ was identified by the authors to be best suited for studying the hydrogen bonding. It was found that a solvent change from pure CH_2Cl_2 to CH_2Cl_2/MeCN mixtures drastically reduced the CD intensity of **18a**$^{2+}$. Since the latter polar solvent mixture can hamper H-bond formation, it was concluded that hydrogen bonding was indeed responsible for inducing the observed diastereomeric excess. In addition to hydrogen bonding, Suzuki *et al*. have also reported similar response systems relying on metal-ligand (dihydrophenanthroline-bipyridine skeletons)[34] or $\pi-\pi$ interactions (biphenyl-2,2'-diyl-type dicationic dyes)[35] as non-covalent forces for the control of axial chirality.

The knowledge gained in the past in understanding hydrogen bonding and designing efficient binding motifs, paved the way for the development of new, self-assembled ligands for asymmetric transformations focusing on the potential of hydrogen bonding. This field took huge benefit from increasing research efforts since the late 1990s. Traditionally, bidentate ligands were regarded as being the key to homogeneous enantioselective transition metal catalysis.[36] These ligands provided two crucial features that raised them above monodentate ligands. Firstly, their defined backbone allowed the for stereodiscrimination often favourable *cis* coordination to the catalytic metal centre, and secondly, the resulting catalyst may take advantage of the increased stability of the chelate complex and the well-defined asymmetric environment it creates around the catalytic centre.[37-41] Hence, strategies for the quick and efficient generation of bidentate ligand libraries are highly sought after. Supramolecular chemistry has proven to offer an alternative approach to do so and as a result several families of new ligands now known as "supramolecular bidentate

ligands" have been developed and can be found in a series of review articles and textbooks.[42-48] Crucial to this new type of ligand is that they are assembled from smaller subunits by non-covalent ligand-ligand interactions. The non-covalent forces include metal-ligand complexation, π–π interactions and the interesting hydrogen bond formation. Overall, these ligand-ligand interactions enabled the supramolecular assemblies in many cases to act as bidentate entities of almost covalent nature but simultaneously maintaining the advantages of the subunits, first and foremost the ease of preparation.

Hydrogen bonding has proven the most convenient and perhaps most powerful non-covalent force in the development of self-assembled ligands so far. This was due to several characteristic features: i) many of the hydrogen bonding motifs used (*e.g.* amides, ureas, guanidines) are quite easy to introduce and also chemically stable, ii) hydrogen bonds are capable of self-assembling (and repairing), thus enabling the thermodynamically driven formation of catalytically active species; iii) hydrogen bonds usually do not interfere negatively with other (desired) interactions such as the complexation between the ligand's donor group and the catalytic metal.[42]

Pioneering work in the exploitation of hydrogen bonds for the construction of bidentate supramolecular ligands was reported by Breit and Seiche.[49-51] In 2003 they described a new concept for the preparation of bidentate ligands by self-assembly through hydrogen bonding. The tautomer system 2-pyridone/2-hydroxypyridine (**20**A/**20**B, Scheme I-9) usually dimerises in aprotic media to form mainly the symmetrical pyridine dimer **22**.[52] Nonetheless, it was reasoned that if X were donor groups capable of coordinating to a metal centre, the equilibrium could be shifted towards the unsymmetrical dimer **23** by taking advantage of the chelate effect. The reaction of 2 equiv. of 6-diphenylphosphanyl-2-pyridone (6-DPPon, **21**) with [$PtCl_2$(COD)]

yielded *cis*-[$PtCl_2$(6-DPPon)$_2$] as was determined by X-ray diffraction. This technique also confirmed the binding mode of 6-DPPon as chelating ligand. A rhodium catalyst was prepared from **21** and tested against established bidentate ligands and the industrially employed monodentate Rh/PPh_3 system in the hydroformylation of 1-octene. The new Rh/6-DPPon catalyst showed excellent regioselectivity and activity, easily exceeding the monodentate PPh_3 ligand in both criteria, and standard bidentate ligands at least in catalytic activity. Furthermore, excellent regioselectivity was afforded in favour of the linear aldehydes in the hydroformylation of several terminal alkenes bearing additional functional groups.[49,50] As can be seen in Scheme I-10, this also included substrates possessing significant hydrogen bonding capabilities of their own which did not affect the high regioselectivity of the Rh/6-DPPon catalytic system. However, it was observed that protic solvents such as MeOH or the addition of AcOH were capable of disrupting the hydrogen bonds. The same was true for elevated temperatures beyond 110 ºC and both led to regioselectivities close to that observed for the monodentate PPh_3 ligand.

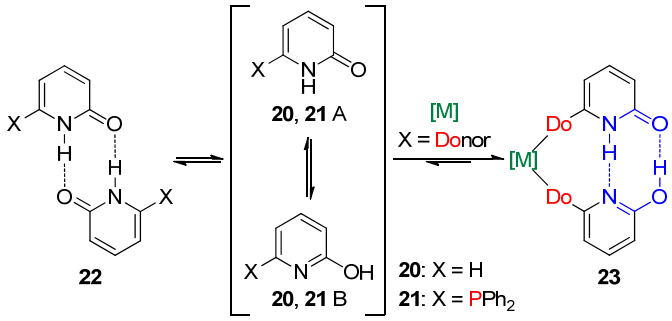

Scheme I-9. 2-Pyridone/2-hydroxypyridine tautomer systems and a possible binding mode to metal centres in the presence of donor groups.[49]

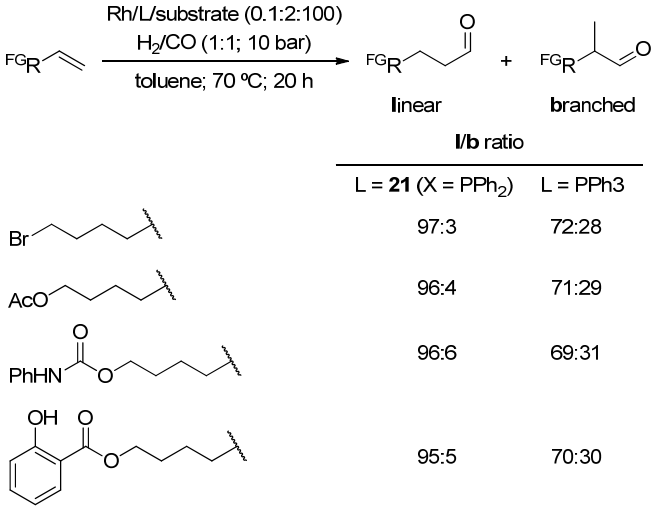

Scheme I-10. Performance of the self-assembling ligand **21** in the Rh-mediated hydroformylation of terminal alkenes.[49]

Based on this concept Breit and Börner *et al*. later reported the application of self-assembling ligands **24a**-**26a** and their non self-assembling analogues **24b**-**26b** in the Rh-mediated enantioselective hydrogenation of prochiral benchmark alkenes (methyl *N*-acetamido acrylate, methyl (*Z*)-2-*N*-acetamido-3-phenylacrylate, and dimethyl itaconate),[53,54] and ligands **25**-**27** as part of a larger library in the Pd-mediated asymmetric allylic amination of *rac*-(*E*)-1,3-diphenyl-3-acetoxyprop-1-ene (Scheme I-11).[55]

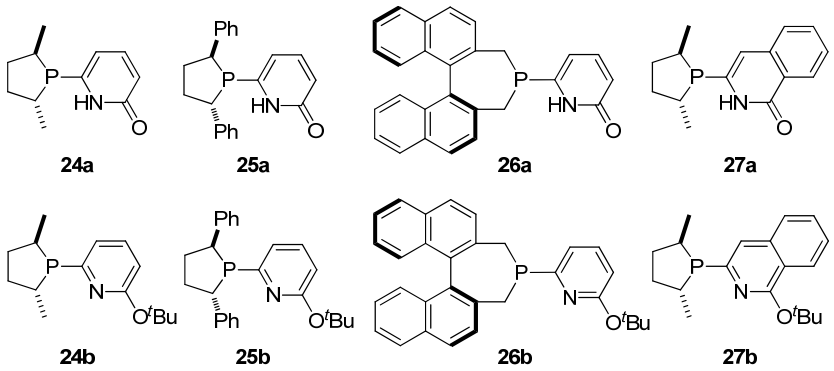

24a **25a** **26a** **27a**

24b **25b** **26b** **27b**

Scheme I-11. Ligands **24a**-**27a** and their non self-assembling analogues **24b**-**27b**.[53-55]

The structure and self-assembly of the ligands **24a**-**26a** and their Rh-complexes in solution was studied by ^{31}P and ^{1}H NMR. Free ligands were present as single species at room temperature and it was further concluded that they also aggregate in non-polar solvents predominantly as pyridone/pyridone dimers similar to **22**. However, in the complexes derived from ligands **24a**-**26a** and $[Rh(COD)_2]BF_4$ the NMR analyses suggest the formation of pyridine/pyridone dimers in *cis* arrangement similar to **23** (Scheme I-9). Strikingly, the ligands capable of self-assembly **24a**-**26a** usually exceeded their non-self-assembling analogues **24b**-**26b** in terms of enantioselectivity in the Rh-mediated hydrogenation of the benchmark alkenes, although at the expense of lower conversions. Ligand **26b** was identified as being the most efficient in these hydrogenations since it provided a good compromise of high enantioselectivities at acceptable reaction rates, the latter being a critical issue for phospholanes **24a** and **25a** (Scheme I-12).

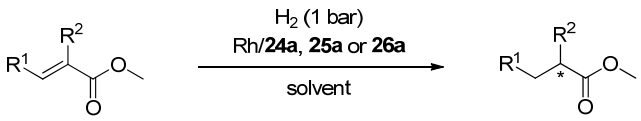

R^1	R^2	ee (%)
H	NHAc	up to 91% (*R*)
Ph	NHAc	up to 94% (*R*)
H	CH_2COOMe	up to 99% (*S*)

Scheme I-12. Performance of self-assembling ligands in the Rh-mediated hydrogenation of benchmark alkenes.[53, 54]

In addition to phosphanes **24**-**26**, new phospholane ligands **27** were tested in the Pd-mediated asymmetric allylic amination of *rac*-(*E*)-1,3-diphenyl-3-acetoxyprop-1-ene. Excellent enantioselectivities (up to 99%) were obtained but, surprisingly, it was the non-self-assembling ligand **27b** based on a small heterocyclic phosphane that gave the best result. The bulkier and self-assembling ligand **26a** led to significantly lower enantioselectivity. This was in sharp contrast to what was found for the hydrogenation reactions.

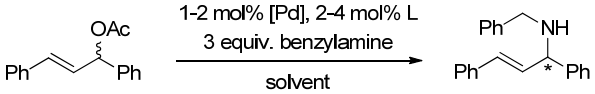

L	ee %
27a	91 (*R*)
27b	99 (*R*)
26a	40 (*S*)

Scheme I-13. Pd-catalysed asymmetric allylic amination of *rac*-(*E*)-1,3-diphenyl-3-acetoxyprop-1-ene using phosphanes **27a**, **27b**, and **26a** as ligands.[55]

Up to this point, only homo-combinations of the two involved monodentate ligands had to be considered since the pyridone/hydroxypyridine tautomers were rapidly interconverting. However, for catalyst optimisation hetero-complexes formed from monodentate ligands bearing different donor sites are of great interest. Unfortunately in such mixtures three potential catalysts would be present at the same time, namely the desired hetero- and two homo-combinations. Only in cases where the hetero-dimeric catalyst is both more reactive and more selective could process optimisation be achieved. Consequently, selective assembly strategies towards hydrogen bonded hetero-complexes were sought.

Breit and co-workers realised such systems by developing a model that was inspired by the complementary adenine–thymine (A–T) base-pair that is found in DNA (Scheme I-14).[51,56-62] The versatility of this model in combinatorial ligand optimisation and catalyst screening becomes apparent immediately. The adenine and thymine analogues, namely aminopyridine **28** and isoquinolone **29** derivatives, respectively, are highly modular with respect to i) the nature of their (phosphorous) donor substituents (influencing the bite angle θ and the coordination geometry at the metal), ii) their backbone, and iii) the steric and electronic factors of the substituent at the H-donor of the aminopyridine. Structures of type **30** were confirmed by X-ray analysis of Pt complexes showing the expected hydrogen bonding mode and *cis*-coordination pattern. Furthermore, ^{31}P and ^{1}H NMR data were in agreement with these findings.

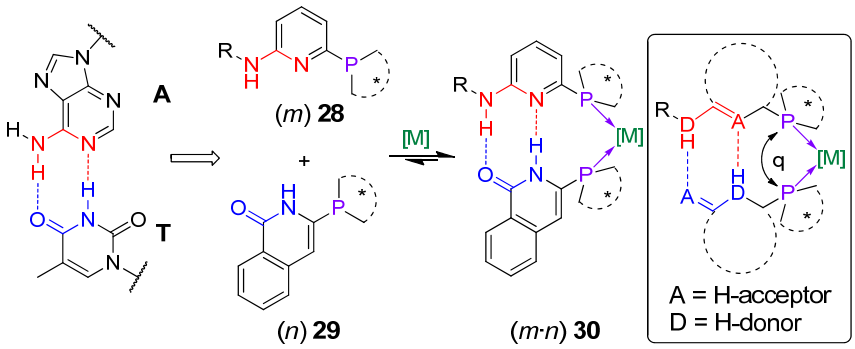

Scheme I-14. A platform inspired by the A–T base pair for the self-assembly of monodentate to hetero-bidentate ligands for combinatorial homogeneous catalysis.[51,56-62]

A library composed of adenine analogues **31** and **32** and thymine analogues **33** was prepared and screened in the regioselective hydroformylation of terminal alkenes (Scheme I-15). Excellent activities (TOF up to 8643 h^{-1}) and regioselectivities (*l*/*b* up to 96:4) were found for Rh-catalysts assembled from **31** and **33** in toluene.[56] The ligands **32** demonstrated their tolerance for protic solvents such as MeOH in a subsequent study against 1-octene (*l*/*b* = 97:3).[60]

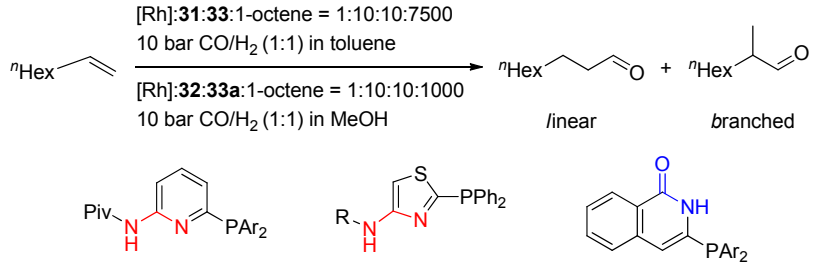

31a: Ar = Ph
b: Ar = 4-MeO-C_6H_4
c: Ar = 3-Me-C_6H_4
d: Ar = 3,5-$(CF_3)_2$-C_6H_3

32a: R = Piv
b: R = CF_3CO

33a: Ar = Ph
b: Ar = 4-MeO-C_6H_4
c: Ar = 3,5-$(CF_3)_2$-C_6H_3
d: Ar = 4-F-C_6H_4

Best result in toluene: **31d**/**33d**, *l*/*b* = 96:4, TOF = 8643 h^{-1}
Best result in MeOH: **32a**/**33a**, *l*/*b* = 97:3

Scheme I-15. Library members and ligand performance in the Rh-mediated hydroformylation of 1-octene in toluene and MeOH.[57,60]

Heterocombinations of ligands derived from the aminopyridine/isoquinolone complementary binding motif were also utilised with success in Rh-mediated asymmetric hydrogenations of benchmark alkenes,[57] and have recently demonstrated their compatibility with high throughput screening following a combinatorial iterative deconvolution strategy for the same reaction.[62] Furthermore, regioselective Ru-mediated *anti*-Markovnikov hydrations of terminal alkynes[58] and nitriles,[59] and the Ni-mediated hydrocyanation of alkenes[61] have also been efficiently mediated by this new ligand family.

The Breit group also reported the generation of new libraries of supramolecular bidentate ligands relying on peptide-functionalised phosphorous moieties. Two strategies were pursued: i) the development of PhanePhos[63,64] analogues **34** by means of an inter-ligand helical hydrogen bond network between identical building blocks (Scheme I-16),[65] and ii) the formation of heterodimeric β-sheet-like strands **35** by combining C-linked peptides with N-linked ones (Scheme I-16).[66]

The helical arrangement including the π–stacking of the two *meta*-substituted aryl-rings (which is similar to the stereogenic plane found in PhanePhos) and the intermolecular hydrogen bonding could be demonstrated by X-ray and NMR analysis of Pt- and Rh-complexes. The latter were used in the enantioselective hydrogenation of methyl *N*-acetyl dehydro-amino acids and dimethyl itaconate. The best enantioselectivities for the dehydro-amino acid derivatives (up to 99% ee) matched those of the PhanePhos derivatives and were obtained with complexes **34b** constituted from peptidyl BINOL-based phosphite ligands. An analogue but non self-assembling phosphite ligand (without peptidyl side chain) resulted in lower ee (82%). In contrast, in the case of dimethyl itaconate, this same ligand yielded the highest ee, thus once more proving that there is no ideal catalyst that is apt for all substrates.

Combination of C-linked phosphane-functionalised peptidyl moieties with their N-linked phosphane-functionalised complements in the presence of suitable Pt(II) or Rh(II) sources resulted in the selective formation of mixed-ligand complexes **35**. Their two-stranded antiparallel β-sheet-like structure was confirmed by in-depth NMR studies, computational methods, and X-ray analysis of a reduced *cis*-Pt(II) model complex. The heterobidentate ligand library generated by this approach was screened against styrene in the Rh-mediated asymmetric hydroformylation reaction. Although only moderate stereoselectivities were obtained (up to 38% ee (*S*)-enantiomer) it could be shown that the remote stereocentres of the peptide side chain can induce enantioselectivity. These results were still significantly better than the ones obtained from homo-combined ligands (5-8% ee), thus demonstrating the superiority of the heterobidentate ligand design.

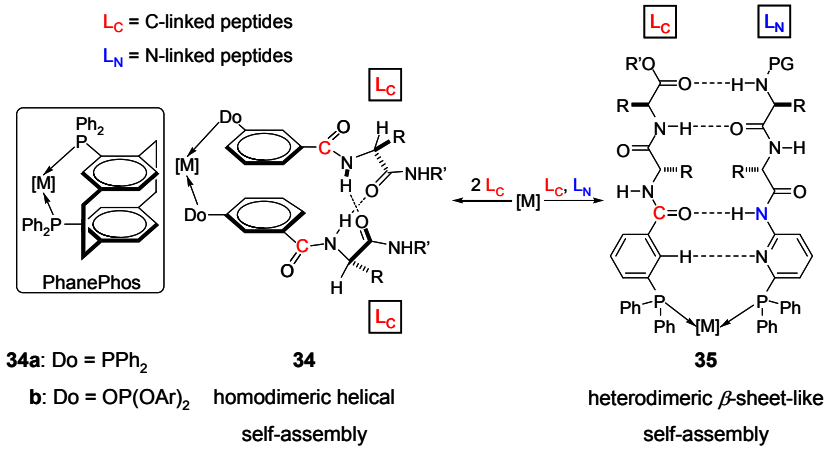

Scheme I-16. Two new concepts of self-assembly of pseudo-bidentate ligands: supramolecular PhanePhos analogue "SupraPhanePhos" (left)[65] and metal-directed antiparallel β-sheet formation of peptide-based phosphane ligands (right).[66]

Further contributions to supramolecular catalysis were made by Breit *et al*. through supramolecularly guided substrate binding and activation (acid-base interaction, hydrogen bonding) in the decarboxylative hydroformylation of α,β-unsaturated carboxylic acids,[67] the regioselective hydroformylation of β,γ-unsaturated carboxylic acids,[68] the hydrogenation of aldehydes and tandem hydroformylation-hydrogenation of terminal alkenes.[69]

Highly noteworthy contributions in the development of catalysts capable of molecular recognition have also been made by Crabtree and co-workers, who have prepared a dimanganese catalyst capable of selectively oxygenating sp^3 C-H bonds.[70] Key to this catalyst are the $Mn(\mu\text{-}O)_2Mn$ reactive centre and the ligands based on Kemp's triacid. This ligand provides a good binding motif for carboxylic acid groups in the substrate *via* its own carboxylic acid function (Scheme I-17). In the hydrogen bonded catalyst-substrate complex with ibuprofen (2-(4-isobutylphenyl)propanoic acid) **36**, the remote methylene group is oriented in proximity to the active manganese centre, thus allowing its preferential oxidation with >98% regioselectivity. With an analogous catalyst not displaying the COOH binding motif, the selectivity dropped to 76%. More recently, the same supramolecular catalyst was applied to the activation of C-H bonds in an alkyl derivative.[71]

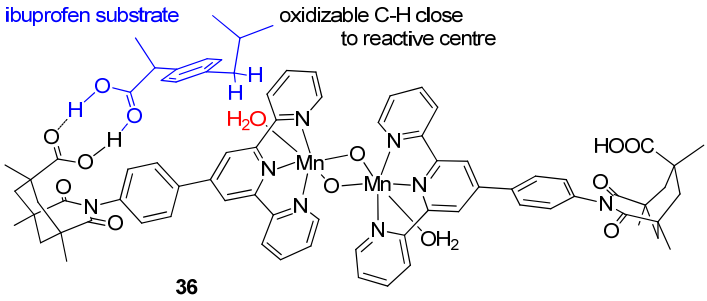

36

Scheme I-17. Selective oxidation of ibuprofen with Crabtree's dimanganese catalyst.[70]

In 2005 Love and co-workers reported the formation of Pd and Rh complexes of type **37** (Scheme I-18) comprised of urea-derived phosphines.[72] However, with $PdCl_2(PhCN)_2$ as Pd source, the complex formation was accompanied by product precipitation in a 1:3 *cis*/*trans* ratio with respect to the coordination mode. It was assumed that this was due to polymerisation caused by intermolecular hydrogen bonding in common organic solvents. It was shown independently by Reek, van Leeuwen, and co-workers that the pure trans-complex **37** could be obtained by using PdCl(COD)(Me) instead.[73] Urea moieties are known to serve as anion receptors[74-76] and indeed both groups have observed an anion templating effect in the presence of *n*-Bu_4NCl. A chloride is bound to the pocket created by the urea units and the interaction with the four urea-NH groups is substituting the former hydrogen bonds (**38**, Scheme I-18). The association constant of chloride in the pocket was determined from NMR titrations to be $K = (10 \pm 2) \cdot 10^2\ M^{-1}$.

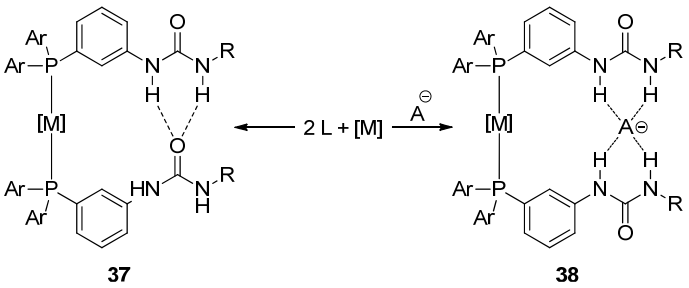

37 **38**

Scheme I-18. Formation of *trans*-coordinating bidentate phosphanes *via* hydrogen bonding (left) or anion templated (right) self-assembly.[72,73]

Based on this interesting way to realise bidentate ligands Reek *et al*. developed new families of modular urea-functionalised phosphane, phosphite, and phosphoramidite ligands named UREAPhos (Scheme I-19). They successfully applied these supramolecular ligands in the asymmetric hydrogenation of structurally diverse and industrially relevant substrates.[77,78]

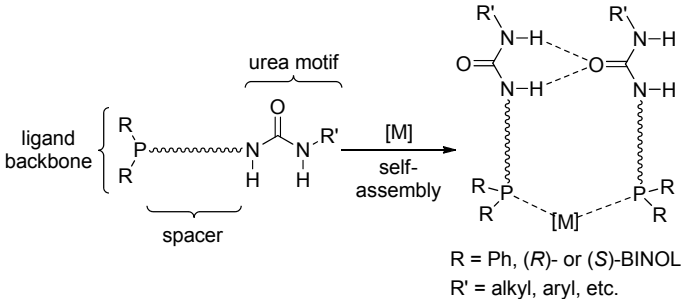

Scheme I-19. Self-assembly of a supramolecular catalyst from an ample library of highly tunable phosphorous ligands *via* hydrogen bonding.[77,78]

Recently Reek and co-workers have shown that the urea-motif of the ureaphosphane moieties bearing flexible spacers (ethyl, chiral 1,2-diphenylethyl) may also coordinate as single bidentate *P*,*O*-ligand to rhodium (using $[Rh(nbd)_2]BF_4$ as the metal source) if the metal/ligand ratio is adjusted properly. Such complexes in which the O-atom of the urea motif forms a chelate together with the phosphane by coordination to Rh(I) were used in the asymmetric hydrogenation of benchmark enamides with high enantioselectivities (up to 88% ee).[79]

The very diverse ligating behaviour of ureaphosphanes in Rh(I) complexes was further investigated with regard to the dependency on the nature of the anion of the Rh-source and the ligand/metal ratio. Controlling these parameters allows the ureaphosphane to preferentially form hybrid *P*,*O*-coordinated bidentate ligands, anionic *P*,*N*-coordinated chelates, or the supramolecular hydrogen bonded bidentate ligands. Furthermore, the influence of the binding mode on the results in the Rh(I)-mediated asymmetric hydrogenation of three benchmark substrates (including a challenging acetamide) was also investigated.[80] Both the activity and enantioselectivity for a given substrate were found to be strongly dependent on the present complex. In conclusion this strategy allowed the optimisation of the catalyst not only based on ligand design but also on the binding mode of the ligand.

Supramolecular ligands are dynamic entities due to the reversibility of their non-covalent interactions. In 2008 an interesting example of such ligands was reported by Reek *et al*. and with regard to its mutability they called it "METAMORPhos".[81] This ligand is capable of adopting various tautomeric forms even when bound to a metal (Scheme I-20). During the complexation of **39** with [Rh(acac)$(CO)_2$], the liberation of acetylacetonate was detected by NMR, suggesting the proton transfer from tautomer **39b** to the acetylacetonate anion under formation of **39c**. The existence of two different *trans*-coordinated ligands in [Rh(**39a**···**39c**)(CO)] was confirmed by ^{31}P NMR whilst IR in solution indicated intermolecular NH···O–S hydrogen bonding. Mixing two slightly different METAMORPhos-type ligands, **39** and **41** which exists as one dominant tautomer, led to the formation of true hetero-bisligated Rh(I)-complexes. In contrast, no hetero-combinations were observed between **39** and **42** as these ligands formed the two possible homo-complexes with Rh(I), most likely due to the lack of pK_a matching with the amino group. However, both neutral Rh(I) complexes, homo and hetero alike, were inactive in the enantioselective hydrogenation of methyl 2-acetamidoacrylate. The active cationic form could be either achieved through activation with HBF_4·OMe_2 or, more elegantly, by direct formation using [Rh$(nbd)_2$]BF_4 as metal source. The obtained active catalysts in this way (homo- and hetero-combinations) were applied to the Rh-mediated asymmetric hydrogenation of methyl 2-acetamidoacrylate with very good enantioselectivities (99% ee (*S*) and 92% ee (*S*), respectively).

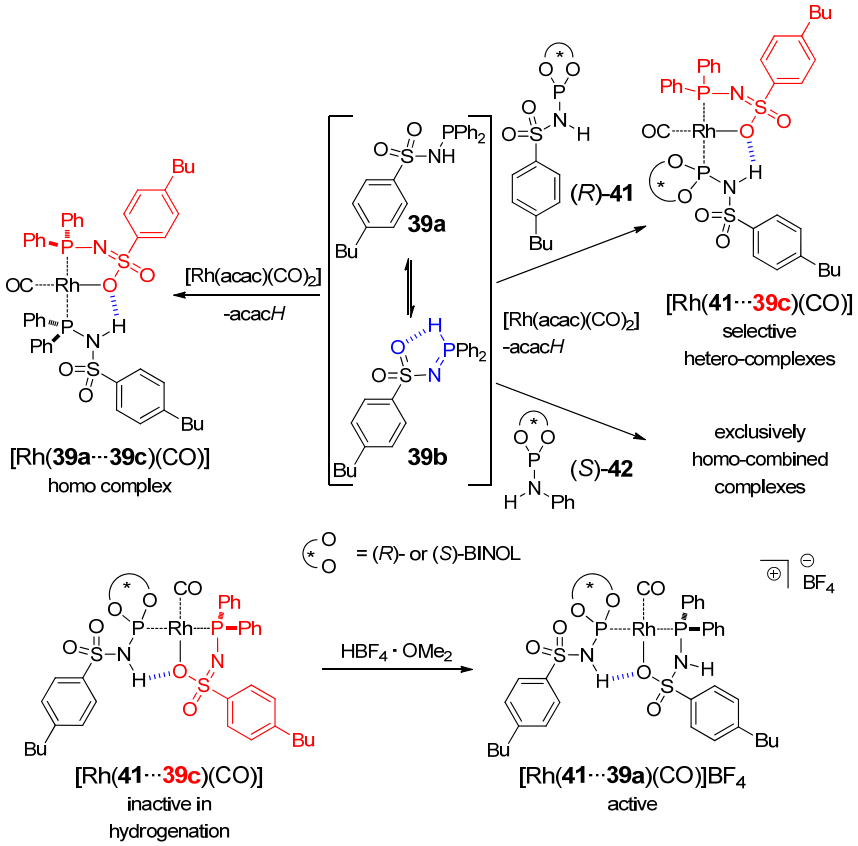

Scheme I-20. Tautomeric equilibrium of METAMORPhos ligand **39** and its coordination behaviour with [Rh(acac)(CO)$_2$]. Formation of quasi-homo complexes from two **39** moieties (top left) and hetero-complexes [Rh(**41**···**39c**)(CO)] with **41** (top right) and activation of the latter complex by protonation with $HBF_4 \cdot OMe_2$ (bottom). Ligand **42** served in a control experiment.[81]

In 2009 Reek's group reported a unique dinuclear Rh-catalyst bridged by two anionic sulfonamido-phosphoramidite ligands. It turned out to be highly selective in the hydrogenation of hindered tri- and tetrasubstituted alkenes (up to 81 and 99% ee, respectively).[82,83] Excellent enantioselectivity (>99% ee) was achieved in the Rh-mediated hydrogenation of *t*-butyl 2-hydroxymethylacrylate with new singly hydrogen bonded supramolecular ligands (LEUPhos).[83]

2 Preliminary Considerations

As shown in the introductory literature section, hydrogen bonding has long been used as a driving force for chiral recognition and binding. Indeed it is one of the most important reversible interactions used in both, supramolecular complexes found in nature or those assembled synthetically. Large numbers of supramolecular complexes are nowadays present in textbooks[43,84] and many of them have been synthesised by making use of hydrogen bonding motifs. In addition, rapidly growing numbers of (asymmetric) catalytic transformations in which the physical and stereochemical properties of the catalyst are dominated by hydrogen bonding have also been reported in recent years.[43] This reflects the attractiveness of the supramolecular approach which provides several interesting virtues. One of the main advantages is the fact that (natural) optically pure molecules are broadly available whereas (artificial) chiral and catalytically active ligands usually have to be prepared. Compounds of the chiral pool already carry stereogenic units but in most cases lack suitable catalytic groups which traditionally have to be introduced by means of covalent chemistry. Thus, catalysis research could benefit even more from these chiral compounds if their chiral information could be transferred into catalytically active ligands by making use of supramolecular chemistry in a (final) self-assembly step of the catalyst.

Below we discuss our approach to form new chiral supramolecular ligands based on the use of reversible hydrogen bonding. The key feature of these compounds was that chirality is induced from a chiral building block into a dynamically racemic building block suitable for the subsequent transformation into a catalytic ligand. Consequently, the aim of this work was to identify and prepare suitable building blocks and study their complexation behaviour. The incorporation of catalytically active groups into the new building blocks was foreseen for a later stage of the project. In this vein, we hoped to avoid the preparation of enantiopure ligands, which rely on covalent chemistry only, and instead control the stereochemical properties through hydrogen bonding in a final complexation step.

Figure I-1 schematically depicts the concept underlying this idea. The chiral unit is combined with a prochiral unit in solvents suitable for the formation of hydrogen bonds of sufficient strength. Through this interaction the chiral inducer is believed to disturb the fast interchanging enantiomers of the dynamically racemic unit from its equilibrium in order to form diastereomerically enriched supramolecular complexes.

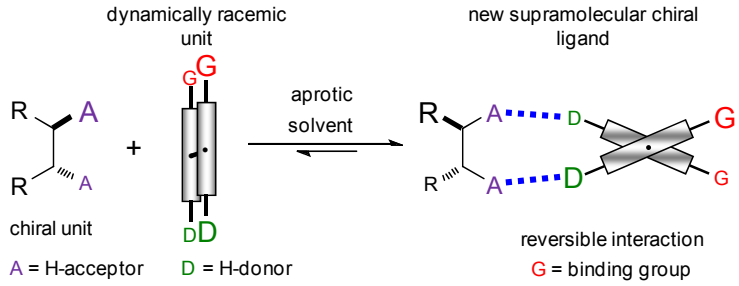

Figure I-1. Schematic concept for the transfer of chirality using hydrogen bonding.

Some considerations had to be made before choosing the building blocks. For both, chiral and dynamically racemic units, precursors close to the required structures should ideally be commercially available at reasonable cost in order to minimise the synthetic effort involved. Furthermore, key for the induction of chirality would be the steric interaction between the two building blocks. Accordingly, the ideal precursors should be easy to derivatise in order to obtain compounds of controllable steric demand. Last but not least, the molecules had to bear complementary binding motifs in order to establish the desired hydrogen bond. We reasoned that freely rotatable (*tropos*) BIPOL- and enantiopure (1,2)-diamine derivatives could fulfil all of the necessary criteria. Receptors based on phenolic groups are known to readily form supramolecular complexes with aliphatic amines. Hydrogen bonding between them has been studied both experimentally[85-91] and using theoretical approaches.[92-95] Furthermore, several examples of induction of axial chirality mediated by hydrogen bonding between BIPOL-derivatives and enantiopure amines or amino alcohols can be found in the literature.[1,2,9,24] Regarding the solvent, we followed the guidelines given by Hunter.[96] Since it was the aim to maximise the strength of the hydrogen bonds, the solvent had to be anhydrous and non-polar in order to minimise solute-solvent interactions. Eventually, we reasoned that toluene would be best suited to combine solvency and the above mentioned requirements. Furthermore, toluene had already proven its suitability as solvent in similar studies.[2] THF was also used in some cases for comparison reasons or when demanded by solubility.

Keeping these considerations in mind, we anticipated that chiral supramolecular complexes of type **43** (Scheme I-21) could be realised from *tropos* 2,2'-biphenols **44a**-**c** and optically active (1,2)-DACH derivatives **45a**-**g** and the N,N-substituted (1,2)-DPEN **45h**, respectively. Ideally, simultaneous formation of two hydrogen bonds between the

hydroxyl and amino groups should result in cyclic structures, benefiting from the chelate effect in solution and thus increasing the strength of the interaction.[97,98] The biphenol's *ortho*-substituents R^1 were crucial to our concept. Due to their electron density-accepting or donating character they should either increase (R^1 = NO_2, **44a**) or decrease (R^1 = Me, **44b**; R^1 = OMe, **44c**) the acidity of the phenol group. This should be reflected in the strength of the resulting hydrogen bonds.[92-95,99-101] Additionally, the biphenol bore an ester group in the *para*-position relative to the hydroxyl function. The purpose of this ester was to allow for the simple transformation into a wide variety of binding groups for future catalytic applications at a later stage of the project.

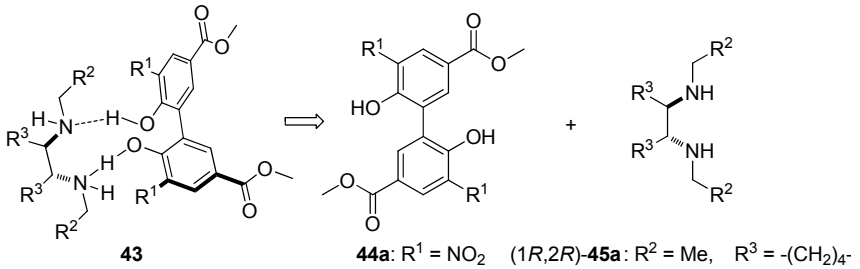

43

44a: R^1 = NO_2
44b: R^1 = Me
44c: R^1 = MeO

(1*R*,2*R*)-**45a**: R^2 = Me, R^3 = -$(CH_2)_4$-
45b: R^2 = Et, R^3 = -$(CH_2)_4$-
45c: R^2 = ^{i}Pr, R^3 = -$(CH_2)_4$-
45d: R^2 = ^{t}Bu, R^3 = -$(CH_2)_4$-
45e: R^2 = ^{c}Hex, R^3 = -$(CH_2)_4$-
45f : R^2 = Np, R^3 = -$(CH_2)_4$-
45g: R^2 = Mes, R^3 = -$(CH_2)_4$-
45h: R^2 = Et, R^3 = Ph

Scheme I-21. Design of chiral complexes **43** by hydrogen bonding-mediated chirality transfer from optically active (1,2)-DACH to prochiral 2,2'-BIPOL derivatives.

In order to analyse the dependence of the chiral induction process on steric interactions between the two building blocks, a wide range of enantiomerically pure diamines **45a**-**f** bearing sterically diverse N-substituents were prepared. Steric interactions between R^1 and R^2 were expected to disfavour the formation of one of the two possible diastereomeric supramolecular complexes and, ideally, the dihedral

angle ϕ of the biphenol could be modified depending on the steric demand of the N-substituent. Diamine **45g** was prepared to study the influence that a π–electron rich substituent might have on the outcome of the hydrogen bonding process. The diamine backbone was also considered to be of great importance to the complexation. A rather rigid backbone such as that provided by the cyclohexane fragment should lower the motion within the chiral unit, thus allowing stronger hydrogen bonds. In order to verify this assumption the more flexible diamine **45h** was synthesised and also applied in the following study.

The strength of hydrogen bonds covers a broad range going from very weak (4-5 kcal mol^{-1}, *e.g.* the $H_2O\cdots H\text{-}OH$ bond in water) to reasonably strong (25-31 kcal mol^{-1}, *e.g.* the very strong $[H_2O\cdots H\cdots OH_2]^+$ and $[HO\cdots H\cdots OH]^-$ bonds).[99] Consequently, getting an idea of the stability of our complexes was of great importance in order to estimate their ability to act as ligands in potential catalysts. Therefore, binding constants *K* had to be determined. We did so by means of UV-vis and isothermal calorimetry (ITC) titrations which are both frequently used for this purpose in supramolecular chemistry.[102-104] Furthermore, together with NMR data, ITC allowed us to draw conclusions about the stoichiometry of the new complexes and provided us with thermodynamic parameters.

Naturally, proof of the successful induction of chirality had to be provided. One of the best tools for doing so is of course the measurement of electronic circular dichroism (ECD). Provided that a chromophore is present, ECD is sensitive to both, stereogenic centres and axes, the latter being of prime importance for us. Indeed the literature tackling the conformational and configurational analysis of organic compounds is so vast that only a small selection of review and textbook references can be given here.[30,105-109]

3 Results and Discussion

3.1 Synthesis of building blocks

3.1.1 Synthesis of 2,2'-biphenol (BIPOL) building blocks

Of the various biaryl homocoupling reaction conditions available in the literature, a modification of a protocol reported by Lemaire *et. al.* turned out to best fit our requirements.[110,111] Aryl halides **46** and **49**, which were required for the synthesis of target biphenols **44b** and **44d** (Scheme I-22), were either commercially available or easily accessible by high yielding synthetic methods.[112] The homocoupling reaction itself was carried out using hexakis(aceto)tripalladium(II) [$(Pd(OAc)_2)_3$] as a catalyst. However, it appeared that yields, although usually moderate, strongly depended on the temperature and especially the work-up conditions. Dehalogenation of the aryl iodides was generally observed and the extent of this side-reaction increased with temperature. Furthermore, separating the reaction product from the slurry of catalyst residues, DMF, DIPEA and TBAB was crucial for controlling the yield. In any case, the major part of DMF and DIPEA should be removed under high vacuum from the extract of the crude product before it could be efficiently purified by either column chromatography on silica gel, or washing with portions of cold CH_2Cl_2. In most cases this simple procedure was superior to column chromatography which often resulted in a significant decrease in yield, especially when DMF and DIPEA were not removed thoroughly prior to chromatography. The preparation of **44a** from its precursor **44d** was achieved following an efficient and straightforward nitration method using $Bi(NO_3)_3$ pentahydrate as nitrating agent.[113]

Unlike **44a** and **44b,** the synthesis of **44c** did not depend on a biaryl coupling reaction since a suitable biaryl precursor was available with 5,5'-bivanillin **50**. The required reaction sequence consisted of an acylation of the hydroxyl group, subsequent oxidation of the aldehyde to give the carboxylic acid, saponification of the acyl ester, and, finally, esterification of the carboxylic acid. All transformations were carried out under standard conditions as found in the literature.

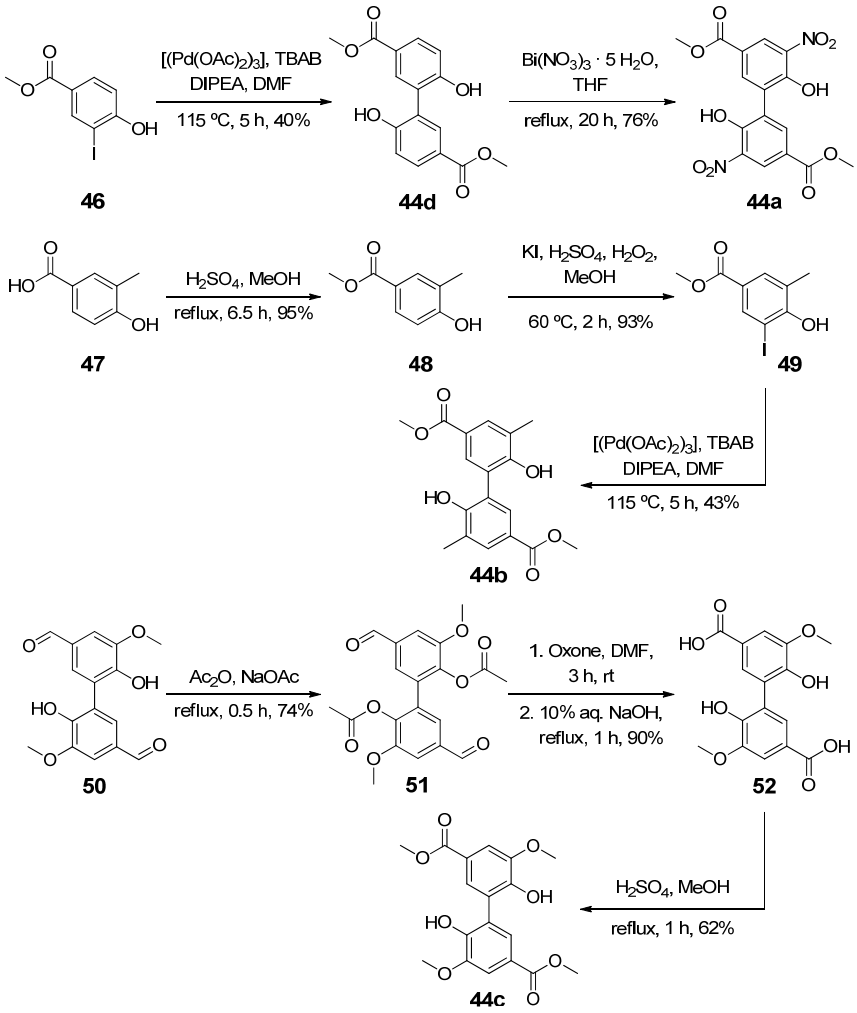

Scheme I-22. Preparation of 2,2'-biphenol derivatives **44a**-**d**.

3.1.2 Synthesis of (1,2)-diamine building blocks

The preparation of the second building block, the chiral (1,2)-DACH and (1,2)-DPEN derivatives was also straightforward using already established synthetic routes.[114-116] An overview of the different methods is given in Scheme I-23. All started either from (1*R*,2*R*)-diaminocyclohexane (1*R*,2*R*)-**53a** (**45a**-**g**) or (1*R*,2*R*)-diphenyl-ethyl-1,2-diamine (1*R*,2*R*)-**53b** (**45h**). In principle any of these synthetic routes is suitable to prepare the diamines **45a**-**h**. Our preference of one particular procedure over the other for a given diamine was mostly based on reagent availability. Nevertheless, each method has certain strengths and weaknesses. Whenever the required carboxylic acid anhydrides and chlorides were available, the route *via* the corresponding diamides was preferred since these intermediate products were easily obtained by precipitation as crystalline solids. In these cases, no further purification was required prior to their reduction. However, it was observed that amides bearing larger aliphatic substituents like **55d**, or longer alkyl chains like $R^2 = {}^n$Pr (a diamine that was synthesised but not used in this study), were not quantitatively reduced with $LiAlH_4$. The use of the borane complex $BH_3 \cdot THF$ as reducing agent solved this problem in most cases.

Since imines are generally easier to reduce than amides, the preparation method involving condensation of amine **53a** with the corresponding aldehyde followed by reduction was also considered for large N-substituents. The condensation reaction between an amine and an aldehyde is reversible and the water formed must be removed in order to shift the equilibrium fully to the product side. Anhydrous $MgSO_4$ or Na_2SO_4 were used in this case to bind water. Still in some cases monoimines were observed but were usually not removed at this point. Instead the crude imines were straightforwardly reduced with $NaBH_4$ and monoamines, if present, were removed by column chromatography.

Subsequently, all diamines were dried by vacuum distillation except for **45g**, which was obtained as a solid and dried under high vacuum. Distillations had to be carried out carefully in order to not suffer from significant yield decreases, especially for diamines bearing larger substituents with high boiling points. The high boiling diamine **45h** could be distilled in a bulb to bulb apparatus only.

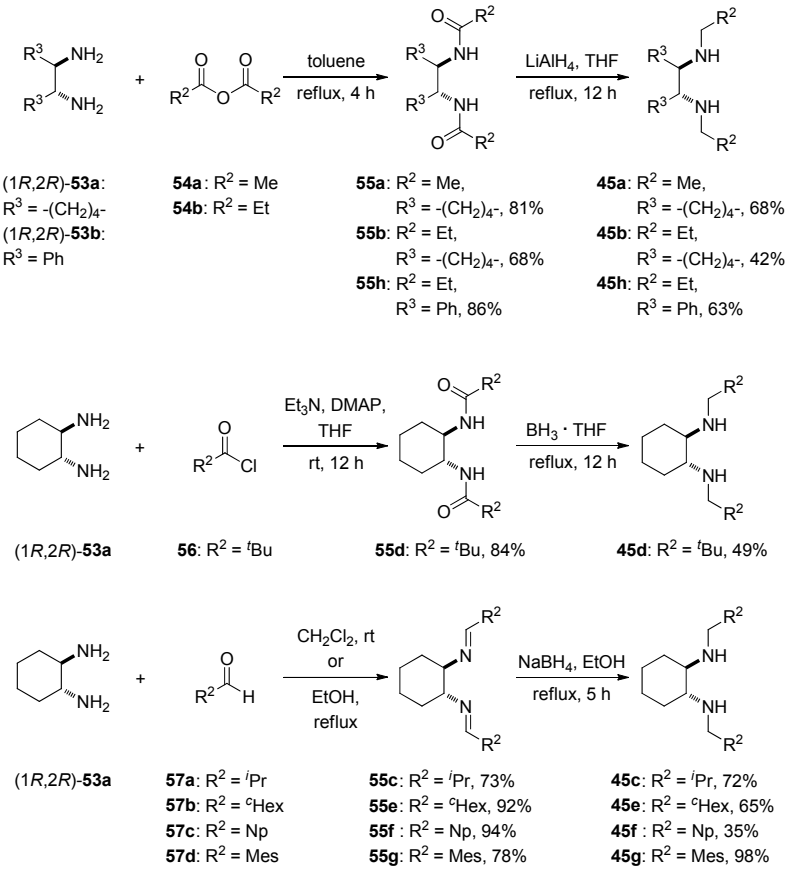

(1*R*,2*R*)-**53a**: R^3 = -$(CH_2)_4$-
(1*R*,2*R*)-**53b**: R^3 = Ph

54a: R^2 = Me
54b: R^2 = Et

55a: R^2 = Me, R^3 = -$(CH_2)_4$-, 81%
55b: R^2 = Et, R^3 = -$(CH_2)_4$-, 68%
55h: R^2 = Et, R^3 = Ph, 86%

45a: R^2 = Me, R^3 = -$(CH_2)_4$-, 68%
45b: R^2 = Et, R^3 = -$(CH_2)_4$-, 42%
45h: R^2 = Et, R^3 = Ph, 63%

(1*R*,2*R*)-**53a**

56: R^2 = ^{t}Bu

55d: R^2 = ^{t}Bu, 84%

45d: R^2 = ^{t}Bu, 49%

(1*R*,2*R*)-**53a**

57a: R^2 = ^{i}Pr
57b: R^2 = ^{c}Hex
57c: R^2 = Np
57d: R^2 = Mes

55c: R^2 = ^{i}Pr, 73%
55e: R^2 = ^{c}Hex, 92%
55f : R^2 = Np, 94%
55g: R^2 = Mes, 78%

45c: R^2 = ^{i}Pr, 72%
45e: R^2 = ^{c}Hex, 65%
45f : R^2 = Np, 35%
45g: R^2 = Mes, 98%

Scheme I-23. Preparation of optically pure diamines **45a**-**h** from (1*R*,2*R*)-diamino-cyclohexane (1*R*,2*R*)-**53a** and (1*R*,2*R*)-diphenylethane-1,2-diamine (1*R*,2*R*)-**53b**.

3.2 Complexation behaviour

3.2.1 NMR studies

The formation of complexes **43** could be confirmed by NMR studies. In all cases 1:1 complexes were observed in samples obtained by mixing equimolar amounts of biphenol **44a** with diamines **45** in dry CD_2Cl_2 and recording ^1H and ^{13}C NMR spectra. In the following, complexes **43** will be named as combinations of their building blocks **44**+**45**. Figure I-2 shows the proton NMR spectrum of the representative hydrogen bonded complex **44a+45d**. The spectrum is in agreement with a C_2-symmetric averaged structure.

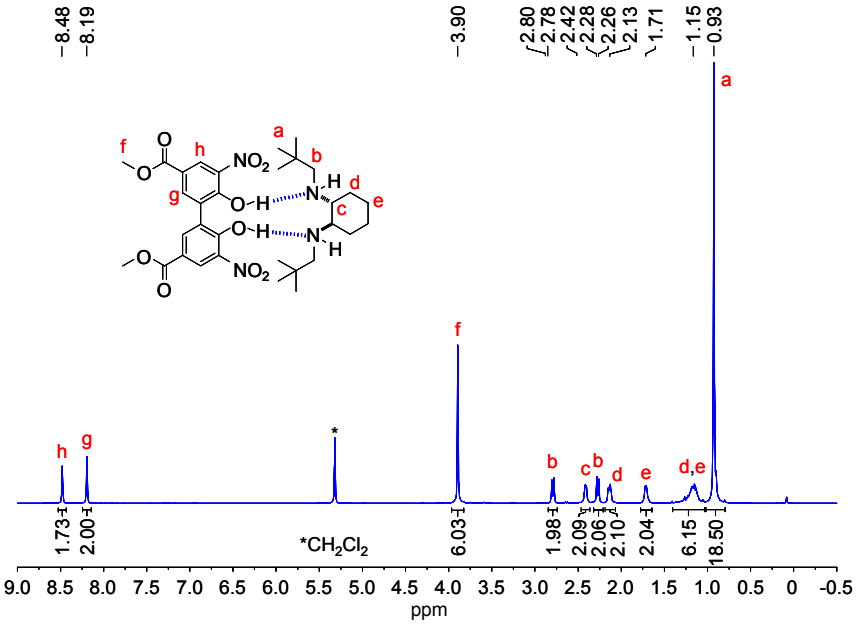

Figure I-2. 1H NMR spectrum of complex **44a**+**45d** (CD_2Cl_2, 500 MHz, 298 K).

Variable temperature ^{1}H NMR analysis of the complex in 1:1 ratio showed only one set of signals across the whole range of studied temperatures (308-193 K). This indicates either the presence of one predominant diastereomer or that possible exchange processes are very fast on the NMR timescale. However, in mixtures of **44a** and **45d** in 1:2 ratios one of the two aromatic signals undergoes clearly visible broadening accompanied by a highfield shift of 0.29 ppm upon cooling from 35 to -80 ºC. Furthermore, at -80 ºC two more signals evolve. One at 7.82 ppm is relatively sharp whereas the other at 7.03 ppm is very broad (Figure I-3).

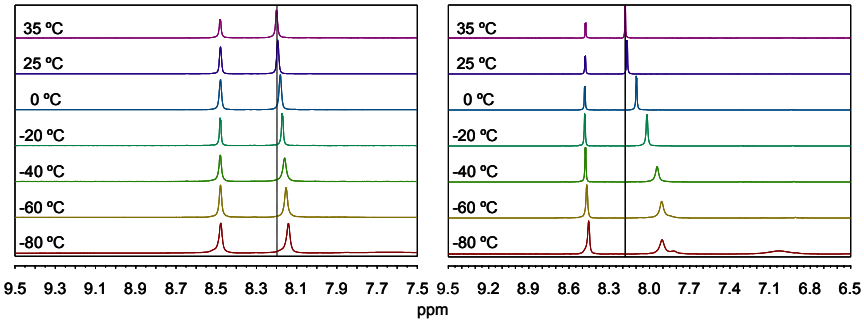

Figure I-3. Variable-temperature ^{1}H NMR (CD_2Cl_2, 500 MHz) of the aromatic region of a mixture of **44a** and **45d** in 1:1 (left panel) and 1:2 ratio (right panel) ([44a ≈ 19 mM]).

Mizutani *et al*. reported that a solution of a *para*-nitrophenol–diisopropylamine hydrogen bonded complex in toluene became yellow at -80 ºC due to proton transfer from the phenol to the amine.[91] Furthermore, an equimolar mixture of diisopropylamine and 3,3'-dibromo-5,5'-dinitro-2,2'-biphenol **1a** (see literature section Scheme I-2) did not show proton transfer at low temperature but turned yellow in the presence of 2 or 10 equivalents of the amine. This so-called thermochromism was also observed in a 1:2 mixture of **1a** with diamine **2a**. Mizutani *et al*. stated that the diamine excess was required to obtain the proton-transferred complex by hydrogen-bonding network formation.

The association constant K_1 for the 1:1 complex of **1a** with **2a** was estimated to $>10^6$ M^{-1} by the authors. Variable-temperature analysis suggested the complete formation of a 1:2 complex at high concentration ([**1a**] ≈ 10 mM) and the presence of both 1:1 and 1:2 complexes at low concentration ([**1a**] ≈ 0.9 mM), both with excess of diamine **2a**. At high concentration the aromatic signals got shifted downfield in toluene-d_8 upon lowering the temperature whereas at low concentration two sets of signals appeared. Therefore the binding of the diamine occurred stepwise and the authors estimated the second association constant K_2 to be roughly 10^3-10^4 M^{-1}.[2]

We presume similar behaviour for our complexes **44a**+**45** based on the 1H NMR data shown in Figure I-3. The binding is strong enough to predominantly form complexes of 1:1 (biphenol/diamine) ratio at room temperature ([**44a**] ≈ 10 mM). However, we estimate the tendency of biphenol **44a** to undergo proton transfer with diamines **45** to be significantly smaller than that of biphenol **1a**, which was used by Mizutani. This is mainly due to the fact that the low temperature ^{1}H NMR spectrum depicted in the right panel of Figure I-3 shows two sets of signals in spite of the high concentration of the sample ([**44a**] ≈ 20 mM). Consequently, a structure as shown in Scheme I-24 is proposed. Intramolecular hydrogen bonding between the two phenolic hydroxyl groups may be facilitated by the electronic influence of the nitro groups but if it occurs it is very fast on the NMR timescale.

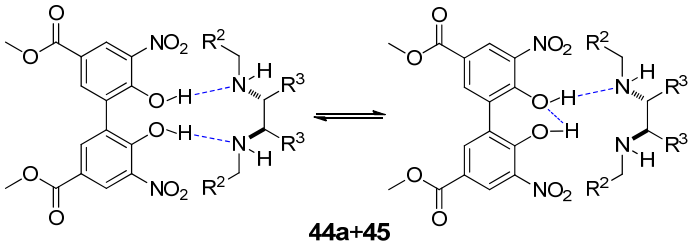

44a+45

Scheme I-24. Proposed structure of complexes **44a**+**45** in a 1:1 mixture in solution.

3.2.2 Binding constant determination*

The determination of binding constants *K* for a given equilibrium between bound and unbound species is the best way to estimate the strength of the interactions (Scheme I-25). For the application of any supramolecular ligand in homogeneous catalysis a large binding constant is required, since the supramolecular complexes should be stable at low concentrations.

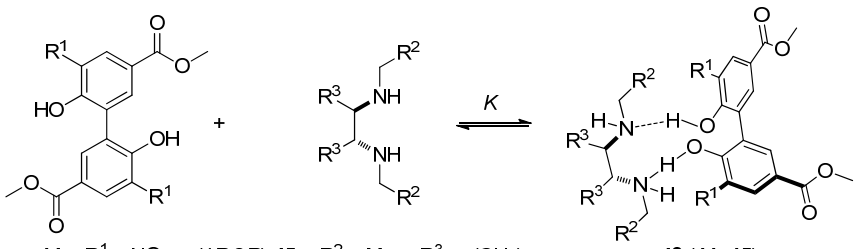

44a: $R^1 = NO_2$
44b: $R^1 = Me$
44c: $R^1 = MeO$

(1*R*,2*R*)-**45a**: $R^2 = Me$, $R^3 = -(CH_2)_4-$
45b: $R^2 = Et$, $R^3 = -(CH_2)_4-$
45c: $R^2 = {}^{i}Pr$, $R^3 = -(CH_2)_4-$
45d: $R^2 = {}^{t}Bu$, $R^3 = -(CH_2)_4-$
45e: $R^2 = {}^{c}Hex$, $R^3 = -(CH_2)_4-$
45f : $R^2 = Np$, $R^3 = -(CH_2)_4-$
45g: $R^2 = Mes$, $R^3 = -(CH_2)_4-$
45h: $R^2 = Et$, $R^3 = Ph$

43 (**44**+**45**)

Scheme I-25. Equilibrium for the formation of complexes **43** (**44**+**45**) from biphenols **44a**-**c** and diamines (1*R*,2*R*)-**45a**-**h**.

*These studies were carried out in collaboration with Dr. Anne-Sophie Felten and Dr. Juan Etxebarria.

Generally, such determinations of *K* are carried out by titration of a host with a guest under observation of a physical variable like UV-vis absorbance-, IR transmission-, chemical shift-, or enthalpy changes. The methods are complementary and the preference for one over another depends primarily on the magnitude of the binding constant *K*. For the systems discussed here, we decided to use UV-vis and ITC titrations since these two techniques are fast and applicable under the required conditions. For UV-vis the ideal working concentration depends on the magnitude of *K* (usually the following approximation holds: $^{1}/_{K} \ll [\text{conc.}] < {}^{10}/_{K}\,M^{-1}$) but in praxis the concentration range may be limited by the magnitude of the extinction coefficients ε. Naturally, the measure of *K* is also decisive in ITC titrations but the practical concentration range also depends on the enthalpy ΔH.

Figure I-4 shows the UV-vis titrations of a solution of **44a** with increasing amounts of **45c** in the aprotic solvents toluene and THF at 298 K. Generally, the addition of diamines **45** led to a decrease of the initial biaryl band around 365 nm and the appearance of a new bathochromically shifted band around 385 nm, a behaviour that was noticeable as colour change from light to strong yellow. Furthermore, in all cases the existence of an isosbestic point was observed, suggesting the presence of only two coloured species (free and hydrogen bonded biphenol **44a**) during the course of the titration. This was also in agreement with the results from the NMR analysis.

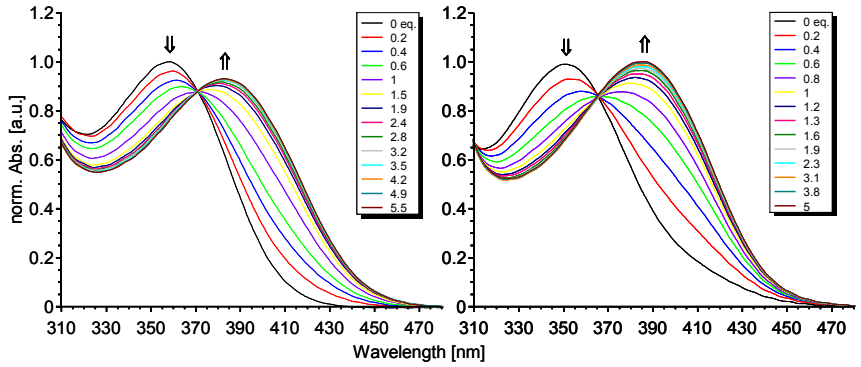

Figure I-4. UV-vis titration of **44a** with **45c** in toluene (left; [**44a**] = $2.6 \cdot 10^{-5}$ M, [**45c**$_{\text{stock solution}}$] = $1.4 \cdot 10^{-4}$ M) and THF (right; [**44a**] = $2.6 \cdot 10^{-5}$ M, [**45c**$_{\text{stock solution}}$] = $1.8 \cdot 10^{-4}$ M) at 298 K, equivalents for each titration point are given in the legends.

UV-vis titration data (310-500 nm) was analysed with *SPECFIT* software[117-119] using multivariate factor analysis and considering a binding model with two absorbing species: unbound biphenol and a 1:1 complex (diamines were found to be UV silent in this wavelength range). In all cases the UV-vis spectra of the free biphenols **44a**-**c** were recorded in the corresponding solvents and used in *SPECFIT* for the fitting algorithm. Generally, very good agreement between the fitted and the experimental curve was observed for the whole wavelength range. The obtained equilibrium constants *K* are summarised together with spectroscopic data in Table I-3. As expected, a correlation between the size of *K* and the identity/acidity of the 3,3'-substituted 2,2'-biphenol was found. Upon changing the nitro group in **44a** for methyl in **44b** the value of *K* decreased by two and finally by three orders of magnitude with the methoxy substituent in **44c** (entries 1-3; THF had to be used due to the low solubility of **44b** and **44c** in toluene). This was in agreement with what we expected on the basis of the biphenol acidity.

It was furthermore observed that the steric hindrance implemented in the complexes by the varying size of the N-substituents of the diamine was only of limited importance for the magnitude of the association constants *K*. For the combination of the nitro-substituted biphenol **44a** with diamines **45a**-**f** (entries 4-9) all values for *K* were within the same range ($6 \cdot 10^4 - 4 \cdot 10^5\ M^{-1}$). However, due to its aromatic N-substituents, the inherently different diamine **45g** (entry 10) showed an association constant with **44a** that was one order of magnitude smaller, presumably due to steric repulsion. Diamine **45g** was also different regarding its chiroptical properties, which will be discussed in the next section. The DPEN derivative **45h** (entry 11) showed a binding constant with **44a** in toluene that was two orders of magnitude smaller compared to that found for the complex **44a**+**45a** (entry 4) and still one order of magnitude smaller than that of **44a**+**45g**. The rigidity of the backbone appears to be decisive for the strength of the rather flexible hydrogen bonds, *i.e.* mobility in this part of the molecule has to be avoided if strong interactions are to be achieved.

Table I-3. Equilibrium constants *K* and UV-vis data of hydrogen bonded complexes **44**+**45**.

entry	complex[a]	solvent	UV data: λ_{max},[b] ε[c]	K[d]
1	**44a**[e]**+45c**	THF	386, 7400	$8.1 \cdot 10^5$
2	**44b**[e]**+45c**	THF	280, 22000	$1.3 \cdot 10^3$
3	**44c**[e]**+45c**	THF	278, 29000	$2.2 \cdot 10^2$
4	**44a+45a**	toluene	385, 6900	$2.0 \cdot 10^5$
5	**44a+45b**	toluene	386, 6700	$2.7 \cdot 10^5$
6	**44a+45c**	toluene	383, 6400	$2.0 \cdot 10^5$
7	**44a+45d**	toluene	382, 6900	$5.6 \cdot 10^4$
8	**44a+45e**	toluene	384, 6600	$2.7 \cdot 10^5$
9	**44a+45f**	toluene	385, 6000	$3.9 \cdot 10^5$
10	**44a+45g**	toluene	379, 8500	$2.5 \cdot 10^4$
11	**44a+45h**	toluene	365, 5600	$2.4 \cdot 10^3$

[a](1*R*,2*R*)-**45** derivatives used in all cases. [b][nm]. [c][M^{-1} cm^{-1}]. [d][M^{-1}], mean value of at least two measurements. [e]UV data for **44**: **44a** (352, $7.3 \cdot 10^3$ in THF; 358, $7.1 \cdot 10^3$ in toluene); **44b** (274, $9.8 \cdot 10^3$ in THF); **44c** (273, $2.1 \cdot 10^4$ in THF).

The formation of hydrogen bonds between phenols and amines is a well studied process.[87-90] It is known that the Brønsted acid/base properties, *i.e.* the pK_a values of the involved proton donor and acceptor groups greatly affect the complexation. The capability to form double charge-assisted hydrogen bonds (±)CAHB, *i.e.* H-bonds resulting from an acid-base equilibrium, is reported to lead to stronger binding than that provided by normal electrostatic hydrogen bonds.[92,93,99,120-122] Ideal (±)CAHB are three-centre-four-electron covalent interactions in which a single bond is split in two half bonds (Scheme I-26).

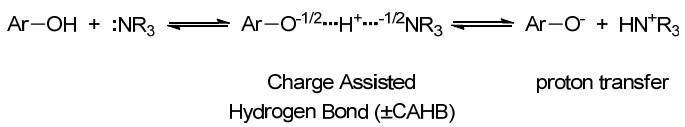

Scheme I-26. Charge Assisted Hydrogen Bond and proton transfer equilibrium.

According to Gilli *et al.* the PA/pK_a equalisation principle can be used to rationalise the strength of H-bonds in terms of matching between the proton affinity (PA) or pK_a acid-base indicators of the proton donor and acceptor partners.[92,93,99,100] In the case of (±)CAHB the proper parameter is given by the pK_a values. The outcome of the above depicted equilibrium then depends on whether the pK_a value of the Ar–OH (or generalised D–H) donor is larger or smaller than the pK_a value of the conjugated acid HN^+R_3 ($H–A^+$) of the acceptor (*i.e.* the question is, if Ar–OH is a weaker or stronger acid than HN^+R_3). In practice this can lead to (±)CAHBs, where accidental pK_a matching occurs to varying degrees, and ordinary hydrogen bonds (OHBs), where it does not, thus covering a large spectrum from neutral weak D–H···A (pK_a (D–H) ≫ pK_a ($H–A^+$)) to strong proton centred $^{-½}D···H^+···A^{-½}$ (pK_a (D–H) ≈ pK_a ($H–A^+$)) and again weak and charged $^-D:···H–A^+$ (pK_a (D–H) ≪ pK_a ($H–A^+$)) hydrogen bonds. However, in the latter case ionic interactions can be present resulting in strong overall binding. The matching criteria for $\Delta pK_a = pK_a$ (D–H) - pK_a ($H–A^+$) was found to be $-4.0 \leq \Delta pK_a \leq 1.0$. In these cases the two limiting structures in Scheme I-26 become more or less isoenergetic which is expressed by the averaged $^{-½}D···H^+···A^{-½}$ structure leading to (±)CAHB.

In the present case (±)CAHB should be possible, particularly so between the (Brønsted-acidic) nitro-substituted 2,2'-biphenol **44a** and diamines **45a**-**h**. In these complexes, except for **44a**+**45h**, the association constant *K* was found to be large, too large in fact to be explained by weak OHBs or the chelate effect alone. The pK_a values reported for 2-nitrophenols (pK_a = 7.2)[123] and protonated dimethylamine (pK_a = 10.7)[124] are relatively close in value and thus facilitating (±)CAHB. Assuming similar parameters for our complexes we estimated Δp$K_a \approx$ -3, *i.e.* well within the required limits. However, the reported pK_a value of methyl 4-hydroxy-3-methoxybenzoate (a suitable model compound for biphenol **44c**) is 8.3,[125] *i.e.* Δp$K_a \approx 0$ should be fulfilled for the combinations of **44c** with diamines **45** as well (Δp$K_a \approx$ -2.4). It must be stressed however, that pK_a values are usually determined in water. Since the solvent polarity has a significant influence on the pK_a values, care must be taken when rationalising H-bond strengths in other solvents based on pK_a matching.

Gilli *et al*. have addressed this problem by comparison of experimental thermodynamic parameters and crystallographic data of a huge number of hydrogen bonded complexes that both serve as binding strength indicators, with predictions made with what they call the pK_a slide rule, a graphical tool for the prediction of H-bond strengths based on pK_a matching.[92,93,99] The range was expanded beyond that of the autoprotolysis equilibrium of water ($0 \leq$ p$K_a \leq 14$) and reliability was confirmed by agreement between predictions and experimental data. On this slide rule we find pK_a matching of mono-nitrated phenols with the second pK_a of diamines which could account for the high binding strength in complexes **44a**+**45**.

In fact, both building blocks, 2,2'-biphenols **44** and chiral (1,2)-diamines **45** alike, possess two pK_a values (Scheme I-27). Following the argument of pK_a matching as being the origin of strong (±)CAHB, we assume better matching between the possible pK_a combinations of **44a** with **45** than between **44b** or **44c** and **45**. As a rule pK_a1 < pK_a2, *i.e.* the first proton abstraction is easier than the second. The nitro-substituents in **44a** may be crucial for acidifying the second proton sufficiently to guarantee proper pK_a matching between both phenol groups and the (dibasic) diamines.

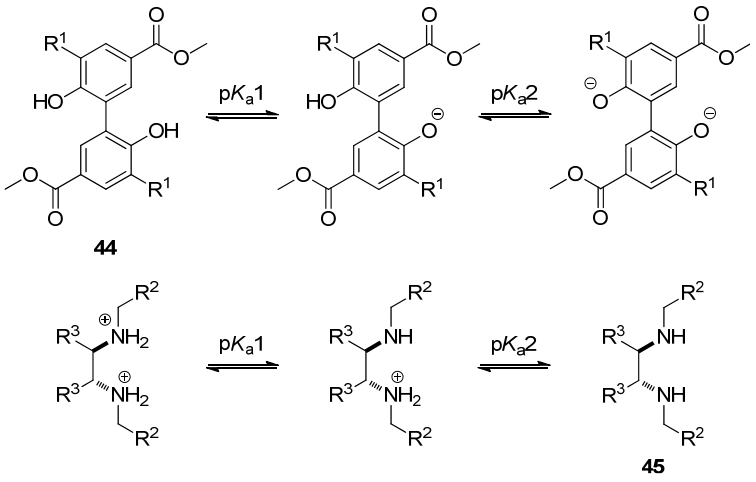

Scheme I-27. Definition of the various pK_a for biphenols **44** and diamine **45** (see Scheme I-25 for the definitions of R^1, R^2, and R^3).

Mizutani *et al.* ascribed the large binding constant ($K > 10^6$ M^{-1}) in complex **3a** (Scheme I-2) to intramolecular hydrogen bonding between the two phenolic hydroxyl groups, which increased the proton donation capability of the OH group.[91] In the solid state structure of the 3,3'-nitro-substituted 2,2'-biphenol **44a** we have observed intramolecular hydrogen bonding between the phenolic groups and including the NO_2 groups. In contrast, no H-bonds were found in the solid state structure of **44b**. We assume similar behaviour to take place in solution, thus

agreeing with the argument made by Mizutani. In the present case however, the NO_2 substituents are not only increasing the acidity of the hydroxyl protons by lowering the π–electron density in the aromatic ring but actively taking part as proton acceptors.

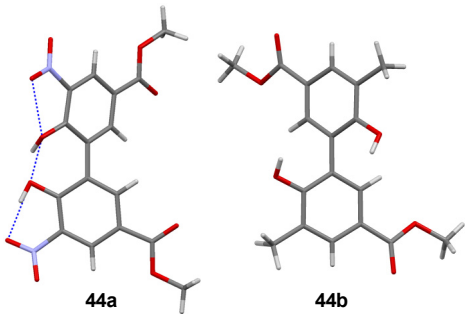

Figure I-5. X-ray structures of 2,2'-biphenols **44a** and **44b** (blue lines indicate hydrogen bonding).

In order to estimate the degree of proton transfer in our systems **44a**+**45** we prepared sodium 5,5'-bis(methoxycarbonyl)-3,3'-dinitro-biphenyl-2,2'-bis(olate) Na_2-**44a** from **44a** with a small excess of NaH. A strong absorbance band was found at 442 nm for the model biphenolate Na_2-**44a** in dry THF. In contrast, the maximum absorbance for the representative complex **44a**+**45c** was found at 386 nm under the same conditions (Figure I-6). Assuming that the intensity of the absorption at 442 nm in a solution of **44a**+**45c** solely resulted from the biphenolate chromophore that was formed by complexation under transfer of both protons from **44a** to **45c**, we evaluated the degree of said transfer to not exceed 8%, and hence being only a minor process in our system. Literature precedents reported the extent of proton transfer in CCl_4 for several chloro-substituted phenol-amine systems with ΔpK_a = 2-3 within the range of 8-35%.[89] However, these are not diprotic systems and the transfer of the second proton is less favoured, consequently leading in our case leading to a small ratio of the doubly charged biphenolate.

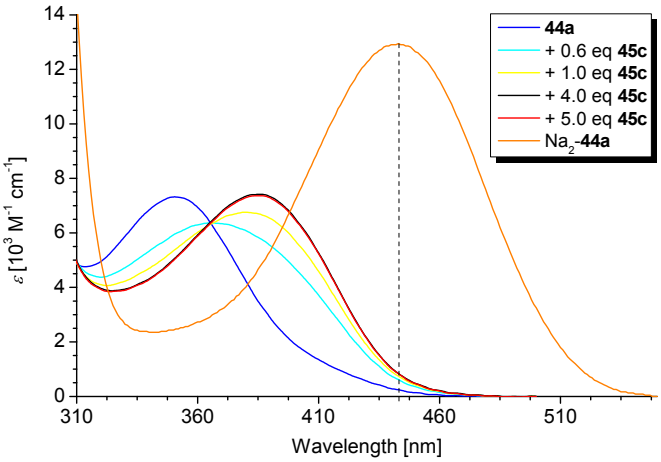

Figure I-6. UV-vis spectra of pure **44a** and the biphenolate Na_2-**44a** together with complex **44a**+**45c** under variation of the **44a**/**45c** ratio (THF, $2.6 \cdot 10^{-5}$ M).

As can be seen in Table I-3 (entries 1 and 6), binding constants for complexes **44a**+**45** may be moderately higher in THF than they are in toluene. This may be due to an increased proton transfer ratio which would be favoured by more polar solvents such as THF compared to toluene.

Apart from UV-vis titrations, the complexation of **44a** with **45c** was also monitored by ITC titrations in toluene and THF (Figure I-7). Good agreement between the two techniques was observed for the determination of *K* at 298 K in both solvents ($2.0 \cdot 10^5$ M^{-1} in toluene, $4.5 \cdot 10^5$ M^{-1} in THF; for UV-vis values see entries 1 and 6 in Table I-3). Moreover, the relative stoichiometry of the complexation process could be determined with the titration data, agreeing with that obtained by NMR to be 1:1 ratio in complexes **44a**+**45** at room temperature. Furthermore, thermodynamic parameters were directly accessible by ITC. The enthalpy change $\Delta H \approx -14$ kcal/mol is consistent with values for strong hydrogen bonding between acidic phenols and amines found in the literature; for example Libus *et al*. reported $\Delta H = -9.8$ kcal/mol for

a single hydrogen bond between *para*-nitrophenol and *n*-dibutylamine in benzene at 298 K.[126] The negative value for ΔS indicates a loss of entropy along the complexation. Conversely, this means an increase of organisation on the molecular level as could be expected for the entropically unfavourable chelation process.

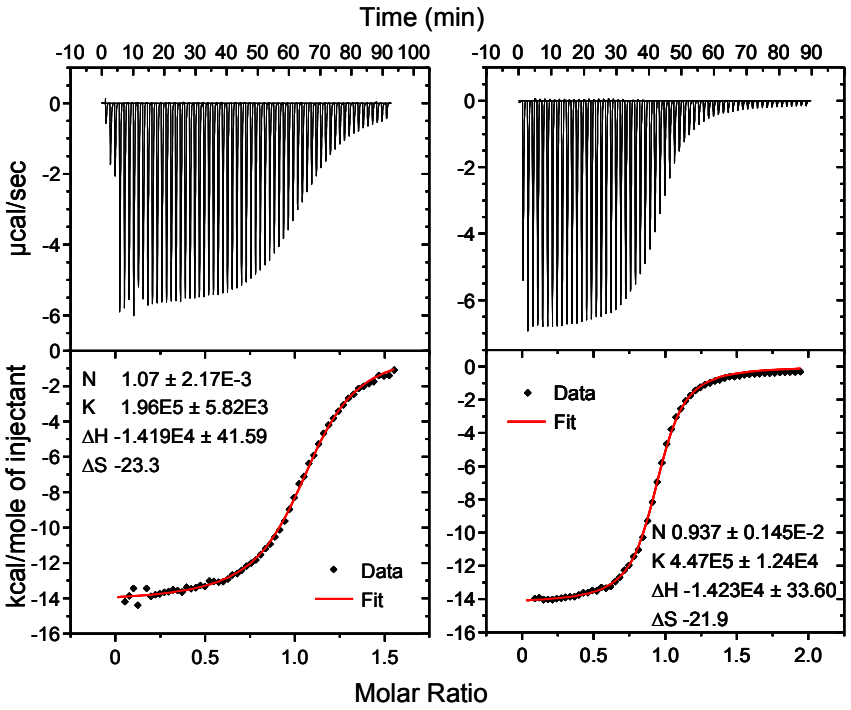

Figure I-7. ITC titration of **44a** with **45c** in toluene (left; [**44a**] = $2.6\cdot10^{-4}$ M, [**45c**] = $1.8\cdot10^{-3}$ M) and THF (right; [**44a**] = $2.2\cdot10^{-4}$ M, [**45c**] = $1.9\cdot10^{-3}$ M), thermodynamic parameters are given in the legends.

3.2.3 Chiroptical properties*

Biaryl compounds of type **44** show a low barrier of rotation that allows interconversion of the two axial conformers at room temperature. Both conformers could, in principle, bind to enantiopure diamines **45** forming two different diastereomeric 1:1 complexes. This is shown in Scheme I-28 where the complexes (*R*,*R*,a*R*)-**43** and (*R*,*R*,a*S*)-**43** differ in the sense of rotation around the biphenol's molecular axis. Provided that the rate of rotation around the prochiral axis in **44** is higher than the rate of the hydrogen bonding event, the ratio of formation between (*R*,*R*,a*R*)-**43** and (*R*,*R*,a*S*)-**43** will depend on the energy difference between the two diastereomers. The whole complexation process can then be regarded as a "*dynamic thermodynamic resolution*" (DTR).[127] This resolution process would be defined by the competing binding events between the two enantiomers (a*R*)-**44** and (a*S*)-**44** for the diamine moiety. Most likely the direct interconversion of (*R*,*R*,a*R*)-**43** into (*R*,*R*,a*S*)-**43** and *vice versa* would be also possible but the equilibration towards the thermodynamically most stable diasteromer cannot be nullified.

*These studies were carried out in collaboration with Dr. Anne-Sophie Felten and Dr. Juan Etxebarria.

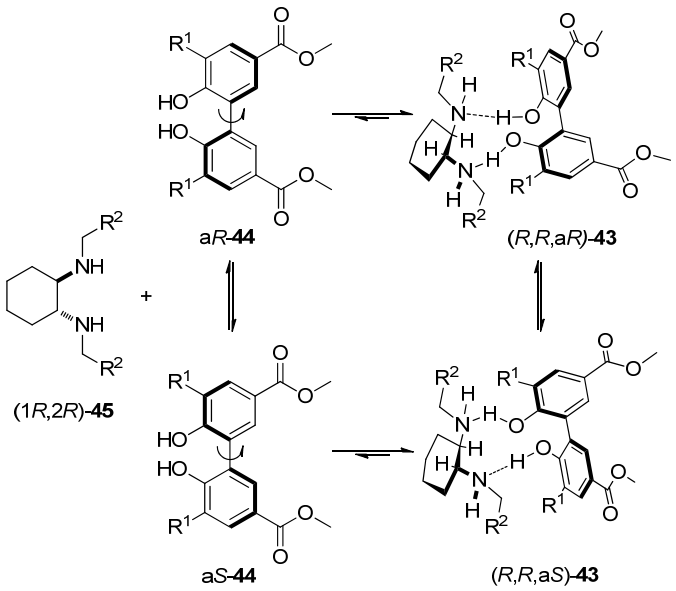

Scheme I-28. Dynamic thermodynamic resolution upon mixing diamines **45** with biphenols **44**.

The biphenyl chromophore has long been and still is the object of intensive CD studies both at the experimental[2,128-134] and theoretical level.[135-137] In fact CD is a particularly powerful method for the assignation of absolute configurations of atropisomeric biaryls, especially when experimental data can be combined with calculated CD spectra.[138,139] This approach was also successfully applied in the use of biaryls as chiral probes by determining the preferred sense of twist induced by stereogenic centres.[140,141] Hence, we decided to study the complexation of **44a** with **45** by recording circular dichroism spectra.

Figure I-8 shows the experimental CD spectra of the complexes **44a**+**45a**-**g** and the calculated CD curve of complex **44a**+**45c** together with the UV-vis spectra of the representative complexes **44a**+**45c** and **44a**+**45g**.* The computed CD data was plotted with GaussSum.[142] Good agreement between the experimental and simulated curves was observed for complex **44a**+**45c**, *i.e.* the signs and numbers of the Cotton effects coincided. The maxima of UV-vis absorption in toluene for these compounds were found in the range 379-386 nm (ε = 6400-8500 M^{-1} cm^{-1}) and were assignable to an allowed $\pi \rightarrow \pi^*$ transition in the substituted biaryl chromophore. All CD bands were in the same range (344-395 nm, $\Delta\varepsilon$ = -1.55-0.98) and thus attributable to the same transition. These results are summarised in Table I-4.

Table I-4. Chiroptical properties of complexes **44a**+**45a**-**h** measured in toluene at 298 K.

Entry	complex[a]	UV data: λ_{max},[b] ε[c]	CD data: λ_{max},[b] $\Delta\varepsilon$[c]
1	**44a**+**45a**	385, 6900	389, 0.07
2	**44a**+**45b**	386, 6700	395, 0.25
3	**44a**+**45c**	383, 6400	381, 0.51
4	**44a**+**45d**	382, 6900	384, 0.98
5	**44a**+**45e**	384, 6600	395, 0.37
6	**44a**+**45f**	385, 6000	394, 0.34
7	**44a**+**45g**	379, 8500	344, -1.55
8	**44a**+**45h**	365, 5600	not measured

[a](1*R*,2*R*)-**45** derivatives used in all cases and measured in toluene. [b][nm]. [c][M^{-1} cm^{-1}].

*Optimised geometries were calculated using the MPWB1K density functional and 6-31g(d) basis set as implemented in Gaussian 03, Rev. C.02 (Gaussian Inc., Wallingford CT, 2004). CD prediction was carried out by TD-DFT methods using the B3LYP functional and aug-cc-pVDZ basis set (see appendix for details). Calculated curve was normalised to experimental values.

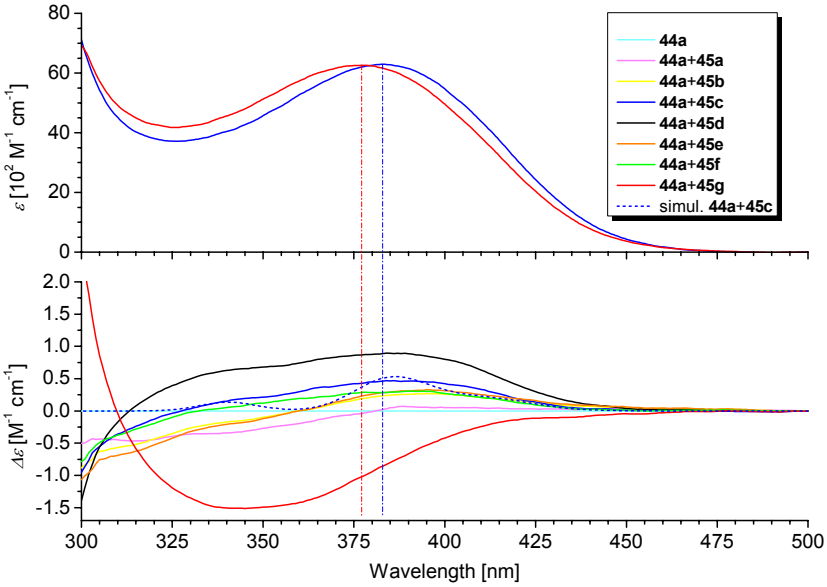

Figure I-8. Experimental UV-vis (top) of complexes **44a**+**45c** and **44a**+**45g** and experimental and calculated CD data (bottom) for complexes **44a**+**45**, spectra were measured in toluene at 298 K.

The existence of CD bands suggested the excess of one of the chiral diastereomers (*R*,*R*,a*R*)-**43** or (*R*,*R*,a*S*)-**43**. CD, *i.e.* chirality was successfully induced in the biaryl. The CD bands were invariably of positive sign for diamines (1*R*,2*R*)-**45a**-**f**, carrying aliphatic N-substituents. In a first approximation the intensities depended on the steric demand of said substituents. Accordingly, the largest amplitude was caused by the bulky ^{t}Bu-substituent in **45d**, followed by ^{i}Pr in **45c**. In contrast, the likewise bulky Np-substituent in diamine **45f** did not induce amplitudes of similar height presumably due to the increased flexibility of the elongated alkyl chain. It must be stressed however, that though merely comparing the amplitudes of a set of CD curves may have been successfully used in the past for indicating the sensitivity of axial chirality towards steric interactions,[1] it may be misleading due to the fact that alterations in the chromophore, like variations of the dihedral angle θ, can result in changes of the position and CD band

intensity in axially chiral biaryl compounds.[105, 143] This is due to the fact that CD arises from transitions between electronic states whose energy depends on conjugation effects and thus on orbital overlapping.

Interestingly, the sign of the Cotton effect was changed from positive to negative when going from aliphatic to an aromatic N-substituent. The complex prepared by the combination of **44a** with the mesitylmethyl-substituted diamine **45g** led to a reversed Cotton effect, furthermore showing the highest absolute amplitude in this series. Naturally, in all cases the chiral inducers **45** were of the same absolute configuration. These results suggested that the dynamically racemic 2,2'-biphenol derivative **44a** can be readily fixed with either preferential a*R*- or a*S* configuration depending on the nature of the N-substituent. Presumably, hydrogen bonding was not the only non-covalent interaction taking place when the aromatic substituent was present. We assumed that aromatic interactions can be a strong driving force, most likely even strong enough to lead to population inversion between the possible a*R* and a*S* diastereomers (Scheme I-28).

In order to gain a deeper understanding of the three dimensional structure of our complexes, full level DFT geometry optimisation was carried out using the MPWB1K density functional as implemented in Gaussian 03 software.* This functional was reported to be particularly well suited for the treatment of non-covalent interactions.[144,145] Two representative complexes **44a**+**45c** (R^2 = isopropyl, positive Cotton effect) and **44a**+**45g** (R^2 = mesityl, negative Cotton effect) were chosen for modelling. Furthermore, only complexes with C_2-symmetry, as observed by NMR, were taken into

*Gaussian 03, Rev. C.02 (Gaussian Inc., Wallingford CT, 2004). Computed relative energies do not take solvent effects into account but include corrections for zero-point energy and free energy (incorporating temperature and entropic effects corrected to 298.15 K).

account. Thus, the number of diastereomers that had to be computed could be reduced to four for each complex. Table I-5 shows the stereogenic nitrogens created in the binding event (due to C_2 symmetry only 1*R*,2*R* or 1*S*,2*S*) and the preferred sense of axial rotation, a*R* or a*S*. As can be seen the energetically most favourable diastereomer for complex **44a**+**45c** shows a*S* sense of rotation and diequatorial arrangement of the N-substituents (entry 1). However, the diastereomer with biaxial orientation of the N-substituents is only slightly less favourable (entry 2) but also showing a*S* configuration. The first a*R*-diastereomer, however, is significantly less favourable (entry 3). Thus, the computed CD data suggested the a*S* sense of rotation for complex **44a**+**45g** by comparison with the experimental data. In contrast, the calculated preferred sense of axial rotation in complex **44a**+**45g** is a*R* (entry 5), thus strengthening the assumption that aromatic N-substituents are capable of inverting the diastereomer populations.

Table I-5. Computed relative energies for complexes **44a**+**45c** and **44a**+**45g**.

entry	diastereomer **44a**+**45c**[a]	energy[b]	entry	diastereomer **44a**+**45g**[a]	energy[b]
1	R_C,R_C,S_N,S_N,a*S*[c]	0.0	**5**	R_C,R_C,R_N,R_N,a*R*	0.0
2	R_C,R_C,R_N,R_N,a*S*	0.2	**6**	R_C,R_C,S_N,S_N,a*S*	3.6
3	R_C,R_C,S_N,S_N,a*R*	2.4	**7**	R_C,R_C,R_N,R_N,a*S*	5.0
4	R_C,R_C,R_N,R_N,a*R*	3.2	**8**	R_C,R_C,S_N,S_N,a*R*	10.4

[a](1*R*,2*R*)-enantiomers. [b]In kcal/mol. [c]Denotations are as follows: the first two characters refer to the configuration at the N-substituted ring-carbons of the amines **45**, the following two indicate the configurations at the tetrahedral nitrogens upon complexation (priorities: C(ring) > C(N-substituent > H(O) > H(N)), a*R* and a*S* mark the sense of rotation in the biaryl unit.

As mentioned earlier, aromatic, *i.e.* π–π interactions might be responsible for the unexpected stereochemical outcome of the hydrogen bonding between **44a** and **45g**. Figure I-9 shows a comparison of the energetically lowest calculated structures of the complexes **44a**+**45c** and **44a**+**45g**. In the latter we observe an off-face arrangement between the nitro-substituted rings of the biaryl unit and the axial N-substituents of the diamine. Such an orientation of the π-systems should facilitate simultaneous π(CH) and π(NO_2) interactions between the aromatic rings.[146] In both cases four intermolecular hydrogen bonds (of which only two are shown for clarity), Ar–OH···HN–alkyl and O=N–O^-···HN–alkyl, were identified.

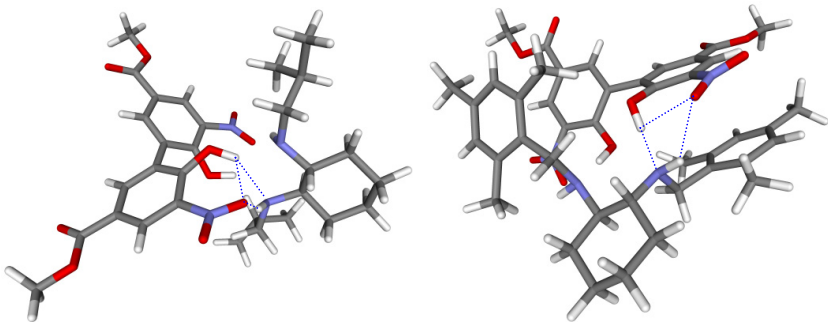

(R_C,R_C,S_N,S_N,a*S*)-**44a+45c** (R_C,R_C,R_N,R_N,a*R*)-**44a+45g**

Figure I-9. Energetically lowest calculated structures of complexes **44a**+**45c** and **44a**+**45g**.

3.2.4 Structural studies by X-ray diffraction.

Single crystals of hydrogen bonded complexes composed of 2,2'-biphenols **44** and chiral (1,2)-diamines **45** were obtained by dissolving the two building blocks in equimolar amounts in dry THF. The solvent was evaporated and the residue dried for several hours under high vacuum. Crystals were grown at 60 ºC by dissolving samples of the products in the minimum amounts required of either dry toluene or dry mesitylene.

Figure I-10 shows the crystal packing of complex **44a**+(1*S*,2*S*)-**45a**. Biphenol moieties **44a** are stacked in layers and flanked by the diamine (1*S*,2*S*)-**45a**. Proton transfer from one biphenol hydroxyl group to one of the two amine functions of (1*S*,2*S*)-**45a** is observed. The amine shows multipoint intermolecular hydrogen bonding with the remaining hydroxyl group, its neighbouring nitro-substituent, and a carboxyl function of the following biphenol, *i.e.* the layers are connected by hydrogen bonds. Taking bond lengths as criterion for binding strength we find hydrogen bonds ranging from weak ($d_{N\text{-}O}$ = 3.03 Å, O=N–O$^-$···HN–alkyl; $d_{N\text{-}O}$ = 2.98 Å, C=O···HN–alkyl) to medium-strong ($d_{N\text{-}O}$ = 2.68 Å aryl–OH···HN–alkyl).[92,93,99]

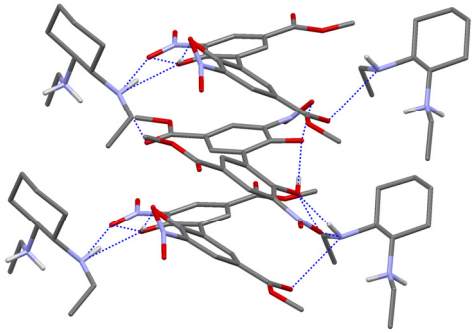

Figure I-10. Crystal packing of complex **44a**+(1*S*,2*S*)-**45a** (non N- and O-bounded protons are omitted for clarity; blue lines indicate hydrogen bonding).

Overall it can be said that the solid state structure is dominated by its comprehensive hydrogen bonding network which overrules energetic effects like 1:1 chelation in solution. Furthermore, all biphenol moieties to be found in the asymmetric unit show a*R* sense of rotation as would be expected from comparison of the experimental CD data (entries 1 and 3 in Table I-4) with calculated relative energies and simulated CD data (entry 1 in Table I-5 and simulated **44a**+**45c** in Figure I-8). It should be noted that in the crystal structure the (1*S*,2*S*)-enantiomer of **45a** was used. In order to compare the data a*S* sense of rotation must be assumed for a crystal of **44a**+(1*R*,2*R*)-**45a**. It must be stressed however, that it cannot be decided whether this preference was caused by (steric) interactions with the enantiopure diamine or the demands of the crystal packing, *i.e.* caution must be taken when interpreting the solution behaviour of complexes **44a**+**45** on the basis of solid state structures.

In conclusion, X-ray analysis only partially confirmed the findings presented in the previous section. This illustrates the difficulties faced when dealing with dynamic systems that are dominated by reversible interactions. In our case there are numerous structures to be considered: apart from different diastereomers complete proton transfer can lead to ionic structures. X-ray analyses revealed proton transfer in the solid state and if a charged species is present in solution, it is more likely to crystallise from non-polar solvents than an uncharged one even though it might be a minor compound only. This could account for the difference in structure between the assumed cyclic 1:1 geometry in solution and the linear 1:1 arrangement between biphenol **44a** and diamine (1*S*,2*S*)-**45a** that is observed in the solid state. Energy lowering effects for cyclic structures in solution, *i.e.* the chelate effect, seem to be dominated by requirements dictated by the incorporation of a molecule into the crystal lattice. Last but not least, conclusions made based on

the Δp*K*a matching model are not totally reliable since the pK_a value is a solution property.[120]

In addition to the above presented complex, single crystals were also obtained from the combination of the 3,3'-unsubstituted 2,2'-biphenol **44d** with the *N*-mesitylmethyl-substituted diamine (1*S*,2*S*)-**45g**. The solid state structure of complex **44d**+(1*S*,2*S*)-**45g** (Figure I-11) can be seen as a chain of alternating diamine and biphenol units held together by intermolecular hydrogen bonds. Proton transfer is observed from one phenolic OH group to one of the two N-atoms of a neighbouring diamine unit. Thus, the presence of the nitro-substituents is not crucial for proton transfer in the solid state. Assuming the H-bond chain starts at the hydroxyl group of one biphenol, we can follow it intramolecularly to the neighbouring hydroxyl group, in the structure present as phenolate ($d_{O\text{-}O}$ = 2.46 Å ,aryl-O–H···$^-$O–aryl), before going intermolecularly to the (protonated) first amine function of (1*S*,2*S*)-**45g** ($d_{N\text{-}O}$ = 2.61Å, aryl–O$^-$···H$_2^+$N–alkyl). The second amine of the same diamine molecule is then H-bonded to the hydroxyl group of the next biphenol in the chain ($d_{N\text{-}O}$ = 3.01 Å, alkyl-NH···HO-aryl) and from there the sequence starts anew. The formation of the H-bond network seems to be the driving force for the crystallisation of complex **44d**+(1*S*,2*S*)-**45g**. The form of a chain is not compatible with chelates. This might be the reason why the in solution energetically favoured 1:1 chelate complexes are not found in the crystal. Aromatic interactions did not seem to play a major role in the crystal lattice due to the distances between biphenol- and mesityl-rings (3.5-4.0 Å). In summary, the structure is again dominated by a hydrogen bonding network in which proton transfer plays a significant role although the hydroxyl groups were not acidified by nitro-substituents. The predominant sense of rotation was found to be a*R*. This is also the case for **44a**+(1*S*,2*S*)-**45a** however, any conclusion drawn from the solid state about the solution

behaviour of **44d**+(1*S*,2*S*)-**45g** or any related complex (like **44a**+**45g**) must be taken with utmost care.

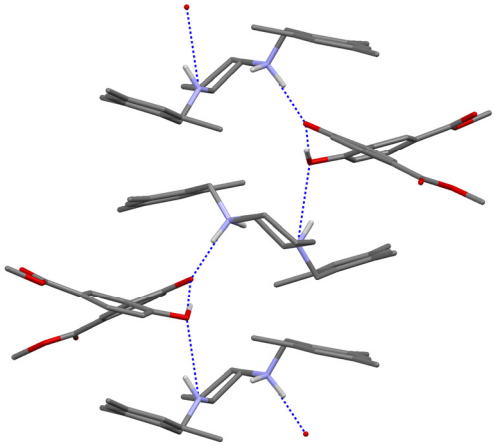

Figure I-11. Crystal packing of complex **44d**+(1*S*,2*S*)-**45g** (non N- and O-attached protons are omitted for clarity; blue lines indicate hydrogen bonding).

The combination of dynamically racemic biphenol **44a** with enantiopure diamines **45** has allowed for biasing the ratios of diastereomeric complexes **44a**+**45** by transfer of chirality from the optically active to the dynamically racemic building block. This thermodynamically controlled resolution resulted in new chiral supramolecular complexes as could be confirmed experimentally by CD measurements and theoretically by in-depth structural analysis and CD prediction. The complexes were found to be highly stable ($K > 10^5$ M^{-1}) as the measurement of binding constants by means of UV-vis and ITC titrations has revealed. Both, thermodynamic values (ΔH, ΔS) determined by ITC, and NMR analysis suggested the formation of (C_2-symmetric) 1:1 adducts between the biphenol and diamine moieties. We proposed the formation of two double charge-assisted hydrogen bonds resulting from favourable pK_a matching between the dibasic diamine and diprotic biphenol to be responsible for the high binding

strength. Additional contribution to the stability should come from the chelate effect. Substitution of the electron-withdrawing nitro-substituent by electron-donating ones such as Me (**44b**) or OMe (**44c**) was followed by a significant decrease of binding strength (*K* dropped by 2-3 orders of magnitude). The intensities and signs of the Cotton effects observed in CD spectra were found to depend on the steric bulk and nature of the N-substituents, with amplitudes increasing when going from chain-like small or flexible to bulky and spherical aliphatics. Aromatic N-substituents like mesitylmethyl on the other hand lead to an inversed Cotton effect, presumably by additional supramolecular (aromatic π–π) interactions. Consequently, it could be shown that the transmission and control of chiral information in such complexes cannot only be achieved directly by stereogenic centres of a chiral inducer but also indirectly by secondary interactions. Investigating the potential for exploitation of this strategy for chiral sensors and the preparation of new ligands for asymmetric transformations will be the purpose of future projects.

References

[1] T. Mizutani, H. Takagi, O. Hara, T. Horiguchi, H. Ogoshi, *Tetrahedron Lett.* **1997**, *38*, 1991.
[2] H. Takagi, T. Mizutani, T. Horiguchi, S. Kitagawa, H. Ogoshi, *Org. Biomol. Chem.* **2005**, *3*, 2091.
[3] Y.-X. Lu, Z.-M. Shi, Z.-T. Li, Z. Guan, *Chem. Commun.* **2010**, *46*, 9019.
[4] Y. Ishii, Y. Onda, Y. Kubo, *Tetrahedron Lett.* **2006**, *47*, 8221.
[5] S. R. Nam, H.-J. Kim, S. Sakamoto, K. Yamaguchi, J.-I. Hong, *Tetrahedron Letters* **2004**, *45*, 1339.
[6] J. J. D. de Jong, L. N. Lucas, R. M. Kellogg, J. H. van Esch, B. L. Feringa, *Science* **2004**, *304*, 278.
[7] K. Maeda, K. Morino, Y. Okamoto, T. Sato, E. Yashima, *J. Am. Chem. Soc.* **2004**, *126*, 4329.
[8] H. Onouchi, K. Maeda, E. Yashima, *J. Am. Chem. Soc.* **2001**, *123*, 7441.
[9] K. Morioka, N. Tamagawa, K. Maeda, E. Yashima, *Chemistry Letters* **2006**, *35*, 110.
[10] T. Hasegawa, K. Morino, Y. Tanaka, H. Katagiri, Y. Furusho, E. Yashima, *Macromolecules* **2006**, *39*, 482.
[11] J.-L. Hou, H.-P. Yi, X.-B. Shao, C. Li, Z.-Q. Wu, X.-K. Jiang, L.-Z. Wu, C.-H. Tung, Z.-T. Li, *Angew. Chem., Int. Ed.* **2006**, *45*, 796.
[12] T. Suzuki, K. Ohta, T. Nehira, H. Higuchi, E. Ohta, H. Kawai, K. Fujiwara, *Tetrahedron Lett.* **2008**, *49*, 772.
[13] J. Yu, T. V. RajanBabu, J. R. Parquette, *J. Am. Chem. Soc.* **2008**, *130*, 7845.
[14] C. Ikeda, Z. S. Yoon, M. Park, H. Inoue, D. Kim, A. Osuka, *J. Am. Chem. Soc.* **2005**, *127*, 534.
[15] Y. Kubo, Y. Ishii, *J. Nanosci. Nanotechnol.* **2006**, *6*, 1489.
[16] T. Ikeda, O. Hirata, M. Takeuchi, S. Shinkai, *J. Am. Chem. Soc.* **2006**, *128*, 16008.
[17] M. Ikeda, M. Takeuchi, A. Sugasaki, A. Robertson, T. Imada, S. Shinkai, *Supramol. Chem.* **2000**, *12*, 321.
[18] H. Ito, M. Ikeda, T. Hasegawa, Y. Furusho, E. Yashima, *J. Am. Chem. Soc.* **2011**, *133*, 3419.
[19] T. W. Anderson, J. K. M. Sanders, G. D. Pantos, *Org. Biomol. Chem.* **2010**, *8*, 4274.
[20] M. M. J. Smulders, I. A. W. Filot, J. M. A. Leenders, P. van der Schoot, A. R. A. Palmans, A. P. H. J. Schenning, E. W. Meijer, *J. Am. Chem. Soc.* **2010**, *132*, 611.
[21] S. J. George, Z. Tomovic, M. M. J. Smulders, T. F. A. de Greef, P. E. L. G. Leclere, E. W. Meijer, A. P. H. J. Schenning, *Angew. Chem., Int. Ed.* **2007**, *46*, 8206.

[22] K. Morino, N. Watase, K. Maeda, E. Yashima, *Chem. Eur. J.* **2004**, *10*, 4703.
[23] M. M. Green, J.-W. Park, T. Sato, A. Teramoto, S. Lifson, R. L. B. Selinger, J. V. Selinger, *Angew. Chem., Int. Ed.* **1999**, *38*, 3139.
[24] R. Eelkema, B. L. Feringa, *J. Am. Chem. Soc.* **2005**, *127*, 13480.
[25] R. Eelkema, B. L. Feringa, *Org. Lett.* **2006**, *8*, 1331.
[26] R. Holzwarth, R. Bartsch, Z. Cherkaoui, G. Solladie, *Chem. Eur. J.* **2004**, *10*, 3931.
[27] A. di Matteo, S. M. Todd, G. Gottarelli, G. Solladie, V. E. Williams, R. P. Lemieux, A. Ferrarini, G. P. Spada, *J. Am. Chem. Soc.* **2001**, *123*, 7842.
[28] H. Stegemeyer, K. J. Mainusch, *Chem. Phys. Lett.* **1970**, *6*, 5.
[29] J. Yoshida, H. Sato, A. Yamagishi, N. Hoshino, *J. Am. Chem. Soc.* **2005**, *127*, 8453.
[30] S. Allenmark, *Chirality* **2003**, *15*, 409.
[31] J.-I. Nishida, T. Suzuki, M. Ohkita, T. Tsuji, *Angew. Chem., Int. Ed.* **2001**, *40*, 3251.
[32] T. Suzuki, R. Yamamoto, H. Higuchi, E. Hirota, M. Ohkita, T. Tsuji, *J. Chem. Soc., Perkin Trans. 2* **2002**, 1937.
[33] T. Suzuki, A. Migita, H. Higuchi, H. Kawai, K. Fujiwara, T. Tsuji, *Tetrahedron Lett.* **2003**, *44*, 6837.
[34] T. Suzuki, R. Tamaki, E. Ohta, T. Takeda, H. Kawai, K. Fujiwara, M. Kato, *Tetrahedron Lett.* **2007**, *48*, 3823.
[35] T. Suzuki, T. Iwai, E. Ohta, H. Kawai, K. Fujiwara, *Tetrahedron Lett.* **2007**, *48*, 3599.
[36] W. Tang, X. Zhang, *Chem. Rev.* **2003**, *103*, 3029.
[37] P. W. N. M. van Leeuwen, P. C. J. Kamer, J. N. H. Reek, P. Dierkes, *Chem. Rev.* **2000**, *100*, 2741.
[38] O. Stelzer, S. Rossenbach, D. Hoff, M. Schreuder-Goedheijt, P. C. J. Kamer, J. N. H. Reek, P. W. N. M. van Leeuwen, in *Multiphase Homogeneous Catalysis*, **2005**, pp. 66.
[39] H. B. Kagan, P. Dang Tuan, *J. Am. Chem. Soc.* **1972**, *94*, 6429.
[40] A. Miyashita, A. Yasuda, H. Takaya, K. Toriumi, T. Ito, T. Souchi, R. Noyori, *J. Am. Chem. Soc.* **1980**, *102*, 7932.
[41] A. Boerner, Editor, *Phosphorus Ligands in Asymmetric Catalysis; Vol. 1-3*, Wiley-VCH, Weinheim, **2008**.
[42] S. Carboni, C. Gennari, L. Pignataro, U. Piarulli, *Dalton Trans.* **2011**, *40*, 4355.
[43] P. W. N. van Leeuwen, Ed., *Supramolecular Catalysis*, WILEY-VCH, Weinheim, **2008**.
[44] B. Breit, *Angew. Chem., Int. Ed.* **2005**, *44*, 6816.
[45] M. J. Wilkinson, P. W. N. M. van Leeuwen, J. N. H. Reek, *Org. Biomol. Chem.* **2005**, *3*, 2371.
[46] A. J. Sandee, J. N. H. Reek, *Dalton Trans.* **2006**, 3385.
[47] J. Meeuwissen, J. N. H. Reek, *Nat. Chem.* **2010**, *2*, 615.

[48] G. Gasparini, M. Dal Molin, L. J. Prins, *Eur. J. Org. Chem.* **2010**, 2429.
[49] B. Breit, W. Seiche, *J. Am. Chem. Soc.* **2003**, *125*, 6608.
[50] W. Seiche, A. Schuschkowski, B. Breit, *Adv. Synth. Catal.* **2005**, *347*, 1488.
[51] B. Breit, W. Seiche, *Pure Appl. Chem.* **2006**, *78*, 249.
[52] P. Beak, *Acc. Chem. Res.* **1977**, *10*, 186.
[53] M.-N. Birkholz, N. V. Dubrovina, H. Jiao, D. Michalik, J. Holz, R. Paciello, B. Breit, A. Boerner, *Chem. Eur. J.* **2007**, *13*, 5896.
[54] B. Schaeffner, J. Holz, S. P. Verevkin, A. Boerner, *Tetrahedron Lett.* **2008**, *49*, 768.
[55] M.-N. Birkholz, N. V. Dubrovina, I. A. Shuklov, J. Holz, R. Paciello, C. Waloch, B. Breit, A. Boerner, *Tetrahedron: Asymmetry* **2007**, *18*, 2055.
[56] B. Breit, W. Seiche, *Angew. Chem., Int. Ed.* **2005**, *44*, 1640.
[57] M. Weis, C. Waloch, W. Seiche, B. Breit, *J. Am. Chem. Soc.* **2006**, *128*, 4188.
[58] F. Chevallier, B. Breit, *Angew. Chem., Int. Ed.* **2006**, *45*, 1599.
[59] T. Smejkal, B. Breit, *Organometallics* **2007**, *26*, 2461.
[60] C. Waloch, J. Wieland, M. Keller, B. Breit, *Angew. Chem., Int. Ed.* **2007**, *46*, 3037.
[61] M. de Greef, B. Breit, *Angew. Chem., Int. Ed.* **2009**, *48*, 551.
[62] J. Wieland, B. Breit, *Nat. Chem.* **2010**, *2*, 832.
[63] P. J. Pye, K. Rossen, R. A. Reamer, R. P. Volante, P. J. Reider, *Tetrahedron Lett.* **1998**, *39*, 4441.
[64] P. J. Pye, K. Rossen, R. A. Reamer, N. N. Tsou, R. P. Volante, P. J. Reider, *J. Am. Chem. Soc.* **1997**, *119*, 6207.
[65] A. C. Laungani, B. Breit, *Chem. Commun.* **2008**, 844.
[66] A. C. Laungani, J. M. Slattery, I. Krossing, B. Breit, *Chem. Eur. J.* **2008**, *14*, 4488.
[67] T. Smejkal, B. Breit, *Angew. Chem., Int. Ed.* **2008**, *47*, 3946.
[68] T. Smejkal, B. Breit, *Angew. Chem., Int. Ed.* **2008**, *47*, 311.
[69] L. Diab, T. Smejkal, J. Geier, B. Breit, *Angew. Chem., Int. Ed.* **2009**, *48*, 8022.
[70] S. Das, C. D. Incarvito, R. H. Crabtree, G. W. Brudvig, *Science* **2006**, *312*, 1941.
[71] S. Das, G. W. Brudvig, R. H. Crabtree, *J. Am. Chem. Soc.* **2008**, *130*, 1628.
[72] P. A. Duckmanton, A. J. Blake, J. B. Love, *Inorg. Chem.* **2005**, *44*, 7708.
[73] L. K. Knight, Z. Freixa, P. W. N. M. van Leeuwen, J. N. H. Reek, *Organometallics* **2006**, *25*, 954.
[74] C. R. Bondy, P. A. Gale, S. J. Loeb, *J. Am. Chem. Soc.* **2004**, *126*, 5030.
[75] B. P. Hay, T. K. Firman, B. A. Moyer, *J. Am. Chem. Soc.* **2005**, *127*, 1810.

[76] L. Pescatori, A. Arduini, A. Pochini, F. Ugozzoli, A. Secchi, *Eur. J. Org. Chem.* **2008**, 109.
[77] J. Meeuwissen, M. Kuil, A. M. van der Burg, A. J. Sandee, J. N. H. Reek, *Chem. Eur. J.* **2009**, *15*, 10272.
[78] A. J. Sandee, A. M. van der Burg, J. N. H. Reek, *Chem. Commun.* **2007**, 864.
[79] J. Meeuwissen, R. J. Detz, A. J. Sandee, B. de Bruin, J. N. H. Reek, *Dalton Trans.* **2010**, *39*, 1929.
[80] J. Meeuwissen, R. Detz, A. J. Sandee, B. de Bruin, M. A. Siegler, A. L. Spek, J. N. H. Reek, *Eur. J. Inorg. Chem.* **2010**, 2992.
[81] F. W. Patureau, M. Kuil, A. J. Sandee, J. N. H. Reek, *Angew. Chem., Int. Ed.* **2008**, *47*, 3180.
[82] F. W. Patureau, S. de Boer, M. Kuil, J. Meeuwissen, P.-A. R. Breuil, M. A. Siegler, A. L. Spek, A. J. Sandee, B. de Bruin, J. N. H. Reek, *J. Am. Chem. Soc.* **2009**, *131*, 6683.
[83] P.-A. R. Breuil, F. W. Patureau, J. N. H. Reek, *Angew. Chem., Int. Ed.* **2009**, *48*, 2162.
[84] J. W. Steed, J. L. Atwood, Ed., *Supramolecular Chemistry*, 2nd ed., WILEY, **2009**.
[85] L. Pu, *Chem. Rev.* **2004**, *104*, 1687.
[86] D. Gurka, R. W. Taft, L. Joris, P. v. R. Schleyer, *J. Am. Chem. Soc.* **1967**, *89*, 5957.
[87] R. Kraemer, G. Zundel, *J. Chem. Soc., Faraday Trans.* **1990**, *86*, 301.
[88] A. Koll, M. Rospenk, L. Sobczyk, *J. Chem. Soc., Faraday Trans. 1* **1981**, *77*, 2309.
[89] G. Albrecht, G. Zundel, *J. Chem. Soc., Faraday Trans. 1* **1984**, *80*, 553.
[90] Z. Pawelka, T. Kuc, *Pol. J. Chem.* **2001**, *75*, 845.
[91] T. Mizutani, H. Takagi, Y. Ueno, T. Horiguchi, K. Yamamura, H. Ogoshi, *J. Phys. Org. Chem.* **1998**, *11*, 737.
[92] P. Gilli, L. Pretto, V. Bertolasi, G. Gilli, *Acc. Chem. Res.* **2009**, *42*, 33.
[93] P. Gilli, G. Gilli, *J. Mol. Struct.* **2010**, *972*, 2.
[94] H. Szatylowicz, *J. Phys. Org. Chem.* **2008**, *21*, 897.
[95] A. Fedorowicz, A. Koll, J. Mavri, *Theor. Chem. Acc.* **2003**, *109*, 220.
[96] C. A. Hunter, *Angew. Chem. Int. Ed.* **2004**, *43*, 5310.
[97] A. G. Blackman, *C. R. Chim.* **2005**, *8*, 107.
[98] D. C. Bowman, *J. Chem. Educ.* **2006**, *83*, 1158.
[99] P. Gilli, L. Pretto, G. Gilli, *J. Mol. Struct.* **2007**, *844-845*, 328.
[100] P. Gilli, V. Bertolasi, L. Pretto, G. Gilli, *J. Mol. Struct.* **2006**, *790*, 40.
[101] A. Hunter Christopher, *Angew. Chem. Int. Ed.* **2004**, *43*, 5310.

[102] K. A. Connors, *Binding Constants. The measurement of molecular complex stability*, John Wiley & Sons, Inc., New York, **1987**.
[103] P. Thordarson, *Chem. Soc. Rev.* **2011**, *40*, 1305.
[104] C. Dethlefs, J. Eckelmann, H. Kobarg, T. Weyrich, S. Brammer, C. Naether, U. Luening, *Eur. J. Org. Chem.* **2011**, 2066.
[105] N. Berova, L. Di Bari, G. Pescitelli, *Chem. Soc. Rev.* **2007**, *36*, 914.
[106] D. A. Lightner, J. E. Gurst, *Organic Conformational Analysis and Stereochemistry from Circular Dichroism Spectroscopy*, John Wiley & Sons, New York, **2000**.
[107] N. Berova, K. Nakanishi, R. W. Woody, *Circular Dichroism: Principles and Applications*, 2nd ed., Wiley-VCH, New York, **2000**.
[108] G. Pescitelli, L. Di Bari, N. Berova, *Chem. Soc. Rev.* **Advance Article**, DOI: 10.1039/C1CS15036G.
[109] G. Pescitelli, L. Di Bari, N. Berova, *Chem. Soc. Rev.* **2011**, DOI: 10.1039/C1CS15036G.
[110] J. Hassan, V. Penalva, L. Lavenot, C. Gozzi, M. Lemaire, *Tetrahedron* **1998**, *54*, 13793.
[111] J. Hassan, C. Gozzi, M. Lemaire, *C. R. Acad. Sci. Paris, Série IIc, Chimie* **2000**, *3*, 517.
[112] J. Iskra, S. Stavber, M. Zupan, *Synthesis* **2004**, 1869.
[113] H.-B. Sun, R. Hua, Y. Yin, *J. Org. Chem.* **2005**, *70*, 9071.
[114] A. P. Cole, V. Mahadevan, L. M. Mirica, X. Ottenwaelder, T. D. P. Stack, *Inorg. Chem.* **2005**, *44*, 7345.
[115] T. Arao, K. Sato, K. Kondo, T. Aoyama, *Chem. Pharm. Bull.* **2006**, *54*, 1576.
[116] A. M. Costa, C. Jimeno, J. Gavenonis, P. J. Carroll, P. J. Walsh, *J. Am. Chem. Soc.* **2002**, *124*, 6929.
[117] R. A. Binstead, A. D. Zuberbühler, B. Jung, SPECFIT Global Analysis System, Version 3.0.38 ed., Spectrum Software Associates, **1993-2006**.
[118] H. Gampp, M. Maeder, C. J. Meyer, A. D. Zuberbuehler, *Talanta* **1986**, *33*, 943.
[119] H. Gampp, M. Maeder, C. J. Meyer, A. D. Zuberbuehler, *Talanta* **1985**, *32*, 95.
[120] T. Steiner, *Angew. Chem., Int. Ed.* **2002**, *41*, 48.
[121] P. Gilli, V. Bertolasi, L. Pretto, V. Ferretti, G. Gilli, *J. Am. Chem. Soc.* **2004**, *126*, 3845.
[122] G. Gilli, P. Gilli, *J. Mol. Struct.* **2000**, *552*, 1.
[123] S.-P. Wang, H.-J. Chen, *J. Chromatogr., A* **2002**, *979*, 439.
[124] S. Fu, *Analyst* **1998**, *123*, 1487.
[125] M. Ragnar, C. T. Lindgren, N.-O. Nilvebrant, *J. Wood Chem. Technol.* **2000**, *20*, 277.
[126] W. Libus, M. Mecik, W. Sulek, *J. Solution Chem.* **1977**, *6*, 865.
[127] W. K. Lee, Y. S. Park, P. Beak, *Acc. Chem. Res.* **2009**, *42*, 224.

[128] W. Kuhn, R. Rometsch, *Helv. Chim. Acta* **1944**, *27*, 1346.
[129] K. Mislow, *Angew. Chem.* **1958**, *70*, 683.
[130] E. Bunnenberg, C. Djerassi, K. Mislow, A. Moscowitz, *J. Am. Chem. Soc.* **1962**, *84*, 2823.
[131] K. Mislow, E. Bunnenberg, R. Records, K. Wellman, C. Djerassi, *J. Am. Chem. Soc.* **1963**, *85*, 1342.
[132] B. Borecka, T. S. Cameron, A. Linden, P. Rashidi-Ranjbar, J. Sandstroem, *J. Am. Chem. Soc.* **1990**, *112*, 1185.
[133] Z. Xie, F. Wuerthner, *Org. Lett.* **2010**, *12*, 3204.
[134] M.-A. Dubois, A. Grandbois, S. K. Collins, A. R. Schmitzer, *J. Mol. Recognit.* **2010**, *24*, 288.
[135] P. Rashidi-Ranjbar, J. Sandstroem, *J. Mol. Struct.* **1991**, *246*, 25.
[136] T. Mori, Y. Inoue, S. Grimme, *J. Phys. Chem. A* **2007**, *111*, 4222.
[137] G. Bringmann, K. Maksimenka, J. Mutanyatta-Comar, M. Knauer, T. Bruhn, *Tetrahedron* **2007**, *63*, 9810.
[138] L. Loncar-Tomascovic, R. Sarac-Arneri, A. Hergold-Brundic, A. Nagl, M. Mintas, J. Sandstrom, *Helv. Chim. Acta* **2000**, *83*, 479.
[139] A. Iuliano, S. Facchetti, G. Uccello-Barretta, *J. Org. Chem.* **2006**, *71*, 4943.
[140] S. Superchi, D. Casarini, A. Laurita, A. Bavoso, C. Rosini, *Angew. Chem., Int. Ed.* **2001**, *40*, 451.
[141] S. Superchi, R. Bisaccia, D. Casarini, A. Laurita, C. Rosini, *Journal of the American Chemical Society* **2006**, *128*, 6893.
[142] N. M. O'Boyle, A. L. Tenderholt, K. M. Langner, *J. Comput. Chem.* **2008**, *29*, 839.
[143] L. Di Bari, G. Pescitelli, P. Salvadori, *J. Am. Chem. Soc.* **1999**, *121*, 7998.
[144] Y. Zhao, N. E. Schultz, D. G. Truhlar, *J. Chem. Theory Comput.* **2006**, *2*, 364.
[145] Y. Zhao, D. G. Truhlar, *J. Chem. Theory Comput.* **2007**, *3*, 289.
[146] C. A. Hunter, K. R. Lawson, J. Perkins, C. J. Urch, *J. Chem. Soc., Perkin Trans. 2* **2001**, 651.

II Design and Preparation of New Chiral Ligands by Chiral Induction Using Metal-Ligand Interactions as the Mediating Force

1 Literature Precedents

The current literature encompasses many examples of coordination complexes involved in chirality transfer processes.[1] Often, the chirality is transferred from an optically pure ligand to the metal centre, a process that is usually referred to as *predetermined chirality*.[2-5] Also well-known is the transfer and propagation of chirality in helicate structures induced by the coordination to one or more metal centres.[6-9] However, coordination compounds in which chiral information is transferred from a chiral to a prochiral moiety or ligand are relatively scarce.

A nice example for the induction of axial chirality mediated by metal-ligand interactions was reported by Kubo *et al*.,[10] who have used an heterotopic Zn(II) porphyrin dimer **58** in which the two porphyrins were attached to a dynamically racemic biphenol derivative. The biphenol's oxygen atoms were furthermore part of a crown ether-like structure, in which one ethyl bridge was substituted by the biphenol moiety (Scheme II-1). Preferential formation of one of the two atropisomers of **58** was achieved by ditopic interaction of the enantiopure inducer **59** with the porphyrins' Zn(II) centres. The stoichiometry of the molecular complex was determined to be 1:1 by Job plot analysis and the resulting CD spectra were in accordance with the exciton coupling model. Interestingly, the addition of $Ba(ClO_4)_2$ resulted in the incorporation of Ba^{2+} ions into the crown ether ring but displaced the inducer base **59** from its coordination site presumably by disrupting the required binding geometry. The CD signal was retained, however, indicating that the induced chirality was memorised. When adding Ba^{2+} before the chiral inducer the compound remained CD silent, *i.e*. was not perturbed from its dynamic equilibrium.

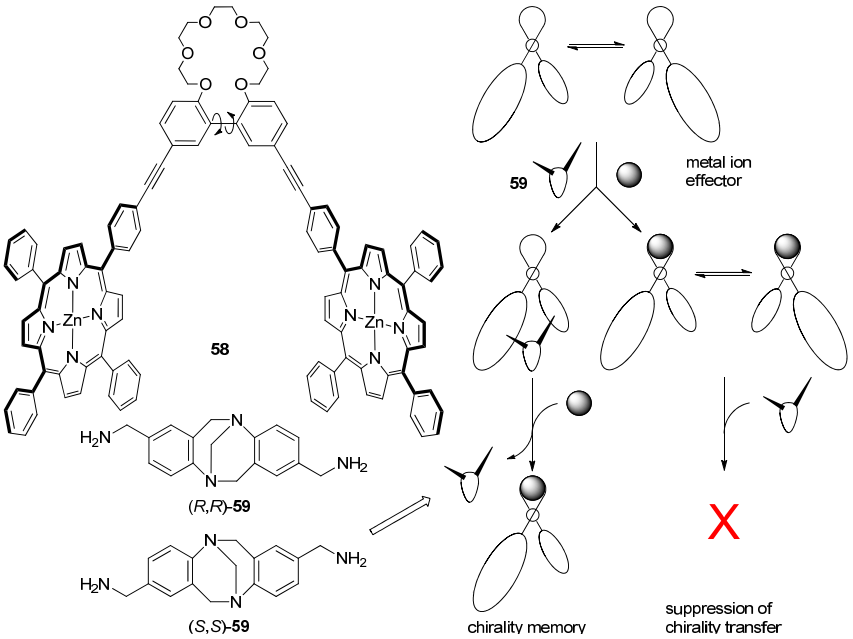

Scheme II-1. Axial chirality-transfer control and memory using a chiral amine and an anti-cooperative binding motif, respectively.[10]

The Zn(II) porphyrin amine binding motif was also utilised in the development of chirality sensors by Nakanishi *et al*.[11] Two tetraphenylporphyrin moieties were connected *via* a pentanediol bridge to form a tweezer **60** capable of coordinating chiral guests like diamines, amino acids, and amino alcohols (Scheme II-2). To achieve efficient chiral recognition, it was crucial for the substrate to have a primary amino group directly attached to the stereogenic centre. Furthermore, the remaining two substituents present at the latter had to be of different size. Enantiomerically pure guests such as **61** induce a preferential screw sense in receptor **60**, thus bringing the two porphyrin units close in space, which as a consequence experience strong exciton coupling of their transitions and exhibit intense CD bands (see general introduction). The absolute configuration of the bound host could be deciphered from the CD of the macrocyclic host-guest complex and the presented

assembly showed great versatility due to some unique features: i) porphyrins are very good chromophores (here λ_{max} = 419 nm, ε = 890000 $M^{-1}cm^{-1}$ in CH_2Cl_2), ii) this enabled the chromophores to couple over ≈ 50 Å,[12] iii) the flexible linker allowed the hosting of guests of variable length and steric bulk, and iv) the direction of the effective electric transition moment was known to run in the 5-15 direction of the *meso*-positions of the porphyrin.[13] Amino acids and amino alcohols required simple derivatisations in order to introduce the required second amino function. After attaching an additional amino group to monoamino derivatives, the scope of chiral hosts suitable for absolute configuration analysis could be further enlarged to primary monoamines and monoalcohols.[14,15] Furthermore, following their porphyrin tweezer approach, Nakanishi *et al.* also elaborated procedures to elucidate the absolute configuration of cyclic α-hydroxyketones[16] and, by applying Mg(II) instead of Zn(II), that of chiral carboxylic acids.[17]

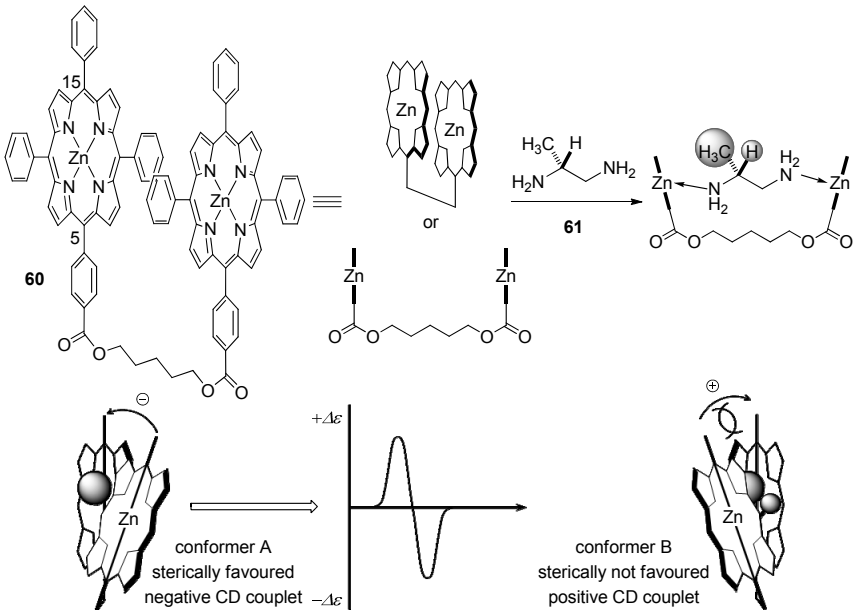

Scheme II-2. Chiral sensing of (*R*)-1,2-diaminopropane **61** by porphyrin tweezer **60**. Of the two possible conformations one is sterically favoured.[11]

In 2001 Gagné and co-workers reported successful asymmetric transformations involving catalyst **62** derived from unresolvable, conformationally dynamic 2,2'-bis(diphenylphosphino)-1,1'-biphenyl (BIPHEP).[18] Key to their approach was locking the BIPHEP ligand into a dynamically frozen moiety and using it as the only source of chirality for catalysis. Enantiomerically pure (*S*)-BINOL served as chiral inducer that allowed the formation of Pt(II) complexes which were relatively stable against atropinversion.[19] The resulting diastereomeric [Pt((*S*)-BINOLate)(BIPHEP)] complexes could be separated and furnished enantiopure Lewis catalysts once the (*S*)-BINOL ligand was removed. Good catalytic performance was observed in the asymmetric Diels-Alder and the asymmetric glyoxolate-ene reactions (Scheme II-3).

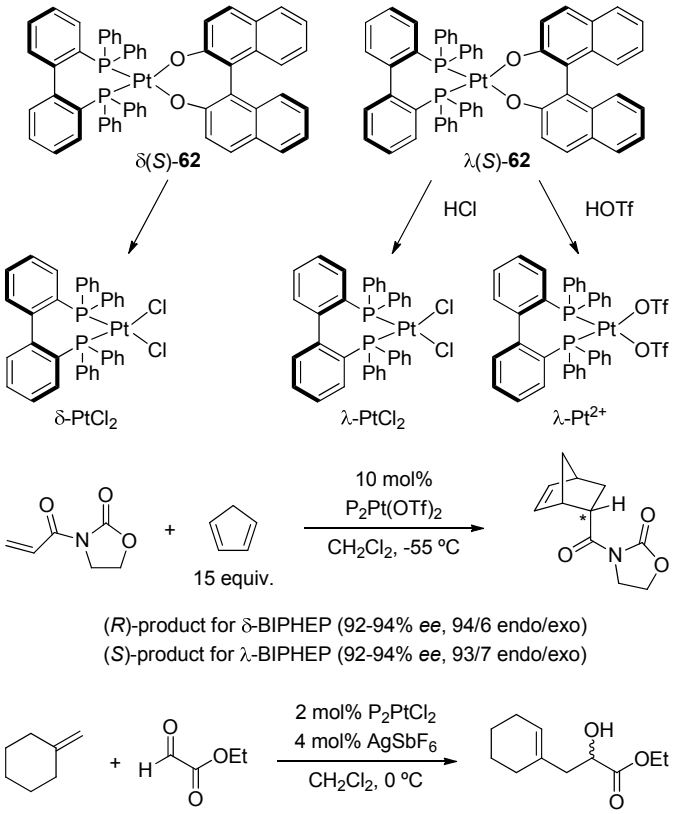

Scheme II-3. Preparation of enantiopure Pt(BIPHEP) complexes **62** and their application in asymmetric catalysis. To distinguish BIPHEP and BINOL stereochemistry the authors arbitrarily labelled the BIPHEP moiety in terms of its skew conformation (λ/δ) and BINOL according to its axial sense of rotation (a*R*/a*S*).[18,19]

Walsh *et al*. pursued a very interesting approach to optimise the activity and enantioselectivity of catalysts by incorporating achiral and *meso* ligands in the catalytic system.[20] Instead of preparing and screening libraries of enantiopure ligands they employed only (*S*)-3,3'-diphenyl-BINOL **63** as the chiral inducer in the Lewis acid catalysed enantioselective addition of dialkylzinc derivatives to benzaldehyde. According to the authors, this work was inspired by the reports of Ding, Ishii, and Mikami, who activated enantiopure Zn(Ph_2-BINOLate) complexes with enantiopure diimine ligands.[21,22] In contrast, here the optimisation of the chiral environment around the active Zn(II) centre was achieved by employing a series of achiral diimine and diamine activators, thus eliminating the necessity of a second enantiopure ligand. These activators included: i) achiral diimine ligands capable of adopting chiral conformations thanks to their *meso* backbones, ii) achiral diimines with backbones that became axially chiral on coordination to the metal, iii) achiral diamines that formed stereocentres as a result of coordinating the metal, and iv) achiral diamine ligands with attached groups that have axially chiral conformations. Catalysts, which were screened in the asymmetric addition of an ethyl group to benzaldehyde, were prepared from diethylzinc, (*S*)-Ph_2-BINOL **63**, and the respective activator. This concept, which the authors called "achiral activation", is shown in Scheme II-4 together with some representative activators of the above-mentioned classes i) to iv) and their performance in said asymmetric addition reaction.

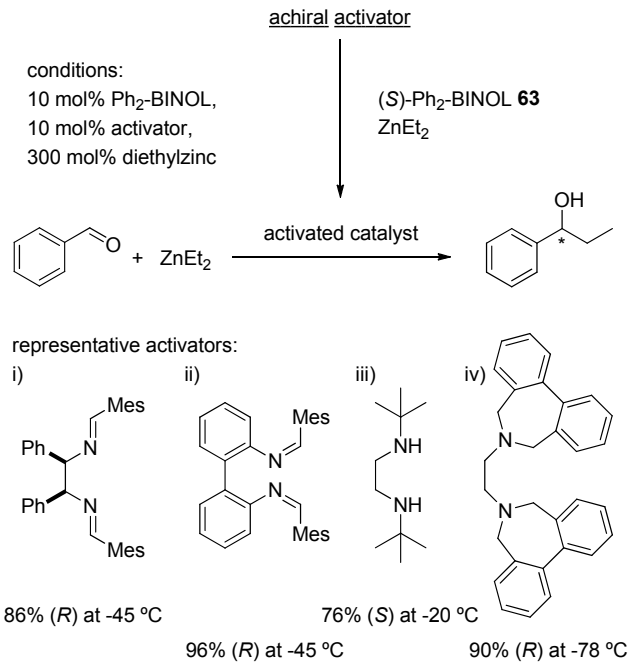

Scheme II-4. Concept of achiral activation employed in the asymmetric addition of an ethyl group to benzaldehyde (top) and representative activators together with their performance in said reaction (bottom). In all cases the indicated reaction conditions were applied.

Of particular interest for the work presented in this thesis were the cases ii) and iv), *i.e.* the ones in which the coordination to the metal centre of the diimine and diamine, respectively, could lead to the freezing of axially chiral conformations. In these cases two different diastereomeric [Zn((*S*)-Ph_2-BINOLate)] complexes were possible (Scheme II-5) and the interaction between the enantiopure (*S*)-Ph_2-BINOLate and the rapidly racemising biaryl groups was thought to cause the latter to adopt chiral conformations. This could be interpreted as the transfer of chirality from the enantiopure (*S*)-Ph_2-BINOL **63** to the dynamically racemic biaryl compound mediated by zinc(II) and contributing to the chiral environment shaped around the metal centre.

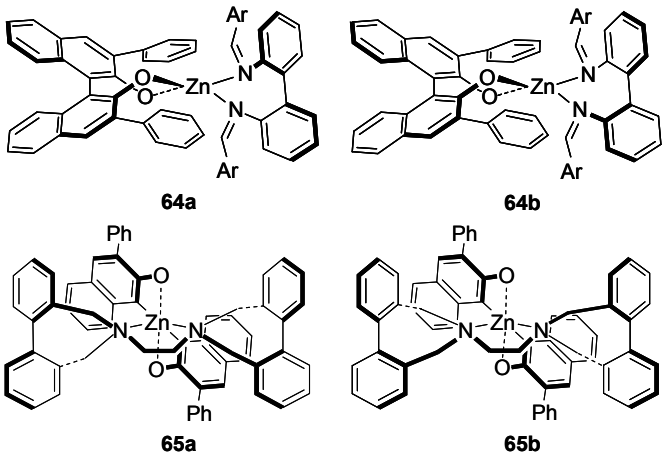

Scheme II-5. Diastereomeric conformations **64a** and **64b** of [Zn((*S*)-Ph_2-BINOLate)] complexes with ligands derived from 2,2'-diiminobiphenyl (top) and **65a** and **65b** of [Zn((*S*)-Ph_2-BINOLate)] complexes with (1,2)-diaminoethane ligands bearing dynamically racemic biaryls.[20]

Walsh's group also investigated the solid state and solution behaviour of two representative complexes. The first was derived from (*S*)-Ph_2-BINOL **63** and the simple achiral diimine **66** (Scheme II-6) by simply mixing them in equimolar amounts with diethylzinc. The crystal structure showed Zn(II) in pseudotetrahedral geometry bonded to the Ph_2-BINOLate and diimino ligands with the latter having *cis* and *trans* configurations with respect to the *N*-imino substituents (*cis*, *trans*-**67** in Scheme II-6). The Zn-O atomic distances were reported to be 1.881(2) and 1.918(2) Å, respectively, whilst Zn-N distances were determined to be 2.080(2) and 2.058(3) Å. The angles amounted to 101.32(10)º (O-Zn-O), 82.37(11)º, and a torsional angle of 59.5º in the BINOLate. However, the ^{1}H and ^{13}C NMR data collected from recrystallised material did not confirm this structure in solution. Although the C_2-symmetric binding mode of the Ph_2-BINOLate ligand was confirmed to come true on the NMR timescale, it was found that the diimine was not coordinated symmetrically to Zn(II). An imaginable open structure such as *cis*-**67** could be discounted due to its inconsistency with

^{13}C NMR and IR data in solution. Eventually, an equilibration between *trans*, *trans*-**67** and *cis*, *trans*-**67** *via* the open structure *cis*-**67** was postulated. Interestingly, when the compound was formed *in situ* and immediately submitted to NMR analysis, the structure to be found corresponded to C_2-symmetric *trans*, *trans*-**67** that isomerised within several days to give the same spectra as *cis*, *trans*-**67**. The latter was also applied instead of the *in situ* generated catalyst in the enantioselective ethyl addition to benzaldehyde with dramatic decrease of both enantioselectivity (18% ee (*R*) compared to 75% ee (*R*)) and catalytic activity (22% conversion after 10 min compared to 98%) at 0 ºC.

Similar studies were carried out by Walsh's group with a Zn(II) complex prepared from (*S*)-Ph$_2$-BINOL and diamine **68** (Scheme II-6). Again in the solid state, the metal centre was found to be present in a pseudotetrahedral environment with both, the BINOL and the diamino unit bound in C_2-symmetric manner. New stereocentres of *R* configuration were created at the two nitrogen atoms as is shown in (*R*,*R*)-**69**. Atomic distances (1.900(4) and 1.940(2) Å for Zn-O, and 2.057(4) and 2.086(4) Å for Zn-N) were very close to those in the previous imine-complex. The same was true for the O-Zn-O bond angle of 101.30(14)º, whereas the N-Zn-N bond angle was found with 86.5(2)º to be slightly wider. The torsional angle between the naphthyl rings of the BINOL spanned to 63.0º. The NMR analysis of this compound indicated that its solution behaviour was dominated by underlying equilibria. In the ^{1}H NMR spectrum three signals assignable to ^{t}Bu groups were found instead of the expected singlet. Furthermore, instead of the expected three resonances attributable to the ethyl backbone plus the N-attached protons, eight signals were found in the relevant region. The ^{13}C NMR spectrum showed three signals for every expected resonance. Unfortunately, it remained unclear whether (*R*,*R*)-**69** was in equilibrium with its diastereomer (*R*,*S*)-**69** or a possible three-

coordinated species with a loose amino nitrogen atom. At any rate, here the catalytic performance of the newly dissolved isolated compound was as good as that of the *in situ* prepared catalyst, suggesting that in both cases the same catalytic species was present.

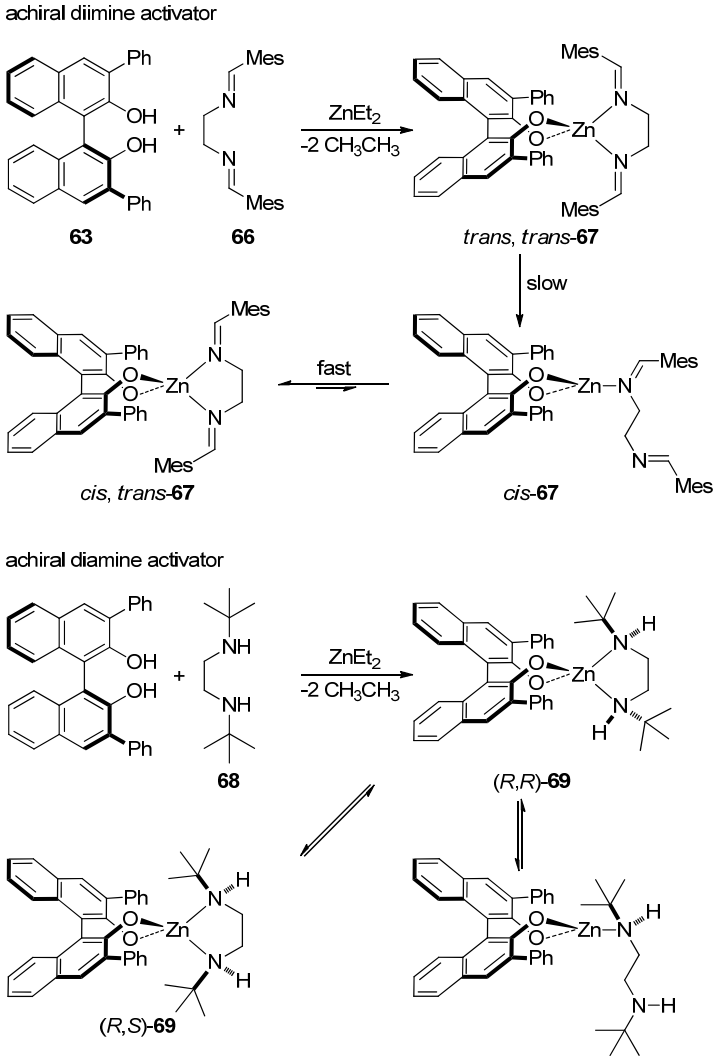

Scheme II-6. Synthesis and possible structures in solution of [Zn((*S*)-Ph_2-BINOLate)(diimine)] **67** and [Zn((*S*)-Ph_2-BINOLate)(diamine)] **69** complexes according to Walsh *et al*.[20]

In summary, Walsh *et al*. presented a piece of work that demonstrated very nicely the possibilities of manipulating chiral environments by employing achiral and *meso* ligands. It was discussed here in detail due to its importance to our approach of preparing new chiral supramolecular ligands, both from the conceptual as well as the preparative point of view.

The previous two examples were representative for metal-ligand mediated chirality control around a metal centre that served for both, catalytic and chirality controlling purposes. However, this is not the only strategy envisaged for utilising supramolecular metal-ligand interactions in asymmetric catalysis. The preparation of ditopic ligands by assembling two chiral constituent monotopic blocks around a template or structural metal has also turned out to be an efficient approach. It is particularly interesting in the formation of heterobidentate ligands. Crucial to this strategy is the ability of the binding moieties to coordinate different metals in a mutually controllable manner, *i.e*. the binding motif for the structural metal (or the template) must not compete for the active metal with the catalytic binding motif and *vice versa*. A good orientation that has been recognised in many literature examples is given by the Pearson-Parr hard and soft acids and bases (HSAB) principle.[23-26] Most notably, P,N-ligands having available the soft phosphorous and the hard nitrogen donor atoms are good candidates for the selective coordination of P-groups to soft, catalytically active metals like rhodium or palladium, and the binding of N-coordination motifs to hard metals like zinc and titanium. All in all, it can be said that contrary to the hydrogen bonded supramolecular complexes that were introduced in the literature section of Chapter I, no direct binding of the two constituting ligands is taking place here, but instead it is mediated by the structural metal or template.

One of the first supramolecular bidentate ligands relying on metal-ligand interactions was introduced in 2003 by Reek and van Leeuwen *et al*. (Figure II-1).[27] Their strategy was based on a dimeric Zn(II) porphyrin template that directed the coordination of two pyridyl-phosphane or pyridyl-phosphite ligands, to rhodium. The thus formed supramolecular assemblies behave like bidentate ligands in the coordination towards rhodium precursors suitable for catalysis. The resulting bidentate rhodium complex **70** efficiently mediated the hydroformylation of 1-octene giving higher linear to branched ratios (*l*/*b* up to 94/6) than their untemplated analogue. Furthermore, with the Rh-mediated hydroformylation of styrene, an example for an asymmetric transformation was given as well. Although only moderate ee values (up to 33% ee) were obtained, this constituted a clear improvement compared to the monodentate analogues (*ca*. 7% ee) involved in the authors' study.

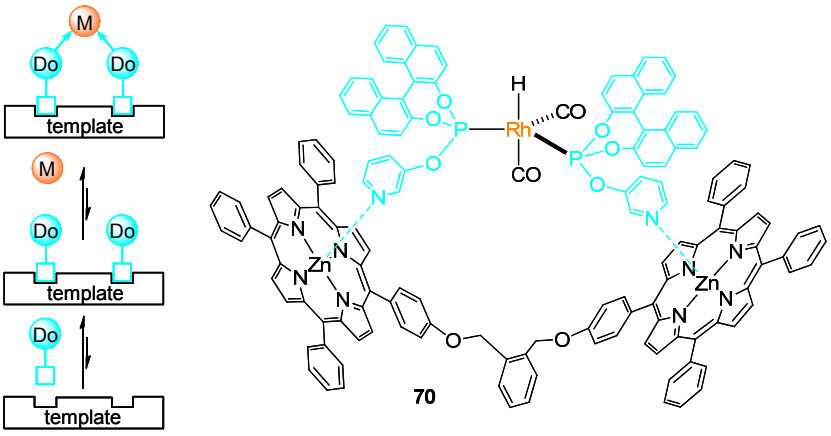

Figure II-1. Illustration of a templated three-component bidentate ligand (left) and Reek's transition metal catalyst **70** (right) formed from a dimeric Zn(II) porphyrin template, a pyridine/BINOL-derived phosphite, and [Rh(acac)$(CO)_2$] under syn gas (1/1 H_2/CO).[27]

Following this work, the same authors reported in 2007 a variation of the template principle indicated in Figure II-1 by using a dihydroxotin(IV) bis-porphyrin platform together with carboxylic phosphorous ligands.[28] The decisive binding motif was realised through the selective coordination of the carboxylate oxygen to Sn(IV). These ligands showed good performance in the Rh-mediated hydroformylation of 1-octene by increasing the catalyst's activity, making it up to forty times faster relative to the untemplated monodentate analogues.

Bis-zinc(II) porphyrin platforms were not the only templates of interest to Reek and van Leeuwen. Another approach focused on more rigid bis-Zn(II) salphen building blocks for the formation of homobidentate[29] as well as heterobidentate ligands **75**.[30] The formation of the latter is shown in Scheme II-7, although the principle is the same for homobidentates which simply require the assembly of two identical monodentate building blocks on the salphen template. Contrary to what could be expected, only the hetero-combined complex was observed by ^{31}P NMR spectroscopy when mixing bis-Zn(II) salphen **71** with ligands **73** and **74**, whereas only the homocombinations were found in complexes without the template. The origin of this selective heterocomplex formation was assumed to be of steric nature since no electronic alterations were included in the templation process. Moreover, the heterobidentate ligands showed higher enantioselectivities (combination of **72** and **73**, 72% ee (*S*), *b*/*l* ratio = 9.2) but often lower activities (19% conv. after 87 h for the same combination) in the asymmetric hydroformylation of styrene than the homobidentate (combination of **74** and **74**, 13% ee (*S*), *b*/*l* ratio = 13.5, >99% conv. after 16 h) or untemplated mixed ligand combinations (combination of **73** and **74**, 10% ee (*S*), *b*/*l* ratio = 12.0, >99% conv. after 87 h).

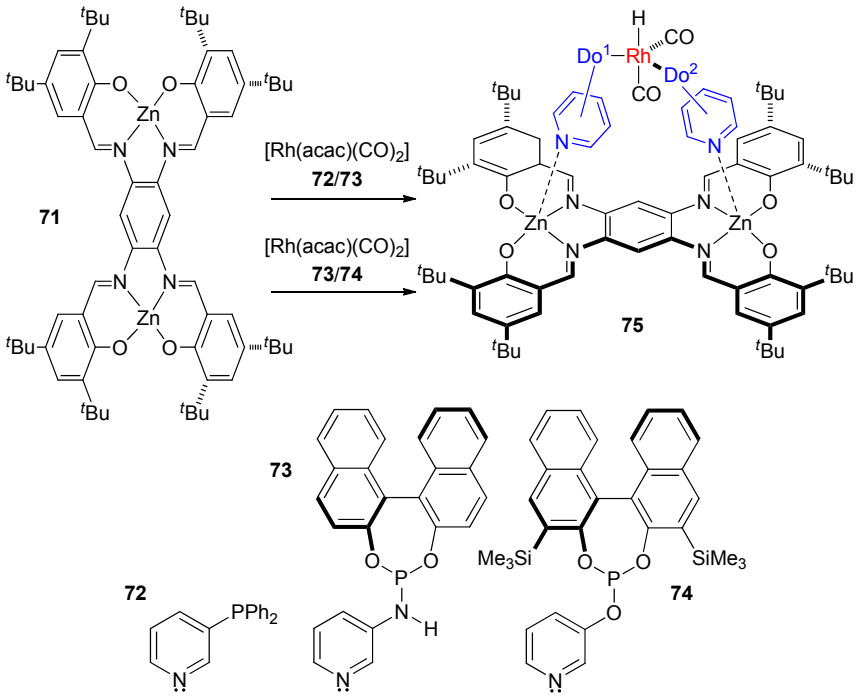

Scheme II-7. Rhodium catalyst formed on a rigid bis-Zn(II)-salphen template **71** from the phosphorous ligands **72**-**74** and $[Rh(acac)(CO)_2]$.[30,31]

Naturally, as was indicated earlier, the bis-Zn(II) salphen template can also be utilised in the formation of homobidentate ligands. Rhodium catalysts derived in that manner from the homocombinations of ligands similar to those shown above were applied in the hydroformylation of 1-octene and styrene, the asymmetric hydrogenation of α-methylcinnamic acid and dimethyl itaconate. However, it was also observed that a more rigid template like bis-Zn(II) salphen does not necessarily lead to better catalytic performances than the more flexible bis-zinc(II) porphyrin.[29]

In the latter two examples, the templates constituted large platforms on which the actual ligands were assembled. However, the template does not necessarily have to be of highly sophisticated structure. Again making use of the excellent zinc(II) porphyrin-amine binding motif, Reek, van Leeuwen, and co-workers prepared multicomponent porphyrin assemblies **78** templated by ditopic 1,4-diazabicyclo[2.2.2]octane (DABCO) **77** (Scheme II-8).[32,33] Although the resulting catalyst was not suitable for asymmetric transformations due to the absence of stereogenic elements, it shall be introduced here briefly owing to its typical supramolecular behaviour. Two tris(zinc(II) porphyrin)phosphite ligands coordinated to rhodium in a sandwich-like fashion in the presence of at least three equivalents of DABCO. The resulting catalyst was applied to the hydroformylation of 1-octene and showed excellent regioselectivities in favour of the linear aldehyde under mild conditions (*l*/*b* ratio = 22.8 at 30 ºC). Supramolecular forces are generally stronger at moderate temperatures. This presumably allowed the DABCO template to better enforce the geometrical disposition of the phosphites enabling them to act as chelating ligands.

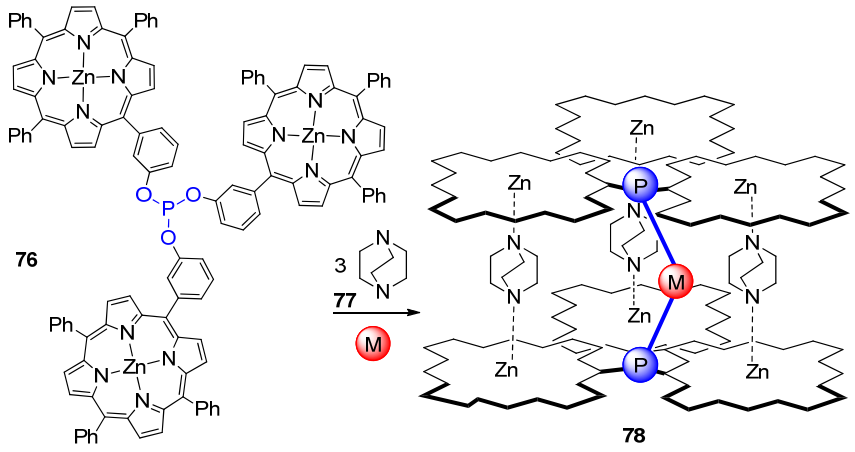

Scheme II-8. Concept of the assembly of a multicomponent catalyst **78** from tris(Zn(II) porphyrin)phosphite **76**, the DABCO template **77**, and a transition metal source M.[32]

Although the template-assisted formation of supramolecular bidentate ligands *via* metal-ligand interactions has proven to be a powerful strategy, it is not stringently necessary to use a template. The successful assembly of such untemplated chelating ligands *via* direct interactions between monomeric ligand building blocks was introduced in 2004 by Reek, van Leeuwen, and co-workers.[34] Again the zinc(II) porphyrin-pyridyl binding motif was used in order to create ligand libraries of the fittingly called SUPRAPhos family (Figure II-2). The first library of 6×8 members gave rise to 48 different chelating ligands, thus demonstrating the applicability of this approach for combinatorial and screening techniques. The binding properties were studied for the representative ligand combination **79a·80b**. UV-vis titrations allowed the determination of the association constant of the pyridyl moiety to the zinc(II) centre ($K_{\mathbf{79a\cdot 80b}} = 3.8 \times 10^3\ M^{-1}$) and revealed the behaviour as a chelate resulting in an increased value of K in the presence of a Rh-source ($K = 64.5 \times 10^3\ M^{-1}$). This value corresponded to a chelate energy of 7 kJ/mol. ^{31}P NMR Spectroscopy confirmed the bidentate coordination mode and the exclusive formation of the heterocomplex.[34,35] This library was subsequently amplified and screened in the Rh-mediated enantioselective hydroformylation of styrene (preference for the branched aldehyde),[36] the Rh-mediated regioselective hydroformylation of styrene forming the linear aldehyde,[37] the enantioselective Pd-mediated allylic alkylation of *rac*-1,3-diphenylallyl acetate **90** using dimethyl malonate **91** as the nucleophile (Scheme II-9A),[35] the challenging asymmetric hydrogenation of a difficult enamide substrate **93** (Scheme II-9B),[38] and the Pd-mediated kinetic resolution of *rac*-cyclohexenyl acetate **95** (Scheme II-9C).[39]

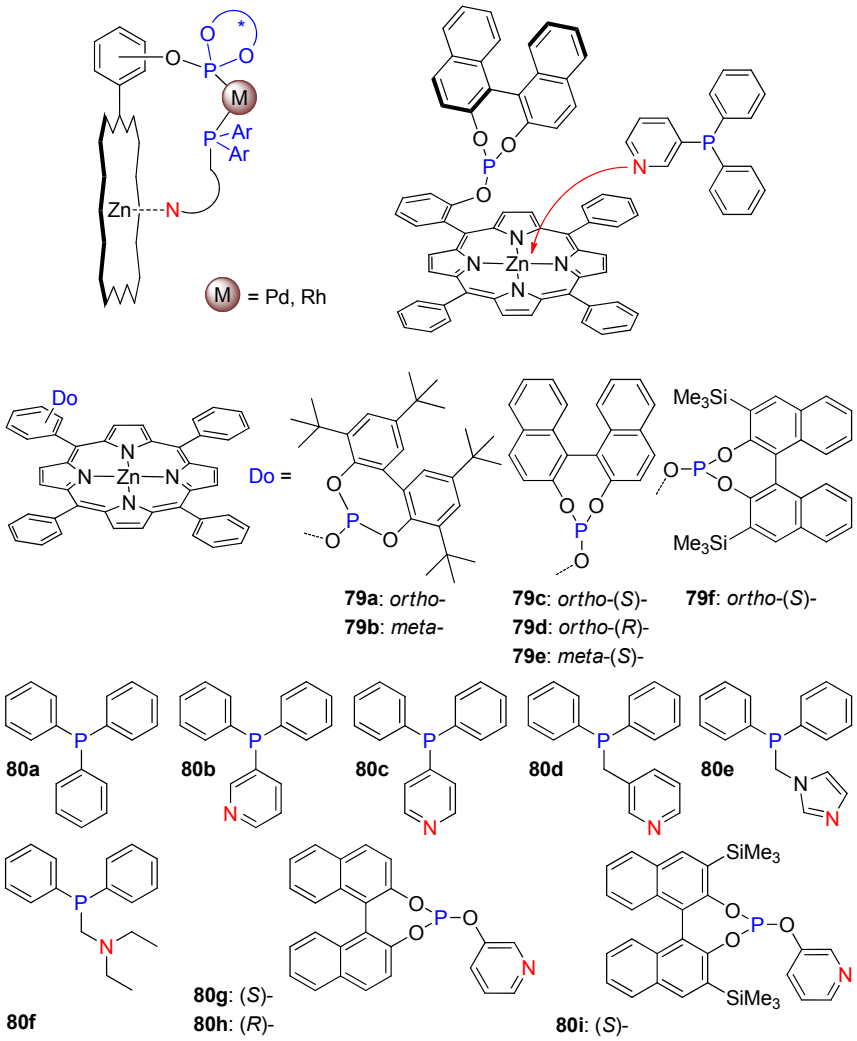

Figure II-2. Assembly of a SUPRAPhos ligand with building blocks **79c** and **80b** (top) and library of constituent phosphite-functionalised porphyrins **79a-f** and monodentate phosphorous ligands **80a-i** (bottom).[34,35]

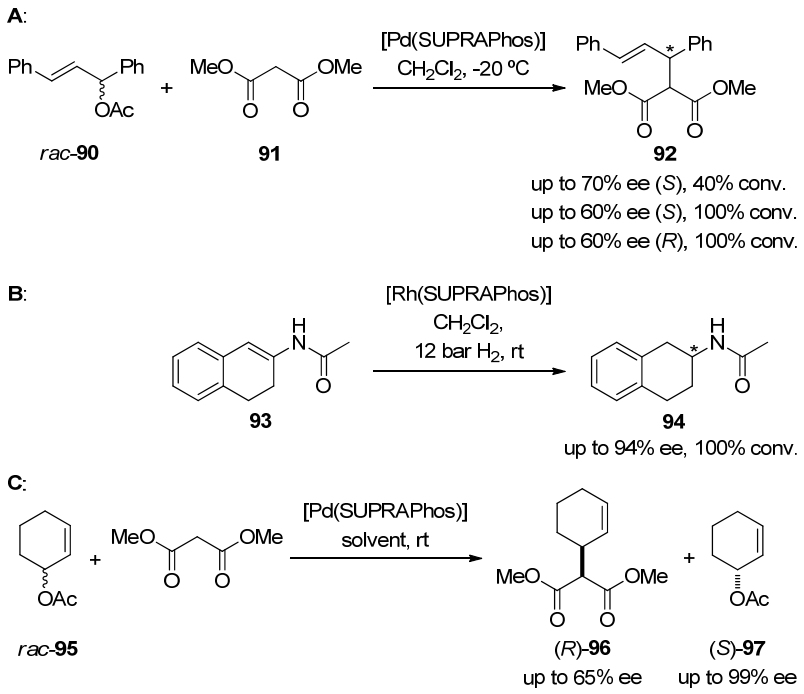

Scheme II-9. SUPRAPhos ligands in catalytic applications.[31, 35, 38, 39]

The demand for new combinatorial and modular strategies in catalyst research was also addressed by Takacs and co-workers who reported in 2004 the development of modular bimetallic catalysts based on chirality-directed self-assembly of bifunctional subunits around a structural metal (Figure II-3).[40] Key to their approach was the metal-directed self-assembly of the ligand backbone in a final step. Thus, avoiding covalent chemistry at the often crucial ligand backbone of the catalyst allowed the rapid construction of a library of structurally diverse bidentate bisphosphite ligands.

Bisoxazoline (BOX) ligands with pendant TADDOL-derived phosphites were chosen to serve as binding motifs for the structural zinc(II) centre. Heteroleptic complexes were exclusively formed by employing "racemic" or "pseudoracemic" mixtures of the BOX ligands driven by chiral self-discrimination in the tetrahedral zinc(II) complexes (Figure II-4), as zinc-bisoxazoline complexes involving two units of either (*S*,*S*)-BOX or (*R*,*R*)-BOX turned out to be less stable than the corresponding heteroleptic dimers.[41,42] Coordination of the TADDOL-phosphite in the envisaged mode to catalytically active metals was confirmed by ^{31}P NMR spectroscopy after addition of one equivalent of $[Rh(COD)_2]BF_4$ to the self-assembled ligand (SAL) SAL-**98bb**.

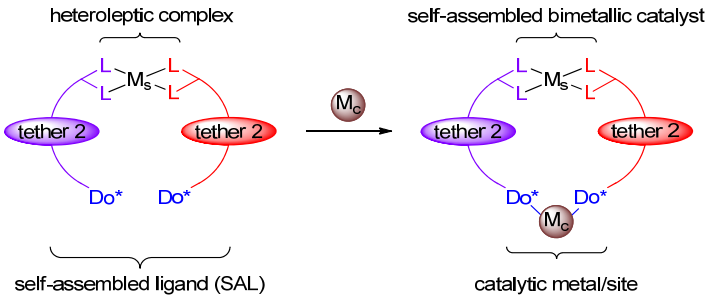

Figure II-3. Self-assembly of bimetallic catalysts guided by a structural metal (M_s) and incorporation of a catalytic metal (M_c) according to Takacs.[40]

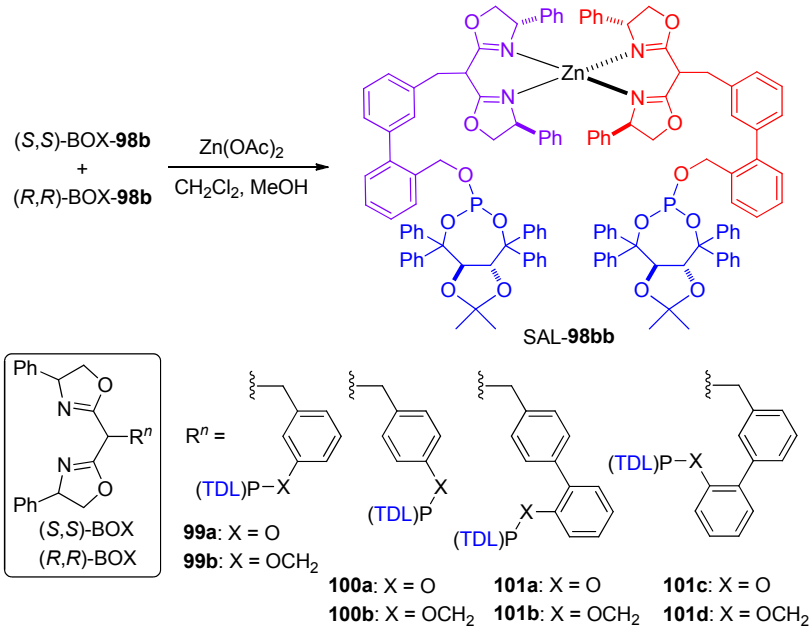

Figure II-4. Preparation of the chiral diphosphite Zn(BOX-**98bb**) (top) and selected bifunctionalised BOX-(TADDOL)phosphite conjugates, (TDL) = (*R*,*R*)-TADDOLate (drawn in blue in the SAL-**98bb** structure).[40]

Takacs *et al*. prepared a library of 50 combinations of SALs varying mostly in their backbone scaffold and screened them in the Pd-mediated allylic amination of the racemic carbonate **102** with various toluenesulfonamides (Scheme II-10A). Nine combinations were found to furnish ee's of 90% or higher (97% ee (*R*) with the combination **101b** with **101d**), thus considerably exceeding their monodentate analogues (48% ee in a test reaction with a related monodentate phosphite).[40]

Subsequently, a library of SALs was tested in the Rh-mediated (asymmetric) hydroboration of sterically and electronically diverse styrene derivatives **104** (Scheme II-10B).[43] Generally good regioselectivities in favour of the branched product with enantioselectivities up to 96% ee (*R*) for 2-methoxystyrene were observed when the combination of **101a** and **101c** was used.

Fine-tuning of the catalyst's ligand scaffold allowed the reaction for all of the diverse styrene compounds to be carried out with high regio- (92-99% branched alcohol) and enantioselectivity (91-96% ee).

A different library was prepared in which the TADDOL moiety was substituted by a biphenylphosphine-phosphite ligating scaffold and tested in the Rh-mediated asymmetric hydrogenation of methyl (*Z*)-2-acetamidocinnamate **107** (Scheme II-10C).[44] The BIPHEP moiety was first identified amongst other phosphorous ligands as the lead structure for the optimisation of new SAL scaffolds and the best catalyst assemblies yielded up to 97% of the hydrogenated product in up to 81% ee.

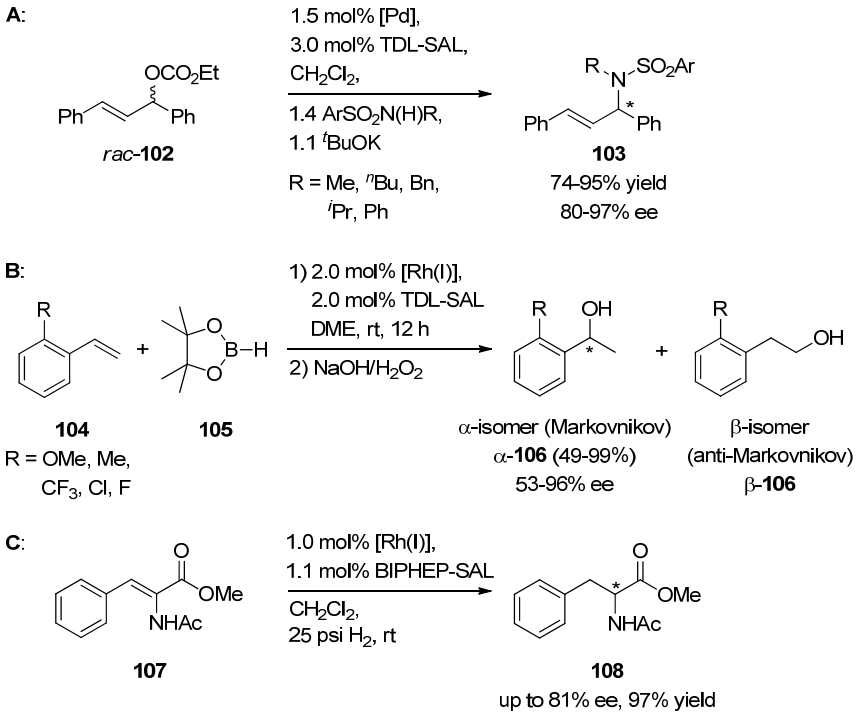

Scheme II-10. Asymmetric catalytic transformations using Takacs' self-assembled ligands (SALs).[40]

The templating effect of a structural metal was used by Gudat and co-workers. In 2007 they reported the template controlled self-assembly of ditopic catechol phosphane complexes with hemilabile coordination behaviour (Scheme II-11).[45] Key to their strategy was the ditopic ligand **109**[46] bearing hard catecholate and a soft phosphane binding site. Complexes **110** were prepared in one pot syntheses by selective coordination of catecholate to the hard main group metal tin(IV) and the phosphanes to the soft transition metal palladium(II). The structure of **110a** was elucidated by single crystal diffraction clearly showing the μ_2-oxo-bridge connecting the two metal centres. Interestingly, this complex showed hemilabile behaviour upon cooling to -55 ºC. Reversible formation of a second species **110a'** was detected by low temperature ^{31}P NMR spectroscopy attributed to dynamic exchange between the two species. The authors assumed that **110a'** arose from the binding of extra solvent molecules by either Pd or Sn. DFT calculations were carried out to model the interaction of **110a** with formamide in the gas phase, which revealed that the coordination of formamide to Pd like in **110a'/b'** was energetically favoured by 3.6 kcal mol^{-1} over the binding of formamide by the Sn metal centre. These findings supported the assertion of a macrocyclic structure with *trans* configuration at the palladium. Thus, the Pd centre can switch between tetradentate O_2P_2 and bidentate P_2L_2 coordination modes.

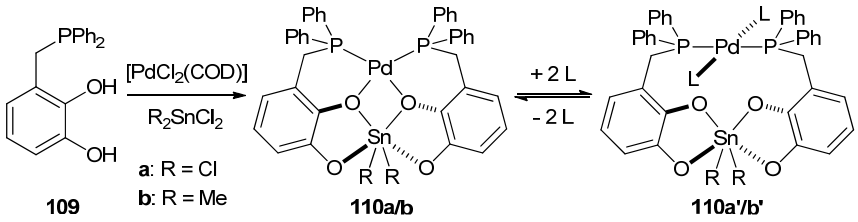

109 **110a/b** **110a'/b'**

Scheme II-11. Molecular bimetallic chelate complexes **110** through self-assembly of catechol based phosphanes **109**, L = solvent (DMF or formamide).[45]

In the same year Gudat *et al*. reported also the preparation of boron templated bidentate catechol phosphanes and their use as ligands in Ag(I) complexes (Scheme II-12A).[47] In contrast to the previous strategy, the synthesis of Ag(I) complexes required the pre-formation of the isolable self-assembled chelate ligand. The rigidity of these new ligand entities was said to be sufficient to lead to specific bite angles (spanned by the two phosphorous atoms and the transition/catalytic metal).

The latter was proven recently by an extension of their approach in which several tri- or tetravalent main group and transition metals of varying atomic radii were used as templating metals (Scheme II-12B).[48] The one-step syntheses were carried out in DMF by treating mixtures of the catechol phosphane, $[PdCl_2(COD)]$, and the chloride of the structural metal M_s with excess triethylamine. The resulting complexes **111** were characterised by single crystal X-ray diffraction and NMR studies. Interestingly, applying zirconium tetrachloride as template source yielded a trinuclear complex **112** including one zirconium and two palladium atoms (Scheme II-13). The octacoordinated Zr(IV) centre templated four catechol phosphane moieties in a pairwise fashion, *i.e*. the structure could be described as a dimer formed from two subunits (structures like those found for the main group metal complexes) under elimination of one of the transition metal centres.

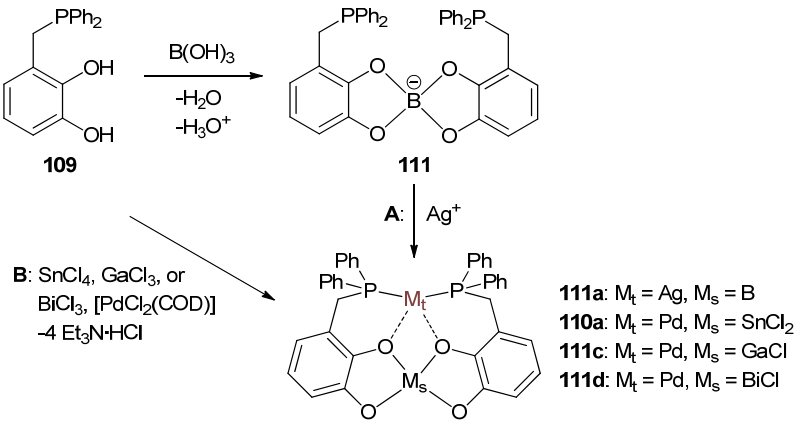

Scheme II-12. Preparation of boron and main group metal templated catechol phosphane chelate complexes through self-assembly.[48]

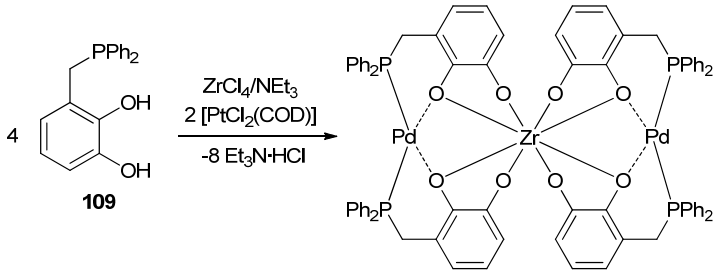

Scheme II-13. Formation of the mixed Pd-Zr trinuclear complex **112**.

The authors also rationalised the variation of the wide P-Pd-P and more acute O-Pd-O bite angles (Table II-1) on the basis of the templates' size, valence, and coordination numbers. Furthermore, it was pointed out that the variation of O-Pd-O bite angles amounting to 5º was well within the variation ranges found for natural bite angles in bisphospholane ligands in which the geometry of the P-C-C-P backbone was determined by rigid hetero- or carbocyclic structures.[49] However, taking into account that the strong preference of Pd(II) centres for square-planar coordination geometries imposes certain restrictions upon the chelate ligands, it may be assumed that the potential variability in the supramolecular frameworks is much larger.

Table II-1. Comparison of covalent radii and coordination numbers of the template metal with observed average phosphorous interatomic distances [Å] and bite angles [º].[48]

	M_m	r_{cov} [a]	C.N.[b]	P···P [Å]	P-Pd-P [º]	O-Pd-O [º]
111c	Ga	1.25	5	3.489	101.8(1)	74.3(1)
110a	Sn	1.40	6	3.419	98.8(1)	77.0(1)
112	Zr	1.45	8	3.404	99.7(1)	75.1(1)
111d	Bi	1.52	7	3.380	97.1(1)	79.7(2)

[a]Data from ref. [50]. [b]C.N. = effective coordination number, including a lone pair for Bi(III).

In summary, the application of metal-ligand interactions in coordinative complexes has enabled the preparation of highly sophisticated supramolecular assemblies under pronounced control of stereochemical aspects. Crucial in all these approaches has been the identification and utilisation of suitable binding motifs. Chiral induction transmitted by metal-ligand interactions has been used in chiral sensors and chiral reporters, respectively, often used in the determination of absolute configurations of organic molecules. The asymmetric environment at catalytic centres has been shaped and amplified not only by the coordination of chiral ligands but also by achiral ones flexible enough to adopt chiral conformations upon coordination to a metal. It has been demonstrated that bimetallic complexes including catalytically active metals can be prepared by careful choice of the underlying binding motifs. Finally, ligand self-assembly driven by metal-ligand interactions has proven to be one of the most promising approaches in modern catalyst research, which, in spite of all efforts of rationalising catalyst design, still far too often depends on trial and error or serendipity, thus, demanding new strategies for the fast and efficient creation of ligand libraries. Solutions have been found for one of the longstanding problems of asymmetric catalysis, namely the facilitation of bidentate ligand preparation relying on highly efficient self-assembly processes. However, to the best of our knowledge, so far no reports

about methodologies allowing the transfer of chiral information contained in simple building blocks *via* metal-ligand interactions into remote prochiral catalytic building blocks have been given. The indispensable combination of several aspects such as finding suitable binding motifs, structural and catalytic metals, the realisation of geometries suitable for the desired chirality transfer, and the control of dynamic processes usually coming with non-covalent forces, make such a project challenging.

2 Preliminary Considerations

As pointed out in the general introduction, hydrogen bonding is just one of several possible reversible interactions in the continuum between the bound and unbound state of two or more molecules (see Introduction Scheme 2). Metal-ligand interactions represent another reversible force that may be used for the formation of new chiral supramolecular ligands. It is indeed a frequently used binding motif and examples from the literature can be found in the several review articles[31,33,51-53] and the references given in the preceding literature section. Generally, molecular complexes that are formed by metal-ligand interactions are of higher stability than those based on hydrogen bonds. The simple reason of which is the binding strength of the underlying force. Analogous to Figure I-1, the concept of transferring chirality by metal-ligand interactions can be summarised as the interplay of three linked components: i) the dynamically racemic building block, ii) the chiral building block, and iii) the mediating structural metal centre (Figure II-5).

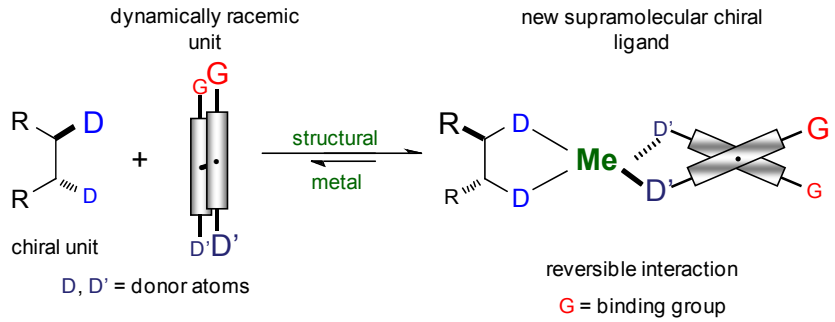

Figure II-5. Schematic concept for the transfer of chirality using metal-ligand interactions.

Regarding the dynamically racemic building blocks, the same considerations that were pointed out in chapter I remain valid here. Again 2,2'-biphenol derivatives were the compounds of choice for the introduction of atropisomerism. We presumed that the coordination of the BIPOL *via* its oxygen atoms to a suitable metal centre would allow the formation of seven-membered chelate rings of sufficient strength and rigidity to hold the biphenol in a chiral conformation. However, some further criteria regarding the properties of the dynamically racemic 2,2'-biphenols, in particular the *ortho*-substituents relative to the hydroxyl groups had to be taken into account. Whilst in the hydrogen-bonding approach these substituents were first and foremost responsible for polarising the oxygen-hydrogen bond, this was of no importance for the metal-ligand interactions. Phenols are generally acidic enough to readily yield the phenolate with one of the various available bases. Thus, the intended role of the *ortho*-substituents was limited to affect the steric demand during the complexation. Of the earlier introduced 2,2'-biphenols (Scheme I-22) the nitro compound **44a** was not found suitable for this strategy. Thus, only the 2,2'-biphenols **44d** (no *ortho*-substituent) and **44b** (*ortho*-Me substituent) were used. Additionally, the bulky iodine-substituted biphenol **44e** (Scheme II-15) was also studied here, albeit to a less extent.

The criteria for choosing the chiral building blocks were basically the same as those for the hydrogen-bonding approach, *i.e*. they should be broadly available at reasonable cost and easy to modify with reasonable preparative effort. Thus, again enantiopure 1,2-diamines were the compounds of choice. Whereas before it was their capability of readily forming hydrogen bonds, here the excellent coordinative behaviour of the amino donor group, especially to hard metal centres, was of main interest.

Some considerations regarding the nature of the structural metal centre should be discussed. Naturally, the metal of choice should not be catalytically active in later transformations of interest. In the case of our group, these include for example asymmetric allylic alkylations and aminations, respectively, and particularly asymmetric hydrogenations. Thus, the structural metal must show low affinity to the binding groups typically used in the respective catalysts in order to not compete for these binding groups with the catalytically active metal. Referring to enantioselective hydrogenations, these would predominantly be phosphorus containing chiral ligands[54] in Rh,[55-57] Ru,[58-60] and Ir[61-63] complexes. Amongst the many success stories, enantioselective hydrogenations of different substrates such as imines,[64] amino ketones,[65] aromatic and heteroaromatic compounds,[66,67] and minimally functionalised terminal alkenes[68] can be found. Nowadays, reactions of these types are of enormous relevance to industry.[69-71] Furthermore, with Knowles[72] and Noyori[73] two of the main protagonists of this research field were awarded with the Nobel Prize in 2001 (together with Sharpless[74] who was awarded for his work on catalytic asymmetric epoxidations).

Moreover, to realise systems as depicted in Figure II-5, metal centres favouring fourfold coordination and ideally adopting the tetrahedral geometry were preferred in order to best take advantage of the transfer of chirality. It was reasoned that said transfer in planar-quadratic or octahedral complexes would be inferior to that in tetrahedral ones. These prerequisites would most likely be fulfilled by metal centres with an electron configuration of either d^0, like Ti(IV) and Zr(IV), or d^{10}, like Zn(II), and, to a lesser extent the d^9 configured Cu(II). It is known that the titanium d^0 configuration often forms polynucleic complexes with alcoholates such as BINOLate. Many of these structures have shown catalytic activity especially in aldol addition reactions and the enantioselective addition of alkyl groups to

aldehydes.[22,75-77] Usually these complexes are formed by mixing enantiopure BINOL or its derivatives and varying proportions of titanium tetraisopropoxide. Moreover, the complex solution behaviour of such mixtures has been studied and a strong dependence on the BINOL/Ti(O^iPr)$_4$ ratio was reported for the variety of species present in solution.[78-80] However, both phenomena had to be avoided in our project since defined complexes of 1:1:1 (prochiral block/structural metal/chiral block) stoichiometries were desired. On the other hand Walsh *et al.* reported the formation of chiral zinc(II) complexes using enantiopure 2,2'-BINOL and achiral or *meso* diimines and diamines, respectively, as ligands.[20] The purpose of their work was to prove that the optimisation of catalyst enantioselectivity and catalytic activity could also be achieved by the modification of achiral and *meso* ligands instead of the more traditional approach of synthesis and screening of chiral ligands. In some cases the ligands were capable of amplifying or extending the asymmetric environment around the zinc(II) centre by adopting chiral conformations. Furthermore, they showed that the latter ligands were the most efficient in increasing the enantioselectivity of the zinc catalysts they used in the addition reaction of diethylzinc to benzaldehyde.

Consequently, zinc(II) seemed to be the most promising of the above mentioned metals and was therefore chosen as the structural metal for the complexation with dynamically racemic 2,2'-biphenols and chiral 1,2-diamines. Regarding the zinc(II) source, three were tested (Scheme II-14): i) diethylzinc, as it was used by Walsh and served as both, the zinc source and deprotonating agent for the BIPOL derivative (method A), ii) zinc bis(bis(trimethylsilyl)amide) ($Zn[N(SiMe_3)_2]_2$) **113** was used as the zinc source and without requiring an additional base for the deprotonation of the BIPOL derivative (method B) and iii) the BIPOL derivative was first deprotonated with NaH and subsequently treated with a preformed [$ZnCl_2$(diamine)] complex (method C).

Darensbourg and co-workers reported the use of $Zn[N(SiMe_3)_2]_2$ **113** for the preparation of Zn(II) phenolates that were capable of binding two pyridine ligands per zinc centre.[81] The groups of Lee and Roh both published structures of $[ZnCl_2((1,2)\text{-DACH})]$ complexes derived from the reaction of $ZnCl_2$ with 1,2-DACH derivatives,[82,83] which were assumed to be suitable precursors for method C. In the following the formation of new zinc(II) coordination complexes according to the named methods is described.

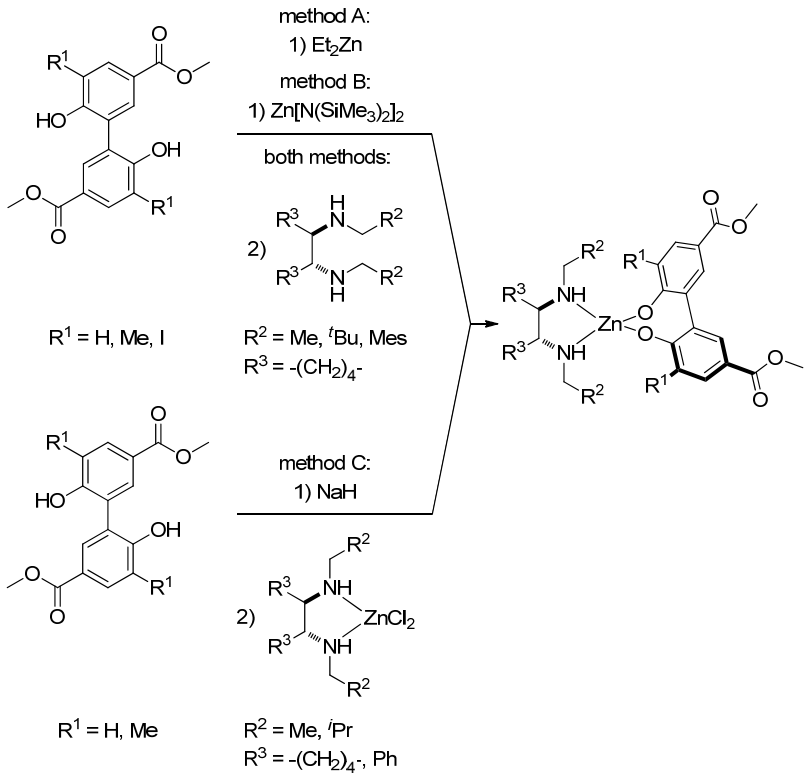

Scheme II-14. Strategies for the formation of new chiral zinc(II) complexes from simple building blocks.

3 Results and Discussion

3.1 Synthesis of Building Blocks

The synthesis of the dynamically racemic 2,2'-biphenol (see Scheme I-22) and the chiral 1,2-diamines (see Scheme I-23) was described in detail in chapter I. Therefore, only a minor complement is necessary here. In addition to the already introduced 3,3'-methyl-substituted biphenol **44b** and the 3,3'-unsubstituted biphenol **44d**, complexation studies were carried out with the 3,3'-iodo-substituted biphenol moiety **44e**. It was obtained straightforwardly by iodination of **44d** following the same protocol as for precursor **49** (Scheme II-15).[84]

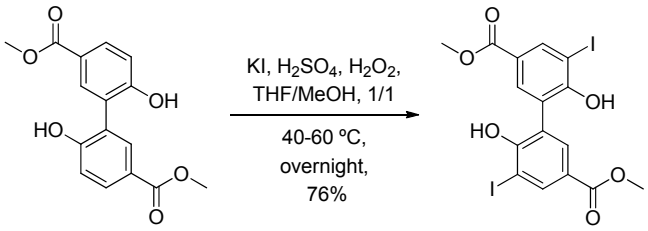

44d **44e**

Scheme II-15. Preparation of the *ortho*-iodinated biphenol **44e**.

3.2 Zinc as the Structural Metal

3.2.1 Complexation methods

As is depicted in Scheme II-14, the new supramolecular chiral [Zn(2,2'-biphenolate)(1,2-diamine)] complexes were formed following one of the three strategies A, B, or C. Whilst method A and B were very similar and did not require an additional base for the deprotonation of the BIPOL moiety, method C was inherently different.

Method A was the first to be tested. Preparations following this method had to be carried out under inert atmosphere by dissolving the BIPOLs **44b** and **44d** in dry THF and subsequently adding 1.1 equivalents of diethylzinc. The resulting mixtures were stirred for about 1 h before 1 equivalent of enantiopure diamine **45** was added dissolved in THF. The advantage of this procedure was that it was clean and simple. No additional base was required since diethylzinc irreversibly deprotonated BIPOL derivatives with ethane release. In several cases crystals suitable for X-ray analysis were obtained under inert conditions by slow diffusion of *n*-hexane into a solution of the crude material in either THF or CH_2Cl_2. Unfortunately, at an early stage of the project, this method suffered heavily from reproducibility problems particularly related to the behaviour in solution. Although it could not be fully proven, we believe that the reaction mixtures were very sensitive towards traces of water or a possible larger excess of diethylzinc. This mostly affected the characterisation of the complexes by NMR, UV-vis, and CD spectroscopy as is exemplified in the respective sections. At any rate these problems could be largely overcome by working under inert conditions in a glove box.

Since the initial experiments following method A long suffered from low reproducibility, an alternative was searched for. Darensbourg and co-workers used $Zn[N(SiMe_3)_2]_2$ for the preparation of aggregates of zinc phenolates which were then reacted with propylene carbonate or pyridine.[81] For the latter they reported a tetrahedral structure in which zinc(II) was coordinated by two phenolate and two pyridine moieties each. This approach seemed promising and therefore we prepared $Zn[N(SiMe_3)_2]_2$ according to standard procedures and stirred it in THF under inert conditions with the BIPOLs **44b**, **44d**, or **44e** and enantiopure diamines **45**. Again, the structure of several of the complexes could be determined by X-ray analysis from crystals grown under similar conditions as mentioned previously. As for method B, the use of $Zn[N(SiMe_3)_2]_2$ as a zinc source and deprotonating agent was straightforward and clean, leaving only the readily extractable bis(trimethylsilyl)amine as the by-product. Additionally, exact amounts of $Zn[N(SiMe_3)_2]_2$ could easily be measured and the reaction seemed to be less sensitive towards a possible excess of the zinc reagent or traces of water. Overall, method B provided a very practical and reliable procedure for the preparation of the [Zn(2,2'-biphenolate)(1,2-diamine)] complexes. Due to their similarities the two methods are summarised together in Scheme II-16. Comparison of crystallographic and IR data demonstrated unequivocally that both procedures lead to the same products which will be discussed in the following discussion.

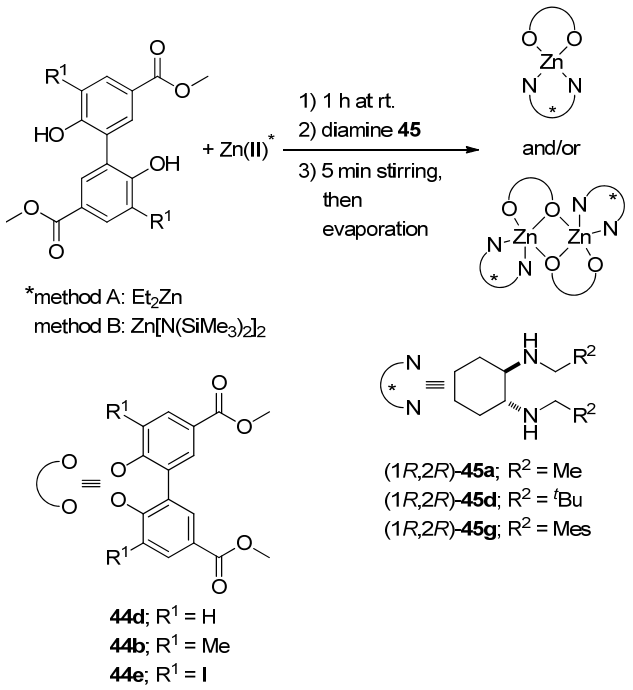

Scheme II-16. Synthetic strategy for the preparation of [Zn(2,2'-biphenolate)(1,2-diamine)] structures using either diethylzinc (method A) or $Zn[N(SiMe_3)_2]_2$ (method B) as zinc source.

Also initially conceived as an alternative to the rather delicate method A, procedure C was elaborated. Most of the initial problems using method A were thought at that time to be associated with the characterisation of the reaction products, *i.e.* it was proven that at least one chiral species was formed but its structure could not be elucidated. Thus, we reasoned that a procedure allowing the formation of well defined and isolable precursors could close that gap. Lee and Roh reported the solid state structure of $[ZnCl_2(1,2\text{-DACH})]$ complexes that were prepared by simply mixing $ZnCl_2$ and 1,2-DACH derivatives.[82,83] We considered the formation of such complexes in order to obtain the desired new chiral structures by the reaction of $[ZnCl_2(1,2\text{-DACH})]$ complexes with biphenolate derivatives as is shown in Scheme II-17.

The driving force of this complexation would be the precipitation of NaCl which greatly favoured the binding event under inert conditions. However, the salt formation turned out to be disadvantageous since NaCl could not be removed easily from the reaction products. Furthermore, using NaH as base was complicated due to difficulties of handling the small quantities that were required here. This constituted a serious problem and with time, method C was abandoned as the other two methods were easier to control. Consequently, this strategy was not studied in-depth and is addressed only briefly at the end of this section.

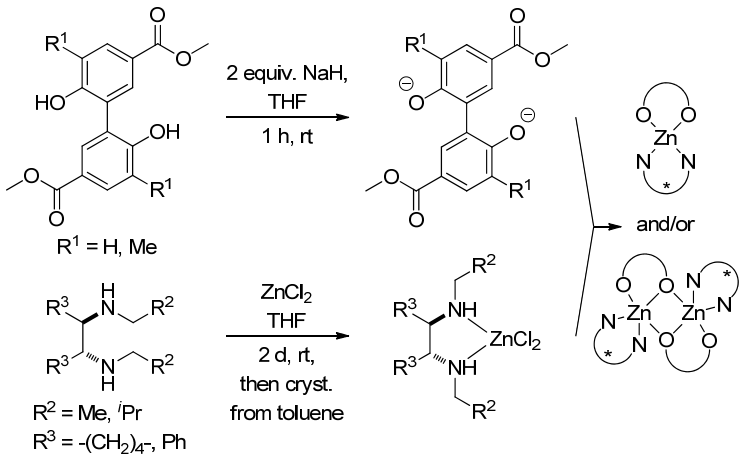

Scheme II-17. Synthetic strategy for the preparation of [Zn(2,2'-biphenolate)(1,2-diamine)] structures using NaH as base and a preformed [$ZnCl_2$(1,2-diamine)] complex (method C).

Single crystal analysis of complexes prepared according to methods A and B generated some unexpected results. Apparently biphenol **44b** bearing 3,3'-methyl substituents, favoured crystallisation as mononuclear complex of 1:1:1 (biphenolate/Zn(II)/diamine) stoichiometry whilst the 3,3'-unsubstituted **44d** predominantly formed dinuclear 2:2:2 complexes in the solid state. Surprisingly, this was largely independent from the steric bulk of the N-substituent of the diamine. Since this appeared as an inherent property of the complexes

it is feasible to classify them according to their mono- and dinuclear nature in the solid state.

3.2.2 Mononuclear zinc complexes of type [Zn(44b)((1*R*,2*R*)-45)].

Preparation of [Zn(Me-BIPOLate)((1*R*,2*R*)-Et-DACH)], complex **114**; [Zn(**44b**)((1*R*,2*R*)-**45a**)]

The complex [Zn(**44b**)((1*R*,2*R*)-**45a**)] (**114**) depicted in Scheme II-18 is one of the best characterised of all the complexes in this series. Owing to its good crystallisability, which allowed both single crystal and powder X-ray diffraction analysis, and the NMR analysis, it can be seen as a model complex. Furthermore, thanks to its relatively small size and molecular weight it was also the most convenient structure to be studied by computational methods. Scheme II-18 shows the preparation of a complex derived from (1*R*,2*R*)-*N*,*N*'-diethyl-1,2-cyclohexanediamine (1*R*,2*R*)-**45a** and Me-BIPOL **44b** as it was envisaged by the concept. Complex **114** was successfully prepared following methods A and B (see also Scheme II-14). Both routes generated identical products (yields are given in Scheme II-18) as could be demonstrated by crystallographic and IR data. Provisionally, no axial chirality is indicated since the stereodiscrimination, if taking place, could not be foretold at this point by merely knowing the configuration of the chiral inducer.

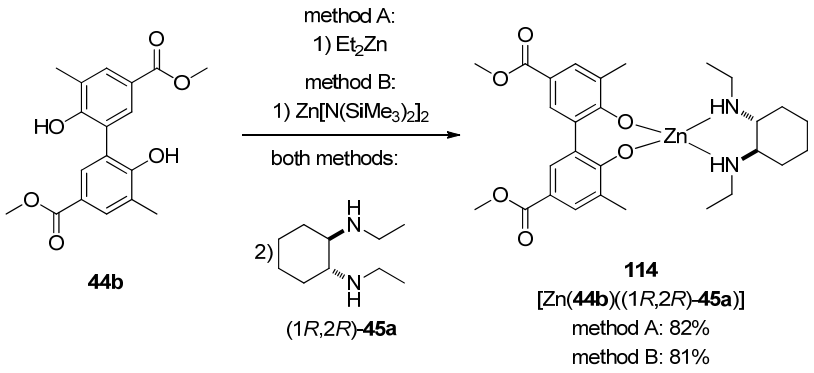

Scheme II-18. Preparation and proposed structure of [Zn(Me-BIPOLate)((1*R*,2*R*)-Et-DACH)]; complex **114**.

In order to determine the solid state structure of compound **114**, a freshly prepared sample was crystallised by diffusion of *n*-hexane into a solution in CH_2Cl_2. An ORTEP plot of the resulting structure is shown in Figure II-6. Complex **114** crystallised in the chiral $C222_1$ space group. Obviously, the space group for complex **114** lacks S_n symmetry operators, since enantiopure diamines were used in their preparation. The structure found was in agreement with the proposal in Scheme II-18. The configuration of the BIPOLate was found to be a*R*, *i.e.* the (1*R*,2*R*)-diamine induced a*R* sense of rotation and the complex is referred to as a*R*-**114** in the following. Apart from co-crystallised solvent molecules (CH_2Cl_2) the asymmetric unit does not contain any other structures, which demonstrates that all biphenol units in the crystal are of the same configuration. The diamine nitrogen atoms became tetrahedral and thus stereogenic upon binding to zinc(II). Having their hydrogens pointing towards opposite directions, both N-atoms adopted the *S* configuration and diamine (1*R*,2*R*)-**45a** is coordinating in C_2-symmetric manner. The zinc(II) centre itself is present in a *quasi*-tetrahedral environment.

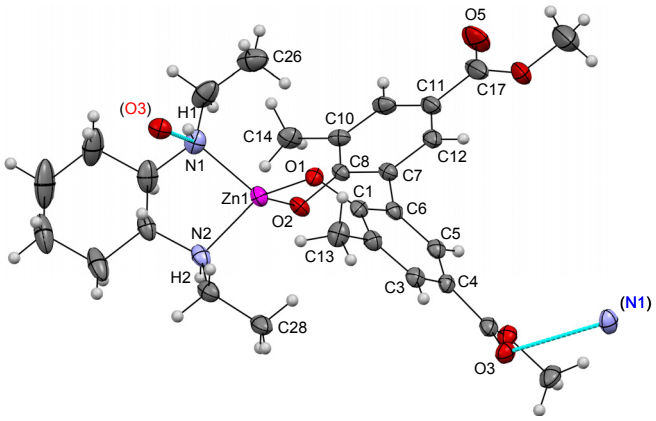

Figure II-6. ORTEP plot of complex a*R*-**114** with partial atomic numbering scheme. Ellipsoids are at the 50% probability level, hydrogens are drawn as size-fixed spheres of 0.15 Å radii, solvent molecules are omitted for clarity, teal lines indicate hydrogen bonding to the O(3) atom and N(1)H group of neighbouring complex molecules.

Selected atom distances, angles, and torsion angles of complex a*R*-**114** are given in Table II-2. The Zn-N(1) and Zn-N(2) distances (entries 1, 2) are comparable to those found in the [$ZnCl_2$(1,2-diamine)] complexes of Lee and Roh, as well as Walsh's [Zn(BINOLate)(1,2-diamine)] complexes. The Zn-O(1) and Zn-O(2) distances (entries 3, 4) are also similar to the ones reported for the latter structures and furthermore match those observed for the phenolate ligands by Darensbourg.[81,85] The acute angle spanned by Zn and the two N-atoms (entry 5) on the one hand and the obtuse one formed by Zn and the two O-atoms (entry 6) on the other are slightly wider than those in Walsh's complexes. Interestingly, two distinct torsional angles (entries 7, 8) between the phenyl rings are obtained. This indicates that the rings themselves are not planar but rather distorted. Furthermore, as can be seen by its torsion angle (entry 9), one of the methoxycarbonyl substituents of the Me-BIPOLate is not coplanar with the phenyl ring it is attached to. A possible explanation may be given by the fact that this substituent's carbonyl oxygen O(3) is hydrogen-bonded to the N(1)H

group of a neighbouring complex molecule. The fact that the carbonyl oxygen atom O(5) does not form hydrogen bonds is in agreement with the coplanarity of this group with the phenyl ring (entry 10 in Table II-2).

Table II-2. Selected bond lengths [Å], angles [º], and torsion angles [º] for complex a*R*-**114**.

entry	atom 1	atom 2	atom 3	atom 4	**length**
1	Zn(1)	N(1)			2.058(2)
2	Zn(1)	N(2)			2.054(2)
3	Zn(1)	O(1)			1.921(2)
4	Zn(1)	O(2)			1.923(2)
					angle
5	N(1)	Zn(1)	N(2)		87.1(1)
6	O(1)	Zn(1)	O(2)		103.98(8)
					torsion
7	C(1)	C(6)	C(7)	C(8)	-64.9(4)
8	C(5)	C(6)	C(7)	C(12)	-58.1(3)
9	C(3)	C(4)	C(15)	O(3)	-12.9(4)
10	C(10)	C(11)	C(17)	O(5)	2.6(5)

Crystallographic data for this compound was also collected from crystals obtained from a solution in THF covered with a layer of *n*-hexane. The results are fully in agreement with the above presented ones. This is important since the solution behaviour of these compounds was almost entirely investigated in THF. Furthermore, crystallisation of the compound using the enantiomeric (1*S*,2*S*)-diamine resulted in structures with a*S* configuration in the BIPOL axis (see appendix for the structure of a*S*-**114**). This finding is fully consistent with what could be expected assuming that it is the configuration of the diamine that is determining the induced sense of axial rotation. Thus, it is clearly demonstrated that axial chirality can be induced and controlled in

dynamically racemic Me-BIPOL **44b** by using inexpensive chiral structures like enantiopure 1,2-cyclohexanediamines.

The good crystallisability of complex a*R*-**114** allowed the collection of powder diffraction data from crystalline material obtained from a bulk crystallisation. Powder X-ray diffraction (PXRD) is a rapid analytical technique usually used for the identification of the phases of crystalline material. It can also provide information on unit cell dimensions.[86] By comparison of collected data with that provided by data bases (*e.g.* the International Center for Diffraction Data (ICDD) listed over 300.000 data sets in its 2010 PDF-4+ release) the phase of a certain compound may be identified even in a mixed crystalline specimen, *i.e.* the phase of a crystalline compound can be regarded as its fingerprint. Alternatively, if the single crystal structure is known, the experimentally obtained powder pattern can be compared with that calculated from the crystal structure. This measurement of (crystallographic) sample purity is particularly useful when other techniques like NMR spectroscopy or mass spectrometry cannot provide the required information. Figure II-7 shows the theoretical diffraction pattern calculated from the single crystal structure together with the experimentally found one. As can be seen both data sets are in very good agreement, *i.e.* the only crystalline material present in the sample corresponds to the structure of the measured single crystal. The fact that the theoretical phase appears slightly shifted at larger angles is a consequence of the experimental setup. The powder pattern was obtained at room temperature whilst the theoretical pattern was calculated from a crystal structure that was measured at 100 K. However, this does not affect the conclusions above.

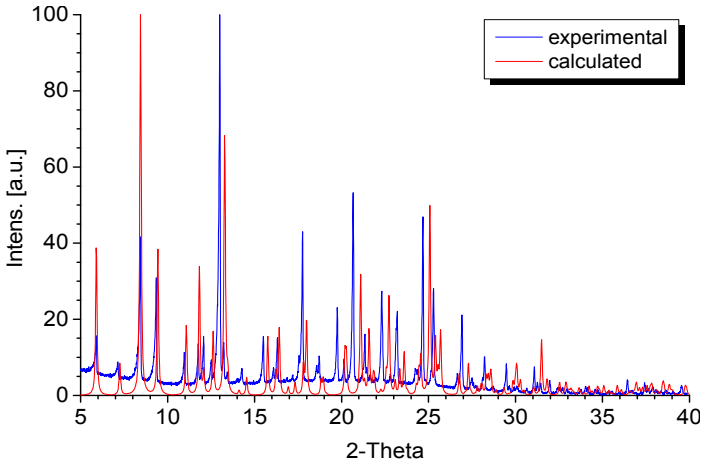

Figure II-7. Experimental (blue) and calculated (red) powder diffraction pattern of complex a*R*-**114**.

IR spectra were recorded from neat samples of a*R*-**114** that were prepared according to methods A (diethylzinc) and B ($Zn[N(SiMe_3)_2]_2$). IR turned out to be a convenient spectroscopic technique to prove the equality and reproducibility of the two methods. To do so, it is sufficient to compare the fingerprint region plus the carbonyl vibrations of the two samples in question. The excellent agreement of the two spectra is apparent at first glance (Figure II-8). Hence, it can be safely assumed that the two spectra are derived from the same chemical structure, namely a*R*-**114**. Upon closer inspection, both spectra show a split carbonyl vibration band (approx. 1700 and 1670 cm^{-1}), *i.e.* in both samples two distinguishable carbonyl groups were present. As we have learned from the X-ray structure this is the case in crystalline material since the O(3) oxygen is participating in a hydrogen bond whereas O(5) is not. Thus, the C-O(3) double bond should be slightly weakened and consequently its vibration appear at lower frequencies (1670 cm^{-1}).

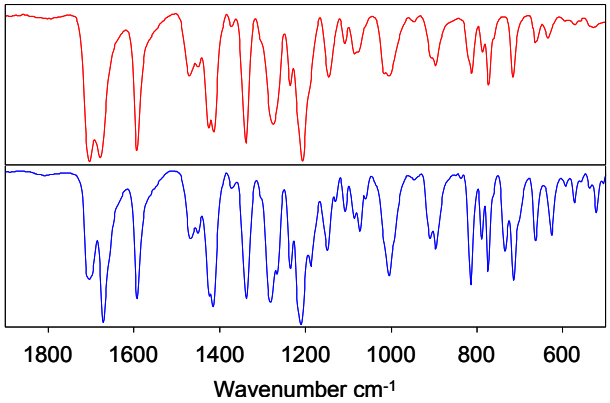

Figure II-8. Comparison of the fingerprint plus carbonyl vibration region of the IR spectra of a*R*-**114** prepared by method A (red) and method B (blue).

In conclusion, solid state data of compound a*R*-**114** were consistent with the structure proposed in Scheme II-18. Furthermore, it was clearly shown that in the solid state a preferential sense of axial rotation was induced, *viz.* a*R* when using the (1*R*,2*R*)-DACH and a*S* when using the (1*S*,2*S*)-DACH derivative **45**.

However, the solution behaviour of coordination compounds is usually far more complex since solvent effects and possible dynamic processes may take place. Consequently, NMR analysis of complex a*R*-**114** was carried out. Figure II-9 shows the ^{1}H NMR spectrum of recrystallised complex a*R*-**114** recorded at room temperature in dry THF-d_8. Using other standard NMR solvents such as $CDCl_3$ or CD_2Cl_2 did not result in interpretable spectra due to massive line broadening. Assignation of the signals was aided by 2D NMR studies and comparison with spectra of complex a*R*-**115** [Zn(Me-BIPOLate)((1*R*,2*R*)-^{t}Bu-DACH)] (see the following section for the complete discussion).

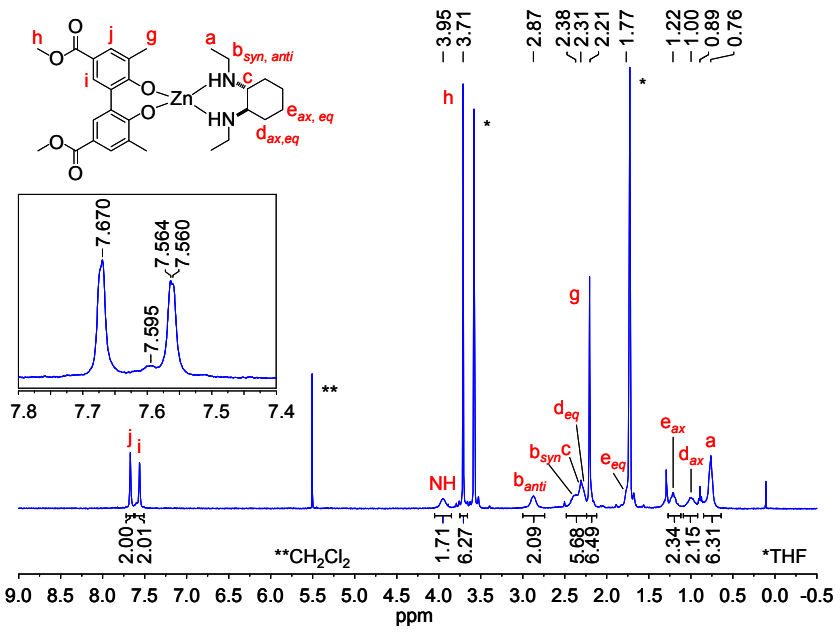

Figure II-9. 1H NMR (400 MHz, THF-d_8, 298 K) of complex a*R*-**114**, the notations b_{syn} and b_{anti} are referenced to the amine proton (see the X-ray structure).

Though 1D NMR spectra were in accordance with the structure of the 1:1 chelate **114**, this technique did not allow for unequivocal proof of the intermolecular interaction between the amine and biaryl units. Thus, in order to gain further insights into the structure of the complexes, 2D ROESY NMR spectra were recorded. Having found atomic distances of 2.44–2.60 Å between protons in positions **b** and **g** and 3.24–3.44 Å between **a** and **g** in the X-ray structure, we expected to observe dipolar cross-relaxation between these nuclei. Indeed crosspeaks most likely attributable to these spatial interactions were found in the spectrum (see picked peaks in Figure II-10). However, due to partial overlapping of the crucial methyl signal **g** with signals caused by cyclohexyl- and methylene protons also in proximity to **a**, the geometry of the molecule observed in the solid state (a*R* sense of axial rotation) could not be unambiguously confirmed in solution.

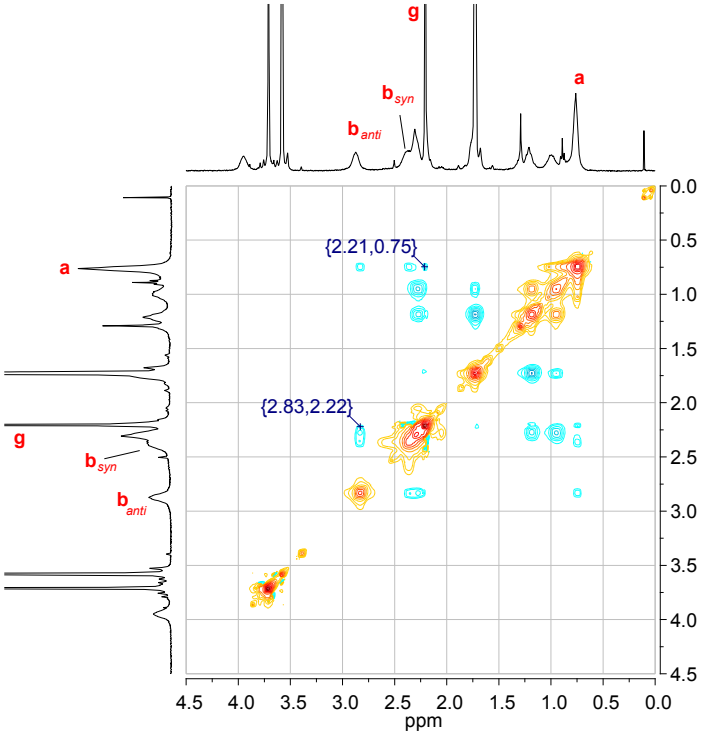

Figure II-10. Detail of the ROESY spectrum (500 MHz, THF-d_8, 298 K) of complex **114**.

Low temperature ^{1}H NMR spectroscopy did not improve the spectral resolution. However, at 273 K weak and poorly resolved signals appeared at 3.08, 2.98, and 2.58 ppm, *i.e.* next to the methylene signals of the *N*-ethyl substituent. At 253 K these signals got shifted to 3.23, 3.00, and 2.56 ppm. Further lowering the temperature caused these signals to disappear probably due to line broadening which affected the whole spectrum at lower temperatures. Unfortunately, the nature of the signals could not be elucidated with the data at hand. One would think that dynamic processes as those shown in Scheme II-19 were responsible for the observed behaviour. Presumably, the relatively small *N*-ethyl substituents are not bulky enough to induce complete diastereomer discrimination through steric interaction with the 3,3'-methyl substituents of the 2,2'-biphenol. Lowering the temperature

should in principle slow down the interconversion rate between the two diastereomers to the NMR timescale, thus, potentially making the energetically disfavoured minor diastereomer observable. However, since separate signals attributable to a*R*-**114** and diasteromeric a*S*-**114'** (both prepared with (1*R*,2*R*)-**45a**, a*S*-**114'** here must not be confused with enantiomeric a*S*-**114** which could be prepared with (1*S*,2*S*)-**45a**) were not observed, this equilibrium could not be demonstrated and thus remains a working hypothesis. At any rate, an (idealised) equilibrium as it is depicted in Scheme II-19 should lead to the predominant formation of the energetically most favoured species, which here is a*R*-**114**.

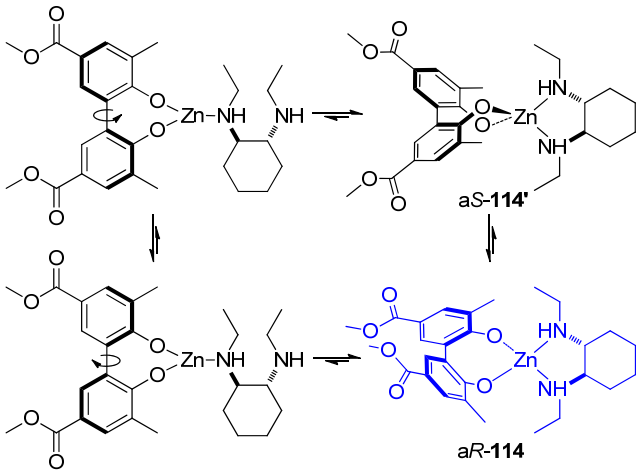

Scheme II-19. Idealised equilibria of species **114** (prepared from **44b** with (1*R*,2*R*)-**45a**) leading predominantly to the a*R*-chelate complex in solution.

The measurement of electronic circular dichroism (ECD and CD are used synonymously in the following) of chromophores in a chiral environment is an excellent tool for the configurational analysis of stereogenic elements. CD analysis of complex **114** was carried out both on the experimental and theoretical level. Figure II-11 shows the CD and UV-vis curves of complexes a*R*-**114** and enantiomeric a*S*-**114** prepared with both *N*,*N*'-diethyl-1,2-cyclohexanediamine enantiomers (1*R*,2*R*)-**45a** and (1*S*,2*S*)-**45a**. Chiral diamine **45a** was proven to be CD silent in the applied wavelength range and consequently the observed Cotton effects are attributable to the phenol rings in a chiral environment. The two curves are almost perfect mirror images, *i.e.* the induced preferential sense of rotation directly depends on the configuration of the diamine.

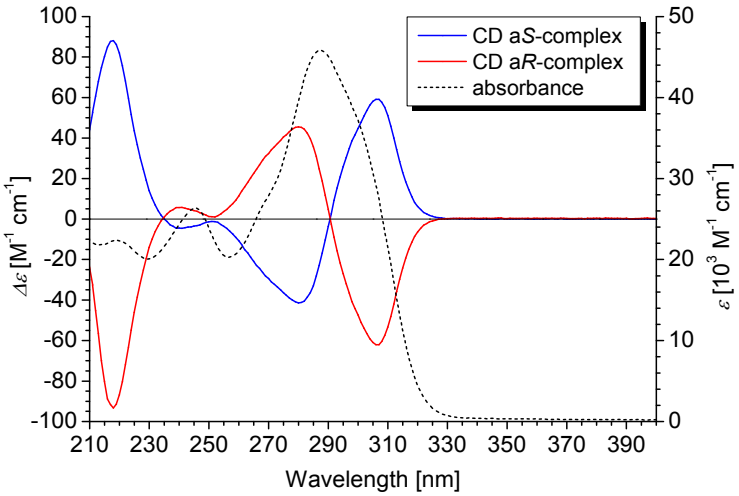

Figure II-11. UV-vis Absorption (dashed black line, identical for a*R*- and a*S*-**114**, right axis) and CD spectra (left axis) of a*R*-**114** (red line) and a*S*-**114** (blue line) (anhydrous THF, 25 ºC).

At longer wavelengths the curves show split-type (or exciton coupling) behaviour with the two constituent Cotton effects being centred at 290 nm. They are attributable to a $\pi-\pi^*$ transition with λ_{max} at 287 nm. This band should also be sensitive to the biphenyl torsion angle θ, *i.e.* variations of λ_{max} of this band in a given series of complexes are significant indicators for the value of θ.[87,88] Towards higher energies, first a local minimum is observed at 241 nm that is followed by a very intense Cotton effect at 218 nm (Table II-3). Due to increased absorbance of the solvent, it was not feasible to measure below 210 nm. Thus, it was impossible to decide whether or not the strong CD band was part of a bisignated signal that is associated to a nearby absorbance.

Table II-3. CD and UV-vis properties of enantiomeric complexes a*R*- and a*S*-**114**.

CD data	1st CE[a] $\Delta\varepsilon^b$ $(\lambda)^c$	2nd CE[a] $\Delta\varepsilon^b$ $(\lambda)^c$	3rd CE[a] $\Delta\varepsilon^b$ $(\lambda)^c$
a*R*-**114**	-62.1 (307)	45.5 (280)	-93.3 (218)
a*S*-**114**	59.2 (306)	-41.4 (280)	88.2 (218)
UV data	λ^c $(\varepsilon)^b$	$\lambda^c(\varepsilon)^b$	$\lambda^c(\varepsilon)^b$
	287 (45800)	246 (26300)	219 (22400)

[a]CE = Cotton effect; [b]M^{-1} cm^{-1}; [c]nm.

In conclusion these findings demonstrated that the induction of axial chirality found in the solid state prevailed also in solution. To answer the question whether or not it is the same species that is causing the CD signal, a computational approach was required. Predictions of CD and UV-vis spectroscopic properties first require an input geometry of the structure in question. Usually this is accomplished by a conformational search of the structures that have to be considered and subsequent geometry optimisation of the energetically favoured conformers. In a complex derived from **44b** and (1*R*,2*R*)-**45a**, there are

five stereogenic elements (four stereocentres and one stereogenic axis) to be found of which two, the ones at the diamine carbon atoms, are fixed. This gives rise to eight (2^n, n = number of stereocentres, here n = 3) diastereomers. In a first approach the geometries of all eight diastereomers were optimised on the moderate B3LYP/6-31G(d) level of theory[*] and without taking solvent effects into account. The resulting structures are shown in Figure II-12. The relative energies for the different diastereomers are arranged in the order of their magnitude in Table II-4. As can be seen the diastereomer showing the same configuration as that found in the X-ray structure (entry 2) is not the energetically lowest structure but rather comes the second lowest. This finding can be interpreted in two ways: i) the energetically most favourable structures in the solid state and in solution are not identical, or ii) calculations at this level of theory are not reproducing the energies properly. We presumed the latter to be more likely due to a decisive factor: all the dichroic spectra calculated from these structures (CAMB3LYP/SVP level of theory) solely depended on the sense of rotation of the biphenol axis and were almost identical, with the signs of all Cotton effects correctly predicted. All diastereomers with a*R* configuration led to negative (exciton) couplets (see Introduction) whereas a*S* configured diastereomers resulted in positive (exciton) couplets. Thus, it was concluded that the in the solid state observed induction (a*R* with (1*R*,2*R*)-**45a** and a*S* with (1*S*,2*S*)-**45a**) was also preserved in solution.

[**] Representative references for all computational methods mentioned here can be found in the Introduction.

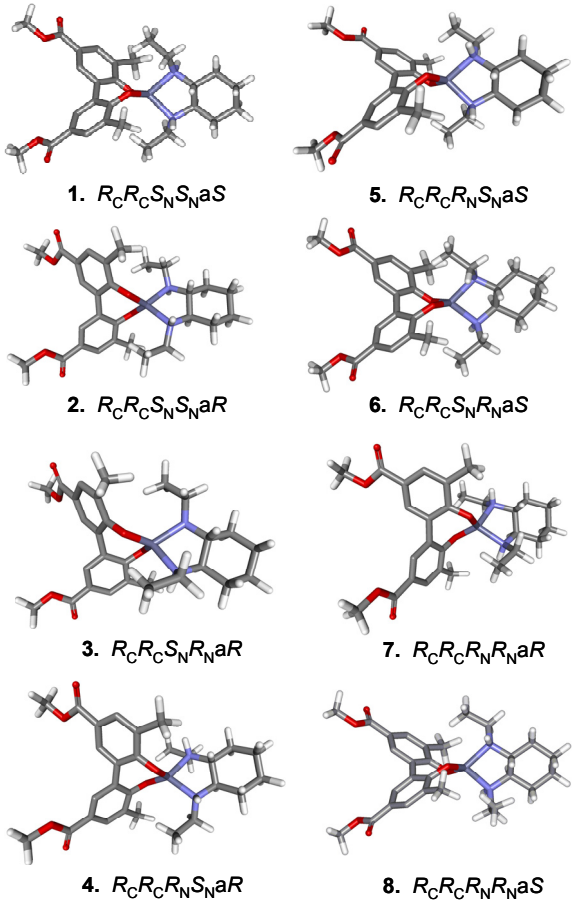

Figure II-12. Geometry optimised (B3LYP 6-31G(d) level of theory) diastereomers of a complex analogue to **114** derived from biphenol **44b** and diamine (1*R*,2*R*)-**45a**.

Table II-4. B3LYP 6-31G(d) calculated relative energies for the eight possible diastereomers of complex **114** (diamine configuration fixed to (1*R*,2*R*)).

entry	diastereomer[a]	relative energy[b]
1	$R_CR_CS_NS_N$a*S*	0.000
2	$R_CR_CS_NS_N$a*R*	2.733
3	$R_CR_CS_NR_N$a*R*	4.959
4	$R_CR_CR_NS_N$a*R*	4.966
5	$R_CR_CR_NS_N$a*S*	5.096
6	$R_CR_CS_NR_N$a*S*	5.099
7	$R_CR_CR_NR_N$a*R*	5.173
8	$R_CR_CR_NR_N$a*S*	8.953

[a]Denotations are as follows: the first two characters refer to the configuration at the N-substituted ring-carbons of amine (1*R*,2*R*)-**45a**, the following two indicate the configuration at the coordinated stereogenic nitrogen atoms (priorities: Zn > C(ring) > C(*N*-substituent > H(N)), a*R* and a*S* mark the sense of axial rotation in the biaryl. [b]In kcal/mol.

The comparison of several calculated UV-vis and CD spectra is shown in Figure II-13. It can be seen that the absorbance spectra of the diastereomers of entries 1 and 2 (Table II-4) are very similar whereas their CD curves are practical mirror images. It must be stressed that the latter do not result from enantiomers but diastereomers which demonstrates that the shape of the curve is determined exclusively by the induced axial chirality in the biphenol moiety. Also depicted are the spectra calculated from the X-ray structure used as input geometry and the experimental UV-vis and CD curves of complex a*R*-**114**. Apparently the overall shape and the number and signs of the Cotton effects are acceptably reproduced in all cases although the calculated curves appear compressed at higher energies compared to the one obtained experimentally. Furthermore, the computed curves had to be red-shifted by 35 nm in order to fit the experimental data. The 35 nm were derived from the shift required to superimpose the calculated and experimental maximum UV-vis absorbance. Moreover, it should be noted that the

calculated curves show strong bisignated Cotton effects centred at 220 nm. Unfortunately, this effect could be observed only partially in the experiment due to the increasing THF absorbance below 210 nm. Nevertheless, this result confirms the previously made assumption that the strong CD band at higher energies forms part of a second exciton couplet. In conclusion, at the B3LYP/6-31G(d) level of theory calculated input geometries did not correctly reproduce the relative energies but provided predicted CD spectra that were in agreement with the experimentally observed ones.

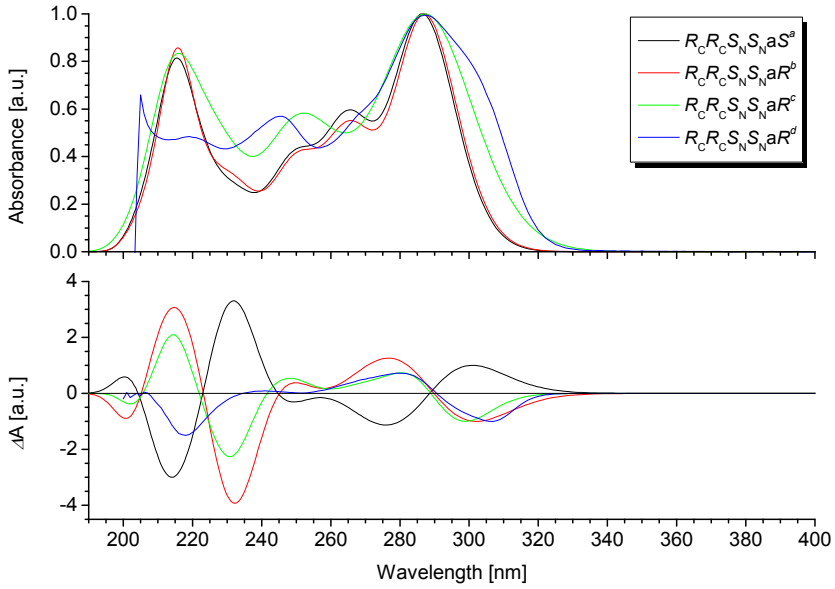

Figure II-13. Comparison of calculated (CAMB3LYP/SVP) and experimental UV-vis (top, λ_{max} arbitrarily normalised to 1) and CD (bottom, λ_{max} of the first Cotton effect arbitrarily normalised to 1) spectra of complex **114**. [a]Geometry optimised diastereomer according to entry 1 of Table II-4. [b]Geometry optimised diastereomer according to entry 2 of Table II-4. [c]Input geometry derived from the X-ray structure of a*R*-**114**. [d]Experimental data of compound a*R*-**114**.

We wanted to know if the problem concerning the relative energies of the diastereomers corresponding to entries 1 and 2 in Table II-4 could be overcome by using an extended basis set in the geometry optimisation of the two input structures. Thus, both diastereomers were optimised with the B3LYP functional in combination with the 6-311++G(d,p) basis set. The relative energies for the two energetically most stable diastereomers $R_CR_CS_NS_N$a*S*-**114** and $R_CR_CS_NS_N$a*R*-**114** calculated at this level of theory were found to be in better agreement with what was expected based on the experimental observations. The computed $R_CR_CS_NS_N$a*R*-**114** diastereomer, which is the one corresponding to the X-ray structure, was calculated to be stabilised by 0.624 kcal/mol relative to $R_CR_CS_NS_N$a*S*-**114**. Figure II-14 shows a comparison of the calculated CD and UV-vis spectra (B3LYP/6-31G(d) geometry optimised, excitations calculated with CAMB3LYP/SVP, and B3LYP/6-311++G(d,p)//CAMB3LYP-SVP, respectively) with the experimentally obtained spectra of compound a*R*-**114** ($R_CR_CS_NS_N$a*R* configuration). In conclusion, almost no differences in the predicted CD spectra were found using the geometries obtained at the two different levels of theory.

The MO6 functional was reported to be better suited than B3LYP to study steric congestion,[89] which probably is responsible for the energy gaps between the different diastereomers. Therefore we decided to repeat the geometry optimisation of the two energetically lowest diastereomers of Table II-4 (entries 1 and 2) with this functional and the 6-31G(d) basis set in order to further study the problem regarding the relative energies also by using another functional. Although the relative energy difference between the two diastereomers was significantly reduced, the a*S*-configured diastereomer was still stabilised by 0.424 kcal/mol compared to the a*R*-configured diastereomer. However, the UV-vis and CD spectra derived from the

MO6/6-31G(d) optimised structures were very similar to those depicted in Figure II-14.

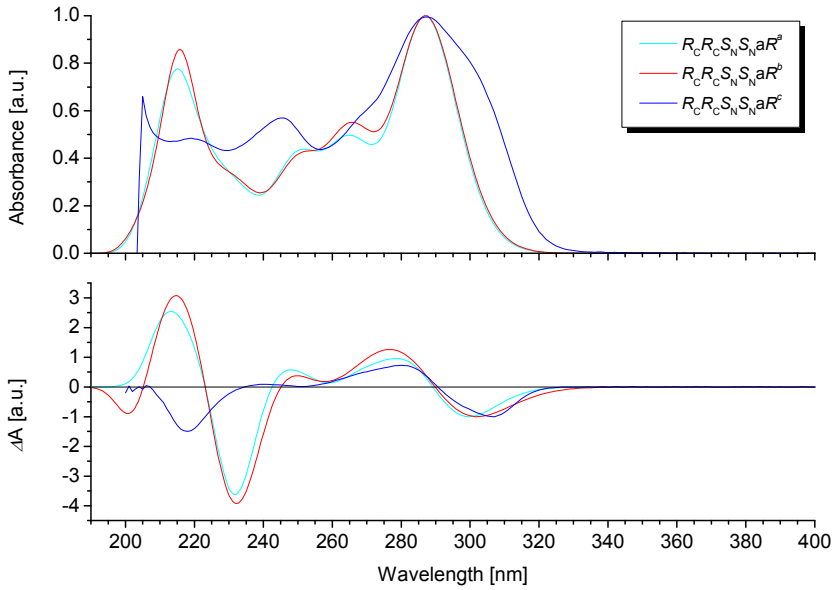

Figure II-14. Comparison of calculated (CAMB3LYP/SVP) and experimental UV-vis (top, λ_{max} arbitrarily normalised to 1) and CD (bottom, λ_{max} of first Cotton effect arbitrarily normalised to 1) spectra of complex **114**. [a]Input geometry B3LYP/6-311++G(d,p) optimised. [b]Input geometry B3LYP 6-31G(d) optimised. [c]Experimental data of a*R*-**114**.

Regarding mass spectrometry, it turned out that the MALDI technique is most convenient for recording routine mass spectra of the zinc(II) complexes. Figure II-15 shows the spectrum of **114**. The base peak corresponds to the ionised mononuclear complex. Upon close inspection, this species was identified as a mixture of the radical cation $M^{+\cdot}$ and protonated **114** $[M+H]^+$ as can be seen by comparison of the experimental data with the theoretical isotopic pattern calculated with *mMass* software.[90] Beyond that no other assignable masses were detected and as a whole the spectrum indicates a fairly pure compound. HRMS was carried out using the ESI technique that allowed the identification of compound **114** as $[M+H]^+$ (m/z = 563.2101 found, m/z = 563.2094 calculated.)

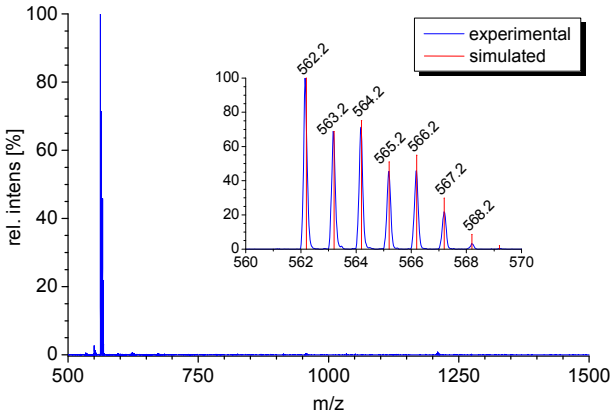

Figure II-15. MALDI-MS (pyrene) of complex **114**, overlaying patterns of $M^{+\cdot}$ and $[M+H]^+$ detected, the insert graph shows the experimental (blue) and simulated (red) isotopic patterns.

Preparation of [Zn(Me-BIPOLate)((1*R*,2*R*)-^{t}Bu-DACH)], complex a*R*-**115**; [Zn(**44b**)((1*R*,2*R*)-**45d**)].

The analysis of compound a*R*-**114** permitted a deep insight into the properties of both the solid state and solution behaviour of the complex. However, it was part of the concept to not only induce axial chirality in dynamically racemic 2,2'-biphenol derivatives, but also to influence the degree of axial rotation of these ligands. Therefore, we extended the study to diamines with bulkier N-substituents. One of the complexes prepared comprised the sterically more demanding *tert*-butyl substituent in the chiral building block. Due to the experience from complex a*R*-**114** the same sign of twist, namely a*R*, was expected to be induced into the biaryl by the DACH derivative (1*R*,2*R*)-**45d** (Scheme II-20). Complex a*R*-**115** was synthesised following methods A and B (see also Scheme II-14), using the 3,3'-substituted 2,2'-biphenol **44b** and the *N*-*tert*-butyl substituted diamine (1*R*,2*R*)-**45d**. Again the equivalence of the two methods was proven by spectroscopic techniques and MS.

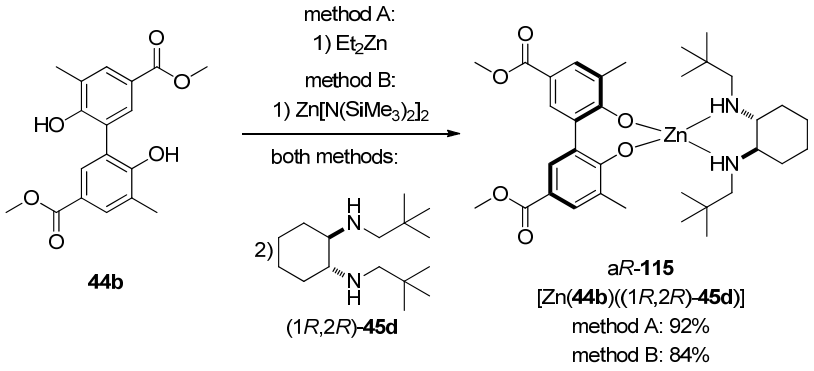

Scheme II-20. Preparation and proposed structure of [Zn(Me-BIPOLate)((1*R*,2*R*)-^{t}Bu-DACH)]; a*R*-**115**.

Crystals of complex a*R*-**115** suitable for X-ray analysis were obtained in the same way as described for complex a*R*-**114**. Complex a*R*-**115** was found to crystallise in the $P2_12_12_1$ space group which is of lower symmetry than that of a*R*-**114**. The asymmetric unit contains three conformationally different molecules which are of the same absolute configuration (a*R* sense of axial rotation) and furthermore show the same coordination mode as complex a*R*-**114**. One of the structures is shown in Figure II-16 as ORTEP. Traces of water were unavoidably incorporated during the crystallisation process and several water molecules were found to participate in a hydrogen bonding network including amine and carbonyl functional groups. The zinc(II) atom is centred in a tetrahedral environment. As can be seen in Table II-5, the tetrahedral angles (entries 5, 6) are very similar to those found for complex a*R*-**114** (Table II-2). The same is valid for the Zn-N (entries 1 and 2) and the Zn-O (entries 3 and 4) atomic distances. Apparently the bulkier ^{t}Bu substituent is not impeding the coordination to the metal or elongating the bonds between the Zn(II) atom and the diamine nitrogen atoms. The axial torsion angles of the biphenol (entries 7 and 8) were also found to be of similar size to those present in a*R*-**114**. Thus, it is concluded that manipulating the degree of the axial torsion angle can be achieved only to a small degree by augmenting the steric bulk of the chiral diamine moiety. It seems that the extent of twist is rather determined by the zinc centre's preferred tetrahedral angle than by steric interactions of the ligands. This seems true at least for the solid state but the possibility of different behaviour in solution cannot be fully excluded. To close this discussion, it should also be said that both carbonyl oxygen atoms of the biphenol form hydrogen bonds with either the NH groups of a neighbouring diamine or water but with a superior number of hydrogen bonds identifiable between the biphenol and the diamine units. The opposite is the case for the two NH groups of a

single diamine molecule which are hydrogen bonded to either biphenol carbonyl oxygen atoms or water.

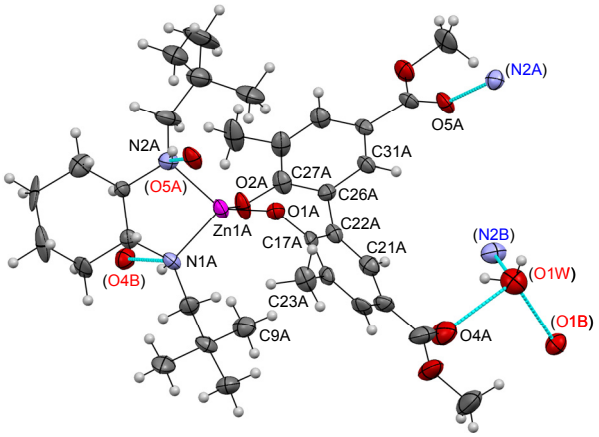

Figure II-16. ORTEP plot of complex **115** with partial atomic numbering. Ellipsoids are at the 50% probability level, hydrogens are drawn as size-fixed spheres of 0.15 Å radii, cyan lines indicate hydrogen bonds.

Table II-5. Selected bond lengths [Å], angles [º], and torsion angles [º] for complex a*R*-**115**.

entry	atom 1	atom 2	atom 3	atom 4	**length**
1	Zn(1)A	N(1)A			2.027(9)
2	Zn(1)A	N(2)A			2.045(8)
3	Zn(1)A	O(1)A			1.901(7)
4	Zn(1)A	O(2)A			1.901(7)
					angle
5	N(1)A	Zn(1)A	N(2)A		88.7(3)
6	O(1)A	Zn(1)A	O(2)A		107.4(3)
					torsion
7	C(17)A	C(22)A	C(26)A	C(27)A	-66.7(14)
8	C(21)A	C(22)A	C(26)A	C(31)A	-53.6(14)

As was done previously, the fingerprint together with the typical carbonyl vibration regions were again used in order to compare the outcome of methods A and B (Figure II-17). Interestingly, here the splitting of the carbonyl band is inferior to that found for complex **114** (Figure II-8). In contrast to the IR spectrum of complex **114**, the splitting of the carbonyl stretching vibration is not clearly observable since the band at 1702 cm-1 appears only as a shoulder. Obviously the more intense vibration appears at lower frequencies (1680 cm^{-1}). Following the argument that this band originates from a hydrogen bonded carbonyl oxygen atom, it was concluded that here the majority of the carbonyl groups are hydrogen bonded. Although in the crystal structure several of these groups were found to interact with water, it was still observed that the tendency to form hydrogen bonds also with the diamine moiety is higher than in complex **114**. It should be noted that contrary to the spectra in Figure II-8, the IR spectra shown here were taken from material that was not recrystallised prior to the measurement. Apparently the complex was, at least partially, obtained crystalline from the reaction.

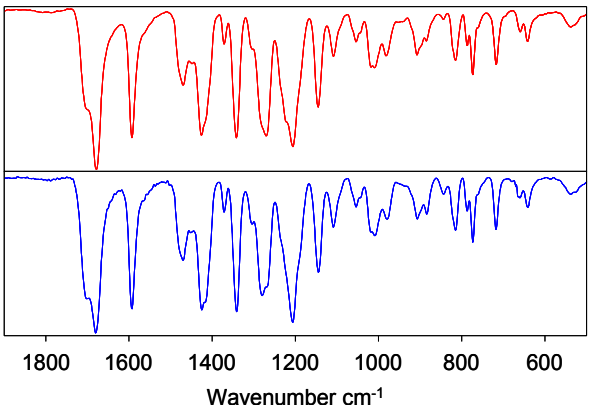

Figure II-17. Comparison of the fingerprint plus carbonyl stretching vibration region of the IR spectra of **115** prepared by method A (red) and method B (blue).

The solution structure of complex a*R*-**115** was elucidated straightforwardly by NMR analysis. Figure II-18 shows the proton NMR spectrum of a*R*-**115** measured at 253 K. At this temperature the NH signal appears shifted downfield relative to its chemical shift at 298 K. At room temperature it overlaps as a broad multiplet with the signal of one of the two diastereotopic methylene protons (**b**$_{anti}$) of the *tert*-butyl substituent. However, when separated these two signals appear as, in case of the NH signal poorly resolved, pseudo-triplets, *i.e.* the scalar coupling of the amine proton was resolved in dry THF-d_8. Coupled nuclei are on the one hand the methylene proton (**b**$_{anti}$) and on the other the methine proton **c** of the cyclohexane backbone. Due to the similarity of the *vicinal* coupling constants ($^3J \approx 9$ Hz) the expected doublet of doublets is observed as a pseudo-triplet.

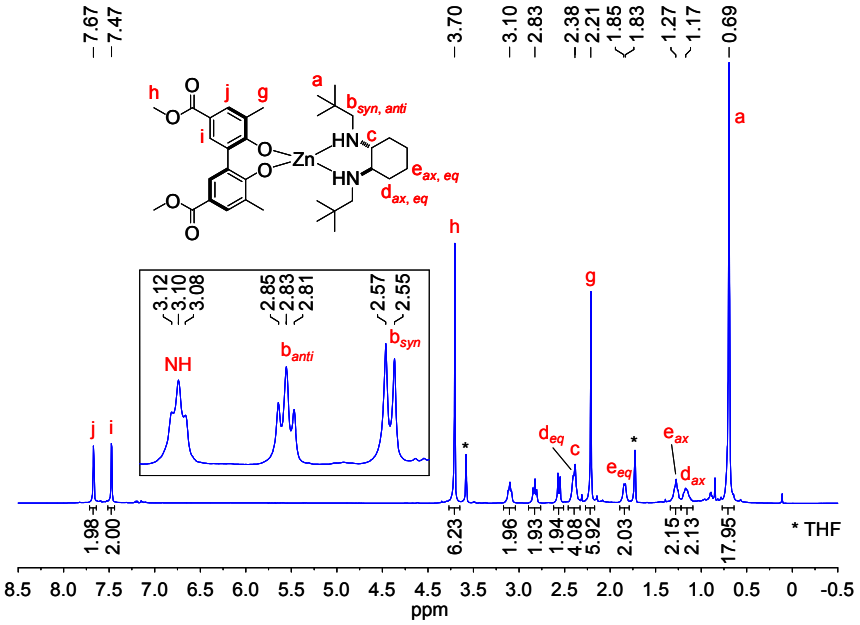

Figure II-18. ^{1}H NMR (500 MHz, THF-d_8, 253 K) of complex a*R*-**115**.

According to the X-ray structure of complex a*R*-**115** the dihedral angles ϕ between the N-attached proton and the two diastereotopic methylene protons are 90º (NH, $\mathbf{b}_{syn}$) and 154º (NH, $\mathbf{b}_{anti}$). Inserting these numbers in the Karplus equation (Equation 1) yields values of approx. 0 Hz and 7.5 Hz for the respective *vicinal* coupling constants. Thus, provided that in solution the dihedral angles are similar, the finding that only one methylene proton, namely $\mathbf{b}_{anti}$, shows *vicinal* coupling, seems reasonable. It must be noted however, that strictly speaking, the Karplus relation is defined for rotations around C-C bonds only. Nevertheless, this may also give a hint as to why the signal of the methylene proton in the $\mathbf{b}_{anti}$ position also splits into a pseudo-triplet. Due to the relatively large dihedral angle we observe a *vicinal* coupling constant of medium to large size as can be seen in Figure II-19. The red curve corresponds to the theoretical values for *vicinal* coupling constants (^3J) as obtained from the Karplus equation, whereas the dotted line roughly indicates the upper limit of the experimentally observed values (apart from ϕ, ^3J also depends on substituents, bond angles, and lengths).[91] Generally, *vicinal* coupling constants are positive and in between these two lines (in particular for ϕ close to 0º and 180º, the experimental values are usually larger than the calculated ones). Thus, the observed *vicinal* H-N-C-H_{anti} coupling constants may be similar to the typical values of *geminal* coupling constants (^2J), *i.e*. the *geminal* coupling between the diastereotopic methylene protons, and as result a pseudo-triplet is observed instead of the expected doublet of doublets.

$$^3J = \begin{cases} 8.5\ cos^2\ \phi\text{-}0.28; & 0º \le \phi \le 90º \\ 9.5\ cos^2\ \phi\text{-}0.28; & 90º \le \phi \le 180º \end{cases}$$

Equation 1. Karplus relation.

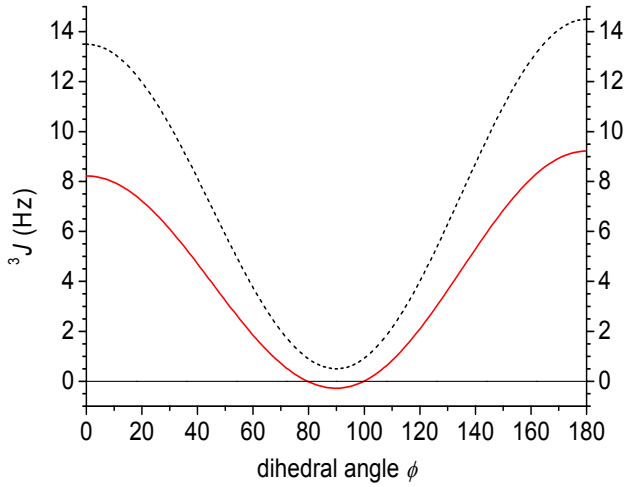

Figure II-19. Dependence of the *vicinal* coupling constant on the dihedral angle ϕ (Karplus curve), red line corresponds to calculated values whereas the dotted line marks the limit of the experimentally found ones.

Contrary to the case described above, the Karplus relation can be applied without reservations for the assignation of signals and the prediction of coupling constants of the cyclohexyl backbone. Looking again at the proton spectra of complex a*R*-**115**, it becomes apparent that the proton **e** in equatorial position ($\mathbf{e}_{eq}$) appears as a poorly resolved doublet instead of the expected multiplet. In the X-ray structure, the only dihedral angles ϕ to be found of suitable size (approx. 178º) for efficient scalar coupling are those including the axial protons of the positions **d** and **e**. All other combinations of equatorial and axial protons show dihedral angles close to 60º and thus the respective *vicinal* couplings result in ^3J values (near 2 Hz as can be seen in the Karplus curve) which are too small to be resolved under the applied magnetic field strength and with the observed linewidths.

Direct proof for an interaction between the chiral diamine and the dynamically racemic biphenol was required for confirming the cyclic structure of the complex in solution. Figure II-20 shows the NOESY spectrum (THF-d_8, 253 K) of the aliphatic region of complex a*R*-**115**. The sought after dipole-dipole interaction is observed for the *tert*-butyl protons **a**, and the 3,3'-methyl protons **g** of the biphenol (2.7-3 Å distance in the solid state). Another through space interaction is found between **g** and $\mathbf{b}_{anti}$ (2.1-2.5 Å distance in the solid state). On the contrary the proximity between **g** and $\mathbf{b}_{syn}$ is indicated in the NOESY spectrum only by very weak crosspeaks, corresponding to larger distances in the solid state structure (3.4-4.1 Å).

In conclusion, it can be safely assumed that the predominant structure in solution must be very similar to the one elucidated by single crystal analysis. Moreover, no hints of possible equilibria including open-ring structures or other diastereoisomers were found by NMR spectroscopy. Most importantly the NOESY spectrum is fully in accordance with the above made assignation of signals and clearly shows the spatial interaction between the two constituent building blocks. Additional spectra like ^{1}H-^{13}C HSQC, and ^{13}C NMR that further strengthen the signal assignation demonstrated here, are included in the appendix.

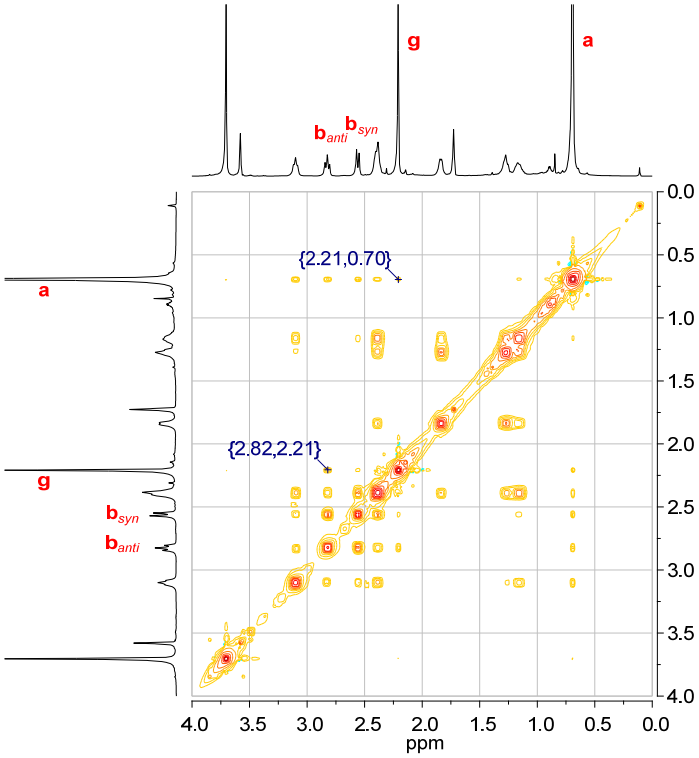

Figure II-20. Detail of the NOESY spectrum (500 MHz, THF-d_8, 253 K) of complex **115**.

The UV-vis and CD spectra of complex a*R*-**115** showed great similarity to those obtained for a*R*-**114** (Figure II-21). In the CD curve the same sequence of Cotton effects corresponding to a negative exciton couplet with intensities closely matching those of a*R*-**114** are observed (Table II-6). Consequently, the same axial configuration can be assigned here, *i.e.* the DACH derivative (1*R*,2*R*)-**45d** induced a*R* configuration in the 2,2'-biphenol unit.

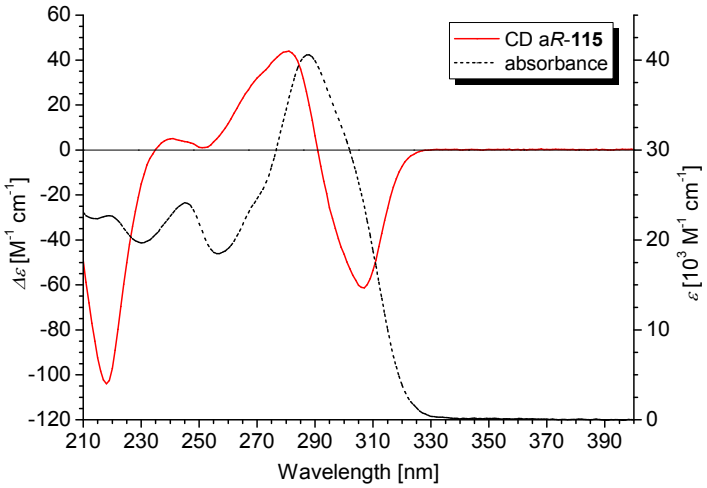

Figure II-21. UV-vis absorption (dashed black line, right axis) and CD spectrum (red line, left axis) of a*R*-**115** (anhydrous THF, 25 ºC).

Table II-6. CD and UV-vis properties of complex a*R*-**115**.

CD data	1st CE[a] $\Delta\varepsilon^b$ $(\lambda)^c$	2nd CE[a] $\Delta\varepsilon^b$ $(\lambda)^c$	3rd CE[a] $\Delta\varepsilon^b$ $(\lambda)^c$
	-61.3 (307)	43.9 (281)	-103 (218)
UV data	λ^c $(\varepsilon)^b$	$\lambda^c(\varepsilon)^b$	$\lambda^c(\varepsilon)^b$
	288 (40600)	245 (24100)	219 (22700)

[a]CE = Cotton effect; [b]M^{-1} cm^{-1}; [c]nm.

Preparation of [Zn(Me-BIPOLate)((1*R*,2*R*)-Mes-DACH)], complex a*S*-**116**; [Zn(**44b**)((1*R*,2*R*)-**45g**)].

In order to further study the influence of the N-substituent on the induction of chirality, a complex (Scheme II-21) incorporating an aromatic group on this position was prepared following both methods A and B. Again their equivalency was proven and no distinction between the two methods will be made in the following. Based on the experience with the previous complexes, we expected a*R* sense of axial rotation to be induced by the diamine (1*R*,2*R*)-**45g**. However, as was proven by CD, this was not the case since the signs of the Cotton effects were inverted. Consequently, we propose the structure shown in Scheme II-21 for complex **116**. Unfortunately, no crystals suitable for X-ray analysis were obtained from this compound.

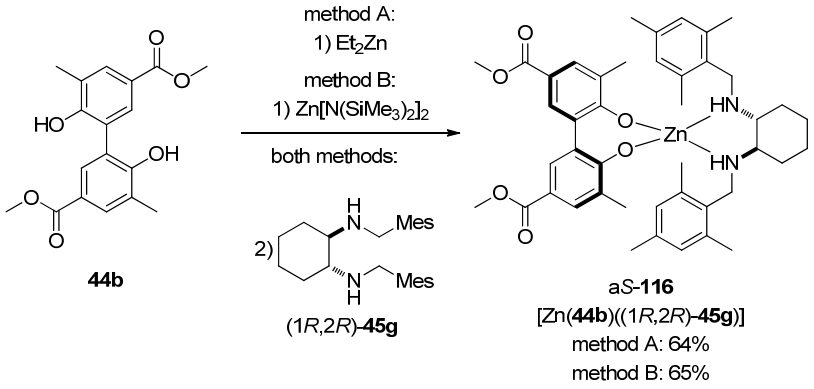

Scheme II-21. Preparation and proposed structure of [Zn(Me-BIPOLate)(1*R*,2*R*)-Mes-DACH)]; a*S*-**116**.

Disregarding the fact that the NMR analysis of compound a*S*-**116** was significantly hampered due to line broadening, its behaviour in solution was generally similar to that of the previous complexes. However, as indicated before, emphasis must be placed on the CD properties. In contrast to what was observed for complexes a*R*-**114** and a*R*-**115**, the zinc(II) complex that was derived from the

(1*R*,2*R*)-enantiomer of DACH derivative **45g** and Me-BIPOL **44b**, showed a positive instead of the expected negative exciton coupled CD signal (Figure II-22). Consequently, we assumed that the biphenol **44b** predominantly adopted a*S* sense of axial rotation in combination with the chiral inducer (1*R*,2*R*)-**45g**. The use of the (1*S*,2*S*)-enantiomer of diamine **45g** rendered the other enantiomer of the complex, a*R*-**116**, which displayed a mirror inverted CD curve with respect to the one of a*S*-**116**. This behaviour was similar to what was already observed in the hydrogen bonding approach when using the *N*-2,4,6-trimethylbenzyl-substituted diamine **45g**. Also noticeable in the CD curves of compound **116** (a*S* and a*R*) are the lower intensities of the Cotton effects compared to those observed for a*R*-**114** and a*R*-**115** whereas the absorbance suffered only a small decrease (Table II-7). Due to the fact that the degree of twist in these complexes was found to be mostly dependent on the preferential tetrahedral angle of the zinc(II) centre, it was concluded that this loss of signal intensity was not due to variations of the torsion angle θ of the biphenol, but rather a consequence of a lower diastereomeric excess of the complex. The aromatic N-substituents seem to be less suited to efficiently induce a predominant axial sense of twist. The possibility of partial decomplexation in solution can also not be fully disregarded since traces of free diamine **45g** were found in the MALDI-MS spectrum. It should also be noted that diamine **45g** is beginning to dominate the UV absorbance curve below 240 nm.

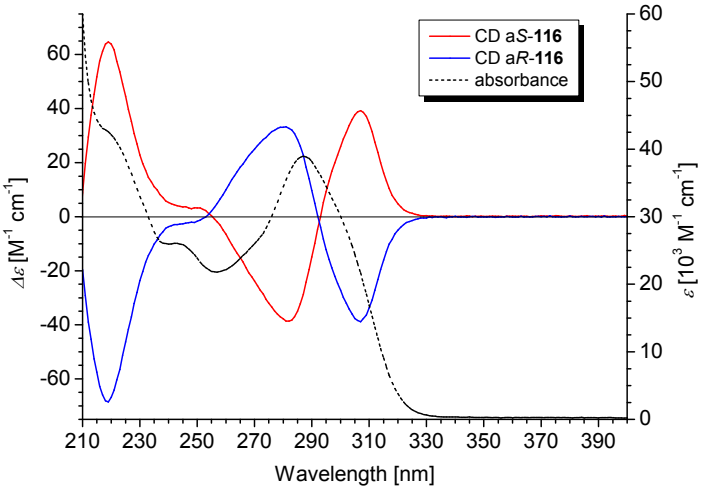

Figure II-22. UV-vis absorption (dashed black curve, identical for a*S*- and a*R*-**116**, right axis) and CD spectra (left axis) of a*S*-**116** (red line, chiral inducer: (1*R*,2*R*)-**45g**) and a*R*-**116** (blue line, chiral inducer: (1*S*,2*S*)-**45g**) measured in anhydrous THF at 25 ºC.

Table II-7. CD and UV-vis properties of enantiomeric complexes a*R*- and a*S*-**116**.

CD data	1st CE[a] $\Delta\varepsilon^b$ $(\lambda)^c$	2nd CE[a] $\Delta\varepsilon^b$ $(\lambda)^c$	3rd CE[a] $\Delta\varepsilon^b$ $(\lambda)^c$
a*S*[d]	39.2 (307)	-38.6 (282)	64.7 (219)
a*R*[d]	-38.8 (306)	33.2 (281)	-68.6 (219)
UV data	λ^c $(\varepsilon)^b$	$\lambda^c(\varepsilon)^b$	$\lambda^c(\varepsilon)^b$
	287 (39000)	243 (26100)	217 (43100)

[a]CE = Cotton effect; [b]M^{-1} cm^{-1}; [c]nm. [d]Biphenol axial sense of rotation in complexes **116**.

Preparation of [Zn(I-BIPOLate)((1*R*,2*R*)-Et-DACH)], complex a*R*-**117**; [Zn(**44e**)((1*R*,2*R*)-**45a**)].

Complex a*R*-**117** is the only compound in this series in which the 3,3'-iodine substituted 2,2'-biphenol **44e** was used. The preparation was carried out following only method B which yielded complex a*R*-**117** as a slightly yellow crystalline powder. Unfortunately, no single crystals suitable for X-ray analysis were obtained from this complex. The assignation of the sense of axial rotation was made mainly on the basis of the underlying recognition event. We assumed that the interaction of biphenol **44e** with diamine (1*R*,2*R*)-**45a** would be similar to that of the 3,3'-methyl-substituted biphenol **44b** with (1*R*,2*R*)-**45a** in the formation of complex a*R*-**114**. Moreover, the CD properties of a*R*-**117** were very similar to those observed for the mononuclear complexes a*R*-**114** and a*R*-**115**, a finding which definitely does not contradict the structure proposal shown in Scheme II-22.

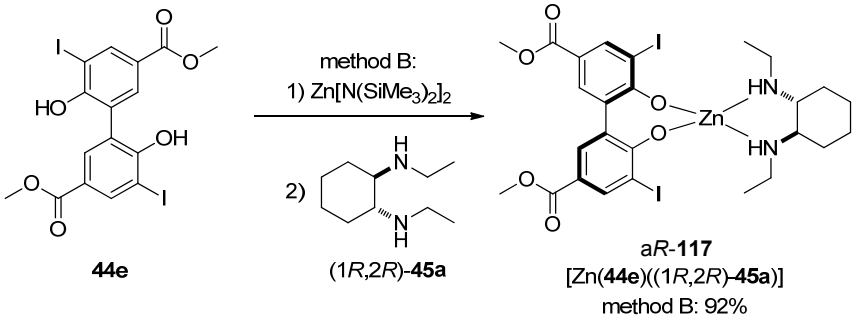

Scheme II-22. Preparation and proposed structure of [Zn(I-BIPOLate)((1*R*,2*R*)-Et-DACH)]; a*R*-**117**.

However, it must be stressed that we are dealing with a different chromophore in this case, *i.e.* CD properties cannot be directly compared with those found for complexes formed with the 3,3'-methyl-substituted 2,2'-biphenol **44b**. The iodine substituent does change the electronic properties of the chromophore and in order to unequivocally determine the absolute configuration of complex a*R*-**117** on the basis of CD, the experimentally obtained CD (Figure II-23) must be compared with the calculated data. Currently this data is not available but this problem may be addressed within a computational approach in the future. Furthermore, CD is not only sensitive to electronic changes in the chromophore but also to changes in the environment of the chromophore in which it is embedded in. A striking example is the dependence of the amplitude of the Cotton effects on the dihedral angle θ in enantiopure 1,1'-binaphthalenes.[92] For very large values of θ the Cotton effect may eventually change its sign although the configuration remains the same. We did not consider this to be the case here since it was found in the mononuclear complexes that θ depended on the tetrahedral angle of the zinc(II) centre which we assume, based on the X-ray data, may not allow such large divergences.

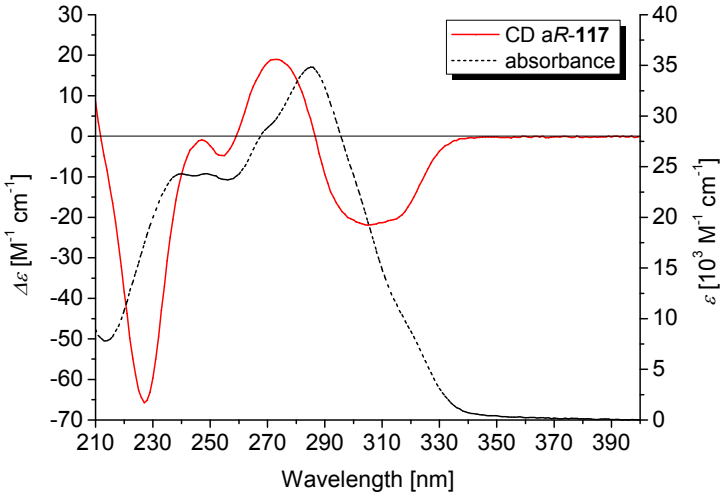

Figure II-23. UV-vis absorption (black line, right axis) and CD spectrum (red line, left axis) of a*R*-**117** (anhydrous THF, 25 ºC).

Table II-8. CD and UV-vis properties of complex a*R*-**117**.

CD data	1st CE[a] $\Delta\varepsilon^b$ $(\lambda)^c$	2nd CE[a] $\Delta\varepsilon^b$ $(\lambda)^c$	3rd CE[a] $\Delta\varepsilon^b$ $(\lambda)^c$
	-22.0 (305)	19.0 (273)	-65.8 (227)
UV data	λ^c $(\varepsilon)^b$	$\lambda^c(\varepsilon)^b$	$\lambda^c(\varepsilon)^b$
	285 (34800)	249 (24300)	239 (24300)

[a]CE = Cotton effect; [b]M^{-1} cm^{-1}; [c]nm.

The IR spectrum of complex a*R*-**117** is in agreement with the structure proposed in Scheme II-22. As observed in several of the IR spectra of the previous complexes, a split carbonyl stretching band is found here as well (1707 cm^{-1} and 1686 cm^{-1}), indicating the presence of two distinguishable carbonyl groups in a*R*-**117**.

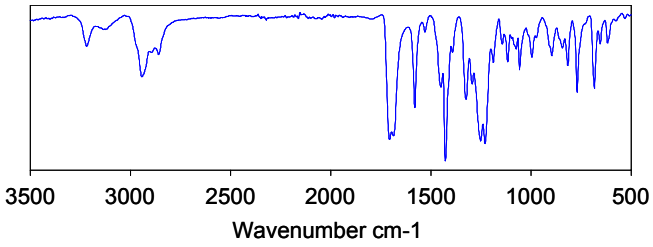

Figure II-24. IR spectrum of complex a*R*-**117**.

3.2.3 Dinuclear zinc complexes of type [{Zn(44d)((1*R*,2*R*)-45)}$_2$].

Preparation of [{Zn(μ-H-BIPOLate)((1*R*,2*R*)-Mes-DACH)}$_2$], complex **118**; [{Zn(**44d**)((1*R*,2*R*)-**45g**)}$_2$].

We expected the outcome of the complexation of ligands **44d** and (1*R*,2*R*)-**45g** with zinc(II) according to methods A and B to be similar to that of the previously described reactions. However, as will be disclosed in this section, a 1:1 chelate structure [Zn(**44d**)((1*R*,2*R*)-Mes-DACH)] as it is depicted in Scheme II-23 was not observed for complex **118**.

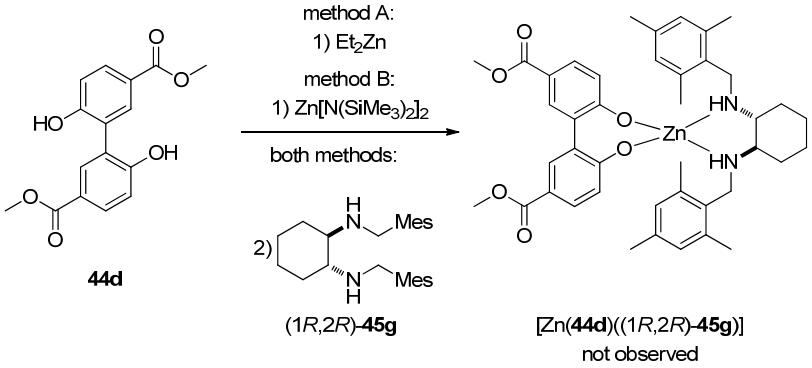

Scheme II-23. Preparation and proposed structure for a complex derived from biphenol **44d** and diamine (1*R*,2*R*)-**45a**.

The compound that was prepared from biphenol **44d** and diamine (1*R*,2*R*)-**45g** according to method B could be crystallised by slow diffusion of *n*-hexane into a solution of THF. The thermal ellipsoid plot of the resulting structure is depicted in Figure II-25. Contrary to what was expected, the solid state structure does not show a mononuclear complex but instead a dinuclear one, in which two zinc(II) centres are coordinated in tetragonal-pyramidal fashion by two diamines and two BIPOLate moieties. Each BIPOLate has one of its oxygen atoms bound as a μ-oxo-bridging ligand. This is in clear contrast to the structures

found for complexes prepared with Me-BIPOL **44b**, exemplified by a*R*-**114** (Figure II-6). Thus, the hypothetical structure of Scheme II-23 could not be confirmed but instead a molecular structure with a 2:2:2 stoichiometry (Zn/**44d**/(1*R*,2*R*)-**45g**) as it is shown in Figure II-26 was obtained. Consequently, when speaking about **118** in its solid state, in the following this will refer to the complex [{Zn(μ-H-BIPOLate)((1*R*,2*R*)-Mes-DACH)}$_2$] or [{Zn(μ-**44d**)((1*R*,2*R*)-**45g**)}$_2$] in short form.

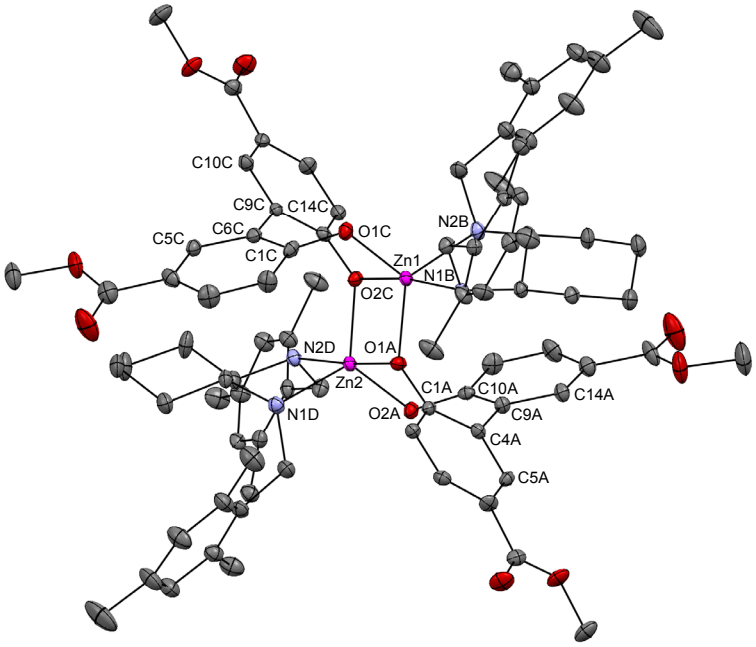

Figure II-25. ORTEP plot of complex **118** with partial atomic numbering scheme. Ellipsoids are at the 50% probability level, co-crystallised solvent and hydrogens are omitted for clarity.

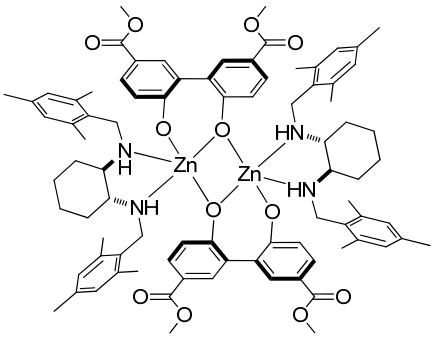

118
[{Zn(*μ*-**44d**)((1*R*,2*R*)-**45g**)}$_2$]

Figure II-26. Solid state structure of [{Zn(*μ*-H-BIPOLate)((1*R*,2*R*)-Mes-DACH)}$_2$] **118**.

Strikingly, it appears that in the solid state structure of complex **118** no induction of a preferential axial twist has taken place, *i.e*. the two axial units of a single complex molecule are present in both a*R* and a*S* configurations with almost identical absolute torsion angles. Also, the two BIPOLate longitudinal axes are *quasi*-parallel and consequently the ligand atomic positions could be transformed into each other by the inversion operation. Furthermore, the two chiral diamine moieties also show unexpectedly different binding from what was observed for complexes **114** and **115**. Here, the chiral units are not coordinated in C_2-like manner but instead the two nitrogens of one diamine unit adopt *R* and *S* configuration, respectively. Naturally, this does not change the configuration of the carbon stereocentres and the cyclohexyl backbone remains in its C_2-symmetric chair conformation. However, the two nitrogen protons and the two 2,4,6-trimethylbenzyl substituents, respectively, are pairwise pointing towards the same direction with the mesitylene rings appearing like “wings”. Two THF molecules were found to have co-crystallised with the structure and the resulting space group is P1. Lastly, no hydrogen bonds between any of the carbonyl oxygen atoms and the diamines’ NH-groups were found. This was in agreement

with the IR spectrum where only one carbonyl band is found around 1700 cm^{-1} (see Figure II-28).

Selected atom distances, bond angles, and torsion angles of complex **118** are given in Table II-9. The Zn-N bonds (entries 1 and 2) are slightly longer than in **114** but still well within earlier reported limits. Regarding the bonds between the Zn(II) centres and the two μ-oxo bridging atoms, it is found that each Zn(II) centre has one longer and one shorter bond (compare entries 5 with 6 and 8 with 9), *i.e.* the four atoms form the corners of a rhomboid. The shorter ones and the remaining Zn-O bonds (entries 7 and 10) are practically of the same length as the ones found for a*R*-**114** and those reported by Darensbourg.[85] Each of the elongated bonds is part of a seven-membered chelate ring formed by one Zn(II) centre plus two oxygens and four sp^2 hybridised carbon atoms of one BIPOLate. Lowering the ring strain might be a possible reason for the elongation of this particular bond since the ligand backbone should be rigid due to the hybridisation of the carbons. Furthermore, the torsion along the BIPOLate's molecular axis seems limited in this structure by steric constraints resulting from the proximity of the diamine cyclohexyl backbone. The Zn-O angles are not directly comparable to those found for the monomeric complexes a*R*-**114** and a*R*-**115** since the binding mode is different here. However, it can be said that they are rather acute. This is true for both types, the ones formed by one Zn(II) centre and the two bridging oxygens (entries 12 and 15), and the ones spanned by Zn(II), one bridging-, and the remaining oxygen (entries 13 and 16). The positive (entries 17 and 18) and negative (entries 19 and 20) signs of the torsion angles indicate the a*S* and a*R* sense of axial rotation in the BIPOLate ligands. These results were confirmed by X-ray diffraction of a crystal derived according to method A using diethylzinc as both deprotonating agent and zinc(II) source.

Table II-9. Selected bond lengths [Å], angles [º], and torsion angles [º] for complex **118**.

entry	atom 1	atom 2	atom 3	atom 4	**length**
1	Zn(1)	N(1)B			2.177(3)
2	Zn(1)	N(2)B			2.086(3)
3	Zn(2)	N(1)D			2.086(3)
4	Zn(2)	N(2)D			2.200(3)
5	Zn(1)	O(1)A			1.975(2)
6	Zn(1)	O(2)C			2.155(2)
7	Zn(1)	O(1)C			1.913(2)
8	Zn(2)	O(1)A			2.153(2)
9	Zn(2)	O(2)C			1.975(2)
10	Zn(2)	O(2)A			1.921(2)
					angle
11	N(2)B	Zn(1)	N(1)B		82.88(10)
12	O(1)A	Zn(1)	O(2)C		77.28(9)
13	O(1)C	Zn(1)	O(2)C		88.26(9)
14	N(1)D	Zn(2)	N(2)D		83.07(10)
15	O(2)C	Zn(2)	O(1)A		77.35(10)
16	O(2)A	Zn(2)	O(1)A		88.46(9)
					torsion
17	C(1)C	C(6)C	C(9)C	C(14)C	51.9(5)
18	C(5)C	C(6)C	C(9)C	C(10)C	46.1(5)
19	C(1)A	C(4)A	C(9)A	C(10)A	-52.0(5)
20	C(5)A	C(4)A	C(9)A	O(14)A	-48.1(5)

Comparison of the experimental and calculated powder diffraction pattern again confirmed the crystallographic purity of the sample (Figure II-27), *i.e*. all of the material present in crystalline form corresponded to the solid state structure of compound **118** (Figure II-25).

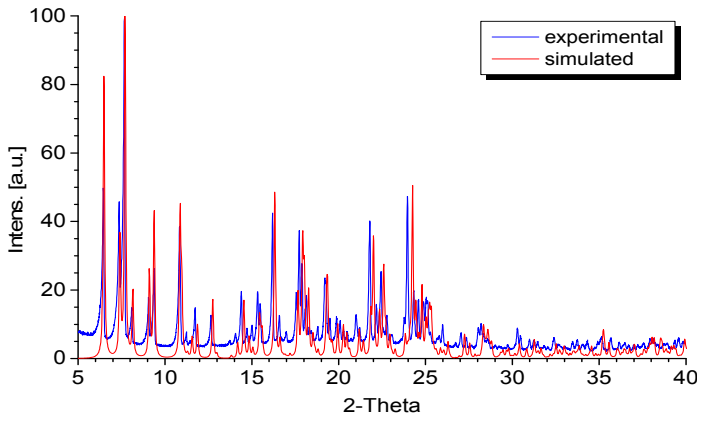

Figure II-27. Calculated (red) and experimental (blue) powder diffraction pattern of complex **118**.

The fingerprint and distinctive carbonyl vibration regions of recrystallised samples of **118** prepared according to methods A and B are identical. Of further interest is the fact that the carbonyl stretching vibration is not split into two bands as it was for complex a*R*-**114** but instead only one band is found at 1709 cm^{-1}, which corresponds to the one found at higher energies in the IR spectrum of compound a*R*-**114** (Figure II-8). It can be interpreted as a consequence of the missing hydrogen bond of the carbonyl oxygen atoms with diamine nitrogen atoms.

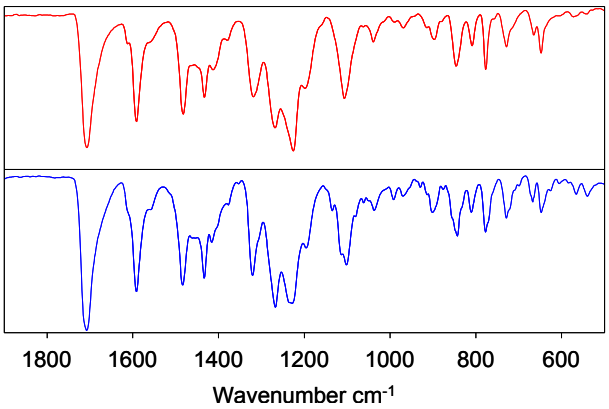

Figure II-28. Comparison of the carbonyl stretching vibration and fingerprint regions of the IR spectra of **118** prepared by method A (red) and method B (blue).

Regarding the behaviour of complex **118** in solution, it was found that the dimeric structure is undergoing dynamic changes on the NMR timescale in the temperature range from 25 to -90 ºC. As can be seen in the ^{1}H NMR spectrum in Figure II-29 (recorded from recrystallised compound **118** at 25 ºC in dry THF-d_8), this dynamic behaviour resulted in line broadening that also affected 2D NMR techniques and most notably ^{13}C NMR spectroscopy (it was not possible to obtain ^{13}C NMR spectra with a high enough signal to noise ratio). Signal assignment in ^{1}H NMR spectra could be carried out only approximately with integrals corresponding roughly to the expected values. In conclusion, we suggest that fluxional equilibria from the dimeric complex could account for the broadened signals observed in ^{1}H NMR. Alternatively or in a parallel way, a fast equilibrium between monomeric and dimeric complexes (Scheme II-24) might account for the line shape of the NMR.

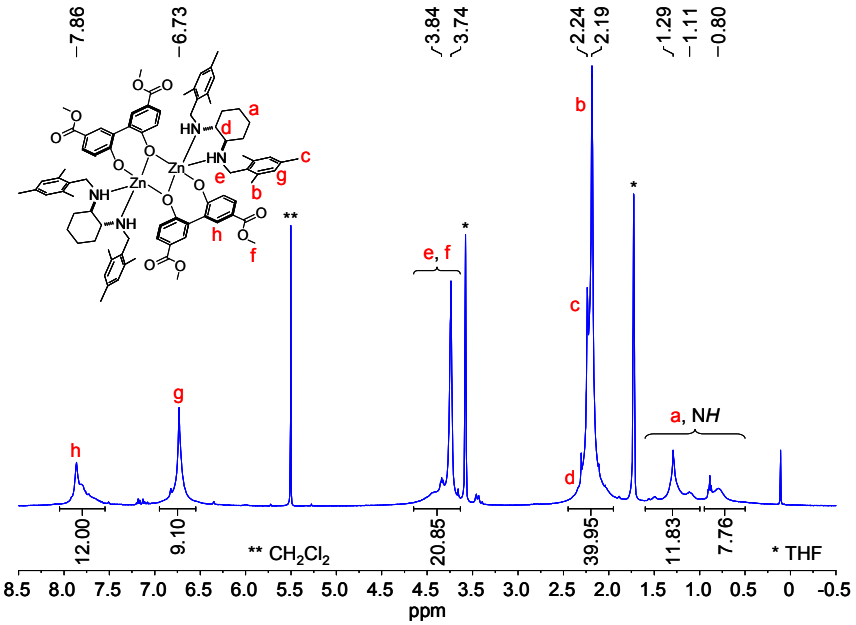

Figure II-29. ^{1}H NMR (400 MHz, THF-d_8, 298 K) of complex **118**.

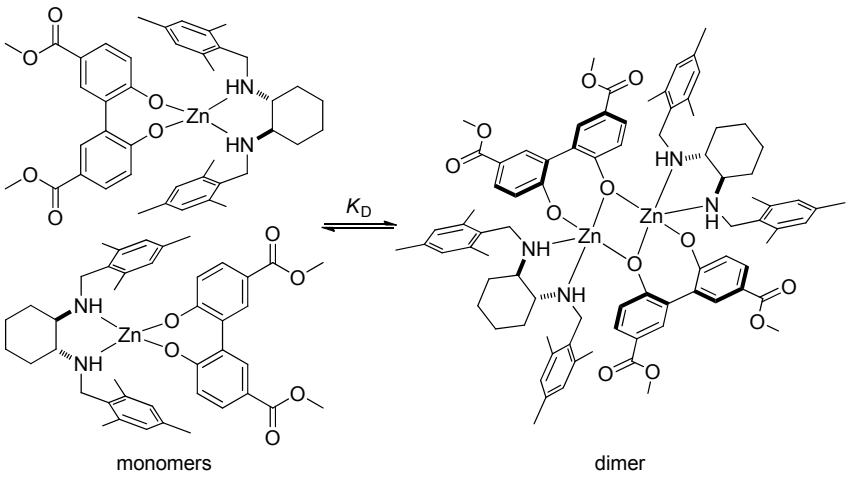

Scheme II-24. Dimerisation equilibrium potentially taking place in solutions of complex **118**.

The proposition of monomeric complexes playing an important role in solutions of complex **118** is supported by mass spectrometry. The MALDI-MS spectrum (Figure II-30) did not show the expected dimer mass peak but instead overlaying patterns of the radical cation and protonated monomer complex. The term monomer complex refers to a 1:1:1 structure as it was found for complexes **114** and **115**. This is a clear indication of differences between the solid state and solution behaviour of Zn(II) complexes prepared with the sterically less hindered H-BIPOL **44d**. At least in the case of compound **118**, although it crystallises as a dinuclear complex, it is present in its mononuclear form if diluted sufficiently. For example, in the ESI-HRMS spectrum, mass peaks for both monomer (*m*/*z* = 743.2747, $[M_{monomer}+H]^+$) and dimer (*m*/*z* = 1489.5979, $[M_{dimer}+H]^+$) structures were found, which indicates that even in high dilution the equilibrium between the two species should be possible.

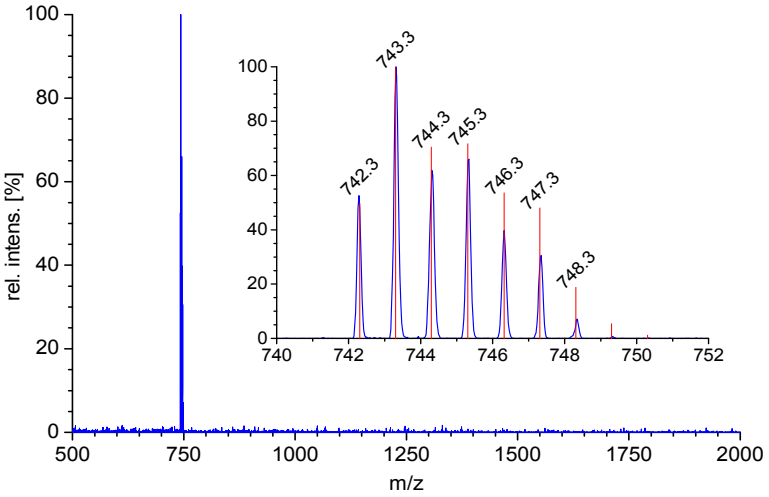

Figure II-30. MALDI-MS (pyrene) of complex **118**, showing overlaying of the detected patterns of both $M^{+\cdot}$ and $[M+H]^+$. The insert shows the experimental (blue) and simulated (red) isotopic patterns.

At first glance the UV-vis and CD properties of complex **118** (Figure II-31) are similar to those of complex a*S*-**116**, *i.e*. the chiral inducer (1*R*,2*R*)-**45g** again led to a positive exciton couplet (Figure II-23). This suggests that the species arising from complex **118** in solution exhibits predominantly a*S* sense of axial rotation. However, as mentioned before one must keep in mind that drawing such conclusions is potentially misleading when comparing the CD of two different chromophores. In contrast to the 3,3'-methyl-substituted biphenol **44b**, which was used in the formation of complex a*S*-**116**, biphenol **44d** is 3,3'-unsubstituted. Consequently, the assumption of a predominant a*S* sense of axial rotation is made under reservation. Nevertheless, the CD of complex **118** shows the form typically observed for the monomeric complexes in this series. Furthermore, the two biphenolate units are *quasi*-inversion symmetric in the solid state structure of **118**, and consequently it is unlikely that the observed CD is caused by such a structure in solution. However, this does not exclude the possibility of complex **118** being present in both monomeric and dimeric form in solution.

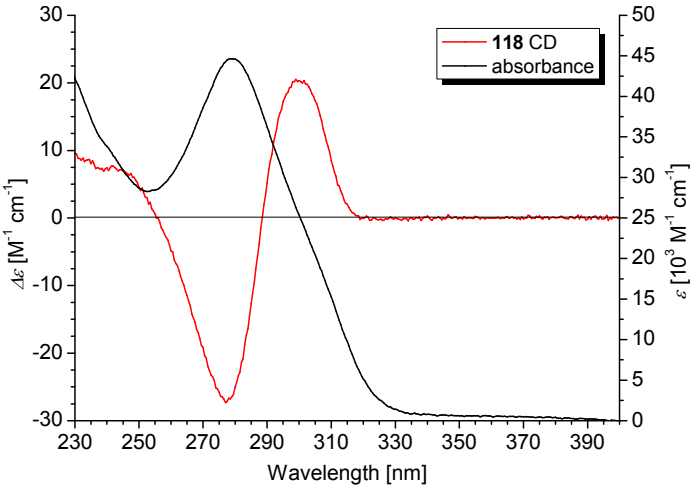

Figure II-31. UV-vis absorption (black line, right axis) and CD spectrum (red line, left axis) of complex **118** (anhydrous THF, 25 ºC, [**118**] = $1.15 \cdot 10^{-4}$ M, concentration calculated as monomer).

Compared to the UV-vis and CD characteristics of complex a*S*-**116** the here observed CD intensities are inferior (Table II-10). This may be due to a lower diastereomeric excess of the CD active species as it can result from a dimerisation equilibrium in solution, but it must again be stressed that two different chromophores are included in this comparison.

Table II-10. CD and UV-vis properties of complex **118**.

CD data	1st CE[a] $\Delta\varepsilon^b$ $(\lambda)^c$	2nd CE[a] $\Delta\varepsilon^b$ $(\lambda)^c$
	20.3 (300)	-27.3 (277)
UV data	λ^c $(\varepsilon)^b$	
	279 (43400)	

[a]CE = Cotton effect; [b]M^{-1} cm^{-1}; [c]nm.

Preparation of [{Zn(μ-H-BIPOLate)((1*R*,2*R*)-^{t}Bu-DACH)}$_2$], complex **119**; [{Zn(**44d**)((1*R*,2*R*)-**45d**)}$_2$].

Compound **119** was prepared following both methods A and B. According to the observations that were made with compound **118**, we propose a solid state structure as it is depicted in Scheme II-25 for complex **119**. However, no single crystals suitable for X-ray analysis could be obtained from **119** but the proposed structure is, however, supported by mass spectrometry. The ESI-HRMS spectrum showed peaks attributable to monomeric (*m*/*z* = 619.3359, $[M_{monomer}+H]^+$) and dimeric (*m*/*z* = 1237.5771, $[M_{dimer}+H]^+$) structures. ^{1}H NMR Spectroscopy did not allow proper signal assignation due to massive line broadening. Moreover, no ^{13}C NMR spectrum was obtained due to a poor signal to noise ratio. Consequently, NMR spectroscopy was not feasible in the structure determination of complex **119**.

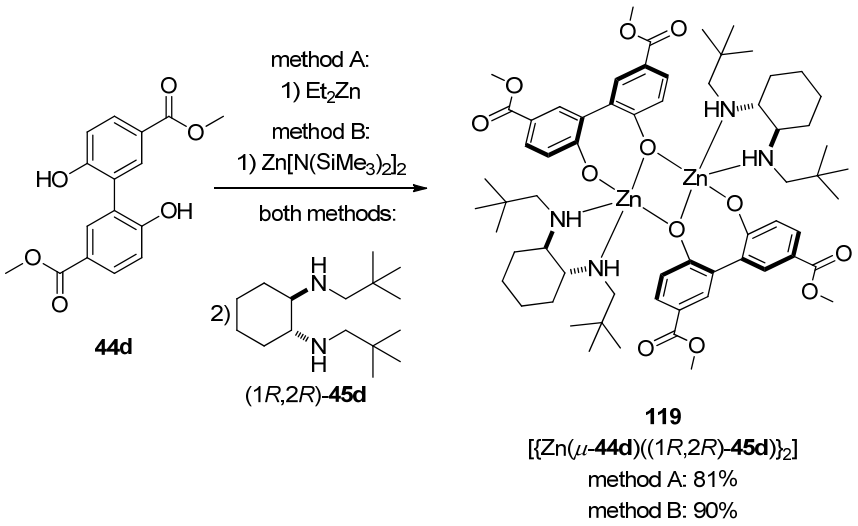

Scheme II-25. Preparation and proposed structure of [{Zn(μ-H-BIPOLate)((1*R*,2*R*)-^{t}Bu-DACH)}$_2$]; **119**.

Owing to the above described problems the analysis of complex **119** is limited to its CD properties. Figure II-32 shows the CD curve of a solution of complex **119** in dry THF measured at three different concentrations. As can be seen, the CD curve undergoes significant changes upon dilution. The shape of the curve resulting from the solution at the highest concentration ($1.85 \cdot 10^{-4}$ M) is unprecedented within this work. Most likely it is attributable to a mixture of two or more CD active species present at this concentration. Such a mixture could arise from an equilibrium between monomeric and dimeric complexes analogous to the proposal made for complex **118** (Scheme II-24) or, from equilibria including other species like homochiral dimers (dimers that exhibit both biphenol units with the same sense of axial rotation, a*R* and a*R* or a*S* and a*S*). CD is additive and all CD active species in solution contribute to the observable CD signal, *i.e.* the exact analysis of such a CD spectrum is impossible unless the CD properties of all the contributing species are known.

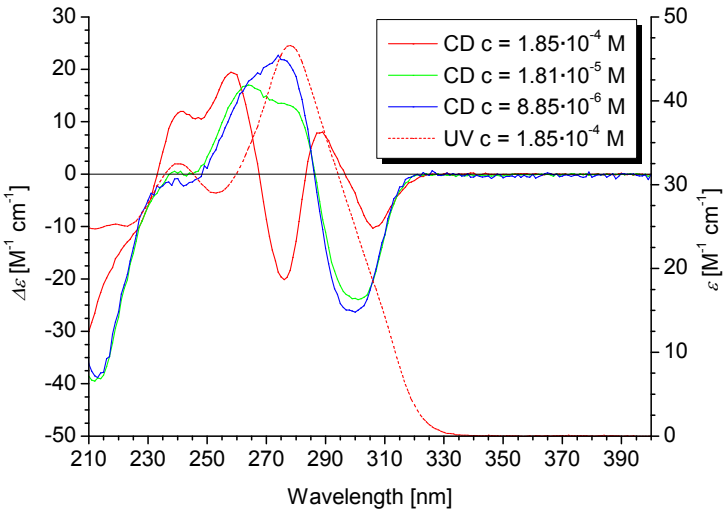

Figure II-32. CD curves of complex **119** measured at different concentrations (anhydrous THF, 25 ºC, red curve was measured at 1 mm, green and blue curves were measured at 1 cm pathlength, concentrations are calculated assuming a monomeric structure).

The possibility of homochiral dimers partaking in the CD curve will be addressed within the next section in the form of a computational approach. Here it should be mentioned that at higher dilutions the CD curve of complex **119** approaches the shape of the curves obtained from monomeric complexes (*e.g.* a*R*-**114** and a*R*-**115**) and complex **118**. Keeping in mind the already mentioned doubts regarding comparing the CD properties of inherently different chromophores, we propose that for adequately diluted solutions of complexes assembled with biphenol **44d**, the predominant species to be found is a monomer according to the formula [Zn(**44d**)(**45**)]. The limiting concentration is a characteristic inherent to each complex [Zn(**44d**)(**45**)] and depending on its dimerisation constant K_D (Scheme II-24). Values for K_D have not been determined yet but might be addressed in the future.

Preparation of [{Zn(μ-H-BIPOLate)((1*R*,2*R*)-Et-DACH)}$_2$], complex **120**; [{Zn(**44d**)((1*R*,2*R*)-**45a**)}$_2$].

The last of the zinc(II) complexes derived from 2,2'-biphenol and enantiopure (1,2)-DACH derivatives to be discussed here is [{Zn(μ-H-BIPOLate)((1*R*,2*R*)-Et-DACH)}$_2$], **120** (Scheme II-26). It was prepared according to methods A and B with identical results as could be proven by IR. As for the previous complexes that were prepared with the 3,3'-unsubstituted 2,2'-biphenol **44d**, we propose a dimeric solid state structure for complex **120**. In contrast to compound **119**, here the structure could be determined by single crystal diffraction.

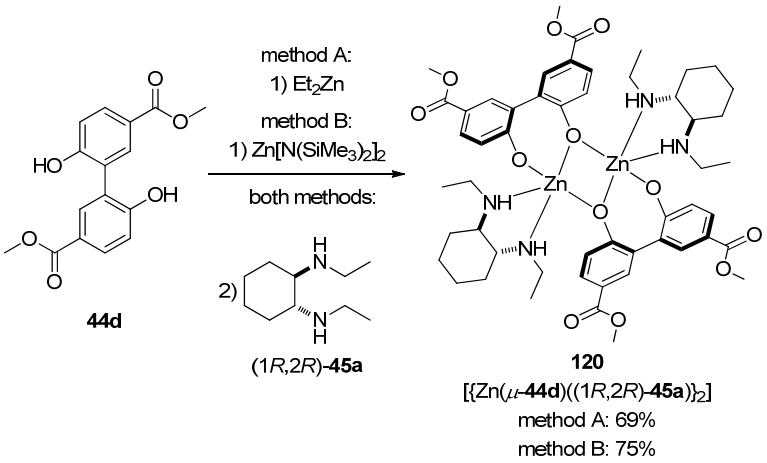

Scheme II-26. Preparation and proposed structure of [{Zn(μ-H-BIPOLate)((1*R*,2*R*)-Et-DACH)}$_2$]; **120**.

Crystals could be obtained from complex **120** by slow diffusion of *n*-hexane into CH_2Cl_2. The structure could be determined (Figure II-33) but unfortunately not be refined owing to the poor quality of the crystal and the heavy disorder found therein. Nevertheless, the only structure to be found in the asymmetric unit corresponded to the proposed dinuclear structure in Scheme II-26. Accordingly, the conclusion that the absence of the 3,3'-substituent in the 2,2'-biphenol unit is preferentially leading to dimeric complexes in the solid state regardless of the size of the N-substituent is reaffirmed.

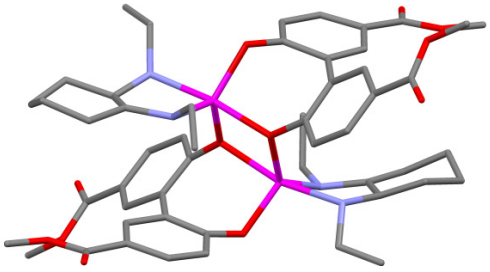

Figure II-33. Crystal structure of complex **120** (hydrogens are omitted for clarity).

The CD of complex **120** was measured in dry THF and dry CH_2Cl_2. As can be seen in Figure II-34, complex **120** shows a negative exciton couplet similar to those found for monomeric complexes [Zn(BIPOLate)(**45**)] in THF. In contrast to complex **119** this is observed at relatively high concentrations ($2.6 \cdot 10^{-4}$ M), *i.e.* **120** readily dissociates into the mononuclear complex in THF. However, at similar concentration ($2.4 \cdot 10^{-4}$ M) in CH_2Cl_2, the shape of the CD curve of complex **120** differs greatly from this behaviour. Solvent polarity may have an influence on CD and indeed in all cases where both solvents were used, intensities were found to be much smaller in CH_2Cl_2 than in THF. Remarkably, this did not affect the absorbance as can be seen in Figure II-34. As a working hypothesis we assumed that possible dimerisation equilibria (see Scheme II-24) explicitly including the formation of homodimers, *i.e.* dimers displaying both biphenol units with the same sense of axial rotation, and the heterodimer as it was found by X-ray diffraction, could be responsible for this finding.

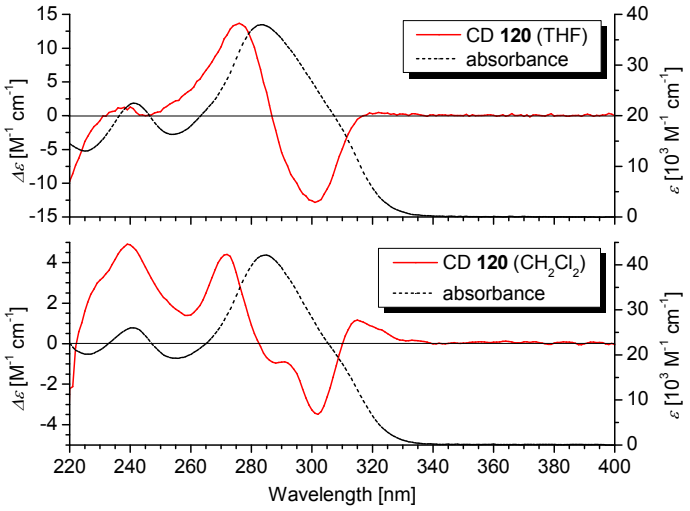

Figure II-34. UV-vis (black lines, right axes) and CD curves (red lines, left axes) of complex **120** in dry THF (top, $2.6 \cdot 10^{-4}$ M) and dry CH_2Cl_2 (bottom, $2.4 \cdot 10^{-4}$ M).

This hypothesis was reassessed by a computational approach. First we optimised the geometries (B3LYP/6-31G(d)) of three dimers of [{Zn(μ-H-BIPOLate)((1*R*,2*R*)-Et-DACH)}$_2$], **120** (no conformational search was carried out here). Two of them were homodimers with a*S* and a*R*, respectively, sense of axial rotation in both BIPOLate units, whereas the third was the heterodimer (one BIPOLate a*S*-, the other a*R*-configured) (Figure II-35).

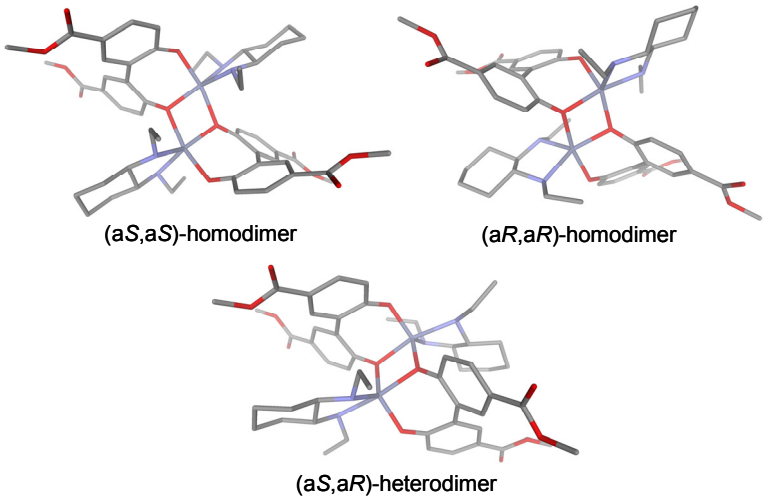

Figure II-35. Geometry optimised (B3LYP/6-31G(d)) structures of the possible homodimers (top) and heterodimer (bottom) of complex **120**; [{Zn(μ-H-BIPOLate)((1*R*,2*R*)-Et-DACH)}$_2$].

The resulting structures where then used as input geometries for the calculation of the CD spectra of each dimer. As can be seen in Figure II-36, the spectra of the two homodimers are almost mirror images with Cotton effects of similar intensities. In contrast, the CD bands of the heterodimer are of much lesser intensity but do not mutually annihilate themselves. Both observations are reasonable since the CD here arises exclusively from the BIPOLate units that are embedded in a chiral environment. This environment is not formed by

the BIPOLate units alone but also by the enantiopure diamine moieties, *i.e.* the BIPOLate ligands of the heterodimer are not necessarily causing mirror inverted CD bands in spite of their opposite sense of axial rotation. Interestingly, the dihedral angles θ of the BIPOLate units in the (a*S*,a*R*)-heterodimer are of practically identical absolute value (-51.4º and 51.3º). It is also apparent the similarity of the calculated CD curve of the (a*S*,a*S*)-homodimer with the experimentally obtained CD curve of complex **120**. Most likely this homodimer is a predominant species in the equilibrium between dimeric and monomeric complexes of compound **120**. Naturally, this does not exclude the contribution of other species to the experimentally observed CD curve.

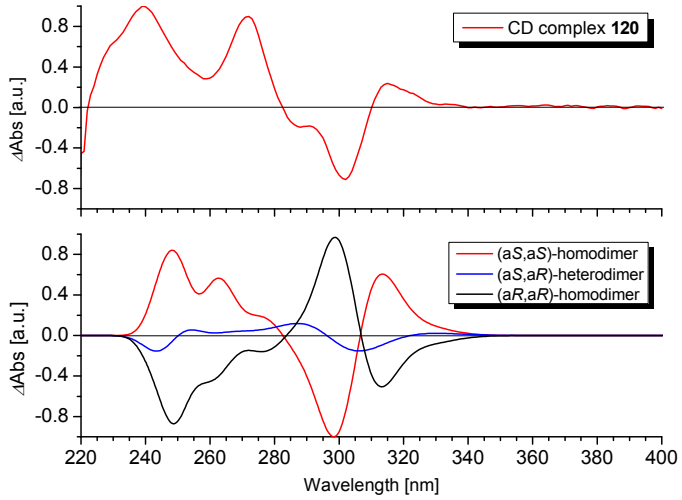

Figure II-36. Comparison of the experimentally obtained CD of complex **120** (top, CH_2Cl_2, 25 ºC, λ_{max} arbitrarily normalised to 1) with the calculated CD (bottom, CAMB3LYP/SVP, resulting curves were 50 nm bathochromically shifted and arbitrarily normalised to 1 relative to λ_{max} of the (a*S*,a*S*)-homodimer) of the two homodimers and the heterodimer of complex **120**; [{Zn(μ-H-BIPOLate)((1*R*,2*R*)-Et-DACH)}$_2$].

3.2.4 Zinc complexes derived from following method C.

In order to bring the discussion of zinc(II) as the structural metal to a close, the until now undiscussed method C (Scheme II-27) shall be briefly addressed. Initially we thought this method could offer an alternative to the use of diethylzinc (method A) since that route did not lead to reproducible results until we started working strictly in a glove box. However, in spite of yielding tangible intermediate products as was desired, method C was not a reliable alternative as will be shown in the following. First of all, this method required the preparation of a Zn(II) precursor complex, namely [$ZnCl_2$((1*R*,2*R*)-**45**)].

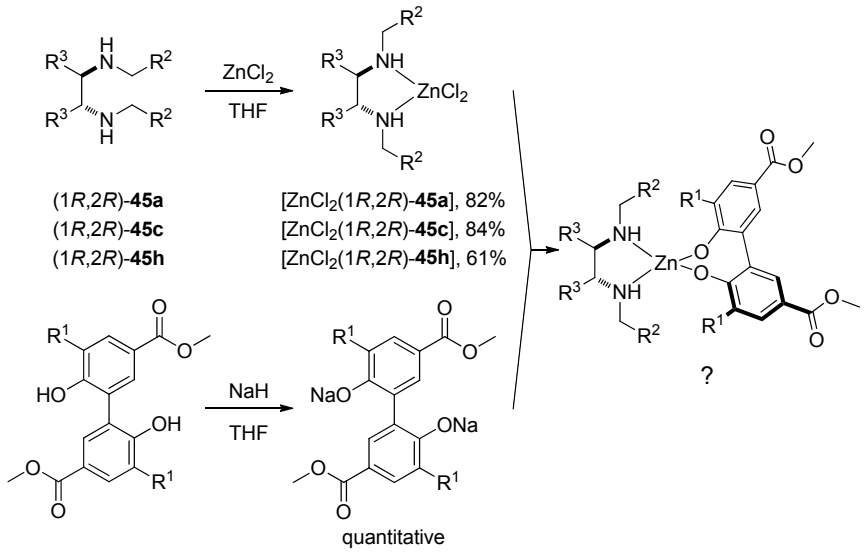

Scheme II-27. Proposed alternative method for the preparation of zinc(II) complexes derived from 2,2'-biphenolates and [$ZnCl_2$((1*R*,2*R*)-**45**)] precursor complexes.

The [$ZnCl_2$((1*R*,2*R*)-**45**)] precursor complexes were readily synthesised following a method reported by Lee and co-workers.[82] Single crystals were obtained by recrystallisation in anhydrous toluene and the solid state structures of three such complexes were determined (Figure II-37). In all cases the atomic distances (Zn-Cl and Zn-N) and bond angles (Cl-Zn-Cl and N-Zn-N) (Table II-11) were close to those reported by Lee for [dichloro(*N*,*N*,*N*',*N*'-tetramethyl-1,2-cyclohexanediamine)]zinc(II). Interestingly, the N-Zn-N bond angles appear to be independent from the flexibility of the diamine backbone, *i.e.* they are dominated by the preferential tetrahedral geometry of the zinc(II) centre. The Cl-Zn-Cl bond angle in [$ZnCl_2$(1*R*,2*R*)-**45c**)] (entry 16) is approximately 5 º wider than the Cl-Zn-Cl bond angles in the remaining two and Lee's complexes. Most likely the wider angle is due to the increased volume of the N-substituents and a similar Cl-Zn-Cl angle (121.42(3) º) was found by Roh and co-workers in the [dichloro(*trans*-(*R*,*R*)-*N*,*N*'-bis-(4-methoxybenzyl)-1,2-cyclohexanediamine)] zinc(II) complex with bulkier substituents.[83] Furthermore, the N-Zn-N angles are also similar to those found in the mononuclear zinc(II) complexes a*R*-**114** (entry 5, Table II-2) and a*R*-**115** (entry 5, Table II-5).

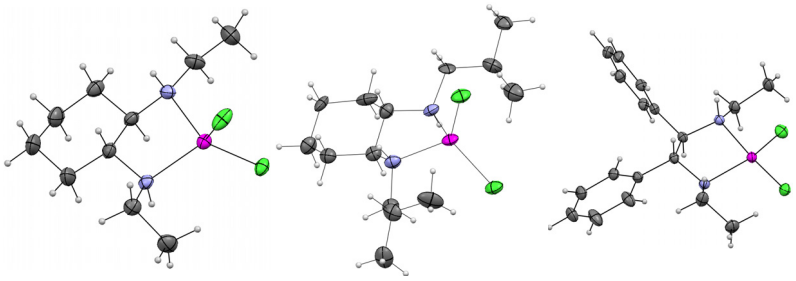

Figure II-37. ORTEP plots of [dichloro((1*R*,2*R*)-*N*,*N*'-diethyl-1,2-cyclohexanediamine)] zinc(II) [$ZnCl_2$((1*R*,2*R*)-**45a**)] (left), [dichloro((1*R*,2*R*)-*N*,*N*'-diisobutyl-1,2-cyclohexanediamine)] zinc(II) [$ZnCl_2$((1*R*,2*R*)-**45c**)] (centre), and [dichloro((1*R*,2*R*)-*N*,*N*'-diethyl-1,2-diphenylethane-1,2-diamine)] zinc(II) [$ZnCl_2$((1*R*,2*R*)-**45h**)] (right). Ellipsoids are at the 50% probability level, hydrogens are drawn as size-fixed spheres of 0.10 Å radii.

Table II-11. Selected bond lengths [Å] and bond angles [º] for complexes [$ZnCl_2$((1*R*,2*R*)-**45a**)], [$ZnCl_2$((1*R*,2*R*)-**45c**)], and [$ZnCl_2$((1*R*,2*R*)-**45h**)].

[$ZnCl_2$((1*R*,2*R*)-**45a**)]	atom 1	atom 2		**length**
1	Zn(1)B	N(1)B		2.062(3)
2	Zn(1)B	N(2)B		2.070(3)
3	Zn(1)B	Cl(1)B		2.2313(10)
4	Zn(1)B	Cl(2)B		2.2530(10)
[$ZnCl_2$((1*R*,2*R*)-**45c**)]				
5	Zn(1)B	N(1)B		2.045(9)
6	Zn(1)B	N(2)B		2.059(10)
7	Zn(1)B	Cl(1)B		2.232(4)
8	Zn(1)B	Cl(2)B		2.228(4)
[$ZnCl_2$((1*R*,2*R*)-**45h**)]				
9	Zn(1)A	N(1)A		2.0576(13)
10	Zn(1)A	N(2)A		2.0658(13)
11	Zn(1)A	Cl(1)A		2.2317(4)
12	Zn(1)A	Cl(2)A		2.2224(4)
[$ZnCl_2$((1*R*,2*R*)-**45a**)]	atom 1	atom 2	atom 3	**angle**
13	N(1)B	Zn(1)B	N(2)B	86.64(10)
14	Cl(1)B	Zn(1)B	Cl(2)B	116.58(4)
[$ZnCl_2$((1*R*,2*R*)-**45c**)]				
15	N(1)B	Zn(1)B	N(2)B	86.4(4)
16	Cl(1)B	Zn(1)B	Cl(2)B	121.94(14)
[$ZnCl_2$((1*R*,2*R*)-**45h**)]				
17	N(1)A	Zn(1)A	N(2)A	86.02(5)
18	Cl(1)A	Zn(1)A	Cl(2)A	116.708(17)

These complexes were then reacted in anhydrous THF with the sodium biphenolates of **44b** and **44d**. Unfortunately, no reproducible CD or NMR data were obtained yet the data suggested the presence of several species in solution. We assumed that this was related to problems of measuring exact amounts (only a few mg were required) of the sodium hydride that furthermore had to be washed free of the mineral oil with dry hexanes before usage. Exemplary for these difficulties is the X-ray structure shown in Figure II-38 that at the same time is the only solid state structure that could be elucidated from complexes prepared according to this strategy. As can be seen the deprotonation of biphenol **44d** was incomplete and as a result could not displace the remaining chloride ligand at the zinc(II) centre. We assumed a deficit of NaH to be the reason. However, experiments with small excesses of NaH resulted in dynamic processes on the NMR timescale in all cases and with other biphenol/diamine combinations. It was reasoned that these problems could be overcome by using another base like *n*-butyllithium instead of sodium hydride but in the meantime the previously described methods have proven to be superior and this strategy was abandoned.

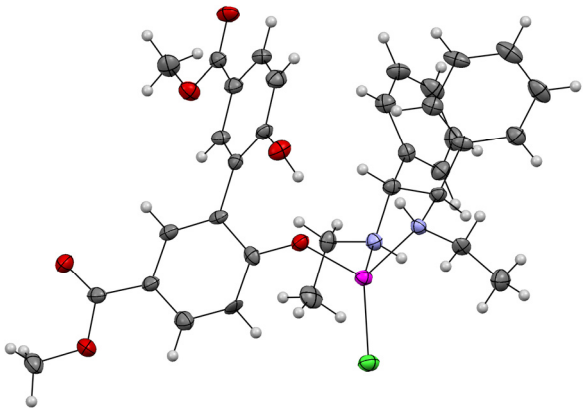

Figure II-38. ORTEP plot of [ZnCl(**44d**)((1*R*,2*R*)-**45h**)], hydrogen atoms are drawn as size-fixed spheres of 0.15 Å radii, solvent molecules (toluene) are omitted for clarity.

3.3 Copper as the Structural Metal

Besides zinc(II), we considered copper(II) as the structural metal in the transfer of chirality from enantiopure (1*R*,2*R*)-DACH compounds to dynamically racemic 2,2'-biphenol derivatives. Regarding the coordination geometry, the d^9 electron configured Cu(II) does not show a pronounced preference for tetrahedral structures but is known to also readily adopt square-planar, trigonal-bipyramidal, tetragonal-pyramidal, and octahedral geometries in mono- or polynuclear complexes.[93] Nevertheless, coordination studies with the aim of obtaining mixed diamine-biphenol complexes were carried out following two distinct methods: i) deprotonation of the biphenol with NaOH in aqueous methanol, in the following referred to as the "reversible deprotonation" method (Scheme II-28R) and ii) an "irreversible deprotonation" procedure under inert conditions using *n*-butyllithium as the base (Scheme II-28I). Studies were made using commercially available 2,2'-biphenol and enantiopure (1,2)-cyclohexanediamine.

Regarding the "reversible deprotonation" method, we followed a procedure reported by Trivedi and co-workers.[94] During the slow addition of the sodium biphenolate to the dark blue Cu(II)-diamine complex in aqueous MeOH, a colour change to greyish-blue and subsequently to green-brown accompanied by precipitation of a green product occurred. The precipitation of the green product also took place when carrying out the reaction under addition of the Cu(II)-diamine species to the sodium biphenolate solution, or with sub-stoichiometric amounts of NaOH. Presumably, the green precipitate consisted of Cu(II) hydroxides and/or mixed Cu(II)amine/hydroxide complexes. Since this was entirely pH-dependent, this problem could not be avoided by this procedure. However, removing the precipitate, which accounted for *ca.* 17% by weight relative to the total amount of isolated products, yielded

a dark violet solution that was concentrated to dryness, re-dissolved in $CHCl_3$, and filtered in order to remove NaCl.

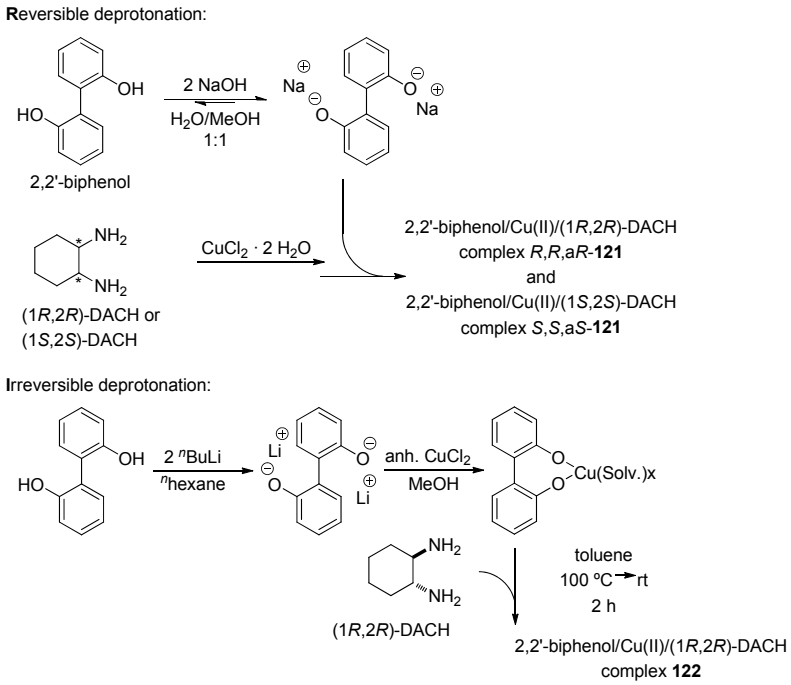

Scheme II-28. Preparation of 2,2'-biphenol/Cu(II)/(1,2)-DACH complexes **121** and **122** following two distinct methods.

Single crystals suitable for X-ray diffraction were grown at -18 ºC within several days from a room temperature semi-saturated solution in MeOH. The intensely violet crystals were cubic and rather small (0.2-0.3 mm edge length). The structures of copper(II) complexes coordinated by 2,2'-biphenol and (1*R*,2*R*)-DACH and (1*S*,2*S*)-DACH, respectively, could be elucidated (Figure II-39) and the Cu(II) centre was found being of octahedral geometry ligated by two diamine and two biphenol moieties. The latter is attached to the metal centre *via* a phenolate oxygen atom, whilst the second phenol function was not deprotonated. Nevertheless, both biphenol units have adopted a preferential axial sense of rotation in the complexes, namely a*R*

($\theta \approx$ -42 º) with the (1*R*,2*R*)- and a*S* ($\theta \approx$ 42 º) with the (1*S*,2*S*)-DACH ligand. We assumed the formation of hydrogen bonds to be essential for the induction of chirality. Both non-ligating phenol groups established weak hydrogen bonds (based on the O···N distances of entries 12 and 13 in Table II-12) with one of the diamines' amino groups. In addition, intramolecular H-bonds were found in both 2,2'-biphenol units between the atoms O(1)···H–O(2) and O(3)···H–O(4). These hydrogen bonds are stronger and shorter than the intermolecular ones (see entries 14 and 15 in Table II-12). Hydrogen bonds from the non-ligating phenol and the remaining amino group to co-crystallised MeOH (not shown here) completed the network. In order to determine the stereogenic elements in Figure II-39, it is helpful to identify the orientation of the (cyan) hydrogen bonds keeping in mind that in *R*,*R*,a*R*-**121** the atoms O(1), O(3), N(1), and N(3) are in front of O(2), O(4), N(2), and N(4), whereas in *S*,*S*,a*S*-**121** they are behind them.

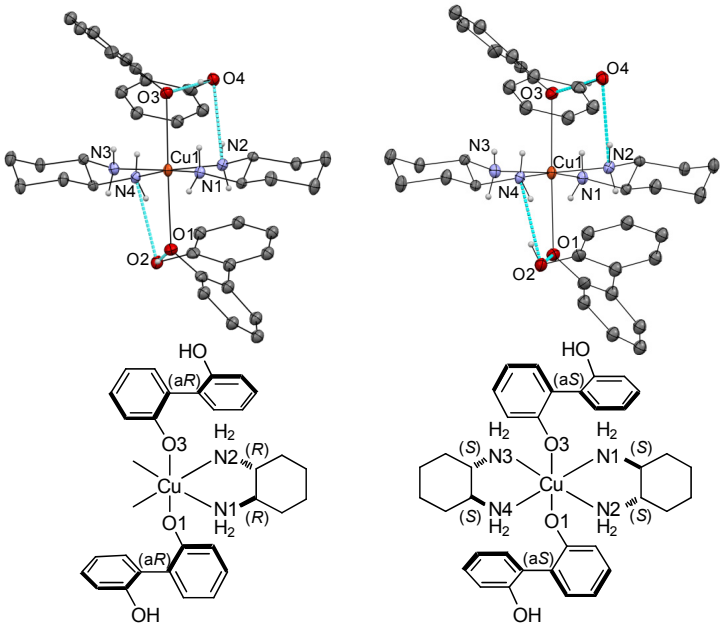

Figure II-39. ORTEP plots of copper(II)-2,2'-BIPOL complexes **121** generated following method R ("reversible deprotonation") with (1*R*,2*R*)-DACH (left) resulting in a*R* configuration of the biphenol and (1*S*,2*S*)-DACH (right) resulting in a*S* configuration of the biphenol. Ellipsoids are at the 50% probability level; hydrogens are drawn as size-fixed spheres of 0.10 Å radii; all C-attached hydrogen atoms and co-crystallised MeOH molecules are omitted for clarity. Cyan lines indicate hydrogen bonding interactions.

Table II-12 includes several atomic distances, angles and H-bond lengths (defined as O···N distances) of complex *R*,*R*,a*R*-**121**. The four short (entries 1-4) and two elongated (entries 5 and 6) bond lengths clearly indicate a tetragonally elongated octahedron. Such Jahn-Teller distorted octahedral geometries are typical for the d^9 configured Cu(II) centre resulting from the unequal occupation of the non-degenerated e_g orbital pair (d_{z^2}, $d_{x^2-y^2}$)[93].

Table II-12. Selected bond lengths [Å], bond angles [º], and H-bond lengths [Å] for complex *R*,*R*,a*R*-**121**.

entry	atom 1	atom 2	atom 3	**length**
1	Cu(1)	N(1)		2.0122(18)
2	Cu(1)	N(2)		2.033(2)
3	Cu(1)	N(3)		2.011(2)
4	Cu(1)	N(4)		2.0308(19)
5	Cu(1)	O(1)		2.6343(19)
6	Cu(1)	O(2)		2.562(2)
				angle
7	N(1)	Cu(1)	N(2)	84.85(8)
8	N(3)	Cu(1)	N(1)	95.29(8)
9	N(3)	Cu(1)	N(2)	173.49(9)
10	O(3)	Cu(1)	O(1)	178.43(6)
11	N(3)	Cu(1)	O(1)	92.71(7)
				H-bond length[a]
12	O(2)	N(4)		2.97
13	O(4)	N(2)		3.01
14	O(1)	O(2)		2.46
15	O(3)	O(4)		2.45

[a]Defined as O···N distance

The IR spectrum of complex *R*,*R*,a*R*-**121** is in agreement with the X-ray structure. The coordination of the diamine to Cu(II) should be visible in a shift of the two amine stretching vibrations towards smaller wave numbers. However, due to the broad bands of the hydrogen bonded phenol and methanol hydroxyl groups, the expected shift cannot be identified unambiguously.

ESI-MS analysis of a solution of **121** did not confirm the structure observed in the solid state. Whilst the molecular ion of complex **121** was not observed in the ESI spectrum, a group of peaks from m/z = 476 to m/z = 480 was observed. These signals clearly confirmed the presence of one Cu atom in the fragment and could be assigned to the fragment which arises from **121** by losing one biphenol ligand ($[MH\text{-}C_{12}H_9O_2]^+$). Unfortunately, several non-assignable peaks together with signals that are compatible with the $[[\{Cu(\mu\text{-BIPOLate})((1,2)\text{-DACH})\}_2]+H]^+$ (m/z = 723-729) and $[[Cu(BIPOLate)((1,2)\text{-DACH})]+H]^+$ (m/z = 362-366) complexes were also observed. Whether these signals correspond to fragmentations of complex **121** during the MS-determination or arise from multiple metal-ligand equilibria in the diluted MeOH solution remains to be clarified.

Given that the outcome of the complexation reaction using reversible deprotonation conditions rendered a diastereomerically pure crystalline material, we wondered whether the BIPOL groups in this neutral Cu(II) complex would be configurationally stable in solution. The suitable spectroscopic techniques for studying this aspect were quite restricted, as NMR turned out to be impracticable due to signal broadening arising from paramagnetic effects. In order to study whether the intramolecular (*i.e.* hydrogen bonds between methanol and two Cu(II) complexes) and intermolecular hydrogen bonds (*i.e.* between the non-deprotonated Ar-OH and amino groups; see Figure II-39) were capable of freezing the rotation around the C-C molecular axis of the BIPOL groups in solution, the UV-vis and CD spectra of the complex were recorded. Complex **121** shows a weak absorbance band attributable to a d-d transition at 555 nm (ε = 200 M^{-1} cm^{-1}) in MeOH and 610 nm (ε = 170 M^{-1} cm^{-1}) in CH_2Cl_2, respectively. This is in accordance with values reported in the literature for Cu(II) complexes.[95] As can be seen in the CD spectrum of complex *R*,*R*,a*R*-**121** measured in MeOH

(Figure II-40), a weak positive Cotton-effect is found at *ca*. 248 nm. The small amplitude is most likely attributable to the protic solvent which disrupts the weak hydrogen bonding that was observed in the solid state structure between the phenol and the amino group. Consequently, the 2,2'-biphenol unit largely regains its rotatory freedom and we eventually reasoned that the uniform sense of axial chirality in the BIPOL fragment was lost in solution.

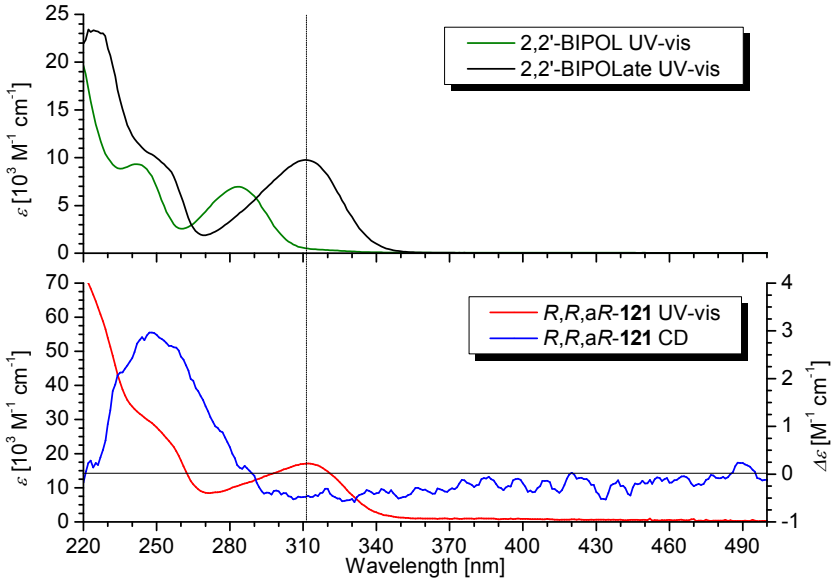

Figure II-40. UV-vis spectra of 2,2'-biphenol and 2,2'-biphenolate (top, MeOH, 298 K) and UV-vis and CD spectrum of complex *R*,*R*,a*R*-**121** (bottom, MeOH, 298 K).

In contrast, the hydrogen bonding network should be more stable in aprotic solvents like CH_2Cl_2. As can be seen in Figure II-41, a very weak CD band attributable to the absorbance at 323 nm is observed for complex *R*,*R*,a*R*-**121**, thus, strengthening the assumption of hydrogen bonds being responsible for the preferential sense of axial rotation. However, the effect is very weak and further complexation studies with enantiomerically pure amines and other dynamically racemic biaryl derivatives and copper as the bonding metal were abandoned for this reason.

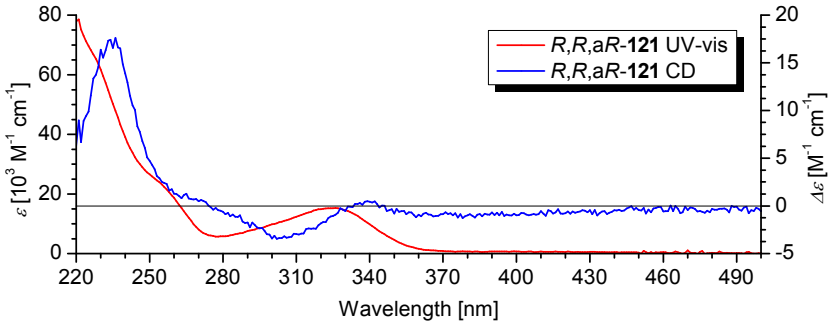

Figure II-41. UV-vis and CD spectrum of complex *R*,*R*,a*R*-**121** (CH_2Cl_2, 298 K)

Using *n*-butyllithium as the deprotonating agent under inert conditions (*i.e.* following the "irreversible deprotonation" strategy in Scheme II-28) lead to the identification of the dinuclear complex structure **122** by X-ray diffraction of single crystals grown in anhydrous 1,4-dioxane (Figure II-42). These structures were similar to the dinuclear ones that were found for zinc(II) complexes. Just as in the latter cases, no preferential sense of axial rotation was induced in the biaryl unit by the use of enantiopure diamine derivatives. It should be furthermore said that the asymmetric unit of the structure shown here also contained two molecules of free biphenol per complex molecule (see appendix). It could not be clarified whether the amounts of free biphenol resulted

from incomplete deprotonation with *n*-butyllithium or the crystallisation of the complexes under not completely anhydrous conditions.

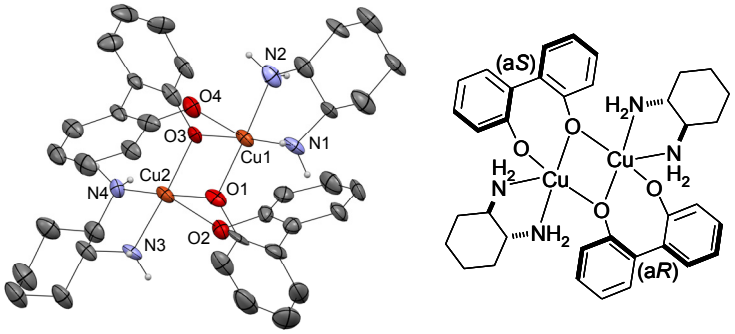

Figure II-42. ORTEP plot of dinuclear copper(II)-2,2'-BIPOL complex **122** generated following method I with (1*R*,2*R*)-DACH. Biphenol units show both a*R* and a*S* configurations. Ellipsoids are at the 50% probability level; hydrogens are drawn as size-fixed spheres of 0.15 Å radii. Co-crystallised solvent (1,4-dioxane) and uncoordinated BIPOL molecules are omitted for clarity (see appendix for the complete structure).

Owing to the fact that the desired tetrahedral chelating structures were not obtained with either of the two methods and furthermore only weak induction of chirality was observed in complexes derived from the "reversible deprotonation" method, we eventually abandoned Cu(II) and concentrated the studies on complexes using Zn(II) as structural metal.

References

[1] J. Crassous, *Chem. Soc. Rev.* **2009**, *38*, 830.
[2] U. Knof, A. von Zelewsky, *Angew. Chem., Int. Ed.* **1999**, *38*, 303.
[3] H. Brunner, *Angew. Chem., Int. Ed.* **1999**, *38*, 1194.
[4] O. Mamula, A. von Zelewsky, *Coord. Chem. Rev.* **2003**, *242*, 87.
[5] M. Fontecave, *ChemCatChem* **2010**, *2*, 1533.
[6] J. M. Lehn, A. Rigault, J. Siegel, J. Harrowfield, B. Chevrier, D. Moras, *Proc. Natl. Acad. Sci. U. S. A.* **1987**, *84*, 2565.
[7] X.-D. Zheng, T.-B. Lu, *CrystEngComm* **2010**, *12*, 324.
[8] C. He, Y. Zhao, D. Guo, Z. Lin, C. Duan, *Eur. J. Inorg. Chem.* **2007**, 3451.
[9] S. Yagi, T. Morinaga, T. Nomura, T. Takagishi, T. Mizutani, S. Kitagawa, H. Ogoshi, *J. Org. Chem.* **2001**, *66*, 3848.
[10] Y. Kubo, T. Ohno, J.-i. Yamanaka, S. Tokita, T. Iida, Y. Ishimaru, *J. Am. Chem. Soc.* **2001**, *123*, 12700.
[11] X. Huang, B. H. Rickman, B. Borhan, N. Berova, K. Nakanishi, *J. Am. Chem. Soc.* **1998**, *120*, 6185.
[12] S. Matile, N. Berova, K. Nakanishi, *Chem. Biol.* **1996**, *3*, 379.
[13] S. Matile, N. Berova, K. Nakanishi, J. Fleischhauer, R. W. Woody, *J. Am. Chem. Soc.* **1996**, *118*, 5198.
[14] T. Kurtan, N. Nesnas, Y.-Q. Li, X. Huang, K. Nakanishi, N. Berova, *J. Am. Chem. Soc.* **2001**, *123*, 5962.
[15] T. Kurtan, N. Nesnas, F. E. Koehn, Y.-Q. Li, K. Nakanishi, N. Berova, *J. Am. Chem. Soc.* **2001**, *123*, 5974.
[16] H. Ishii, Y. Chen, A. Miller Ross, S. Karady, K. Nakanishi, N. Berova, *Chirality* **2005**, *17*, 305.
[17] G. Proni, G. Pescitelli, X. Huang, K. Nakanishi, N. Berova, *J. Am. Chem. Soc.* **2003**, *125*, 12914.
[18] J. J. Becker, P. S. White, M. R. Gagne, *J. Am. Chem. Soc.* **2001**, *123*, 9478.
[19] M. D. Tudor, J. J. Becker, P. S. White, M. R. Gagne, *Organometallics* **2000**, *19*, 4376.
[20] A. M. Costa, C. Jimeno, J. Gavenonis, P. J. Carroll, P. J. Walsh, *J. Am. Chem. Soc.* **2002**, *124*, 6929.
[21] K. Ding, A. Ishii, K. Mikami, *Angew. Chem., Int. Ed.* **1999**, *38*, 497.
[22] K. Mikami, R. Angelaud, K. Ding, A. Ishii, A. Tanaka, N. Sawada, K. Kudo, M. Senda, *Chem. Eur. J.* **2001**, *7*, 730.
[23] R. G. Parr, R. G. Pearson, *J. Am. Chem. Soc.* **1983**, *105*, 7512.
[24] R. G. Pearson, *J. Chem. Educ.* **1968**, *45*, 581.
[25] R. G. Pearson, *J. Chem. Educ.* **1968**, *45*, 643.
[26] R. G. Pearson, J. Songstad, *J. Am. Chem. Soc.* **1967**, *89*, 1827.
[27] V. F. Slagt, P. W. N. M. van Leeuwen, J. N. H. Reek, *Chem. Commun.* **2003**, 2474.

[28] V. F. Slagt, P. W. N. M. van Leeuwen, J. N. H. Reek, *Dalton Trans.* **2007**, 2302.
[29] M. Kuil, P. E. Goudriaan, A. W. Kleij, D. M. Tooke, A. L. Spek, P. W. N. M. van Leeuwen, J. N. H. Reek, *Dalton Trans.* **2007**, 2311.
[30] M. Kuil, P. E. Goudriaan, P. W. N. M. van Leeuwen, J. N. H. Reek, *Chem. Commun.* **2006**, 4679.
[31] S. Carboni, C. Gennari, L. Pignataro, U. Piarulli, *Dalton Trans.* **2011**, *40*, 4355.
[32] V. F. Slagt, P. W. N. M. van Leeuwen, J. N. H. Reek, *Angew. Chem., Int. Ed.* **2003**, *42*, 5619.
[33] A. J. Sandee, J. N. H. Reek, *Dalton Trans.* **2006**, 3385.
[34] V. F. Slagt, M. Roeder, P. C. J. Kamer, P. W. N. M. van Leeuwen, J. N. H. Reek, *J. Am. Chem. Soc.* **2004**, *126*, 4056.
[35] J. N. H. Reek, M. Roeder, P. E. Goudriaan, P. C. J. Kamer, P. W. N. M. van Leeuwen, V. F. Slagt, *J. Organomet. Chem.* **2005**, *690*, 4505.
[36] P. E. Goudriaan, X.-B. Jang, M. Kuil, R. Lemmens, P. W. N. M. van Leeuwen, J. N. H. Reek, *Eur. J. Org. Chem.* **2008**, 6079.
[37] P. E. Goudriaan, M. Kuil, X.-B. Jiang, P. W. N. M. van Leeuwen, J. N. H. Reek, *Dalton Trans.* **2009**, 1801.
[38] X.-B. Jiang, L. Lefort, P. E. Goudriaan, A. H. M. de Vries, P. W. N. M. van Leeuwen, J. G. de Vries, J. N. H. Reek, *Angew. Chem., Int. Ed.* **2006**, *45*, 1223.
[39] X.-B. Jiang, P. W. N. M. van Leeuwen, J. N. H. Reek, *Chem. Commun.* **2007**, 2287.
[40] J. M. Takacs, D. S. Reddy, S. A. Moteki, D. Wu, H. Palencia, *J. Am. Chem. Soc.* **2004**, *126*, 4494.
[41] J. M. Atkins, S. A. Moteki, S. G. DiMagno, J. M. Takacs, *Org. Lett.* **2006**, *8*, 2759.
[42] J. M. Takacs, P. M. Hrvatin, J. M. Atkins, D. S. Reddy, J. L. Clark, *New J. Chem.* **2005**, *29*, 263.
[43] S. A. Moteki, J. M. Takacs, *Angew. Chem., Int. Ed.* **2008**, *47*, 894.
[44] J. M. Takacs, K. Chaiseeda, S. A. Moteki, D. S. Reddy, D. Wu, K. Chandra, *Pure Appl. Chem.* **2006**, *78*, 501.
[45] S. Chikkali, D. Gudat, M. Niemeyer, *Chem. Commun.* **2007**, 981.
[46] S. Chikkali, D. Gudat, *Eur. J. Inorg. Chem.* **2006**, 3005.
[47] S. H. Chikkali, D. Gudat, F. Lissner, M. Nieger, T. Schleid, *Dalton Trans.* **2007**, 3906.
[48] S. H. Chikkali, D. Gudat, F. Lissner, M. Niemeyer, T. Schleid, M. Nieger, *Chem. Eur. J.* **2009**, *15*, 482.
[49] J. Holz, O. Zayas, H. Jiao, W. Baumann, A. Spannenberg, A. Monsees, T. H. Riermeier, J. Almena, R. Kadyrov, A. Boerner, *Chem. Eur. J.* **2006**, *12*, 5001.
[50] J. D. Lee, *Concise Inorganic Chemistry V*, Blackwell, **1996**.
[51] J. Meeuwissen, J. N. H. Reek, *Nat. Chem.* **2010**, *2*, 615.

[52] M. J. Wilkinson, P. W. N. M. van Leeuwen, J. N. H. Reek, *Org. Biomol. Chem.* **2005**, *3*, 2371.
[53] B. Breit, *Angew. Chem., Int. Ed.* **2005**, *44*, 6816.
[54] W. Tang, X. Zhang, *Chem. Rev.* **2003**, *103*, 3029.
[55] W. S. Knowles, M. J. Sabacky, *Chem. Commun.* **1968**, 1445.
[56] I. D. Gridnev, T. Imamoto, *Chem. Commun.* **2009**, 7447.
[57] H. B. Kagan, P. Dang Tuan, *J. Am. Chem. Soc.* **1972**, *94*, 6429.
[58] T. Ohkuma, M. Koizumi, M. Yoshida, R. Noyori, *Org. Lett.* **2000**, *2*, 1749.
[59] Y. Li, Y. Zhou, Q. Shi, K. Ding, R. Noyori, C. A. Sandoval, *Adv. Synth. Catal.* **2011**, *353*, 495.
[60] C. A. Sandoval, Q. Shi, S. Liu, R. Noyori, *Chem. Asian J.* **2009**, *4*, 1221.
[61] J. L. Nunez-Rico, H. Fernandez-Perez, J. Benet-Buchholz, A. Vidal-Ferran, *Organometallics* **2010**, *29*, 6627.
[62] K. Kaellstroem, I. Munslow, P. G. Andersson, *Chem. Eur. J.* **2006**, *12*, 3194.
[63] S. J. Roseblade, A. Pfaltz, *Acc. Chem. Res.* **2007**, *40*, 1402.
[64] N. Fleury-Bregeot, V. de la Fuente, S. Castillon, C. Claver, *ChemCatChem* **2010**, *2*, 1346.
[65] F. D. Klingler, *Acc. Chem. Res.* **2007**, *40*, 1367.
[66] F. Glorius, *Org. Biomol. Chem.* **2005**, *3*, 4171.
[67] Y.-G. Zhou, *Acc. Chem. Res.* **2007**, *40*, 1357.
[68] O. Pamies, P. G. Andersson, M. Dieguez, *Chem. Eur. J.* **2010**, *16*, 14232.
[69] C. S. Shultz, S. W. Krska, *Acc. Chem. Res.* **2007**, *40*, 1320.
[70] H. Shimizu, I. Nagasaki, K. Matsumura, N. Sayo, T. Saito, *Acc. Chem. Res.* **2007**, *40*, 1385.
[71] N. B. Johnson, I. C. Lennon, P. H. Moran, J. A. Ramsden, *Acc. Chem. Res.* **2007**, *40*, 1291.
[72] W. S. Knowles, *Angew. Chem., Int. Ed.* **2002**, *41*, 1998.
[73] R. Noyori, *Angew. Chem., Int. Ed.* **2002**, *41*, 2008.
[74] K. B. Sharpless, *Angew. Chem., Int. Ed.* **2002**, *41*, 2024.
[75] T. J. Davis, J. Balsells, P. J. Carroll, P. J. Walsh, *Org. Lett.* **2001**, *3*, 699.
[76] K. Mikami, Y. Matsumoto, L. Xu, *Inorg. Chim. Acta* **2006**, *359*, 4159.
[77] B. Schetter, B. Ziemer, G. Schnakenburg, R. Mahrwald, *J. Org. Chem.* **2008**, *73*, 813.
[78] G. Pescitelli, L. Di Bari, P. Salvadori, *Organometallics* **2004**, *23*, 4223.
[79] K. M. Waltz, P. J. Carroll, P. J. Walsh, *Organometallics* **2004**, *23*, 127.
[80] T. J. Boyle, N. W. Eilerts, J. A. Heppert, F. Takusagawa, *Organometallics* **1994**, *13*, 2218.

[81] D. J. Darensbourg, M. W. Holtcamp, G. E. Struck, M. S. Zimmer, S. A. Niezgoda, P. Rainey, J. B. Robertson, J. D. Draper, J. H. Reibenspies, *J. Am. Chem. Soc.* **1999**, *121*, 107.
[82] N. Y. Lee, J. U. Yoon, J. H. Jeong, *Acta Crystallogr., Sect. E: Struct. Rep.* **2007**, *E63*, m2471.
[83] S. G. Roh, J. U. Yoon, J. H. Jeong, *Polyhedron* **2004**, *23*, 2063.
[84] J. Iskra, S. Stavber, M. Zupan, *Synthesis* **2004**, 1869.
[85] D. J. Darensbourg, M. S. Zimmer, P. Rainey, D. L. Larkins, *Inorg. Chem.* **2000**, *39*, 1578.
[86] R. Jenkins, R. Snyder, Editors, *Introduction to X-Ray Powder Diffractometry*, WILEY, New York, **1996**.
[87] K. Mislow, E. Bunnenberg, R. Records, K. Wellman, C. Djerassi, *J. Am. Chem. Soc.* **1963**, *85*, 1342.
[88] E. Bunnenberg, C. Djerassi, K. Mislow, A. Moscowitz, *J. Am. Chem. Soc.* **1962**, *84*, 2823.
[89] Y. Zhao, D. G. Truhlar, *Theor. Chem. Acc.* **2008**, *120*, 215.
[90] M. Strohalm, D. Kavan, P. Novak, M. Volny, V. Havlicek, *Anal. Chem.* **2010**, *82*, 4648.
[91] M. Hesse, H. Meier, B. Zeeh, Editors, *Spectroscopic Methods in Organic Chemistry*, Thieme, **1997**.
[92] N. Berova, L. Di Bari, G. Pescitelli, *Chem. Soc. Rev.* **2007**, *36*, 914.
[93] N. N. Greenwood, A. Earnshaw, *Chemistry of the Elements*, 2nd ed., ELSEVIER, **1997**.
[94] M. J. Patel, B. M. Trivedi, *J. Chem. Res.* **2004**, 198.
[95] R. N. Jadeja, J. R. Shah, E. Suresh, P. Paul, *Polyhedron* **2004**, *23*, 2465.

III Perspectives of the Supramolecular Assemblies as Catalytic Ligands

1 Preliminary Considerations

The ultimate goal of our ongoing project “supramolecular approaches to catalysis”, for which the present thesis sets the synthetic principles for the required chiral building blocks by means of supramolecular interactions, is the development of catalytic ligands from the model assemblies, and assessment of their catalytic properties in asymmetric transformations of interest. Key aspects in the design of our supramolecular ligands are shown together with a synthetic strategy for their preparation in Scheme III-1. The methyl ester was originally chosen as a versatile functional group that, in principle, should be readily transformable into a wide variety of binding groups relevant for catalysis. The catalytic group should fulfil the following criteria: i) it should be catalytically active in enantioselective transformations of interest, ii) it should not interfere with the supramolecular recognition event, iii) ideally the donor group itself should be tunable in a modular way, thus, taking influence on its steric and electronic properties or allowing the implementation of a second stereogenic element, iv) the distance between the two donor functionalities and the rigidity of the overall supramolecular complex should be balanced for achieving well-established catalysts or catalyst precursors. This last criterion includes two aspects: v) the distance between the donor groups should be within a certain range to efficiently chelate a catalytically active metal, and vi) a certain degree of rigidity should be given in order to effectuate the induced axial chirality to the catalytic centre.

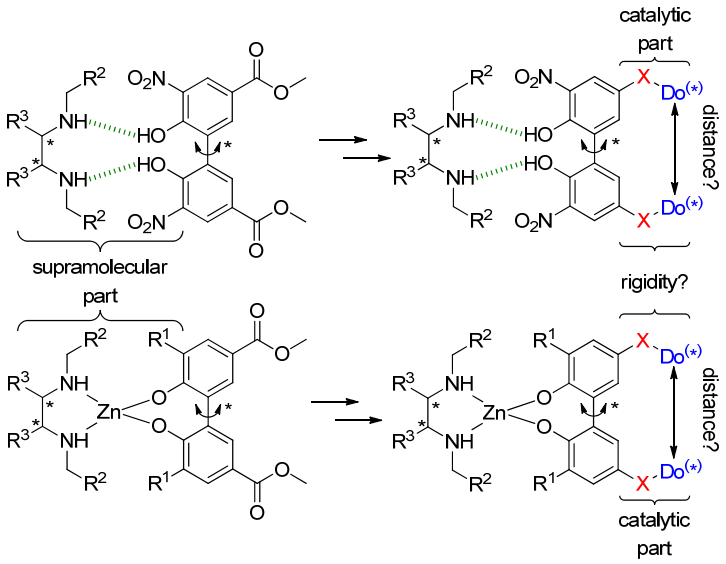

Scheme III-1. Transformation of the supramolecular hydrogen bonded (top) and zinc(II) templated (bottom) model complexes into catalytic ligands with modular characteristics.

In Scheme III-1 is shown the, in principle, high modularity of our approach. The supramolecular part of this catalyst assembly was addressed in the previous sections in form of model systems. The rigidity and distance parameters in the catalytic part in the assembly should be tunable by choosing appropriate scaffolds. For the long-term objectives of the project we have envisaged the preparation of a broad array of structurally diverse bidentate phosphorus ligands with several P-binding groups with varying stereoelectronic properties: bisphosphines, bisphosphonites and bisphosphites (Scheme III-2). At this stage conclusions about the feasibility of preparing such compounds can be drawn only for the bisphosphite **125** (Scheme III-3) and the bisphosphine **131** (Scheme III-4). The remaining structures have not been studied in sufficient detail to be evaluated yet.

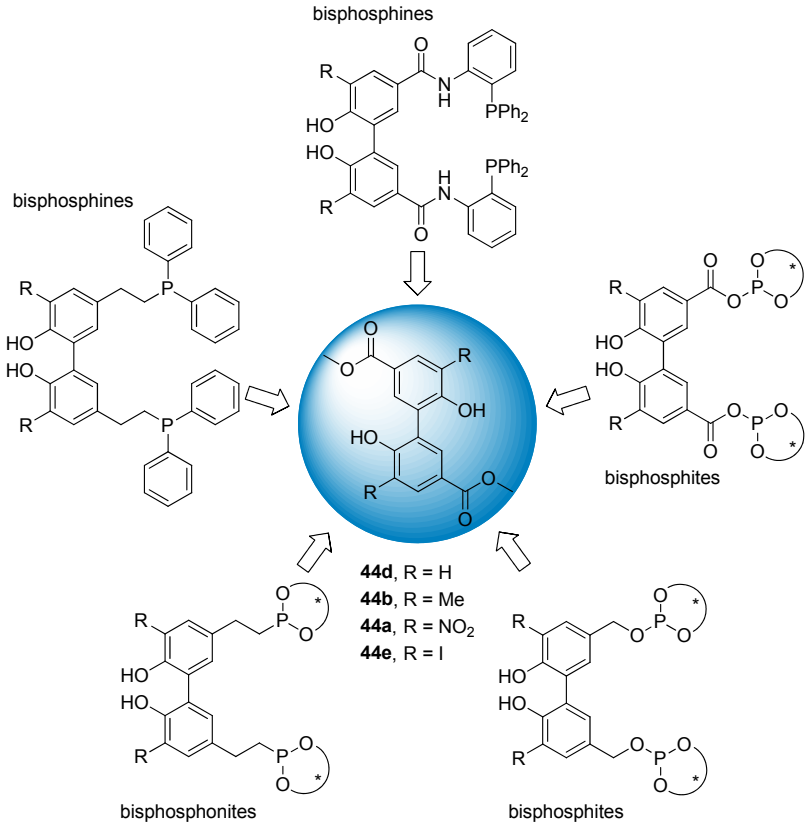

Scheme III-2. Transformation of 2,2'-biphenols **44** into diverse phosphorus ligands.

2 Results and Discussion

The synthetic strategy towards bisphosphite ligands **126** was developed by Dr. Anne-Sophie Felten, a former member of our group, who performed and studied the preparations depicted in Scheme III-3. Starting from the already introduced 2,2'-biphenols **44d** and **44b**, the alcohols **123d** and **123b** were obtained in quantitative yield by reduction of the methyl ester groups with $LiAlH_4$. The next step was the selective protection of the phenol group in compounds **123d** and **123b**, which was achieved by using NaH and acetic anhydride in DMF affording compounds **124d** and **124b**, although in moderate yields (50%) in both cases. Phosphorylation of compounds **124d** and **124b** with the corresponding chlorophosphite (Cl–P–BIPOL) in the presence of an auxiliary base gave the desired compounds **125d** and **125b** in 82% and 88% isolated yield, respectively. Unfortunately, until now it was not possible to isolate the target building blocks **126d** and **126b** since the different experimental procedures for the removal of the acetate protecting group (including basic and acid conditions) led to decomposition and rearrangement side processes of the phosphite moiety. Alternative orthogonal phenol protecting groups need to be considered and implemented in this synthesis in the future.

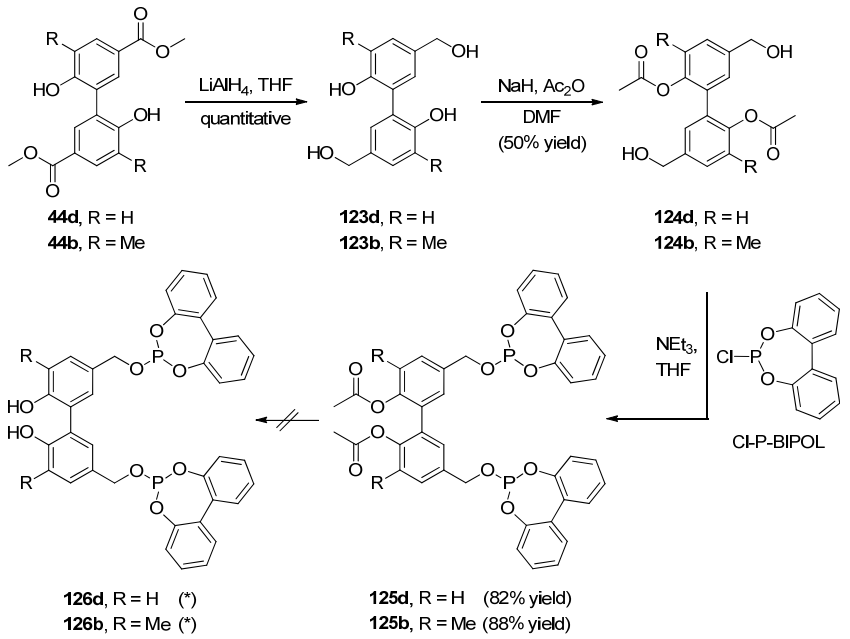

Scheme III-3. Preparation of the precursor ligand **125** and bisphosphite ligand **126** (*this ligand could not be prepared yet).

Despite the fact that the deprotection step failed for compounds **125d** and **125b**, complexation experiments were carried out using phosphite ligand **125d** in order to investigate the coordination behaviour with suitable metal precursors for future catalytic studies. Building block **125d** was mixed with one equivalent of $[Rh(NBD)_2]BF_4$ (NBD = 2,5-norbornadiene) as the metal precursor in dry CD_2Cl_2. The $^{31}P\{^1H\}$ NMR spectrum (Figure III-1) showed a doublet centred at 164.2 ppm with a direct coupling constant (J_{Rh-P} = 219 Hz) that indicated the formation of the cationic C_2-symmetric complex [Rh(NBD)(**125d**)]BF_4, as expected for a 1/1 Rh/ligand complex.[1-3] These results suggest the suitability of the catalytic blocks for future applications in catalysis.

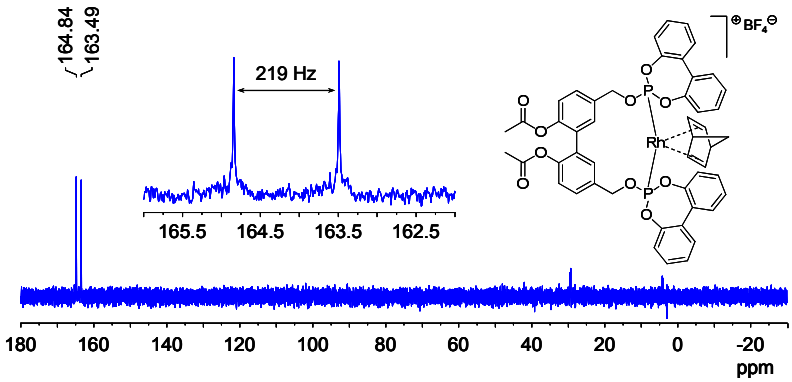

Figure III-1. ^{31}P NMR (CD_2Cl_2, 162 MHz, 298 K) spectrum of [Rh(NBD)(**125d**)]BF_4.

From the remaining potentially catalytic ligands depicted in Scheme III-2 only the synthesis of one bisphosphine, namely **131**, has been developed (in cooperation with Dr. Felten) and studied in detail. (Scheme III-4). In this compound the catalytic binding group is attached to the biaryl fragment *via* amide linkers. The resulting was intended to have the potential to serve as basis for the later preparation of a highly modular ligand library (Figure III-2).

The preparation of the new bidentate phosphorus ligand **131** was achieved in five high yielding syntheses steps starting from biphenol **44b** (Scheme III-4). We decided to first test **44b** since the complexation studies with zinc(II) have shown that the desired tetrahedral structures can be reliably obtained with the 2,2'-biphenol that is bearing methyl substituents in the 3,3'-positions. All transformations in the preparation of **131** were carried out according to standard procedures as they can be found in the literature. The first step was the methylation of the phenol groups with methyl iodide to give the protected biphenol **127**. Subsequent basic saponification of the methyl ester yielded the dicarboxylic acid **128**. This compound had to be coupled with 2-(diphenylphosphino)aniline, which could be purchased but here was synthesised from commercially available 2-iodoaniline.[4]

Since direct coupling with *N*,*N*'-dicyclohexylcarbodiimide (DCC) was not feasible the acyl chloride **129** was prepared with thionyl chloride and subsequently coupled to give the methyl protected derivative **130**.[5] Finally, the protecting methyl group had to be removed with BBr_3 in CH_2Cl_2 before obtaining the target building block **131** as a slightly orange powder.[6] The ligands **130** and **131** were fully characterised.

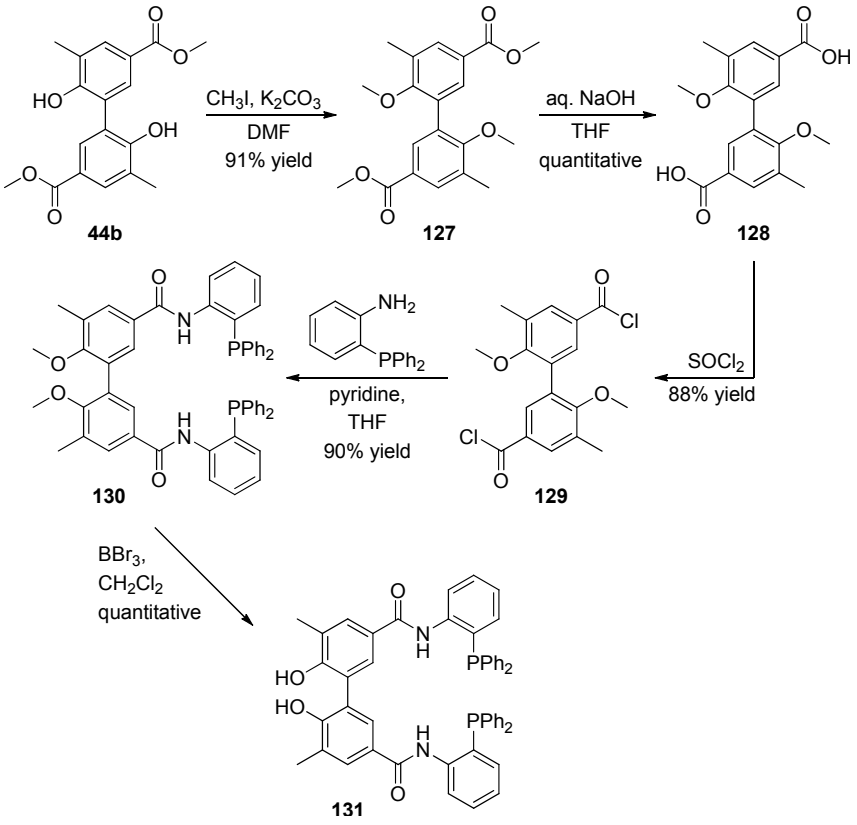

Scheme III-4. Synthesis of the new bidentate phosphine ligand **131**.

We believe that building blocks like **131** may be utilised to generate libraries of structurally and electronically diverse ligands. As can be seen in Figure III-2, this structure allows modifications at several points, provided that the required synthetic operations are viable for other scaffolds. However, first complexation studies with ligand **131** will have to be carried out in order to evaluate the feasibility of the mixed dinuclear complexes.

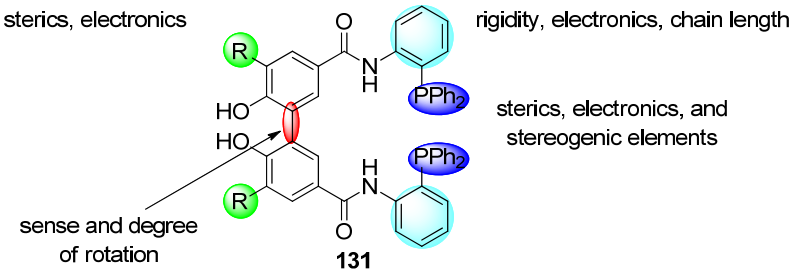

Figure III-2. Basis structure of a modular, potentially catalytic ligand.

Preliminary modelling studies of supramolecular catalysts derived from **131** or analogue ligands suggest that this kind of compounds present the right balance between the distances of the two phosphorus binding groups and the rigidity of the supramolecular complex, which makes them suitable *a priori* for catalytic studies in the future.

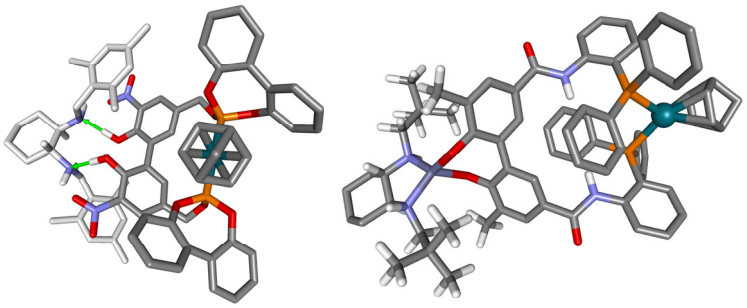

Figure III-3. 3D structure (generated with CAChe) of supramolecular catalysts assembled *via* hydrogen bonding (left) of metal-ligand interactions (right).

References

[1] H. Fernández-Pérez, S. M. A. Donald, I. J. Munslow, J. Benet-Buchholz, F. Maseras, A. Vidal-Ferran, *Chem. Eur. J.* **2010**, *16*, 6495.
[2] A. J. Sandee, A. M. van der Burg, J. N. H. Reek, *Chem. Commun.* **2007**, 864.
[3] P. C. J. Kamer, J. N. H. Reek, P. W. N. M. van Leeuwen, *Catal. Met. Complexes* **2000**, *22*, 35.
[4] D. Gelman, L. Jiang, S. L. Buchwald, *Org. Lett.* **2003**, *5*, 2315.
[5] D. Hedden, D. M. Roundhill, *Inorg. Chem.* **1985**, *24*, 4152.
[6] X.-B. Wang, Y.-G. Zhou, *J. Org. Chem.* **2008**, *73*, 5640.

Conclusions

- Two families of building blocks, namely enantiopure (1,2)-diamine and dynamically racemic 2,2'-biphenol derivatives, were efficiently synthesised according to literature procedures. These building blocks were designed based on the requirements to be utilised in the assembly of new supramolecular ligands by hydrogen bonding (Chapter I) and metal-ligand interactions (Chapter II). In both approaches the induction of chirality by the enantiopure (1,2)-diamines into the dynamically racemic 2,2'-biphenol units was of predominant interest.
- In Chapter I the complexation process between the two building blocks, (1,2)-diamines and 2,2'-biphenols, was studied. The binding constants of several new hydrogen bonded complexes could be reliably determined by UV-vis and ITC titrations. The latter also allowed the determination of thermodynamic parameters of the binding event, which, together with NMR spectroscopic data, revealed the stoichiometry of the new supramolecular complexes (1:1 in all cases). Furthermore, the successful induction of chirality by interaction of the N-substituents of the diamine with the biaryl unit was confirmed by CD measurements. In all cases except one the observed Cotton effects induced by (1*R*,2*R*)-diamine derivatives were positive, which was attributable to an a*R* sense of rotation of the biaryl unit. This particular behaviour could be explained by the electronically different nature of the N-substituents of the inducing (1,2)-diamines. All positive Cotton effects were induced by aliphatic substituents whereas the negative Cotton effect was observed only with the aromatic 2,4,6-trimethylbenzyl substituent at the nitrogen atom of the diamino moiety. Furthermore, for the aliphatic substituents a correlation between the substituents size and the

observed intensity of the Cotton effect was found: the larger the aliphatic substituent, the more intense was the induced Cotton effect.

- In Chapter II the induction of axial chirality mediated by structural metals, principally zinc(II) was studied. The resulting zinc(II) complexes could be clearly divided into two classes in the solid state, mononuclear and dinuclear complexes. Complexes of the first class were found to be formed with Me-BIPOL **44b**, *i.e*. the biphenol bearing methyl groups in the 3,3'-positions, whereas the dinuclear ones were preferentially formed with the 3,3'-unsubstituted H-BIPOL **44d**. The solid state structures of representative examples for both classes could be determined by single crystal analysis. Furthermore, crystallographic purity could be confirmed by powder diffraction for one mononuclear and one dinuclear complex. An unambiguous structural correlation between the absolute configuration of the chiral (1,2)-diamine and the induced sense of axial rotation of the biphenol was found for mononuclear complexes by experimental and theoretical CD studies. In all cases, except for the *N*-(2,4,6-trimethylbenzyl)-substituted one, (1*R*,2*R*)-diamines induced negative chirality that was attributable to an a*R* twist of the biphenol, whereas the (1*S*,2*S*)-enantiomers resulted in positive chirality and a*S* configurations. Unfortunately the dinuclear 2:2:2 complexes did not show preferential induction of axial chirality since they contained two biphenol units of opposite sense of axial rotation. Furthermore, they showed a pronounced dynamic behaviour on the NMR timescale.
- The study of copper(II) as structural metal revealed that a preferential sense of rotation in the solid state can be induced into 2,2'-biphenol using enantiopure (1,2)-diaminocyclohexane.
- Chapter III is about the transformation of the new building blocks into catalytic units. One particularly interesting candidate could be identified and synthesised. Preparation of the diastereomerically enriched zinc(II) chelates followed by complexation studies with

catalytically active transition metals will be carried out in the near future.

Experimental Procedures

Experimental Procedures

All commercially available chemicals were used as received from the corresponding supplier unless otherwise stated. Preparations requiring inert conditions were carried out either in a MBRAUN Unilab glove box or by using standard Schlenk techniques and anhydrous and deoxygenated solvents. Dichloromethane, diethyl ether, *N*,*N*'-dimethylformamide, *n*-hexane, tetrahydrofuran, and toluene were dried *via* a SPS Solvent Purification System THF-d_8 was purchased from Armar Chemicals, dried over sodium metal and degassed by three freeze-thaw cycles under high vacuum. Silica gel 60 (230-400 mesh) was used as received from the supplier, where necessary it was treated with distilled triethylamine or aqueous ammonia as noted in the respective preparations. Alternatively, products were purified on a Teledyne Isco liquid chromatography system (model Combiflash Companion) using RediSep® silica gel cartridges.

NMR spectra were recorded on Bruker Avance 400 and 500 Ultrashield spectrometers. ^{1}H and ^{13}C NMR chemical shifts are quoted relative to solvent residual signals as found in the literature.[1] IR spectra were recorded on Bruker Tensor 27 or Bruker Alpha FTIR spectrometers. UV-vis spectra and titrations were recorded on a Shimadzu UV-Vis spectrophotometer model UV-2401 PC. ITC titrations were carried out on a MicroCal VP-ITC micro calorimeter. CD spectra were measured on an Applied Photophysics Chirascan spectrophotometer. ESI mass spectra were obtained on a Waters LCT Premier mass spectrometer and MALDI mass spectra were obtained on a Bruker Autoflex MALDI-TOF mass spectrometer. Single crystal structure determinations were carried out using a Bruker-Nonius diffractometer equipped with a APPEX 2 4K CCD area detector, a FR591 rotating anode with Mo Kα radiation, Montel mirrors as

monochromator and a Kryoflex low temperature device. Fullsphere data was collected using omega and phi scans. Crystal structure solution was achieved using direct methods as implemented in SHELXTL version 6.14. All non-hydrogen atoms were refined including anisotropic displacement parameters. Powder diffraction was carried out on a D8 Advance Series 2Theta/Theta powder diffraction system using Cu Kα-radiation in transmission geometry equipped with a VÅNTEC-1 single photon counting PSD and a Ge monochromator.

Quantities of reagents and reaction products given in grams or ml and resultant moles are quoted according to the number of significant digits limited by the respective balance or volumetric gauge. The volumes and molarity of solvents and other bulk chemicals like aqueous NaCl, $NaHCO_3$, NH_4Cl, etc. are generally rounded to whole-number values but in exceptional cases given with one decimal place. Yields are always rounded to whole-number values.

Synthesis of methyl 4-hydroxy-3-methylbenzoate 48.

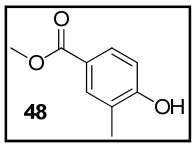

48

Concentrated H_2SO_4 (4.5 ml) was added to a solution of 4-hydroxy-3-methylbenzoic acid **47** (5.0 g, 32 mmol) in MeOH (45 ml). The reaction mixture was refluxed for 6.5 h. After reaching room temperature the solution was brought to approx. pH 6.5 with 2.5 M NaOH and left standing for 15 min after which it was poured into ice-cold H_2O (100 ml). The white precipitate that had formed was filtered off, washed with cold H_2O (75 ml), and dried *in vacuo*. The product was obtained as a white powder (5.0 g, 95%) of sufficient purity for the following iodination reaction.

^{1}H NMR (400 MHz, $CDCl_3$, 298 K): δ = 7.82 (s, 1H, C*H*); 7.77 (d, ^3J = 8.4 Hz, 1H, C*H*); 6.79 (d, ^3J = 8.4 Hz, 1H, C*H*); 5.66 (s, 1H, O*H*); 3.86 (s, 3H, CH_3O); 2.26 (s, 3H, CH_3) ppm.

^{13}C NMR (100 MHz, $CDCl_3$, 298 K): δ = 167.8 (*C*=O); 158.8 (*C*OH); 133.2 (*C*H); 129.8 (*C*H); 124.4 (*C*); 122.5 (*C*); 115.0 (*C*H); 52.3 (*C*H_3O); 16.0 (*C*H_3) ppm.

IR (neat): $\tilde{\nu}$ = 3252 (*s*, OH stretch); 2960 (*w*); 1682 (*s*, C=O); 1598 (*s*, C=C, ar) cm^{-1}.

Physical and spectroscopic data were in agreement with those present in the literature.[2, 3]

Synthesis of methyl 4-hydroxy-3-iodo-5-methylbenzoate 49.[4]

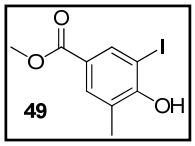

49

Methyl 4-hydroxy-3-methylbenzoate (1.00 g, 6.02 mmol) **48** was added to a solution of conc. H_2SO_4 (0.50 ml, 9.02 mmol) in MeOH (35 ml). Subsequently, solid KI (1.10 g, 6.62 mmol) and H_2O_2 (35% vol., 1.10 ml, 12.0 mmol) were added and the solution was kept stirring at 60 ºC until completion of the reaction (TLC, 1:1 EtOAc/*n*-hexane, R_f (**49**) = 0.56, R_f (**48**) = 0.53). The crude product was then carefully extracted from the reaction mixture with CH_2Cl_2 (3 x 50 ml) and the organic layer was consecutively washed with aqueous Na_2SO_3 (0.1 M, 60 ml), saturated aqueous $NaHCO_3$ (60 ml), and brine (120 ml). The organic layer was dried over Na_2SO_4, filtered, and the solvent evaporated. The product was obtained as a white solid (1.63 g, 93%).

^{1}H NMR (400 MHz, $CDCl_3$, 298 K): δ = 8.20 (d, ^4J = 1.8 Hz, 1H, C*H*); 7.79 (d, ^4J = 1.8 Hz, 1H, C*H*); 5.68 (s, 1H, O*H*); 3.88 (s, 3H, CH_3O); 2.33 (s, 3H, CH_3) ppm.

^{13}C NMR (100 MHz, $CDCl_3$, 298 K): δ = 165.7 (*C*=O); 156.9 (*C*-OH); 137.8 (*C*H); 133.1 (*C*H); 124.8 (*C*); 124.2 (*C*); 85.7 (*C*-I); 52.5 (*C*H_3O); 17.4 (*C*H_3) ppm.

IR (neat): $\tilde{\nu}$ = 3325 (*s*, OH stretch); 2947 (*w*); 1696 (*s*, C=O); 1601 (*m*, C=C, ar) cm^{-1}.

Mp: 132-134 ºC.

HRMS (ESI-): *m*/*z* = 290.9507 found; 290.9518 calcd for $[M-H]^-$ (M = $C_9H_9O_3I$).

Synthesis of dimethyl 6,6'-dihydroxybiphenyl-3,3'-dicarboxylate 44d.

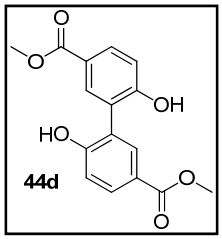

Methyl 4-hydroxy-3-iodobenzoate (2.50 g, 8.90 mmol), TBAB (1.46 g, 4.45 mmol), hexakis(aceto)-tripalladium(II) (0.102 g, 0.151 mmol), and DIPEA (1.57 ml, 8.90 mmol) were mixed with 1.6 ml of anhydrous DMF under inert atmosphere. The reaction mixture was stirred at 115 ºC for 5 h. Subsequently, the mixture was allowed to cool down to room temperature, treated with 2 M HCl (4.50 ml) and stirred for 2 h. The crude product was extracted with EtOAc (3 x 25 ml) and the combined organic layers were washed with saturated aqueous solutions of NH_4Cl and NaCl (each of 20 ml volume) and dried over $MgSO_4$. The drying agent was filtered off and the solvents removed *in vacuo*. The thus obtained brown solid was washed with small portions of cold CH_2Cl_2 until a slightly yellow solid was obtained (534 mg, 40%).

^{1}H NMR (400 MHz, THF-d_8, 298 K): δ = 8.80 (s, 2H, O*H*); 7.89 (d, ^4J = 2.1 Hz, 2H, C*H*), 7.87 (dd, ^3J = 8.4 Hz, ^4J = 2.1 Hz, 2H, C*H*), 6.89 (d, ^3J = 8.4 Hz, 2H, C*H*), 3.80 (s, 6H, CH_3O) ppm.

^{13}C NMR (100 MHz, THF-d_8, 298 K): δ = 166.9 (*C*=O); 160.2 (*C*-OH); 134.6 (*C*H), 131.6 (*C*H), 126.06 (*C*), 122.8 (*C*), 116.7 (*C*), 51.8 (*C*H_3O) ppm.

IR (neat): $\tilde{\nu}$ = 3356 (*s*, OH-stretch); 1685 (*s*, C=O); 1598 (*s*, C=C, ar) cm^{-1}.

UV-vis (CH_2Cl_2, 298 K): λ_{max} (ε) = 240 (31500); 284 (3800) nm ($M^{-1}cm^{-1}$).

UV-vis (THF, 298 K): λ_{max} (ε) = 238 (34200); 254 (28900) nm ($M^{-1}cm^{-1}$).

Mp: 268-270 ºC.

HRMS (ESI+): *m*/*z* = 302.0797 found; 302.0790 calcd for $[M]^{+\cdot}$ (M = $C_{16}H_{14}O_6$).

Synthesis of dimethyl 6,6'-dihydroxy-5,5'-dimethylbiphenyl-3,3'-dicarboxylate 44b.[5]

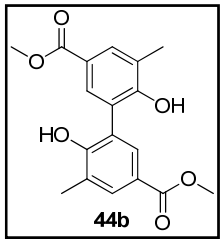

44b

Methyl 4-hydroxy-3-iodo-5-methylbenzoate (4.00 g, 13.7 mmol) **49**, TBAB (510 mg, 1.37 mmol), hexakis(aceto)tripalladium(II) (160 mg, 230 μmol), and DIPEA (2.40 ml, 13.7 mmol) were mixed with 1.4 ml of anhydrous DMF under inert atmosphere. The reaction mixture was stirred at 115 ºC for 5 h. Subsequently, the mixture was allowed to cool down to room temperature, treated with 2 M HCl (7.0 ml) and stirred for 2 h. The crude product was extracted with EtOAc (3 x 60 ml) and the combined organic layers were washed with saturated aqueous solutions of NH_4Cl and NaCl (each of 50 ml volume) and dried over $MgSO_4$. The drying agent was filtered off and the solvents removed *in vacuo*. The thus obtained brown solid was washed with portions of cold CH_2Cl_2 until a slightly yellow solid was obtained (983 mg, 43%).

^{1}H NMR (400 MHz, THF-d_8, 298 K): δ = 8.11 (s, 2H, O*H*); 7.82 (d, ^4J = 1.4 Hz, 2H, C*H*), 7.69 (d, ^4J = 2.0 Hz, 2H, C*H*); 3.79 (s, 6H, CH_3O); 2.30 (s, 6H, CH_3) ppm.

^{13}C NMR (100 MHz, THF-d_8, 298 K): δ = 167.0 (*C*=O); 158.3 (*C*-OH); 132.9 (*C*H); 132.4 (*C*H); 126.7, 125.1 (*C*); 122.9 (*C*); 51.8 (*C*H_3O); 16.9 (*C*H_3) ppm.

UV-vis (CH_2Cl_2, 298 K): λ_{max} (ε) = 241 (30400) nm ($M^{-1}cm^{-1}$).

UV-vis (THF, 298 K): λ_{max} (ε) = 242 (33200); 255 (30100) nm ($M^{-1}cm^{-1}$).

IR (neat): $\tilde{\nu}$ = 3236 (*s*, OH stretch); 2961 (*w*); 1685 (*s*, C=O); 1595 (*m*, C=C, ar) cm^{-1}.

Mp: 249-252 ºC.

HRMS (ESI+): *m*/*z* = 353.1001 found; 353.1006 calcd for $[M+Na]^+$ ($M = C_{18}H_{18}O_6$).

Single crystal structure: see appendix.

Synthesis of dimethyl 6,6'-dihydroxy-5,5'-diiodobiphenyl-3,3'-dicarboxylate 44e.[4]

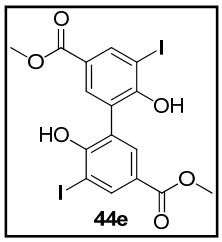

Biphenol **44d** (100 mg, 328 μmol) was added to a solution of conc. H_2SO_4 (55.0 μl, 984 μmol) in a solvent mixture of THF and MeOH (4.50 ml, 0.8 ratio). Subsequently, solid KI (131 mg, 786 μmol) and H_2O_2 (35% vol., 126 μl 1.44 mmol) were added and the solution was kept stirring at 60 ºC for the initial 2 h followed by stirring at 40 ºC overnight. The crude product was obtained by filtration of the precipitate and washing it with saturated aqueous $NaHCO_3$ (3 ml) and a semi-saturated aqueous solution of Na_2SO_3 until it remained only slightly yellow. Subsequent washing of the product with portions of cold THF and CH_2Cl_2 (1 ml each) yielded the pure product as a white solid (137 mg, 76%).

^{1}H NMR (400 MHz, THF-d_8, 298 K): δ = 8.27 (d, ^4J = 1.9 Hz, 2H, C*H*); 7.66 (d, ^4J = 1.9 Hz, 2H, C*H*); 3.80 (s, 6H, CH_3O) ppm.

^{13}C NMR (100 MHz, DMSO-d_6, 298 K): δ = 164.7 (*C*=O); 159.2 (*C*-OH); 139.8 (*C*H); 132.8 (*C*H); 124.9 (*C*); 122.1 (*C*); 87.9 (*C*-I), 52.0 (*C*H_3O) ppm.

UV-vis (THF, 298 K): λ_{max} (ε) = 234 (32500); 250 (26300); 288 (5700) nm ($M^{-1}cm^{-1}$).

IR (neat): $\tilde{\nu}$ = 3294 (*s*, OH stretch); 2948 (*w*); 1701 (*s*, C=O); 1594 (*m*, C=C, ar) cm^{-1}.

Mp: decomposition at T > 260 ºC.

HRMS (ESI+): *m*/*z* = 576.8632 found; 576.8621 calcd for $[M+Na]^+$ (M = $C_{16}H_{12}I_2O_6$).

Synthesis of dimethyl 6,6'-dihydroxy-5,5'-dinitrobiphenyl-3,3'-dicarboxylate 44a.

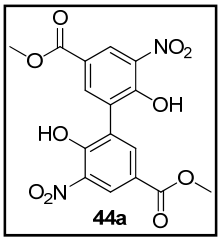

44a

Solid $Bi(NO_3)_3 \cdot 5\ H_2O$ (1.00 g, 2.08 mmol) was added in one portion to a solution of dimethyl-6,6'-dihydroxybiphenyl-3,3'-dicarboxylate **44d** (300 mg, 0.99 mmol) in THF (6.00 ml). The resulting mixture was stirred at 80 ºC for 20 h. After cooling the reaction mixture to room temperature the precipitate was filtered off and the solvent was removed under reduced pressure. The resulting residue was treated with water (25 ml) and the product extracted with EtOAC (3 x 30 ml). Subsequently, the combined organic layers were washed with brine (2 x 20 ml), dried with $MgSO_4$, filtered, and freed of the solvent under reduced pressure. The crude product was purified by column chromatography (Combiflash Companion, RediSep® 12 g silica gel cartridge, detection at 254 nm, eluant: *n*-hexane/EtOAc, gradient from 9:1 to 7:3 ratios). After evaporation of the solvent the pure product was obtained as yellow needle-like crystals (536 mg, 76%).

^{1}H NMR (400 MHz, $CDCl_3$, 298 K): δ = 11.28 (bs, 2H, O*H*); 8.91 (d, ^4J = 2.0 Hz, 2H, C*H*); 8.28 (d, ^4J = 2.0 Hz, 2H, C*H*); 3.96 (s, 6H, OCH_3) ppm.

^{13}C NMR (100 MHz, $CDCl_3$, 298 K): δ = 164.6 (*C*=O); 156.1 (*C*-OH); 139.5 (*C*H); 133.8 (*C*); 127.8 (*C*H); 127.0 (*C*); 122.46 (*C*); 52.9 (CH_3O) ppm.

IR (neat): $\tilde{\nu}$ = 3215 (*s*, OH stretch); 3099 (*m*); 2916 (*w*); 1731 (*s*, C=O); 1617 (*s*, C=C, ar) cm^{-1}.

UV-vis (toluene, 298 K): λ_{max} (ε) = 357 (6300) nm ($M^{-1}cm^{-1}$).

Mp: 227-229 ºC.

HRMS (ESI-): *m*/*z* = 391.0403 found; 391.0419 calcd for $[M-H]^-$ ($M = C_{16}H_{12}N_2O_{10}$).

Single crystal structure: see appendix.

Synthesis of 6,6'-diacetoxy-5,5'-dimethoxybiphenyl-3,3'-dicarbaldehyde 51.[6]

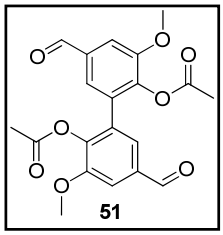
51

5,5'-Bivanillin (1.20 g, 90%, 3.60 mmol) was refluxed for 30 min with acetic anhydride (2.70 ml, 21.4 mmol) and anhydrous sodium acetate (0.30 g, 3.60 mmol). After completion of the reaction the solution was poured into ice-water and the resulting precipitate was filtered and washed with cold MeOH (2 x 10 ml). Product **51** was obtained as a white solid (1.03 g, 74%) and required no further purification.

^{1}H NMR (400 MHz, $CDCl_3$, 298 K): δ = 9.98 (s, 2H, C*H*O); 7.58 (d, ^4J = 1.8 Hz, 2H, C*H*); 7.43 (d, ^4J = 1.8 Hz, 2H, C*H*); 3.98 (s, 6H, CH_3O); 2.15 (s, 6H, CH_3-C=O) ppm.

^{13}C NMR (100 MHz, $CDCl_3$, 298 K): δ = 190.7 (*C*(H)=O); 167.8 (*C*=O); 152.4 (*C*); 142.8 (*C*); 134.7 (*C*); 131.3 (*C*); 126.5 (*C*H); 110.3 (*C*H); 56.4 (*C*H_3O); 20.4 (*C*H_3-C=O) ppm.

Mp: 115-117 ºC.

Physical and spectroscopic data were in agreement with those present in the literature.[6]

Synthesis of 6,6'-dihydroxy-5,5'-dimethoxybiphenyl-3,3'-dicarboxylic acid 52.

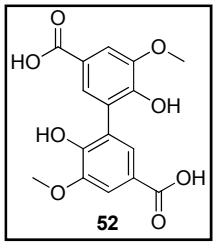

52

To a solution of 6,6'-diacetoxy-5,5'-dimethoxybiphenyl-3,3'-dicarbaldehyde **51** (0.91 g, 2.40 mmol) in DMF (24 ml) Oxone® (3.00 g, 5.00 mmol) was added. The mixture was stirred for 3 h at room temperature and subsequently quenched with 1 M HCl (20 ml). The product was extracted with EtOAc (4 x 20 ml) and the combined organic layers were washed with HCl (2 x 20 ml) and brine (2 x 20 ml), dried with $MgSO_4$, filtered and freed of the solvent under reduced pressure. The intermediate product 6,6'-diacetoxy-5,5'-dimethoxybiphenyl-3,3'-dicarboxylic acid was obtained as slightly yellow oil and used without further purification in the next step. Saponification was achieved by refluxing the acetyl compound for 1 h in 10% aqueous NaOH (10 ml). The mixture was cooled to 0 ºC in an ice/water bath before being acidified to pH 6 with 1 M HCl. The resulting precipitate was filtered off, washed with portions of hot EtOH (2 x 5 ml), and dried. The product was obtained as a white solid (0.42 g, 90%) and was used without further purification in the next step.

Physical and spectroscopic data were in agreement with those present in the literature.[6]

Synthesis of dimethyl 6,6'-dihydroxy-5,5'-dimethoxybiphenyl-3,3'-dicarboxylate 44c.

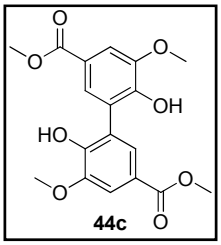

Concentrated H_2SO_4 (0.30 ml, 5.05 mmol) was added carefully to a suspension of 6,6'-dihydroxy-5,5'-dimethoxybiphenyl-3,3'-dicarboxylic acid **52** in MeOH (2.30 ml). The reaction mixture was refluxed for 1 h and neutralised with 2 M aqueous NaOH after cooling to room temperature. The resulting precipitate was filtered off and washed with cold MeOH (10 ml) in order to yield the desired compound as a white solid (0.28 g, 62%) that required no further purification.

^{1}H NMR (400 MHz, DMSO-d_6, 298 K): δ = 9.50 (bs, 2H, O*H*); 7.47 (d, ^4J = 2.0 Hz, C*H*); 7.44 (d, ^4J = 2.0 Hz, C*H*); 3.90 (s, 3H, CH_3O); 3.80 (s, 3H, CH_3O) ppm.

^{13}C NMR (100 MHz, DMSO-d_6, 298 K): δ = 166.1 (*C*=O); 148.8 (*C*-OH); 147.6 (*C*-OCH$_3$); 125.4 (*C*H); 124.3 (*C*); 119.6 (*C*); 110.9 (*C*); 56.0 (*C*H$_3$O); 51.8 (*C*H$_3$-OCO) ppm.

Physical and spectroscopic data were in agreement with those present in the literature.[7]

Standard synthesis procedure (SSP 1)* for the preparation of enantiopure *N*,*N*'-(cyclohexane-1,2-diyl)diamide and *N*,*N*'-(1,2-diphenylethane-1,2-diyl)diamide derivatives.[8]

Enantiopure cyclohexane-1,2-diamine and 1,2-diphenylethane-1,2-diamine, respectively, was refluxed in anhydrous toluene for approx. 4 h with large excesses (8-12-fold) of, depending on availability, either the required carboxylic acid anhydride or acyl chloride. The crude product was isolated by cooling the reaction mixture to 0 ºC and filtering the resulting white precipitate through a suitable frit (D3). Washing with portions of cold toluene and Et_2O yielded products that were sufficiently pure for the following reduction (see SSP 2).

Standard synthesis procedure (SSP 2)* for the preparation of enantiopure *N*,*N*'-substituted 1,2-cyclohexanediamine and 1,2-diphenylethane-1,2-diamine derivatives from the corresponding diamides.

A suspension of the *N*,*N*'-(cyclohexane-1,2-diyl)diamide or *N*,*N*'-(1,2-diphenylethane-1,2-diyl)diamide derivative in anhydrous THF (*ca*. 30 ml/mmol of substrate) was cooled to 0 ºC in an ice/water bath. The reaction vessel had to be of reasonable size and be equipped with an efficient reflux condenser and a large magnetic stirring bar (quench formed large amounts of insoluble salts). Subsequently, an excess of solid $LiAlH_4$ (up to 8-fold) was added carefully avoiding boiling of the THF. In some cases the reduction with BH_3·THF proved to be more efficient and is indicated for the respective compounds. After the addition was completed the flask and condenser were flushed with N_2 and the mixture was stirred at room temperature for 1 h before being refluxed overnight. Quenching of the reaction and destruction of the excess $LiAlH_4$ was carried out following a standard method.[9] The crude products were isolated by evaporation of the solvent and extensive

extraction of the resulting residue with Et_2O. The combined organic layers were dried with $MgSO_4$, filtered and freed of the solvent by rotary evaporation. Purification of the crude compound was achieved as noted at the respective diamine compounds.

Standard synthesis procedure (SSP 3)* for the synthesis of enantiopure (1*R*,2*R*)-*N*,*N*'-dialkylidene-1,2-cyclohexanediamine and (1*R*,2*R*)-*N*,*N*'-diarylidene-1,2-cyclohexanediamine derivatives.[10]

Enantiopure 1,2-cyclohexanediamine was dissolved together with two equivalents of the corresponding aldehyde in anhydrous CH_2Cl_2 or absolute EtOH and stirred for 2 h. Then, anhydrous $MgSO_4$ (approx. 2 equivalents) was added and the mixture was stirred overnight. The $MgSO_4$ was filtered off and washed with CH_2Cl_2 before the solvent was removed *in vacuo*. The remaining colourless to yellow oils or white solids were used in the following reduction without further purification.

Standard synthesis procedure (SSP 4)* for the preparation of enantiopure *N*,*N*'-substituted 1,2-cyclohexanedamine and 1,2-diphenylethane-1,2-diamine derivatives from the corresponding diimines.

The diimine was refluxed in absolute EtOH (5-6 ml/mmol) for 5 h in a nitrogen flushed round bottomed flask of adequate size (quench formed large amounts of insoluble salts) with a large excess of $NaBH_4$ (*ca*. tenfold). After completion of the reaction the excess of $NaBH_4$ was destroyed at room temperature with H_2O. The solvent was removed *in vacuo* and the crude product extracted from the residue with CH_2Cl_2. Purification was achieved through column chromatography and subsequent vacuum distillation when required (for details see the entry at the respective compounds).

*Generally, both synthesis routes were suitable for the preparation of the desired diamines. The choice between the diamide and the diimine route was mainly based on the cost and availability of the required aldehyde or acyl chloride and carboxylic acid anhydride, respectively. Nevertheless, it should be noted that when possible the diamide route was preferred since it yielded crude products of higher purity.

Synthesis of (1*R*,2*R*)-*N*,*N*'-diacetyl-1,2-cyclohexanediamine (1*R*,2*R*)-55a, SSP 1.

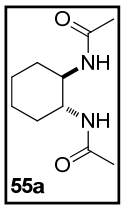

55a

The synthesis of (1*R*,2*R*)-*N*,*N*'-diacetyl-1,2-cyclohexanediamine (1*R*,2*R*)-**55a** was carried out following the standard synthesis procedure SSP 1. (1*R*,2*R*)-DACH (4.00 g, 35.0 mmol) was refluxed for 4 h in anhydrous toluene (100 ml) together with acetic anhydride (70 ml, 556 mmol). The product was obtained as white needle-like crystals (5.64 g, 81%) of sufficient purity for the following reduction.

^{1}H NMR (400 MHz, $CDCl_3$, 298 K): δ = 6.05 (bs, 2H, N*H*); 3.68-3.58 (m, 2H, C*H*); 2.05-1.98 (m, 2H, CH_2); 1.93 (s, 6H, CH_3); 1.79-1.69 (m, 2H, CH_2); 1.38-1.15 (m, 4H, CH_2) ppm.

^{13}C NMR (100 MHz, $CDCl_3$, 298 K): δ = 171.0 (*C*=O); 54.0 (*C*H); 32.4 (*C*H_2); 24.8 (*C*H_2); 23.5 (*C*H_3) ppm.

IR (neat): $\tilde{\nu}$ = 3282 (*s*, NH stretch); 1634 (*s*, C=O) cm^{-1}.

Mp: 296-297 ºC.

Physical and spectroscopic data were in agreement with those present in the literature.[11]

(1*S*,2*S*)-*N*,*N*'-Diacetyl-1,2-cyclohexanediamine (1*S*,2*S*)**-55a** was synthesised in an analogous manner starting from (1*S*,2*S*)-DACH (76% yield).

Synthesis of (1*R*,2*R*)-*N*,*N*'-diethyl-1,2-cyclohexanediamine (1*R*,2*R*)-45a, SSP 2.

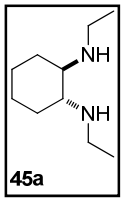

45a

The synthesis of (1*R*,2*R*)-*N*,*N*'-diethyl-1,2-cyclohexanediamine was carried out following the standard synthesis procedure SSP 2. (1*R*,2*R*)-*N*,*N*'-diacetyl-1,2-cyclohexanediamine (1*R*,2*R*)-**55a** (5.50 g, 28.0 mmol) and solid $LiAlH_4$ (10.5 g, 280 mmol) as the reducing agent were refluxed for 12 h in anhydrous THF (600 ml). The resulting slightly yellow crude product was purified by distillation under reduced pressure (46 ºC, $4 \cdot 10^{-2}$ mbar) in order to obtain the final product as a colourless oil (3.22 g, 68%).

^{1}H NMR (400 MHz, THF-d_8, 298 K): δ = 2.76-268 (m, 2H, NHCH_2); 2.46-2.38 (m, 2H, NHCH_2); 2.09-1.99 (m, 4H, CH, CH_2); 1.70-1.61 (m, 2H, CH_2); 1.41 (bs, 2H, NH); 1.44-1.13 (m, 2H, CH_2); 1.02 (t, ^3J = 7.1 Hz, 6H, CH_3); 0.99-0.86 (m, 2H, CH_2) ppm.

^{13}C NMR (100 MHz, $CDCl_3$, 298 K): δ = 61.9 (*C*H); 41.5 (NH*C*H_2); 32.0 (*C*H_2); 25.4 (*C*H_2); 16.4 (*C*H_3) ppm.

IR (neat): $\tilde{\nu}$ = 3298 (*w*, NH stretch) cm^{-1}.

$[\alpha]_D^{27}$ = -59.7 (*c* 0.50, $CHCl_3$).

Physical and spectroscopic data were in agreement with those present in the literature.[11]

(1*S*,2*S*)-*N*,*N*'-diethyl-1,2-cyclohexanediamine (1*S*,2*S*)-**45a** was synthesised in an analogous manner starting from (1*S*,2*S*)-**55a** (63% yield).

Synthesis of (1*R*,2*R*)-*N*,*N*'-dipropionyl-1,2-cyclohexanediamine (1*R*,2*R*)-55b, SSP 1.

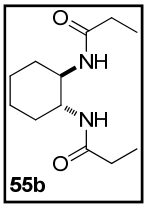

The synthesis of (1*R*,2*R*)-*N*,*N*'-dipropionyl-1,2-cyclohexanediamine (1*R*,2*R*)-**55b** was carried out following standard synthesis procedure SSP 1. (1*R*,2*R*)-DACH (1.67 g, 14.6 mmol) was refluxed for 5 h in anhydrous toluene (35 ml) together with propionic anhydride (19.0 g, 146 mmol). The product was obtained as white needle-like crystals (2.24 g, 68%) of sufficient purity for the following reduction.

^{1}H NMR (400 MHz, $CDCl_3$, 298 K): δ = 6.03 (bs, 2H, N*H*); 3.72-3.60 (m, 2H, C*H*); 2.22-2.07 (m, 4H, CH_2CH$_3$); 2.01 (m, 2H, CH_2); 1.81-1.69 (m, 2H, CH_2); 1.38-1.17 (m, 4H, CH_2); 1.10 (t, ^3J = 7.6 Hz, 6H, CH_3) ppm.

^{13}C NMR (125 MHz, $CDCl_3$, 298 K): δ = 174.8 (*C*=O); 53.9 (*C*H); 32.5 (*C*H$_2$); 30.1 (*C*H$_2$); 25.0 (*C*H$_2$); 10.2 (*C*H$_3$) ppm.

IR (neat): $\tilde{\nu}$ = 3284 (*s*, NH stretch); 3077 (*w*, NH stretch); 1637 (*s*, C=O) cm^{-1}.

Mp: 245-247 ºC.

Physical and spectroscopic data were in agreement with those present in the literature.[12]

Synthesis of (1*R*,2*R*)-*N*,*N*'-di-*n*-propyl-1,2-cyclohexanediamine (1*R*,2*R*)-55b, SSP 2.

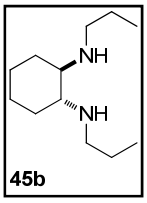

The synthesis of (1*R*,2*R*)-*N*,*N*'-di-*n*-propyl-1,2-cyclohexanediamine was carried out following standard synthesis procedure SSP 2. *N*,*N*'-(1*R*,2*R*)-Dipropionyl-1,2-cyclohexanediamine **55b** (2.2 g, 9.7 mmol) and solid $LiAlH_4$ (3.7 g, 97 mmol) as the reducing agent were refluxed overnight in anhydrous THF (250 ml). The resulting slightly yellow crude product was purified by distillation under reduced pressure

(70 ºC, $4.5 \cdot 10^{-2}$ mbar) in order to obtain the final compound as a colourless oil (0.81 g, 42%).

^{1}H NMR (400 MHz, $CDCl_3$, 298 K): δ = 2.68 (dt, ^2J = 11.1 Hz, ^3J = 7.1 Hz, 2H, NHCH_2); 2.39 (dt, ^2J = 11.1 Hz, ^3J = 7.1 Hz, 2H, NHCH_2); 2.15-2.00 (m, 4H, CH, CH_2); 1.76-1.63 (m, 2H); 1.47 (m, 6H, CH_3CH_2, NH); 1.28-1.13 (m, 2H, CH_2); 1.05-0.92 (m, 2H, CH_2); 0.91 (t, ^3J = 7.4 Hz, 6H, CH_3) ppm.

^{13}C NMR (100 MHz, $CDCl_3$, 298 K): δ = 61.9 (*C*H); 49.2 (NH*C*H_2); 32.0 (*C*H_2); 25.3 (*C*H_2); 23.8 (*C*H_2); 12.0 (*C*H_3) ppm.

$[\alpha]_D^{27}$ = -106.5 (*c* = 0.60, $CHCl_3$).

Physical and spectroscopic data were in agreement with those present in the literature.[13]

Synthesis of (1*R*,2*R*)-*N*,*N*'-diisobutyl-1,2-cyclohexanediamine (1*R*,2*R*)-45c, SSP 3, SSP 4.

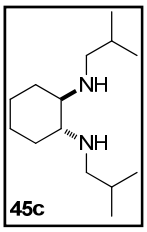

45c

The synthesis of (1*R*,2*R*)-*N*,*N*'-diisobutyl-1,2-cyclohexanediamine (1R,2R)-**45c** was carried out following standard synthesis procedure SSP 3 and subsequently SSP 4. (1*R*,2*R*)-DACH (1.00 g, 8.80 mmol) was reacted with freshly distilled isobutyraldehyde (1.60 ml, 17.5 mmol) in anhydrous CH_2Cl_2 (60 ml). After evaporation of the solvent *in vacuo*, the crude Schiff base was obtained as a slightly brown oil (1.62 g, 73%) that was used without further purification in the following reduction with $NaBH_4$ (1.38 g, 36.4 mmol) in absolute EtOH (30 ml). The crude diamine was obtained as a yellow oil and required purification by column chromatography (silica gel, CH_2Cl_2/MeOH/ammonia as eluant going from 70:30:0.2 to 50:50:0.2 ratio) and subsequent distillation under reduced pressure (70 ºC, $3 \cdot 10^{-2}$ mbar) to yield the pure product as a colourless oil (1.19 g, 72%).

^{1}H NMR (400 MHz, $CDCl_3$, 298 K): δ = 2.56 (dd, ^2J = 11.3 Hz, ^3J = 6.4 Hz, 2H, NHCH_2); 2.20 (dd, ^2J = 11.3 Hz, ^3J = 7.0 Hz, 2H, NHCH_2); 2.12-2.01 (m, 4H, NHCH, CH_2); 1.74-1.57 (m, 4H, CH_2, isopropyl-CH); 1.49 (bs, 2H, NH); 1.27-1.11 (m, 2H, CH_2); 1.02-0.92 (m, 2H, CH_2); 0.90 (d, ^3J = 2.1 Hz, 6H, CH_3); 0.89 (d, ^3J = 2.1 Hz, 6H, CH_3) ppm.

^{13}C NMR (100 MHz, $CDCl_3$, 298 K): δ = 62.1 (NH*C*H); 55.4 (NH*C*H_2); 32.0 (*C*H_2); 28.9 (*C*H); 25.3 (*C*H_2); 21.0 (*C*H_3); 20.8 (*C*H_3) ppm.

IR (neat): $\tilde{\nu}$ = 3309 (*w*); 2926 (*s*); 2868 (*m*); 1463 (*m*); 1365 (*w*); 1123 (*m*) cm^{-1}.

$[\alpha]_D^{26}$ = -97.4 (*c* 0.50, $CHCl_3$).

HRMS (ESI+): *m*/*z* = 226.2405 found; 226.2409 calcd for $M^{+\cdot}$ (M = $C_{14}H_{30}N_2$).

(1*S*,2*S*)-*N*,*N*'-Diisobutyl-1,2-cyclohexanediamine (1*S*,2*S*)-**45c** was synthesised in an analogous manner starting from (1*S*,2*S*)-DACH (53%).

Synthesis of (1*R*,2*R*)-*N*,*N*'-pivaloyl-1,2-cyclohexanediamine (1*R*,2*R*)-55d, SSP 1.[14]

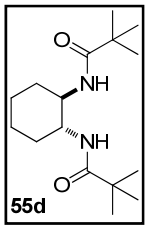

55d

The synthesis of (1*R*,2*R*)-*N*,*N*'-pivaloyl-1,2-cyclohexanediamine (1*R*,2*R*)-**55d** was carried out following a modification of the standard synthesis procedure SSP 1. (1*R*,2*R*)-DACH (2.00 g, 17.5 mmol) was dissolved in anhydrous THF (140 ml) and cooled to 0 ºC in an ice/water bath. Subsequently, Et_3N (6.10 ml, 43.8 mmol), DMAP (430 mg, 3.50 mmol) and, finally, pivaloyl chloride (17.3 ml, 140 mmol) were added under vigorous stirring. The reaction mixture was kept stirring overnight at room temperature, the solvent evaporated to *ca*. ⅓ of its original volume before being diluted with water

(*ca*. 80 ml). The crude product was extracted with EtOAc (2 x 50 ml) and the combined organic layers were successively washed with 10% NaOH, 10% HCl (each 1 x 20 ml), and brine (30 ml) before being dried over $MgSO_4$. After filtration, the solvent was evaporated under reduced pressure and the product was obtained as a white cotton-like solid (4.13 g, 84%) of sufficient purity for the following reduction.

^{1}H NMR (400 MHz, $CDCl_3$, 298 K): δ = 6.12 (bs, 2H, N*H*); 3.67-3.55 (m, 2H, C*H*); 2.10-2.00 (m, 2H, CH_2); 1.80-1.67 (m, 2H, CH_2); 1.39-1.27 (m, 2H, CH_2); 1.27-1.16 (m, 2H, CH_2); 1.14 (s, 18H, CH_3) ppm.

^{13}C NMR (100 MHz, $CDCl_3$, 298 K): δ = 179.2 (*C*=O); 53.8 (*C*H); 38.6 (*C*); 32.5 (*C*H_2); 27.6 (*C*H_3); 24.8 (*C*H_2) ppm.

IR (neat): $\tilde{\nu}$ = 3355 (*m*, NH stretch); 3328 (*s*, NH stretch); 1630 (*s*, C=O) cm^{-1}.

Mp: 247-248 ºC.

Physical and spectroscopic data were in agreement with those present in the literature.[15]

Synthesis of (1*R*,2*R*)-*N*,*N*'-dineopentyl-1,2-cyclohexanediamine (1*R*,2*R*)-45d, SSP 2.[14]

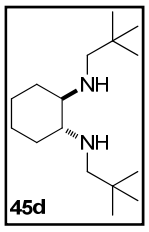

45d

The synthesis of (1*R*,2*R*)-*N*,*N*'-dineopentyl-1,2-cyclohexanediamine (1*R*,2*R*)-**45d** was carried out following a modification of the standard synthesis procedure SSP 2. (1*R*,2*R*)-*N*,*N*'-dineopentanoyl-1,2-cyclohexanediamine (1*R*,2*R*)-**55d** (2.0 g, 7.1 mmol) was refluxed overnight in anhydrous THF(20 ml) together with BH_3·THF (1M in THF, 42 ml, 42 mmol) as the reducing agent. The solution was cooled to 0 ºC in an ice/water bath and MeOH (60 ml) was added carefully under vigorous stirring. Subsequently, the whole mixture was heated to reflux for 1 h and finally concentrated. The residue was treated with water and the

crude product was extracted with an excess of EtOAc (3 x 80 ml). The combined organic layers were washed with brine (30 ml), dried over $MgSO_4$, filtered, and concentrated. Distillation under reduced pressure (83 ºC, $4 \cdot 10^{-2}$ mbar) yielded the pure product as a colourless oil (870 mg, 49%).

^{1}H NMR (400 MHz, THF-d_8, 298 K): δ = 2.47 (d, ^2J = 11.1 Hz, 2H, NHCH_2); 2.13 (d, ^2J = 11.1 Hz, 2H, NHCH_2); 2.08-2.00 (m, 4H, CH, CH_2); 1.71-1.63 (m, 2H, CH_2); 1.60 (bs, 2H, NH); 1.28-1.14 (m, 2H, CH_2); 1.02-0.90 (m, 2H, CH_2); 0.89 (s, 18H, CH_3) ppm.

^{13}C NMR (100 MHz, THF-d_8, 298 K): δ = 63.95 (*C*H); 60.37 (NH*C*H$_2$); 33.07 (*C*H$_2$); 32.52 (*C*H$_2$); 28.35 (*C*H$_3$); 26.34 (*C*) ppm.

IR (neat): $\tilde{\nu}$ = 3316 (*w*); 2928 (*s*); 2859 (*s*); 1464 (*m*); 1361 (*m*); 1117 (*m*) cm^{-1}.

$[\alpha]_D^{26}$ = -77.8 (*c* 0.50, $CHCl_3$).

HRMS (ESI+): *m*/*z* = 254.2714 found; 254.2721 calcd for $M^{+\cdot}$ (M = $C_{16}H_{34}N_2$).

Synthesis of (1*R*,2*R*)-*N*,*N*'-biscyclohexylmethylene-1,2-cyclohexanediamine (1*R*,2*R*)-55e, SSP 3.

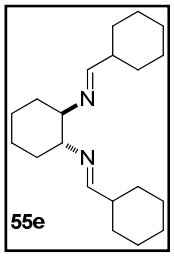

55e

The synthesis of (1*R*,2*R*)-*N*,*N*'-biscyclohexylmethylene-1,2-cyclohexanediamine (1*R*,2*R*)-**55e** was carried out following a modification of the standard synthesis procedure SSP 3. (1*R*,2*R*)-DACH (1.00 g, 8.70 mmol) was refluxed with cyclohexanecarboxaldehyde (2.03 g, 17.5 mmol) in absolute EtOH. The reaction mixture was filtered while still hot and concentrated under reduced pressure, affording diimine (1*R*,2*R*)-**55e** as a slightly yellow oil (2.50 g, 92%) of sufficient purity for the following reduction.

^{1}H NMR (400 MHz, $CDCl_3$, 298 K): δ = 7.43 (d, ^3J = 5.4 Hz, 2H, N=C*H*); 3.03-2.97 (m, 2H, N-C*H*); 2.13-2.07 (m, 2H, C*H*); 1.77-1.35 (m, 16H, CH_2); 1.30-1.13 (m, 12H, CH_2) ppm.

^{13}C NMR (100 MHz, $CDCl_3$, 298 K): δ = 169.0 (N=*C*H); 73.6 (N-*C*H); 43.6 (*C*H); 33.0 (*C*H_2); 30.0 (*C*H_2); 26.0 (*C*H_2); 25.4 (*C*H_2); 24.5 (*C*H_2) ppm.

IR (neat): $\tilde{\nu}$ = 1666 (*m*, C=N) cm^{-1}.

HRMS (ESI+): *m*/*z* = 303.2804 found; 303.2800 calcd for $[M+H]^+$ (M = $C_{20}H_{34}N_2$).

Synthesis of (1*R*,2*R*)-*N*,*N*'-biscyclohexylmethyl-1,2-cyclohexanediamine (1*R*,2*R*)-45e, SSP 4.

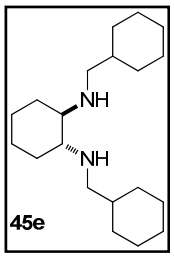

The synthesis of (1*R*,2*R*)-*N*,*N*'-biscyclohexylmethyl-1,2-cyclohexanediamine (1*R*,2*R*)-**45e** was carried out following the standard synthesis procedure SSP 4. (1*R*,2*R*)-*N*,*N*'-biscyclohexylmethylene-1,2-cyclohexanediamine (1*R*,2*R*)-**55e** (1.30 g, 4.30 mmol) and $NaBH_4$ (1.66 g, 43.8 mmol) were refluxed in absolute EtOH. The pure product was obtained as colourless oil (0.87 g, 65%) by distillation under reduced pressure (205 ºC, 4 mbar).

^{1}H NMR (400 MHz, $CDCl_3$, 298 K): δ = 2.57 (m, 2H, NHCH_2); 2.25 (m, 2H, NHCH_2); 2.07-1.98 (m, 4H); 1.78-1.56 (m, 10H); 1.53 (bs, 2H, N*H*); 1.40-1.29 (m, 2H); 1.23-0.94 (m, 10H); 0.92-0.82 (m, 6H) ppm.

^{13}C NMR (100 MHz, $CDCl_3$, 298 K): δ = 61.9 (NH*C*H); 53.8 (NH*C*H_2); 38.5 (*C*H); 31.9 (*C*H_2); 31.5 (*C*H_2); 26.5 (*C*H_2); 26.1 (*C*H_2); 25.2 (*C*H_2) ppm.

IR (neat): $\tilde{\nu}$ = 3300 (*w*, NH stretch) cm^{-1}.

$[\alpha]_D^{28}$ = -66.1 (*c* 0.60, $CHCl_3$).

HRMS (ESI+): *m*/*z* = 306.3023 found; 306.3035 calcd for $M^{+\cdot}$ (M = $C_{20}H_{38}N_2$).

Synthesis of (1*R*,2*R*)-*N*,*N*'-bis(3,3-dimethylbutylidene)-1,2-cyclohexanediamine (1*R*,2*R*)-55f, SSP 3.

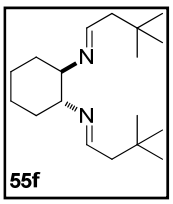

55f

The synthesis of (1*R*,2*R*)-*N*,*N*'-bis(3,3-dimethylbutylidene)-1,2-cyclohexanediamine (1*R*,2*R*)-**55f** was carried out following standard synthesis procedure SSP 3. (1*R*,2*R*)-DACH (856 mg, 7.58 mmol) was reacted with 3,3'-dimethylbutyraldehyde (2.00 ml, 16.2 mmol) in 50 ml of anhydrous CH_2Cl_2. The diimine (1*R*,2*R*)-**55f** was obtained as a colourless oil (1.99 g, 94%) of sufficient purity for the following reduction.

^{1}H NMR (400 MHz, $CDCl_3$, 298 K): δ = 7.64 (dd, ^3J = 5.8 Hz, ^3J = 5.8 Hz, 2H, N=C*H*); 3.13-3.05 (m, 2H, N-C*H*); 2.02 (d, ^3J = 5.8 Hz, 4H, CH_2); 1.77-1.70 (m, 2H, CH_2); 1.64-1.57 (m, 4H, CH_2); 1.40-1.30 (m, 2H, CH_2); 0.90 (s, 18H, CH_3) ppm.

^{13}C NMR (100 MHz, $CDCl_3$, 298 K): δ = 163.7 (N=*C*H); 74.3 (*C*H); 49.5 (^{t}Bu*C*H_2); 33.5 (*C*); 31.1 (*C*H_2); 29.8 (*C*H_3); 24.7 (*C*H_2) ppm.

IR (neat): $\tilde{\nu}$ = 2952 (*m*); 2929 (*m*); 2858 (*w*); 1664 (*m*) cm^{-1}.

Synthesis of (1*R*,2*R*)-*N*,*N*'-bis(3,3'-dimethylbutyl)-1,2-cyclohexanediamine (1*R*,2*R*)-45f, SSP 6.

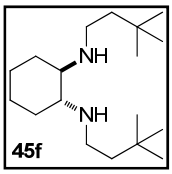

45f

The synthesis of (1*R*,2*R*)-*N*,*N*'-bis(3,3'-dimethylbutyl)-1,2-cyclohexanediamine (1*R*,2*R*)-**45f** was carried out following the standard synthesis procedure SSP 4. (1*R*,2*R*)-*N*,*N*'-Bis(3,3-dimethylbutylidene)-1,2-cyclohexanediamine (1*R*,2*R*)-**55f** (1.95 g, 7.00 mmol) was refluxed for 5 h with $NaBH_4$ (2.65 g, 70.0 mmol) in EtOH (70 ml). The crude diamine was purified by column chromatography (silica gel, CH_2Cl_2/MeOH/ammonia as eluant going from 70:30:0.2 to 50:50:0.2 ratio) and subsequent distillation under reduced pressure (114 ºC, $3.3 \cdot 10^{-2}$ mbar). The pure product was obtained as a white wax-like solid (0.20 g, 35%).

^{1}H NMR (400 MHz, $CDCl_3$, 298 K): δ = 2.70 (ddd, ^2J = 10.8 Hz, ^3J = 10.8 Hz, ^3J = 5.4 Hz, 2H, NHCH_2); 2.38 (ddd, ^2J = 10.8 Hz, ^3J = 10.8 Hz, ^3J = 5.6 Hz, 2H, NHCH_2); 2.11-2.00 (m, 4H, CH, CH_2); 1.74-1.62 (m, 2H, CH_2); 1.46 (bs, 2H, NH); 1.43-1.27 (m, 4H, CH_2); 1.25-1.16 (m, 2H, CH_2); 1.01-0.91 (m, 2H, CH_2); 0.87 (s, 18H, CH_3) ppm.

^{13}C NMR (100 MHz, $CDCl_3$, 298 K): δ = 62.3 (NH*C*H); 44.9 (*C*H_2); 43.4 (*C*H_2); 32.0 (cyclohexyl-*C*H_2); 30.1 (*C*); 29.9 (*C*H_3); 25.4 (cyclohexyl-*C*H_2) ppm.

IR (neat): $\tilde{\nu}$ = 3272 (*m*, NH stretch); 3226 (*m*, NH stretch) cm^{-1}.

$[\alpha]_D^{28}$ = -88.4 (*c* 0.50, $CHCl_3$).

Physical and spectroscopic data were in agreement with those present in the literature.[16]

Synthesis of (1*R*,2*R*)-*N*,*N*'-bis(2,4,6-trimethylbenzylidene)-1,2-cyclohexanediamine (1*R*,2*R*)-55g, SSP 3

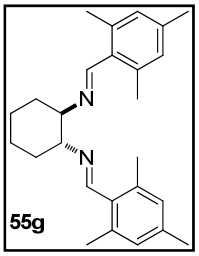

The synthesis of (1*R*,2*R*)-*N*,*N*'-bis(2,4,6-trimethylbenzylidene)-1,2-cyclohexanediamine (1*R*,2*R*)-**55g** was carried out following a modification of the standard synthesis procedure SSP 3. (1*R*,2*R*)-DACH (1.50 g, 12.9 mmol) was refluxed with mesitaldehyde (3.90 ml, 26.5 mmol) in 60 ml of absolute EtOH. The reaction mixture was filtered while still hot and concentrated under reduced pressure, affording diimine (1*R*,2*R*)-**55g** as a white powder (3.76 g, 78%) of sufficient purity for the following reduction.

^{1}H NMR (400 MHz, $CDCl_3$, 298 K): δ = 8.58 (s, 2H, N=C*H*); 6.80 (s, 4H, Ar-C*H*); 3.51-3.39 (m, 2H, C*H*); 2.29 (s, 12H, *o*-CH_3-mesityl); 2.26 (s, 6H, *p*-CH_3-mesityl); 1.93-1.79 (m, 6H, CH_2); 1.61-1.46 (m, 2H, CH_2) ppm.

^{13}C NMR (100 MHz, $CDCl_3$, 298 K): δ = 160.3 (N=*C*H); 138.3 (*C*); 137.5 (*C*); 131.4 (*C*); 129.2 (aryl-*C*H); 75.6 (*C*H); 33.7 (CH_2); 24.7 (CH_2); 21.2 (CH_3); 20.7 (CH_3) ppm.

IR (neat): $\tilde{\nu}$ = 1646 (*s*, C=N); 1611 (*m*); 1437 (*m*); 1374 (*m*) cm^{-1}.

Physical and spectroscopic data were in agreement with those present in the literature.[17]

(1*S*,2*S*)-*N*,*N*'-Bis(2,4,6-trimethylbenzylidene)-1,2-cyclohexanediamine (1*S*,2*S*)-**55g** was synthesised in an analogous manner starting from (1*S*,2*S*)-DACH (73%).

Synthesis of (1*R*,2*R*)-*N*,*N*'-bis(2,4,6-trimethylbenzyl)-1,2-cyclohexanediamine (1*R*,2*R*)-45g, SSP 4.

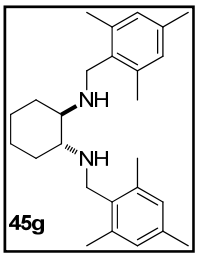

The synthesis of (1*R*,2*R*)-*N*,*N*'-bis(2,4,6-trimethylbenzyl)-1,2-cyclohexanediamine (1*R*,2*R*)-**45g** was carried out following the standard synthesis procedure SSP 4. (1*R*,2*R*)-*N*,*N*'-Bis(2,4,6-trimethylbenzylidene)-1,2-cyclohexanediamine (1*R*,2*R*)-**55g** (3.73 g, 9.96 mmol) was refluxed overnight with $NaBH_4$ (3.80 g, 100 mmol) in absolute EtOH (170 ml). The product was obtained as a white crystalline solid (3.68 g, 98%) that required no further purification.

^{1}H NMR (400 MHz, $CDCl_3$, 298 K): δ = 6.81 (s, 4H, C*H*); 3.85 (d, ^2J = 11.4 Hz, 2H, NHCH_2); 3.48 (d, ^2J = 11.4 Hz, 2H, NHCH_2); 2.38-2.28 (m, 2H, NHC*H*); 2.28 (s, 12H, *o*-CH_3-mesityl); 2.25 (s, 6H, *p*-CH_3-mesityl); 2.22-2.14 (m, 2H, CH_2); 1.83-1.73 (m, 2H, CH_2); 1.53 (bs, 2H, N*H*); 1.35-1.26 (m, 2H, CH_2); 1.15-1.00 (m, 2H, CH_2) ppm.

^{13}C NMR (100 MHz, $CDCl_3$, 298 K): δ = 136.9 (*C*); 136.3 (*C*); 134.2 (*C*); 129.0 (*C*H); 62.1 (NH*C*H); 45.2 (NH*C*H_2); 32.0 (*C*H_2); 25.3 (*C*H_2); 21.0 (*C*H_3); 19.6 (*C*H_3) ppm.

IR (neat): $\tilde{\nu}$ = 3297 (*m*, NH stretch); 2920 (*s*); 2854 (*s*); 1614 (*m*) cm^{-1}.

$[\alpha]_D^{28}$ = -61.8 (*c* 0.50, $CHCl_3$).

Mp: 163-164 ºC.

MS (ESI+): *m*/*z* = 379.2, $[M+H]^+$ (M = $C_{36}H_{50}N_4O_{10}$).

Physical and spectroscopic data were in agreement with those present in the literature.[18]

(1*S*,2*S*)-*N*,*N*'-Bis(2,4,6-trimethylbenzyl)-1,2-cyclohexanediamine (1*R*,2*R*)-**45g** was synthesised in analogue manner starting from (1*S*,2*S*)-**55g** (57%).

Synthesis of (1*R*,2*R*)-*N*,*N*'-diacetyl-1,2-diphenylethane-1,2-diamine (1*R*,2*R*)-55h, SSP 1.

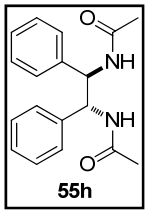

55h

The synthesis of (1*R*,2*R*)-*N*,*N*'-diacetyl-1,2-diphenylethane-1,2-diamine (1*R*,2*R*)-**55h** was carried out following the standard synthesis procedure SSP 1. (1*R*,2*R*)-DPEN (2.00 g, 9.42 mmol) was refluxed for 4 h in anhydrous toluene (100 ml) together with acetic anhydride (70 ml, 556 mmol). The product was obtained as a white powder (2.65 g, 95%) of sufficient purity for the following reduction.

^{1}H NMR (400 MHz, $CDCl_3$, 298 K): δ = 7.21-7.05 (m, 10H, C*H*); 6.72 (bs, 2H, N*H*); 5.25 (s, 2H, NHC*H*); 1.99 (s, 6H, CH_3) ppm.

^{13}C NMR (125 MHz, $CDCl_3$, 298 K): δ = 170.9 (*C*=O); 139.1 (*C*); 128.8 (*C*H); 128.1 (*C*H); 127.9 (*C*H); 59.6 (NH*C*H); 23.5 (*C*H_3) ppm.

IR (neat): $\tilde{\nu}$ = 3273 (*m*, NH stretch) 1643 (*s*, C=O) cm^{-1}.

Mp: 275-277 ºC.

MS (ESI+): *m*/*z* = 319.1, $[M+Na]^+$ (M = $C_{18}H_{20}N_2O_2$).

Synthesis of (1*R*,2*R*)-*N*,*N*'-diethyl -1,2-diphenylethane-1,2-diamine (1*R*,2*R*)-55h, SSP 1.

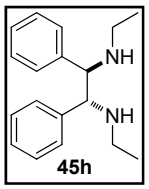

45h

The synthesis of (1*R*,2*R*)-*N*,*N*'-diethyl-1,2-diphenylethane-1,2-diamine (1*R*,2*R*)-**45h** was carried out following the standard synthesis procedure SSP 2. (1*R*,2*R*)-*N*,*N*'-Diacetyl-1,2-diphenylethane-1,2-diamine (1*R*,2*R*)-**55h** (2.80 g, 9.50 mmol) and solid $LiAlH_4$ (4.33 g, 114 mmol) as the reducing agent were refluxed for 12 h in anhydrous THF (300 ml). The resulting slightly yellow crude product was purified by distillation under reduced pressure (110 ºC, $3 \cdot 10^{-2}$ mbar) in order to obtain the final compound as a colourless oil (1.59 g, 63%).

^{1}H NMR (400 MHz, $CDCl_3$, 298 K): δ = 7.15-7.04 (m, 6H, C*H*); 7.03-6.98 (m, 4H, C*H*); 3.63 (s, 2H, NHC*H*); 2.51-2.35 (m, 4H, CH_2); 2.01 (bs, 2H, N*H*); 1.03 (t, ^3J = 7.1 Hz, 6H, CH_3) ppm.

^{13}C NMR (100 MHz, $CDCl_3$, 298 K): δ = 141.9 (*C*); 128.1 (*C*H); 128.0 (*C*H); 126.9 (*C*H); 69.4 (NH*C*H); 42.2 (*C*H_2); 15.6 (*C*H_3) ppm.

IR (neat): $\tilde{\nu}$ = 3309 (*w*); 3061 (*m*); 2963 (*s*); 2805 (*s*); 1452 (*s*); 1121 (*m*); 756 (*m*); 697 (*s*) cm^{-1}.

MS (ESI+): *m*/*z* = 269.2, $[M+H]^+$ (M = $C_{18}H_{24}N_2$).

Synthesis of the hydrogen bonded dimethyl-6,6'-dihydroxy-5,5'-dinitrobiphenyl-3,3'-dicarboxylate/(1*R*,2*R*)-*N*,*N*'-diethyl-1,2-cyclohexanediamine complex, 44a+45a.

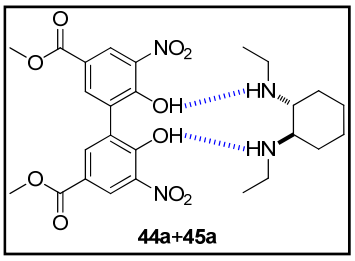

44a+45a

Equimolar amounts of **44a** (8.0 mg, 20 μmol) and **45a** (3.8 mg, 20 μmol) were mixed and dried for 12 h in vacuo in the presence of P_2O_5. Then anhydrous and degassed $CDCl_3$ (1.0 ml) was added and the sample was submitted for NMR analysis.

^{1}H NMR (500 MHz, $CDCl_3$, 298 K): δ = 8.54 (d, ^4J = 2.2 Hz, 2H, C*H*); 8.20 (d, ^4J = 2.2 Hz, 2H, C*H*); 7.57 (bs, 4H, N*H*, O*H*); 3.90 (s, 6H, OCH_3), 3.03-2.96 (m, 2H, NHCH_2); 2.68-2.61 (m, 2H, NHCH_2); 2.43-2.33 (m, 2H, C*H*), 2.10-2.17 (m, 2H, CH_2), 1.80-1.68 (m, 2H, CH_2); 1.26-1.17 (m, 4H, CH_2); 1.15 (t, ^3J = 7.2 Hz, 6H, CH_3) ppm.

^{13}C NMR (125 MHz, $CDCl_3$, 298 K): δ = 166.0 (*C*=O); 160.0 (*C*-OH); 140.2 (*C*); 136.7 (*C*H); 132.4 (*C*); 127.4 (*C*H); 118.3 (*C*); 60.07 (NH*C*H); 52.4 (O*C*H_3); 40.7 (NH*C*H_2); 29.3 (*C*H_2); 24.5 (*C*H_2); 14.1 (*C*H_3) ppm.

Synthesis of the hydrogen bonded dimethyl 6,6'-dihydroxy-5,5'-dinitrobiphenyl-3,3'-dicarboxylate/(1*R*,2*R*)-*N*,*N*'-di-*n*-propyl-1,2-cyclohexanediamine complex, 44a+45b.

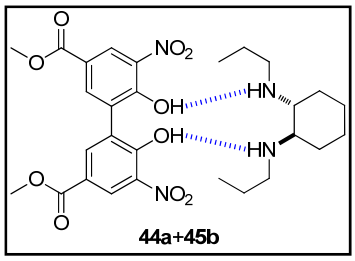

44a+45b

Equimolar amounts of **44a** (9.4 mg, 24 μmol) and **45b** (4.8 mg, 24 μmol) were mixed and dried for 12 h in vacuo in the presence of P_2O_5. Then anhydrous and degassed $CDCl_3$ (1.0 ml) was added and the sample was submitted for NMR analysis.

^{1}H NMR (400 MHz, $CDCl_3$): δ = 8.59 (d, ^4J = 2.1 Hz, 2H, C*H*); 8.19 (d, ^4J = 2.1 Hz, 2H, C*H*); 6.90 (bs, 4H, O*H*, N*H*); 3.90 (s, 6H, OCH_3); 2.89-2.83 (m, 2H, NHCH_2); 2.54-2.48 (m, 2H, NHCH_2); 2.36-2.32 (m, 2H, C*H*); 2.13-2.09 (m, 2H, CH_2); 1.75-1.70 (m, 2H, CH_2); 1.55-1.46 (m, 4H, CH_2); 0.90 (t, ^2J = 8.5 Hz, 6H, CH_3) ppm.

^{13}C NMR (100 MHz, $CDCl_3$, 298 K): δ = 165.8 (*C*=O); 160.2 (*C*-OH); 140.0 (*C*); 136.3 (*C*H); 132.4 (*C*); 127.2 (*C*H); 117.6 (*C*); 60.2 (NH*C*H); 52.1 (O*C*H$_3$); 47.5 (NH*C*H$_2$); 29.3 (*C*H$_2$); 24.4 (*C*H$_2$); 22.0 (*C*H$_2$); 11.2 (*C*H$_3$) ppm.

Synthesis of the hydrogen bonded dimethyl 6,6'-dihydroxy-5,5'-dinitrobiphenyl-3,3'-dicarboxylate/(1*R*,2*R*)-*N*,*N*'-diisobutyl-1,2-cyclohexanediamine complex, 44a+45c.

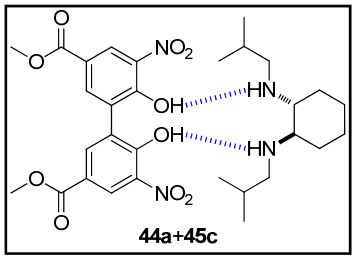

44a+45c

Equimolar amounts of **44a** (9.4 mg, 24 μmol) and **45c** (5.4 mg, 24 μmol) were mixed and dried for 12 h in vacuo in the presence of P_2O_5. Then anhydrous and degassed $CDCl_3$ (1.0 ml) was added and the sample was submitted for NMR analysis.

^{1}H NMR (500 MHz, $CDCl_3$): δ = 8.56 (d, ^4J = 2.2 Hz, 2H, C*H*); 8.21 (d, ^4J = 2.2 Hz, 2H, C*H*); 3.91 (s, 6H, OCH_3); 2.78 (dd, ^2J = 11.8 Hz, ^3J = 6.8 Hz, 2H, NHCH_2); 2.41-2.38 (m, 2H, NHC*H*); 2.38-2.33 (dd, ^2J = 11.8 Hz, ^3J = 6.8 Hz, 2H, NHCH_2); 2.16-2.11 (m, 2H, CH_2); 1.79-1.71 (m, 4H, C*H*, CH_2); 1.24-1.13 (m, 4H, CH_2); 0.91 (d, ^3J = 6.6 Hz, 6H, CH_3); 0.89 (d, ^3J = 6.6 Hz, 6H, CH_3) ppm.

^{13}C NMR (125 MHz, $CDCl_3$, 298 K): δ = 165.7 (*C*=O); 159.6 (*C*-OH); 139.8 (*C*); 136.6 (*C*H); 131.9 (*C*); 127.2 (*C*H); 118.2 (*C*); 60.5 (NH*C*H); 53.2 (NH*C*H_2); 52.2 (O*C*H_3); 29.0 (*C*H_2); 27.3 (*C*H); 24.3 (*C*H_2); 20.2 (*C*H_3); 20.1 (*C*H_3) ppm.

Synthesis of the hydrogen bonded dimethyl 6,6'-dihydroxy-5,5'-dinitrobiphenyl-3,3'-dicarboxylate/(1*R*,2*R*)-*N*,*N*'-2,2-dineopentyl-1,2-cyclohexanediamine complex, 44a+45d.

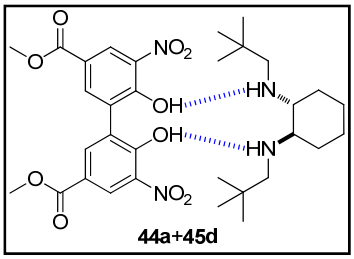

44a+45d

Equimolar amounts of **44a** (7.48 mg, 19.1 μmol) and **45d** (4.86 mg, 19.1 μmol) were mixed and dried for 12 h in vacuo in the presence of P_2O_5. Then anhydrous and degassed CD_2Cl_2 (0.7 ml) was added and the sample was submitted for NMR analysis.

^{1}H NMR (500 MHz, CD_2Cl_2): δ = 8.48 (s, 2H, C*H*); 8.19 (s, 2H, C*H*); 3.90 (s, 6H, OCH_3); 2.79 (d, ^2J = 11.5 Hz, 2H, NHCH_2); 2.45-2.36 (m, 2H, NHC*H*); 2.27 (d, ^2J = 11.5 Hz, 2H, NHCH_2); 2.19-2.09 (m, 2H, CH_2); 1.77-1.66 (m, 2H, CH_2); 1.28-1.08 (m, 4H, CH_2); 0.93 (s, 18H, CH_3) ppm.

^{13}C NMR (125 MHz, CD_2Cl_2, 298 K): δ = 166.1 (*C*=O); 160.4 (*C*-OH); 140.9 (*C*); 136.7 (*C*H); 132.8 (*C*); 127.4 (*C*H); 118.6 (C); 62.2 (NH*C*H); 58.2 (NH*C*H_2); 52.6 (O*C*H_3); 31.5 (*C*); 29.5 (*C*H_2); 27.7 (*C*H_3); 24.9 (*C*H_2) ppm.

Synthesis of the hydrogen bonded dimethyl 6,6'-dihydroxy-5,5'-dinitrobiphenyl-3,3'-dicarboxylate/(1*R*,2*R*)-*N*,*N*'-dicyclohexylmethyl-1,2-cyclohexanediamine complex, 44a+45e.

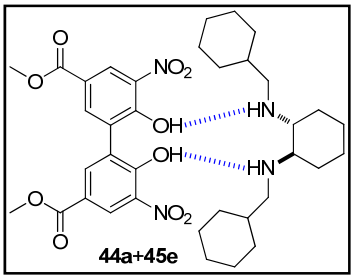

44a+45e

Equimolar amounts of **44a** (9.4 mg, 24 μmol) and **45e** (7.4 mg, 24 μmol) were mixed and dried for 12 h in vacuo in the presence of P_2O_5. Then anhydrous and degassed $CDCl_3$ (1.0 ml) was added and the sample was submitted for NMR analysis.

^{1}H NMR (500 MHz, $CDCl_3$): δ = 8.57 (d, ^{4}J = 2.4 Hz, 2H, C*H*); 8.23 (d, ^{4}J = 2.4 Hz, 2H, C*H*); 3.94 (s, 6H, OCH_3); 2.77 (dd, ^{2}J = 11.7 Hz, ^{3}J = 6.5 Hz, 2H, NHCH_2); 2.42-2.36 (m, 3H); 2.15-2.12 (m, 2H); 1.72-1.63 (m, 12H); 1.46-1.40 (m, 2H); 1.20-1.11 (m; 10H); 0.95-0.86 (m, 5H) ppm.

^{13}C NMR (125 MHz, $CDCl_3$, 298 K): δ = 165.8 (*C*=O); 160.0 (*C*-OH); 140.1 (*C*); 136.3 (*C*H); 132.3 (*C*); 127.1 (*C*H); 117.9 (*C*); 60.5 (NH*C*H); 52.1 (NH*C*H_2); 52.0 (O*C*H_3); 36.7 (*C*H); 30.8 (*C*H_2); 29.1 (*C*H_2); 26.1 (*C*H_2); 25.5 (*C*H_2); 24.3 (*C*H_2) ppm.

MS (ESI+): *m*/*z* = 699.4, $[M+H]^+$, 721.3, $[M+Na]^+$ (M = $C_{36}H_{50}N_4O_{10}$).

Synthesis of the hydrogen bonded dimethyl 6,6'-dihydroxy-5,5'-dinitrobiphenyl-3,3'-dicarboxylate/(1*R*,2*R*)-*N*,*N*'-(3,3'-dimethylbutyl)-1,2-cyclohexanediamine complex, 44a+45f.

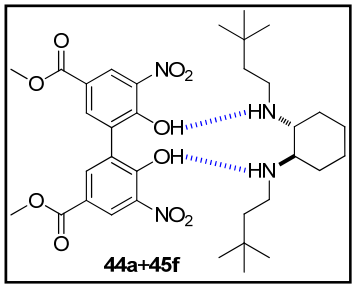

44a+45f

Equimolar amounts of **44a** (9.4 mg, 24 μmol) and **45f** (6.8 mg, 24 μmol) were mixed and dried for 12 h in vacuo in the presence of P_2O_5. Then anhydrous and degassed $CDCl_3$ (1.0 ml) was added and the sample was submitted for NMR analysis.

^{1}H NMR (400 MHz, $CDCl_3$, 298 K): δ = 8.55 (d, ^4J = 2.2 Hz, 2H, C*H*); 8.20 (d, ^4J = 2.2 Hz, 2H, C*H*); 3.90 (s, 6H, OCH_3); 2.91 (ddd, ^2J = 11.5 Hz, ^3J = 11.5 Hz, ^3J = 5.1 Hz, 2H, NHCH_2); 2.57 (ddd, ^2J = 11.5 Hz, ^2J = 11.5 Hz, ^3J = 5.2 Hz, 2H, NHCH_2); 2.46-2.37 (m, 2H, NHC*H*); 2.19-2.10 (m, 4H, CH_2); 1.50-1.40 (m, 2H, ^{t}BuCH_2); 1.37-1.28 (m, 2H, ^{t}BuCH_2); 1.27-1.10 (m, 4H, CH_2); 0.84 (s, 18H, CH_3) ppm.

^{13}C NMR (100 MHz, $CDCl_3$, 298 K): δ = 165.9 (*C*=O); 159.8 (*C*-OH); 139.8 (*C*); 136.9 (*C*H); 132.0 (*C*); 127.4 (*C*H); 118.6 (*C*); 60.3 (NH*C*H); 52.4 (O*C*H$_3$); 42.6 (*C*H$_2$); 42.4 (*C*H$_2$); 30.0 (*C*); 29.5 (*C*H$_3$); 29.2 (*C*H$_2$); 24.6 (*C*H$_2$) ppm.

Synthesis of the hydrogen bonded dimethyl 6,6'-dihydroxy-5,5'-dinitrobiphenyl-3,3'-dicarboxylate/(1*R*,2*R*)-*N*,*N*'-dimesitylmethyl-1,2-cyclohexanediamine complex, 44a+45g.

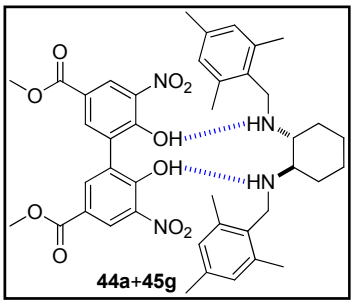

44a+45g

Equimolar amounts of **44a** (9.4 mg, 24 μmol) and **45g** (9.1 mg; 24 μmol) were mixed and dried for 12 h in vacuo in the presence of P_2O_5. Then anhydrous and degassed $CDCl_3$ (1.0 ml) was added and the sample was submitted for NMR analysis.

^{1}H NMR (400 MHz, $CDCl_3$, 298 K): δ = 8.61 (d, ^4J = 2.2 Hz, 2H, biphenol-C*H*); 8.27 (d, ^4J = 2.2 Hz, 2H, biphenol-C*H*); 6.78 (s, 4H, mesityl-C*H*); 4.08 (d, ^2J = 12.8 Hz, 2H, NHCH_2); 3.96 (s, 6H, OCH_3); 3.83 (d, ^2J = 12.8 Hz, 2H, NHCH_2); 2.37-2.29 (m, 3H); 2.24 (s, 6H, *p*-CH_3-mesityl); 2.20 (s, 12H, *o*-CH_3-mesityl); 1.86-1.82 (m, 2H); 1.28-1.13 (m, 8H); 0.90-0.85 (m, 1H) ppm.

^{13}C NMR (125 MHz, $CDCl_3$, 298 K): δ = 165.6 (*C*=O); 159.2 (*C*-OH); 139.3 (*C*); 138.2 (*C*); 137.0 (*C*H); 136.7 (*C*); 131.6 (*C*); 129.5 (*C*H); 128.3 (*C*); 127.2 (*C*H); 118.6 (*C*); 59.4 (NH*C*H); 52.2 (O*C*H_3); 43.4 (NH*C*H_2); 29.2 (*C*H_2); 24.3 (*C*H_2); 20.9 (*p*-*C*H_3-mesityl); 19.5 (*o*-*C*H_3-mesityl) ppm.

Synthesis of zinc bis(trimethylsilyl)amide, $Zn[N(TMS)_2]_2$ 113.[19,20]

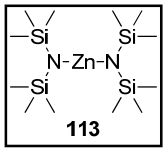

113

Anhydrous $ZnCl_2$ (0.86 g, 6.32 mmol) was placed together with a substoichiometric amount of $NaN(SiMe_3)_2$ (2.08 g, 11.3 mmol) and under inert conditions in a 25 ml Schlenk flask that was equipped with an efficient reflux condenser. Subsequently, anhydrous diethyl ether (10 ml) was added and the reaction mixture was stirred without heating (reaction exothermic) for 1 h. After cooling to room temperature, the precipitated NaCl was filtered off through a Schlenk frit and washed twice with small portions of diethyl ether (2 ml). The resulting solution was freed of the solvent under reduced pressure and the thus obtained crude product was distilled *in vacuo* (approx. 100 ºC at 4 mbar pressure) in a micro-distillation apparatus. The pure product was obtained as colourless oil (1.60 g, 73%).

^{1}H NMR (400 MHz, $CDCl_3$, 298 K): δ = 0.10 (s, CH_3) ppm.

Standard synthesis procedure (SSP 5) for the preparation of [Zn(BIPOLate)(DACH)] complexes using $Zn[N(TMS)_2]_2$ as the zinc source (method A in Chapter II).

The syntheses following SSP 5 were carried out under inert atmosphere in anhydrous solvents by using either Schlenk techniques or working in a glove box. The required biphenol **44** was dissolved in THF (approx. 1.5 ml/0.10 mmol) in a suitable round bottomed flask. Subsequently, 1 equiv. of $Zn[N(TMS)_2]_2$ **113**, dissolved in THF (approx. 0.6 ml/0.1 mmol), was added and the mixture was kept stirring for 45 min at room temperature. Occasionally, a white precipitate presumably consisting of aggregates of zinc biphenolate appeared. Finally, a solution of enantiopure (1,2)-DACH derivatives **45** in THF (1 equiv., approx. 0.6 m/0.1 mmol) was added and the reaction mixture was stirred for 5 min during which the precipitate generally disappeared. The solvent was removed *in vacuo* for which the solution was moderately heated to 35 ºC in a water bath. The crude products were obtained by taking up the residue with either Et_2O or, for solubility reasons, with *n*-hexane where indicated, and filtering through a D3 Schlenk frit. The thus isolated products could be further purified where denoted by crystallisation through slow diffusion of *n*-hexane into solutions in either CH_2Cl_2 or THF.

Standard synthesis procedure (SSP 6) for the preparation of [Zn(BIPOLate)(DACH)] complexes using Et_2Zn as the zinc source (method B in Chapter II).

The syntheses following SSP 6 were carried out under inert atmosphere in anhydrous solvents by either using Schlenk techniques or working in a glove box. The required biphenol **44** was dissolved in THF (approx. 2.5 ml/0.10 mmol) in a suitable round bottomed flask. Subsequently, 1 equiv. of an approx. 1 M solution of Et_2Zn in toluene (evaluated by NMR against COD and C_6D_6 inlet) was added directly to the stirring solution and the mixture was kept stirring for 45 min at room temperature. Occasionally, a white precipitate presumably consisting of aggregates of zinc biphenolate appeared. Finally, a solution of enantiopure (1,2)-DACH derivatives **45** in THF (1 equiv., approx. 0.6 m/0.1 mmol) was added and the reaction mixture was stirred for 5 min during which the precipitate generally disappeared. The crude products were obtained by taking up the residue with either Et_2O or, for solubility reasons, with *n*-hexane where indicated, and filtering through a D3 Schlenk frit. The thus isolated products could be further purified where denoted by crystallisation through slow diffusion of *n*-hexane into solutions in either CH_2Cl_2 or THF.

Synthesis of [Zn(Me-BIPOLate)((1*R*,2*R*)-Et-DACH)], a*R*-114; SSP 5.

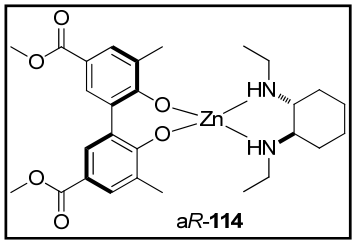

The synthesis of complex a*R*-**114** was carried out following the standard synthesis procedure SSP 5, using biphenol **44b** (108 mg, 0.328 mmol), $Zn[N(TMS)_2]_2$ **113** (0.13 ml 0.33 mmol, 1.0 ml ≡ 2.6 mmol), and (1*R*,2*R*)-Et-DACH, (1*R*,2*R*)-**45a**, (55.8 mg, 0.328 mmol). The product was obtained as a white powder (150 mg, 81%) and could be crystallised by slow diffusion of *n*-hexane into CH_2Cl_2.

^{1}H NMR (400 MHz, THF-d_8, 298 K): δ = 7.68 (s, 2H, C*H*); 7.57 (d, ^4J = 1.3 Hz, 2H, C*H*); 3.98 (bs, 2H, N*H*); 3.71 (s, 6H, CH_3O); 2.92-2.75 (m, 2H, NHCH_2); 2.44-2.23 (m, 6H, NHCH_2, NHC*H*, CH_2); 2.21 (s, 6H, CH_3); 1.77-1.70 (m, 2H, CH_2); 1.24-1.14 (m, 2H, CH_2); 1.02-0.90 (m, 2H, CH_2); 0.83-0.69 (m, 6H, CH_2CH_3) ppm.

^{13}C NMR (125 MHz, THF-d_8, 298 K): δ = 170.3 (*C*=O); 167.8 *C*-O); 134.4 (*C*H); 133.1 (*C*); 131.2 (*C*H); 127.9 (*C*); 117.3 (*C*); 63.0 (NH*C*H); 51.1 (O*C*H_3); 42.6 (*C*H_2); 30.6 (*C*H_2); 25.7 (*C*H_2, superimposed by the THF quintuplet); 18.5 (*C*H_3); 14.6 (CH_2*C*H_3) ppm.

IR (neat): $\tilde{\nu}$ = 3200 (*m*, NH stretch); 2937 (*s*); 2860 (*m*); 1705 (*s*, C=O); 1678 (*s*, C=O); 1593 (*s*); 1417 (*s*); 1339 (*s*); 1275 (*s*); 1207 (*s*); 1147 (*m*); 1086 (*w*); 1006 (*m*); 897 (*m*); 774 (*m*) cm^{-1}.

UV-vis (THF, 298 K): λ_{max} (ε) = 287 (45800); 246 (26300) nm (M^{-1} cm^{-1}).

HRMS (ESI+): *m*/*z* = 563.2101 found; 563.2094 calcd for $[M+H]^+$ (M = $C_{28}H_{39}N_2O_6Zn$).

EA: C, 56.32; H, 6.45; N, 4.53 found; calcd for $C_{28}H_{38}N_2O_6Zn \cdot ½\ CH_2Cl_2$: C, 56.44; H, 6.48; N, 4.62.

Single crystal structure: see appendix.

Synthesis of [Zn(Me-BIPOLate((1*S*,2*S*)-Et-DACH)], a*S*-114; SSP 5.

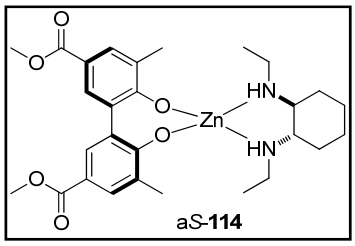

The synthesis of complex a*S*-**114** was analogous to that of a*R*-**114** following the standard synthesis procedure SSP 5, using biphenol **44b** (120 mg, 0.363 mmol), $Zn[N(TMS)_2]_2$ **113** (0.14 ml, 0.36 mmol, 1.0 ml ≡ 2.6 mmol), and (1*S*,2*S*)-Et-DACH, (1*S*,2*S*)-**45a**, (61.9 mg, 0.363 mmol). The product was obtained as a white powder (173 mg, 85%) and could be crystallised by slow diffusion of *n*-hexane into CH_2Cl_2.

Spectroscopic and physical data were in agreement with that of a*R*-**114**.

Single crystal structure: see appendix.

Synthesis [Zn(Me-BIPOLate)((1*R*,2*R*)-Et-DACH)], a*R*-114; SSP 6.

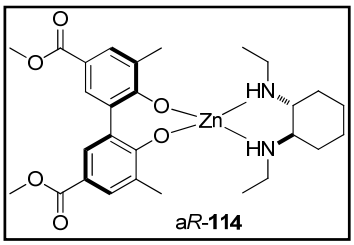

The synthesis of complex a*R*-**114** was also successful following the standard synthesis procedure SSP 6, using biphenol **44b** (86 mg, 0.26 mmol), a solution of Et_2Zn in toluene (1.03 M, 0.25 ml, 0.26 mmol), and (1*R*,1*R*)-Et-DACH, (1*R*,2*R*)-**45a**, (55.8 mg, 0.328 mmol). The product was obtained as a white powder (120 mg, 82%) and could be crystallised by slow diffusion of *n*-hexane into CH_2Cl_2.

Single crystal structure, spectroscopic, and physical data were in agreement with that of a*R*-**114** obtained following protocol SSP 5.

Synthesis of [Zn(Me-BIPOLate)((1*R*,2*R*)-^{t}Bu-DACH)], a*R*-115; SSP 5.

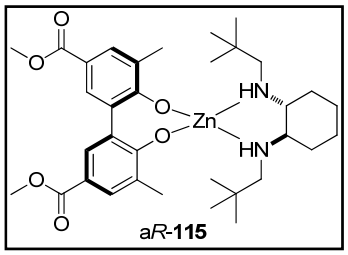

a*R*-**115**

The synthesis of **45d** was carried out following the standard synthesis procedure SSP 5, using biphenol **44b** (72.7 mg, 0.220 mmol), $Zn[N(TMS)_2]_2$ **113** (0.85 ml 0.22 mmol, 1.0 ml ≡ 2.6 mmol), and (1*R*,2*R*)-^{t}Bu-DACH, (1*R*,2*R*)-**45d**, (55.9 mg, 0.220 mmol). The product was obtained as a white powder (120 mg, 84%) and could be crystallised by slow diffusion of *n*-hexane into CH_2Cl_2.

^{1}H NMR (500 MHz, THF-d_8, 253 K): δ = 7.67 (d, ^4J = 1.8 Hz, 2H, C*H*); 7.47 (d, ^4J = 1.8 Hz, 2H, C*H*); 3.70 (s, 6H, OCH_3); 3.10 (dd, ^2J = 11.0 Hz, ^3J = 8.8 Hz, 2H, N*H*); 2.83 (dd, ^2J = 11.0 Hz, ^3J = 8.8 Hz, 2H, NHCH_2); 2.56 (d, ^2J = 11.0 Hz, 2H, NHCH_2); 2.46-2.33 (m, 4H, NHC*H*, CH_2); 2.21 (s, 6H, CH_3); 1.84 (d, *J* = 7.2 Hz, 2H, CH_2); 1.34-1.22 (m, 2H, CH_2); 1.22-1.09 (m, 2H, CH_2); 0.69 (s, 18H, ^{t}Bu-CH_3) ppm.

^{1}H NMR (500 MHz, THF-d_8, 298 K): δ = 7.66 (d, ^4J = 2.2 Hz, 2H, C*H*); 7.47 (d, ^4J = 2.2 Hz, 2H, C*H*); 3.70 (s, 6H, OCH_3); 2.95-2.80 (m, 4H, NHCH_2, N*H*); 2.53 (d, ^2J = 10.5 Hz, 2H, NHCH_2); 2.45-2.35 (m, 4H, NHC*H*, CH_2); 2.21 (s, 6H, CH_3); 1.84 (d, *J* = 7.4 Hz, 2H, CH_2); 1.34-1.24 (m, 2H, CH_2); 1.23-1.12 (m, 2H, CH_2); 0.70 (s, 18H, ^{t}Bu-CH_3) ppm.

^{13}C NMR (125 MHz, THF-d_8, 298 K): δ = 170.9 (*C*=O); 167.9 (*C*-O); 135.1 (*C*H); 133.3 (*C*); 131.3 (C*H*); 127.2 (*C*); 117.0 (*C*); 63.26 (NH*C*H); 59.6 (NH*C*H_2); 51.0 (O*C*H_3); 31.8 (^{t}Bu-*C*); 30.6 (*C*H_2); 27.7 (^{t}Bu-*C*H_3); 26.2 (*C*H_2); 18.9 (*C*H_3) ppm.

IR (neat): $\tilde{\nu}$ = 3253 (*m*, NH stretch); 2948 (*s*); 2866 (*m*); 1702 (*s*, C=O); 1680 (*s*, C=O); 1593 (*s*); 1425 (*s*); 1341 (*s*); 1280 (*s*); 1206 (*s*); 1144 (*m*); 1108 (*m*); 1054 (*w*); 1016 (*m*); 773 (*m*) cm^{-1}.

UV-vis (THF, 298 K): λ_{max} (ε) = 287 (40600); 245 (24100) nm (M^{-1} cm^{-1}).

HRMS (ESI+): *m*/*z* = 669.2603 found; 669.2853 calcd for $[M+Na]^+$ (M = $C_{34}H_{50}N_2O_6Zn$).

MS (MALDI): *m*/*z* = 646.2, $M^{+\cdot}$ (M = $C_{34}H_{50}N_2O_6Zn$).

Single crystal structure: see appendix.

Synthesis of [Zn(Me-BIPOLate)((1*R*,2*R*)-Mes-DACH)], a*S*-116; SSP 5.

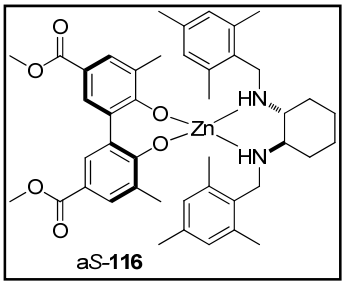

a*S*-**116**

The synthesis of complex a*S*-**116** was carried out following the standard synthesis procedure SSP 5, using biphenol **44b** (100 mg, 0.30 mmol), $Zn[N(TMS)_2]_2$ **113** (0.12 ml 0.30 mmol, 1.0 ml ≡ 2.6 mmol), and (1*R*,2*R*)-Mes-DACH, (1*R*,2*R*)-**45g**, (115 mg, 0.30 mmol). The product was obtained as a white powder (150 mg, 64%).

^{1}H NMR (400 MHz, THF-d_8, 298 K): δ = 7.62 (d, ^4J = 2.1 Hz, 2H, biphenyl-C*H*); 7.47 (d, ^4J = 2.1 Hz, 2H, biphenyl-C*H*); 6.64 (s, 4H, mesityl-C*H*); 4.04 (dd, ^2J = 13.2 Hz, ^3J = 5.2 Hz, 2H, NHCH_2); 3.95 (dd, ^3J = 13.1 Hz,^3J = 8.2 Hz, NHCH_2); 3.73 (s, 6H, OCH_3); 2.88-2.77 (m, 2H, NHC*H*); 2.63-2.52 (m, 2H, N*H*); 2.40-2.34 (m, 2H, CH_2); 2.17 (s, 6H, *p*-CH_3-mesityl); 2.09 (s, 12H, *o*-CH_3-mesityl); 1.90 (s, 6H, biphenyl-CH_3); 1.83-1.78 (m, 2H, CH_2); 1.37-1.29 (m, 2H, CH_2); 1.22-1.12 (m, 2H, CH_2) ppm.

^{13}C NMR (125 MHz, THF-d_8, 298 K): δ = 170.0 (C=O); 168.0 (C-O); 138.6 (mesityl-*C*); 137.9 (mesityl-*C*); 134.3 (biphenyl-*C*H); 132.8 (biphenyl-*C*); 131.3 (biphenyl-*C*H); 131.1 (mesityl-*C*); 130.5 (mesityl-*C*H); 127.8 (biphenyl-*C*); 117.2 (biphenyl-*C*); 64.3 (NH*C*H); 51.0 (O*C*H_3);

46.6 (NH*C*H_2); 32.6 (cyclohexyl-*C*H_2); 26.1 (cyclohexyl-*C*H_2); 21.2 (*p*-*C*H_3-mesityl); 20.0 (*o*-*C*H_3-mesityl); 18.7 (biphenyl-*C*H_3) ppm.

IR (neat): $\tilde{\nu}$ = 3585 (*w*, NH stretch); 2946 (*s*); 2858 (*m*); 1707 (*s*, C=O); 1594 (*m*); 1428 (*m*); 1340 (*m*); 1275 (*m*); 1205 (*s*); 1146 (*m*); 1121 (*m*); 772 (*m*) cm^{-1}.

UV-vis (THF, 298 K): λ_{max} (ε) = 287 (35300); 246 (23300); 218 (40300) nm (M^{-1} cm^{-1}).

HRMS (ESI+): *m*/*z* = 771.3185 found; 771.3346 calcd for $[M+H]^+$ (M = $C_{44}H_{54}N_2O_6Zn$).

MS (MALDI+): *m*/*z* = 771.4, $[M+H]^+$ (M = $C_{44}H_{54}N_2O_6Zn$).

Complex a*R*-**116** was prepared by following SSP 6 using the diamine (1*S*,2*S*)-**45g** resulting in a similar yield (65%).

Synthesis of [Zn(I-BIPOLate)((1*R*,2*R*)-Et-DACH)], a*R*-117; SSP 5.

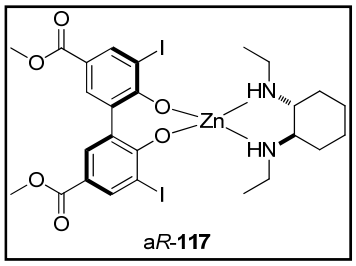

a*R*-**117**

The synthesis of complex a*R*-**117** was carried out following the standard synthesis procedure SSP 5, using biphenol **44e** (183 mg, 0.33 mmol), $Zn[N(TMS)_2]_2$ **113** (128 µl 0.33 mmol, 1.0 ml ≡ 2.6 mmol), and (1*R*,2*R*)-Et-DACH, (1*R*,2*R*)-**45a**, (56.3 mg, 0.33 mmol). The product was obtained as a slightly yellow crystalline powder (239 mg, 92%).

^{1}H NMR (400 MHz, THF-d_8, 298 K): δ = 8.31 (s, 2H, C*H*); 7.68 (s, 2H, C*H*); 4.02 (bs, 2H, N*H*); 3.75 (s, 6H, OCH_3); 3.10-2.97 (m, 2H, NHCH_2); 2.96-2.82 (m, 2H, NHCH_2); 2.50-2.34 (m, 4H, NHC*H*, CH_2); 1.92-1.76 (m, 2H, CH_2); 1.40-1.08 (m, 4H, CH_2); 0.86-0.75 (m, 6H, CH_3) ppm.

^{13}C NMR (125 MHz, THF-d_8, 298 K): δ = 169.5 (*C*=O); 166.3 (*C*-O); 140.2 (C*H*); 136.0 (C*H*); 132.2 (*C*); 119.7 (*C*); 95.1 (*C*-I); 63.5 (NH*C*H); 51.5 (O*C*H$_3$); 43.2 (NH*C*H$_2$); 30.6 (*C*H$_2$); 23.7 (*C*H$_2$); 15.1 (*C*H$_3$) ppm.

IR (neat): $\tilde{\nu}$ = 3219 (*w*, NH stretch); 3125 (*w*, NH stretch); 2943 (*m*); 2859 (*m*); 1707 (*s*, C=O); 1686 (*s*, C=O); 1580 (*m*); 1427 (*s*); 1251 (*s*); 1229 (*s*); 770 (*m*) cm^{-1}.

UV-vis (THF, 298 K): λ_{max}, (ε) = 287 (35300); 246 (23300); 218 (40300) nm (M^{-1} cm^{-1}).

EA: C, 39.78; H, 4.06; N, 3.37 found; calcd for $C_{26}H_{32}I_2N_2O_6Zn$: C, 39.64; H, 4.09; N, 3.56.

Synthesis of [{Zn(μ-H-BIPOLate)((1*R*,2*R*)-Mes-DACH)}$_2$], 118; SSP 5.

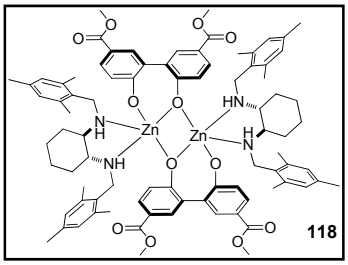

The synthesis of complex **118** was carried out following the standard synthesis procedure SSP 5, using biphenol **44d** (100 mg, 0.33 mmol), Zn[N(TMS)$_2$]$_2$ **113** (0.13 ml 0.34 mmol, 1.0 ml ≡ 2.6 mmol), and (1*R*,2*R*)-Mes-DACH, (1*R*,2*R*)-**45g**, (127 mg, 0.33 mmol). The product was obtained as a white powder (214 mg, 83%) and could be crystallised by slow diffusion of *n*-hexane into THF.

[{Zn(μ-H-BIPOLate)((1*S*,2*S*)-Mes-DACH)}$_2$] was synthesised following SSP 5 (80% yield) and SSP 6 (84% yield) starting from (1*S*,2*S*)-**45g**.

^{1}H NMR (400 MHz, THF-d_8, 298 K): δ = 7.98-7.55 (m, 8H, C*H*); 6.94-6.58 (m, 4H, biphenyl-C*H*, 8H, mesityl-C*H*); 4.08-3.66 (m, 8H, NHC*H*$_2$); 3.84 (s, 12H, OC*H*$_3$); 2.24 (s, 12H, *p*-C*H*$_3$-mesityl) 2.19 (s, 24H, *o*-C*H*$_3$-mesityl); (the missing protons are not unequivocally assignable due to broadened lines) ppm.

^{13}C NMR: Due to the poor signal/noise ratio no ^{13}C NMR spectrum was obtained for this compound.

IR (neat): $\tilde{\nu}$ = 3335 (*w*, NH stretch); 2947 (*m*); 2858 (*m*); 1709 (*s*, C=O); 1592 (*m*); 1484 (*m*); 1324 (*m*); 1266 (*s*); 1225 (*s*); 1101 (*m*); 779 (*m*) cm^{-1}.

UV-vis (THF, 298 K): λ_{max} (ε) = 279 (43400) nm (M^{-1} cm^{-1}).

HRMS (ESI+): *m*/*z* = 1489.5979 found, 1489.5993 calcd for $[M+H]^+$ (M_{dimer} = $C_{84}H_{100}N_4O_{12}Zn_2$); 743.2747 found, 743.3033 calcd for $[M+H]^+$ ($M_{monomer}$ = $C_{42}H_{50}N_2O_6Zn$).

MS (MALDI): *m*/*z* = 743.3, $[M+H]^+$ ($M_{monomer}$ = $C_{42}H_{50}N_2O_6Zn$).

Synthesis of [{Zn(μ-H-BIPOLate)((1*R*,2*R*)-^{t}Bu-DACH)}$_2$], 119; SSP 5.

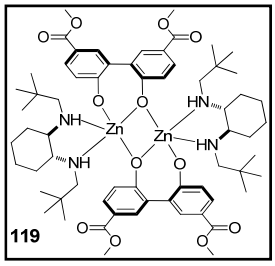

The synthesis of complex **119** was carried out following the standard synthesis procedure SSP 5, using biphenol **44d** (66.9 mg, 0.22 mmol), $Zn[N(TMS)_2]_2$ **113** (85.0 µl 0.22 mmol, 1.0 ml ≡ 2.6 mmol), and (1*R*,2*R*)-^{t}Bu-DACH, (1*R*,2*R*)-**45d**, (56.3 mg, 0.22 mmol). The product was obtained as a white powder (80.0 mg, 90%).

Complex **119** was also prepared by following SSP 6 resulting in a similar yield (81%).

^{1}H NMR (400 MHz, THF-d$_8$, 298 K): δ = 8.30- 7.35 (m, 8H, C*H*); 7.25-6.40 (m, 4H, C*H*); 3.79 (s, 12H, OCH_3); 2.80-0.25 (m, 64H, C*H*, CH_2); (the protons are not unequivocally assignable due to broadened lines) ppm.

^{13}C NMR: Due to the poor signal/noise ratio no ^{13}C NMR spectrum was obtained for this compound.

IR (neat): $\tilde{\nu}$ = **IR (neat):** $\tilde{\nu}$ = 3258 (*w*, NH stretch); 3165 (*w*, NH stretch); 2949 (*s*); 2866 (*m*); 1709 (*s*, C=O); 1593 (*s*); 1481 (*s*); 1370 (*m*); 1271 (*s*); 1227 (*s*); 1108 (*m*); 777 (*m*) cm^{-1}.

UV-vis (THF, 298 K): λ_{max} $(\varepsilon) = 278$ (47900), 240 (34200) nm (M^{-1} cm^{-1}).

HRMS (ESI+): *m*/*z* = 1237.5771 found, 1237.5367 calcd for $[M+H]^+$ ($M_{dimer} = C_{64}H_{92}N_4O_{12}Zn_2$); 619.3359 found, 619.2720 calcd for $[M+H]^+$; 641.2973 found, 641.2540 calcd for $[M+Na]^+$ ($M_{monomer} = C_{32}H_{46}N_2O_6Zn$).

MS (MALDI+): *m*/*z* = 618.3, $M^{+\cdot}$ ($M_{monomer} = C_{32}H_{46}N_2O_6Zn$).

Synthesis of [{Zn(*μ*-H-BIPOLate)((1*R*,2*R*)-Et-DACH)}$_2$], 120; SSP 5.

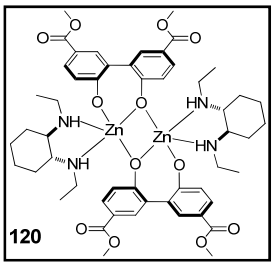

The synthesis of complex **120** was carried out following the standard synthesis procedure SSP 5, using biphenol **44d** (87.8 mg, 0.29 mmol), $Zn[N(TMS)_2]_2$ **113** (112 μl 0.29 mmol, 1.0 ml ≡ 2.6 mmol), and (1*R*,2*R*)-Et-DACH, (1*R*,2*R*)-**45a**, (49.5 mg, 0.29 mmol). The product was obtained as a white powder (117 mg, 75%) and could be crystallised by slow diffusion of *n*-hexane into CH_2Cl_2.

[{Zn(*μ*-H-BIPOLate)((1*S*,2*S*)-Et-DACH)}$_2$] was synthesised following SSP 5 (74% yield) and SSP 6 (69% yield) starting from(1*S*,2*S*)-**45a**

^{1}H NMR (500 MHz, THF-d_8, 298 K): δ = 7.84 (s, 4H, C*H*); 7.78 (d, ^3J = 7.3 Hz, 4H, C*H*); 6.86-6.70 (m, 4H, C*H*); 3.76 (s, 12H, OCH_3); 2.77-2.56 (m, 4H, NHCH_2); 2.55-2.33 (m, 4H, N*H*); 2.14-1.84 (m, 12H, NHCH_2, C*H*, CH_2); 1.68-1.55 (m, 4H, CH_2); 1.21-1.03 (m, 4H, CH_2); 1.01-0.84 (m, 12H, CH_3); 0.82-0.65 (m, 4H, CH_2) ppm (the dimeric structure was assumed for the integration of the signals).

^{13}C NMR: Due to the poor signal/noise ratio no ^{13}C NMR spectrum was obtained for this compound.

IR (neat): $\tilde{\nu}$ = 3232 (*w*, NH stretch); 2945 (*m*); 2865 (*w*); 1700 (*s*, C=O); 1589 (*m*); 1481 (*m*); 1318 (*m*); 1267 (*s*); 1224 (*s*); 1105 (*m*); 780 (*m*) cm^{-1}.

UV-vis (THF, 298 K): λ_{max} (ε) = 283 (41200); 241 (23700) nm (M^{-1} cm^{-1}).

UV-vis (CH_2Cl_2, 298 K): λ_{max} (ε) = 284 (40000); 240 (24700) nm (M^{-1} cm^{-1}).

HRMS (ESI+): 557.1542 found, 557.1601 calcd for $[M+Na]^+$ ($M_{monomer}$ = $C_{26}H_{34}N_2O_6Zn$); 1091.3115 found, 1091.3309 calcd for $[M+Na]^+$ (M_{dimer} = $C_{52}H_{68}N_4O_{12}Zn_2$).

MS (MALDI+): *m*/*z* = 534.1, $M^{+\cdot}$ ($M_{monomer}$ = $C_{26}H_{34}N_2O_6Zn$).

EA: C, 57.59; H, 6.29; N, 5.19 found; calcd for $C_{52}H_{68}N_4O_{12}Zn_2 \cdot \frac{1}{3}CH_2Cl_2$: C, 57.13; H, 6.29; N, 5.09.

Synthesis of [dichloro((1*R*,2*R*)-*N*,*N*'-diethyl-1,2-cyclohexane-diamine)zinc(II)]; [$ZnCl_2$((1*R*,2*R*)-45a)].[21]

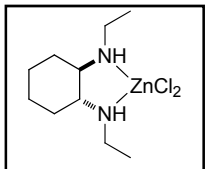

[$ZnCl_2$((1*R*,2*R*)-**45a**)]

To a solution of $ZnCl_2$ (100 mg, 0.59 mmol) in THF (5 ml) was added dropwise a solution of (1*R*,2*R*)-*N*,*N*'-diethyl-1,2-cyclohexanediamine (1*R*,2*R*)-**45a** (79.0 mg, 0.58 mmol) in THF (10 ml) and the mixture was stirred for 2 d at rt. The solvent was removed *in vacuo* and the resulting residue washed with portions of cold diethyl ether (2 × 1 ml). Recrystallisation of the slightly yellow powder from warm toluene yielded long needle-like white crystals (148 mg, 82%).

^{1}H NMR (500 MHz, $CDCl_3$, 298 K): δ = 3.10-2.98 (m, 2H, NHCH_2); 2.78-2.65 (m, 2H, NHCH_2); 2.43-2.32 (m, 4H, NHCH, CH_2); 2.24-2.13 (m, 2H, CH_2); 1.32 (t, ^3J = 7.1 Hz, 6H, CH_3); 1.28-1.19 (m, 2H, CH_2); 1.17-1.06 (m, 2H, CH_2) ppm.

^{13}C NMR (125 MHz, $CDCl_3$, 298 K): δ = 62.2 (NHCH_2); 41.9 (NHCH); 30.6 (CH_2); 24.7 (CH_2); 15.0 (CH_3) ppm.

IR (neat): $\tilde{\nu}$ = **IR (neat):** $\tilde{\nu}$ = 3196 (*m*, NH stretch); 2970 (*m*); 2936 (*m*); 1467 (*m*); 1450 (*m*); 1079 (*s*); 1004 (*s*); 899 (*m*) cm^{-1}.

MS (MALDI+): *m*/*z* = 327.1, $[M+Na]^+$ (M = $C_{10}H_{22}Cl_2N_2Zn$).

Single crystal structure: see appendix.

Synthesis of [dichloro((1*R*,2*R*)-*N*,*N*'-diisobutyl-1,2-cyclohexanediamine)zinc(II)]; [$ZnCl_2$((1*R*,2*R*)-45c)].[21]

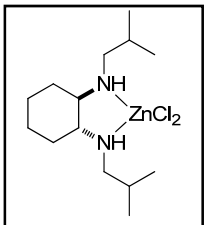

[$ZnCl_2$((1*R*,2*R*)-**45c**)]

To a solution of $ZnCl_2$ (300 mg, 1.33 mmol) in THF (10 ml) was added dropwise a solution of (1*R*,2*R*)-*N*,*N*'-diisobutyl-1,2-cyclohexanediamine (1*R*,2*R*)-**45c** 179 mg, 1.31 mmol) in THF (15 ml) and the mixture was stirred for 2 d at rt. The solvent was removed *in vacuo* and the resulting residue washed with portions of cold diethyl ether (2 × 2 ml). Recrystallisation of the slightly yellow powder from warm toluene yielded needle-like white crystals (402 mg, 83%).

^{1}H NMR (500 MHz, $CDCl_3$, 298 K): δ = 2.74 (ddd, ^2J = 11.5 Hz, ^3J = 11.5 Hz, ^3J = 3.6 Hz, 2H, NHCH_2); 2.50 (ddd, ^2J = 11.5 Hz, ^3J = 10.5 Hz, ^3J = 1.9 Hz, 2H, NHCH_2); 2.45-2.35 (m, 4H, CH, CH_2); 2.19-2.08 (m, 2H, ^{i}PrCH); 1.99-1.89 (m, 2H, NH); 1.88-1.79 (m, 2H, CH_2); 1.30-1.19 (m, 2H, CH_2); 1.13-1.01 (m, 2H, CH_2), 0.97 (d,^3J = 6.6 Hz, 6H, CH_3); 0.94 (d, ^3J = 6.6 Hz, 6H, CH_3) ppm.

^{13}C NMR (125 MHz, $CDCl_3$, 298 K): δ = 62.3 (NH*C*H); 55.2 (NH*C*H_2); 30.8 (*C*H_2); 28.2 (*C*H); 24.7 (*C*H_2); 21.3 (*C*H_3); 20.2 (*C*H_3) ppm.

IR (neat): $\tilde{\nu}$ = 3219 (*m*, NH stretch); 2938 (*s*); 2869 (*m*); 1465 (*s*); 1441 (*m*); 1083 (*s*); 988 (*s*) cm^{-1}.

MS (MALDI+): *m*/*z* = 383.1, $[M+Na]^+$ (M = $C_{14}H_{30}Cl_2N_2Zn$).

Single crystal structure: see appendix.

Synthesis of [dichloro((1*R*,2*R*)-*N*,*N*'-diethyl-1,2-diphenylethane-1,2-diamine)zinc(II)]; [$ZnCl_2$((1*R*,2*R*)-45h)].[21]

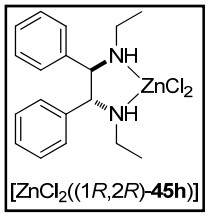

[$ZnCl_2$((1*R*,2*R*)-**45h**)]

To a solution of $ZnCl_2$ (76.0 mg, 0.55 mmol) in THF (8 ml) was added dropwise a solution of (1*R*,2*R*)-*N*,*N*'-diethyl-1,2-diphenylethane-1,2-diamine (1*R*,2*R*)-**45h** 148 mg, 0.55 mmol) in THF (4 ml) and the mixture was stirred for 2 d at rt. The solvent was removed *in vacuo* and the resulting residue washed with portions of cold diethyl ether (2 × 2 ml). Recrystallisation of the slightly yellow powder from warm toluene yielded small white crystals (154 mg, 69%).

^{1}H NMR (400 MHz, $CDCl_3$, 298 K): δ = 7.22-7.13 (m, 6H, C*H*); 7.05-6.98 (m, 4H, C*H*); 3.94-3.84 (m, 2H, NHC*H*); 2.98-2.84 (m, 2H, NHCH_2); 2.84-2.73 (m, 2H, N*H*); 2.67-2.56 (m, 2H, NHCH_2); 1.29 (t, ^3J = 7.1 Hz, 6H, CH_3) ppm.

^{13}C NMR (100 MHz, $CDCl_3$, 298 K): δ = 136.2 (*C*); 129.3 (*C*H); 129.0 (*C*H); 127.5 (*C*H); 68.7 (NH*C*H); 42.9 (NH*C*H_2); 14.9 (CH_3) ppm.

IR (neat): $\tilde{\nu}$ = 3212 (*m*, NH stretch); 2972 (*w*); 2866 (*w*); 1456 (*m*); 1434 (*m*); 1066 (*s*) cm^{-1}.

Single crystal structure: see appendix.

Synthesis of [Cu(BIPOLate)$_2$((1*R*,2*R*)-DACH)$_2$], *R*,*R*-a*R*-121.

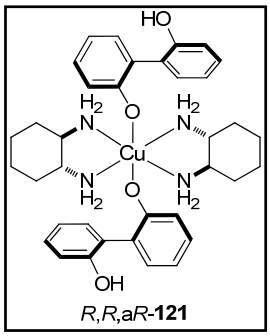

R,*R*,a*R*-**121**

To a solution of $CuCl_2 \cdot 2H_2O$ (122 mg, 1.07 mmol) in CH_3OH/H_2O (1:1, 30 ml), was added under stirring in CH_3OH/H_2O (1:1, 10 ml) dissolved (1*R*,2*R*)-cyclohexanediamine. A second solution of [1,1'-biphenyl]-2,2'-diol (200 mg, 1.07 mmol) together with NaOH (86 mg, 2.14 mmol) in CH_3OH/H_2O (1:1, 20 ml) was prepared and slowly added to the first solution after stirring both for 1 h at rt. The combined reaction mixtures were stirred for 1 h and the green precipitate that had formed was filtered off. The remaining violet filtrate is reduced to approx. ⅓ of its original volume by rotary evaporation and again filtered. Subsequently, the solvent was completely removed, the purple crude product dissolved in the minimum amount of warm (45 ºC) CH_3OH required, filtered warm in order to eliminate NaCl, and crystallized at -18 ºC. The product was obtained in purple, plate like crystals (259 mg, 34% (calc. for M + 2 MeOH)).

UV-vis (MeOH, 298 K): λ_{max} (ε) = 560 (200); 312 (17100); 243 (30700, shoulder) nm (M^{-1} cm^{-1}).

UV-vis (CH_2Cl_2, 298 K): λ_{max} (ε) = 608 (170); 326 (15300); 250 (26500, shoulder) nm (M^{-1} cm^{-1}).

Single crystal structure: see appendix.

Synthesis of [{Cu(μ-BIPOLate)((1*R*,2*R*)-DACH)}$_2$], 122.

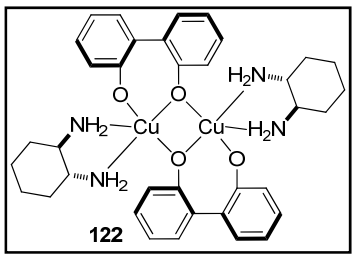

122

To a suspension of 2,2'-biphenol in *n*-hexane in a two-necked round bottomed flask equipped with a reflux condenser, a solution of *n*-BuLi in hexanes was added dropwise and under inert atmosphere. Subsequently, the reaction mixture was kept at reflux until no further butane formation could be observed. The resulting white product was filtered through a Schlenk frit, washed with anhydrous *n*-hexane, and dried under high vacuum. The thus prepared lithium biphenyl-2,2'-bis(olate) was dissolved in anhydrous CH_3OH in a two-necked round bottomed flask equipped with a reflux condenser. Subsequently, a solution of anhydrous $CuCl_2$ in anhydrous CH_3OH was added dropwise under inert atmosphere and the mixture was stirred for 2 h at reflux. The resulting precipitate was filtered through a Schlenk frit, washed with anhydrous CH_3OH, and dried under high vacuum. The resulting Cu(II)-bipolate was suspended in anhydrous toluene and refluxed together with (1*R*,2*R*)-cyclohexanediamine for 2 h. The final product was filtered off through a Schlenk frit, washed with anhydrous *n*-hexane and again dried under high vacuum.

Single crystal structure: see appendix.

Synthesis of dimethyl 6,6'-dimethoxy-5,5'-dimethylbiphenyl-3,3'-dicarboxylate 127.

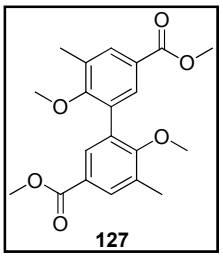
127

Biphenol **44b** (482 mg, 1.46 mmol) and K_2CO_3 (1.00 g, 7.24 mmol) were mixed together in DMF (15 ml) under argon. CH_3I (0.36 ml, 5.85 mmol) was then syringed dropwise. The resulting mixture was heated to reflux for one hour then allowed to cool to rt and quenched with water (10 ml). The solvent was removed under vacuum and the resulting residue was partitioned between water (20 ml) and EtOAc (20 ml). The aqueous layer was extracted two more times with EtOAc (2 × 20 ml), the organic extracts were combined, washed with brine (20 ml), and dried over $MgSO_4$. The drying agent was filtered off, the solution concentrated under reduced pressure and the crude product was purified by column chromatography (silicagel, eluant: 1:9 EtOAc/hexanes). The resulting product was obtained as a white solid (523 mg, quantitative yield).

^{1}H NMR (400 MHz, $CDCl_3$, 298 K): δ = 7.93 (d, ^4J = 2.2 Hz, 2H, C*H*); 7.86 (d, ^4J = 2.0 Hz, 2H, C*H*); 3.90 (s, 6H, COOCH_3); 3.44 (s, 6H, OCH_3); 2.39 (s, 6H, CH_3) ppm.

^{13}C NMR (100 MHz, $CDCl_3$, 298 K): δ = 166.6 (*C*=O); 160.2 (*C*-O); 132.3 (*C*H); 131.5 (*C*); 131.3 (*C*); 130.6 (*C*H); 125.2 (*C*); 60.2 (O*C*H$_3$); 51.9 (COO*C*H$_3$); 16.3 (*C*H$_3$) ppm.

IR (neat): $\tilde{\nu}$ = 3053 (*m*); 2949 (*s*); 1712 (*s*, C=O) cm^{-1}.

HRMS (ESI+): *m*/*z* = 381.1316 found; 381.1314 calcd for [M+Na]$^+$ (M = $C_{20}H_{22}O_6$).

Synthesis of dimethyl 6,6'-dimethoxy-5,5'-dimethylbiphenyl-3,3'-dicarboxylic acid 128.

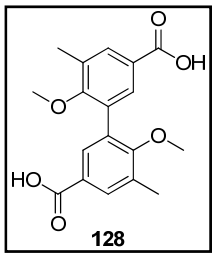

128

Biphenol **127** (523 mg, 1.46 mmol) was dissolved in THF (15.0 ml) before a solution of NaOH. (2 N in water, 15.0 ml) was added and the resulting mixture stirred during 4 h at rt. The solvent was evaporated to approx. ⅓ of its original volume and the product precipitated by addition of concentrated HCl. The crude product was collected by filtration, washed with small amounts of cold water, and dried under high vacuum overnight to give the pure compound as a white solid (450 mg, 93%).

^{1}H NMR (400 MHz, DMSO-d_6, 298 K): δ = 12.9 (bs, 2H, COO*H*); 7.84 (d, ^{4}J = 1.7 Hz, 2H, C*H*); 7.69 (d, ^{4}J = 2.0 Hz, 2H, C*H*); 3.42 (s, 6H, OCH_3); 2.39 (s, 6H, CH_3) ppm.

^{13}C NMR (100 MHz, DMSO-d_6, 298 K): δ = 167.3 (*C*=O); 159.9 (*C*-O); 132.4 (*C*H); 131.7 (*C*); 131.2 (*C*); 130.8 (*C*H); 126.2 (*C*); 60.3 (O*C*H_3); 16.7 (*C*H_3); ppm.

IR (neat): $\tilde{\nu}$ =2945 (*s*); 2860 (*s*); 2612 (*s*); 1671 (*s*, C=O); 1599 (*m*) cm^{-1}.

Synthesis of 6,6'-dimethoxy-5,5'-dimethylbiphenyl-3,3'-dicarbonyl dichloride 129.

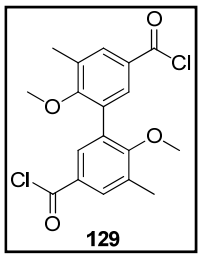

129

Biphenol **128** (440 mg, 1.33 mmol) and $SOCl_2$ (2.00 mL, 26.0 mmol) were mixed together under argon atmosphere and the resulting mixture was heated to reflux for 3 h. Removal of the excess of $SOCl_2$ gave the product **122** as a white foam which was sufficiently pure to be used without further purification (430 mg, 88%).

^{1}H NMR (400 MHz, $CDCl_3$, 298 K): δ = 8.04 (d, ^4J = 2.1 Hz, 2H, C*H*) 7.97 (d, ^4J = 2.4 Hz, 2H, C*H*); 3.53 (s, 6H, OCH_3); 2.44 (s, 6H, CH_3) ppm.

^{13}C NMR (100 MHz, $CDCl_3$, 298 K): δ = 167.4 (*C*=O); 162.3 (*C*-O); 134.5 (*C*H); 132.7 (*C*); 132.6 (*C*); 131.1 (*C*H); 128.2 (*C*); 60.5 (O*C*H_3); 16.6 (*C*H_3) ppm.

Synthesis of the diphosphane ligand 130.

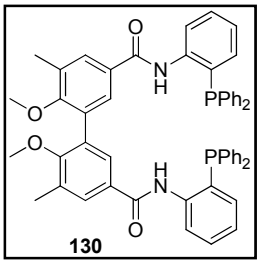

130

2-(Diphenylphosphino)aniline (634 mg, 2.28 mmol) and anhydrous pyridine (0.45 ml, 2.28 mmol) were dissolved under argon atmosphere in anhydrous THF (10 ml). The benzoyl chloride **122** (420 mg, 1.14 mmol) was dissolved in anhydrous THF (5 ml) and rapidly added to the stirred solution *via* cannula. The resulting suspension was stirred for 2 h. The precipitate was filtered and washed with anhydrous THF (20 ml in portions). After removal of the solvent the crude product was obtained as a viscous oil that had to be purified by silicagel column chromatography (eluant: 95:5 CH_2Cl_2/acetone) to give the pure compound **130** as a white solid (870 mg, 90%).

^{1}H NMR (400 MHz, $CDCl_3$, 298 K):δ = 8.55 (d, $^4J_{H\text{-}P}$ = 7.1 Hz, 2H, N*H*); 8.37-8.41 (m, 2H, C*H*); 7.59 (d, ^4J = 2.2 Hz, 2H, C*H*); 7.42-7.47 (m, 2H, C*H*); 7.23-7.35 (m, 20H, C*H*); 7.22 (d, ^4J = 2.2 Hz, 2H, C*H*); 7.06-7.10 (m, 2H, C*H*); 6.89-6.93 (m, 2H, C*H*); 3.39 (s, 6H, OCH_3); 2.39 (s, 6H, CH_3) ppm.

^{13}C NMR (100 MHz, $CDCl_3$, 298 K): δ = 164.5 (*C*=O); 159.2 (*C*-O), 140.9 (d, *J* = 16.4 Hz, *C*), 134.0 (d, *J* = 6 Hz, *C*H); 133.8 (d, *J* = 19 Hz, *C*H); 133.4 (d, *J* = 4 Hz, *C*H); 131.9 (*C*, biphenol); 131.4 (*C*, biphenol); 130.3 (*C*H); 130.1 (*C*H, biphenol), 129.8 (*C*); 129.4 (*C*, biphenol); 128.9

(d, *J* = 7.3 Hz, *C*H); 127.5 (*C*H, biphenol); 126.5 (d, *J* = 10.7 Hz, *C*); 124.6 (*C*H); 121.8 (*C*); 60.3 (O*C*H_3), 16.5 (*C*H_3) ppm.

^{31}P NMR (126 MHz, $CDCl_3$, 298 K): δ = -16.3 ppm.

IR (neat): $\tilde{\nu}$ = 3394 (*m*, NH stretch); 3333 (*m*, NH stretch); 1676 (*s*, C=O); 1572 (*m*); 1508 (*s*); 1432 (*s*); 1296 (*m*); 1200 (*w*); 1152 (*w*) cm^{-1}.

HRMS (ESI+): *m*/*z* = 871.2803 found; 871.2831 calcd for $[M+Na]^+$ (M = $C_{54}H_{46}N_2O_4P_2$).

Synthesis of diphosphane ligand 131.

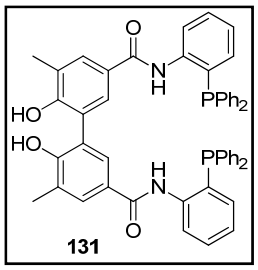

131

A solution of bisphosphane **131** (800 mg, 10 mmol) in anhydrous CH_2Cl_2 (20 ml) was cooled to -78ºC. To this solution was syringed during a period of 30 min BBr_3 (0.5 ml, 30 mmol). The reaction mixture was stirred at -78 ºC for 1 h. Subsequently, the mixture was allowed to come slowly to rt and was stirred overnight. After cooling the mixture to 0ºC, degassed water (20 ml) was added. The solvent was removed *in vacuo* and the resulting crude product dissolved in anhydrous THF and filtered through silicagel pad. Evaporating the THF and drying of the product under high vacuum gave compound **131** as a slightly orange powder (770 mg, quantitative yield).

^{1}H NMR (400 MHz, THF-d_8, 298 K): δ = 8.55 (d, $^4J_{H\text{-}P}$ = 5.8 Hz, N*H*); 8.35-8.37 (m, 2H, C*H*); 7.61 (bs, 2H, C*H*); 7.38-7.42 (m, 2H, C*H*); 7.29-7.34 (m, 20H, C*H*); 7.22 (bs, 2H, C*H*); 7.04-7.08 (m, 2H, C*H*); 6.93-6.96 (m, 2H, C*H*); 2.35 (s, 6H, CH_3) ppm.

^{13}C NMR (100 MHz, THF-d_8, 298 K): δ = 164.5 (*C*=O); 159.2 (*C*-O); 140.9 (d, *J* = 16.4 Hz, *C*); 134.0 (d, *J* = 6 Hz, *C*H); 133.8 (d, *J* = 19 Hz, *C*H); 133.4 (d, *J* = 4 Hz, *C*H); 131.9 (*C*, biphenol); 131.4 (*C*, biphenol); 130.3 (*C*H); 130.1 (*C*H, biphenol); 129.8 (*C*); 129.4 (*C*, biphenol); 128.9

(d, J = 7.3 Hz, *C*H); 127.5 (*C*H, biphenol); 126.5 (d, J = 10.7 Hz, *C*); 124.6 (*C*H); 121.8 (*C*); 60.3 (O*C*H_3); 16.5 (*C*H_3) ppm.

^{31}P NMR (126 MHz, THF-d_8, 298 K): δ = -15.9 ppm.

IR (neat): $\tilde{\nu}$ = 3324 (*m*, OH stretch); 3054 (*w*, NH stretch); 2924 (*w*); 1658 (*m*, C=O); 1572 (*m*); 1517 (*m*); 1433 (*s*) 1301 (*s*); 1233 (*s*) cm^{-1}.

HRMS (MALDI-): *m*/*z* = 819.2515 found; 819.2547 calcd for $[M-H]^-$ (M = $C_{52}H_{42}N_2O_4P_2$).

References

[1] G. R. Fulmer, A. J. M. Miller, N. H. Sherden, H. E. Gottlieb, A. Nudelman, B. M. Stoltz, J. E. Bercaw, K. I. Goldberg, *Organometallics* **2010**, *29*, 2176.
[2] S. Danishefsky, C.-F. Yan, R. K. Singh, R. B. Gammill, P. M. McCurry, Jr., N. Fritsch, J. Clardy, *J Am Chem Soc* **1979**, *101*, 7001.
[3] R. J. Payne, M. D. Toscano, E. M. M. Bulloch, A. D. Abell, C. Abell, *Org. Biomol. Chem.* **2005**, *3*, 2271.
[4] J. Iskra, S. Stavber, M. Zupan, *Synthesis* **2004**, 1869.
[5] J. Etxebarria, H. Degenbeck, A. S. Felten, S. Serres, N. Nieto, A. Vidal-Ferran, *J Org Chem* **2009**, *74*, 8794.
[6] H. Booth, B. C. Saunders, *J. Chem. Soc.* **1956**, 940.
[7] G. Wells, A. Seaton, M. F. G. Stevens, *J. Med. Chem.* **2000**, *43*, 1550.
[8] A. P. Cole, V. Mahadevan, L. M. Mirica, X. Ottenwaelder, T. D. P. Stack, *Inorg. Chem.* **2005**, *44*, 7345.
[9] J. Leonard, B. Lygo, G. Procter, Editors, *Advanced Practical Organic Chemistry, 2nd Edition*, **1995**.
[10] A. M. Costa, C. Jimeno, J. Gavenonis, P. J. Carroll, P. J. Walsh, *J Am Chem Soc* **2002**, *124*, 6929.
[11] Y. L. Bennani, S. Hanessian, *Tetrahedron* **1996**, *52*, 13837.
[12] N. Zweep, A. Hopkinson, A. Meetsma, W. R. Browne, B. L. Feringa, J. H. van Esch, *Langmuir* **2009**, *25*, 8802.
[13] S. G. Davies, A. A. Mortlock, *Tetrahedron* **1993**, *49*, 4419.
[14] T. Arao, K. Sato, K. Kondo, T. Aoyama, *Chem. Pharm. Bull.* **2006**, *54*, 1576.
[15] D. M. Cermak, Y. Du, D. F. Wiemer, *J. Org. Chem.* **1999**, *64*, 388.
[16] S. Hanessian, P. Meffre, M. Girard, S. Beaudoin, J. Y. Sanceau, Y. Bennani, *J. Org. Chem.* **1993**, *58*, 1991.
[17] M. J. Bainbridge, J. R. L. Smith, P. H. Walton, *Dalton Trans.* **2009**, 3143.
[18] G. Desimoni, G. Faita, P. Righetti, N. Sardone, *Tetrahedron* **1996**, *52*, 12019.
[19] H. Buerger, W. Sawodry, U. Wannagat, *J. Organomet. Chem.* **1965**, *3*, 113.
[20] D. J. Darensbourg, M. W. Holtcamp, G. E. Struck, M. S. Zimmer, S. A. Niezgoda, P. Rainey, J. B. Robertson, J. D. Draper, J. H. Reibenspies, *J Am Chem Soc* **1999**, *121*, 107.
[21] N. Y. Lee, J. U. Yoon, J. H. Jeong, *Acta Crystallogr., Sect. E: Struct. Rep.* **2007**, *E63*, m2471.

Appendix

Appendix

The majority of the results of Chapter I is published:

Etxebarria, J.; Degenbeck, H.; Felten, A. S.; Serres, S.; Nieto, N.; Vidal-Ferran, A. *J. Org. Chem.* **2009**, *74*, 8794.

Experimental details, characterisation data, ^{1}H and ^{13}C NMR data for compounds **44a**, **45a**-**g**, general procedures used for UV-vis, CD and computational data, and molecular modelling coordinates, are available free of charge via the Internet at http://pubs.acs.org. Here only some examples of ^{1}H and ^{13}C NMR spectra are given.

NMR data of the hydrogen bonded complex **44a**+**45d** (1:1 ratio).

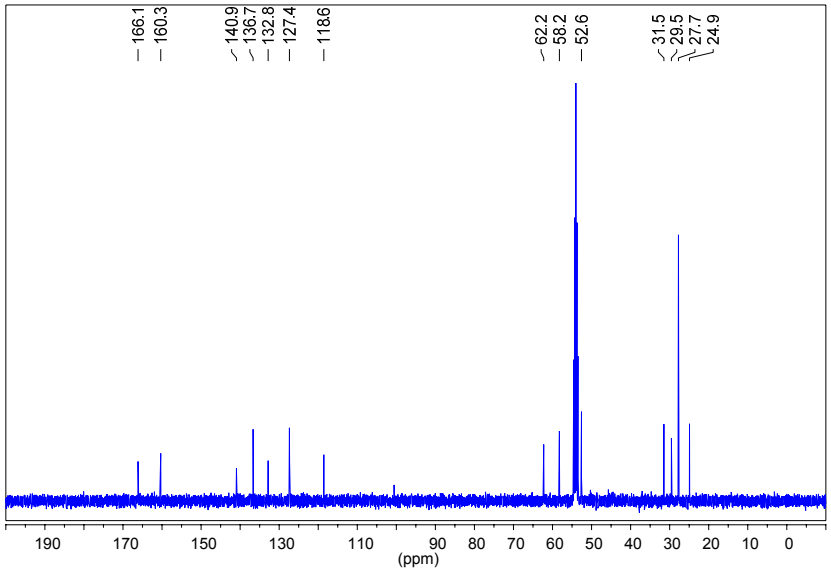

^{13}C NMR (CD_2Cl_2, 100 MHz, 298 K).

Appendix

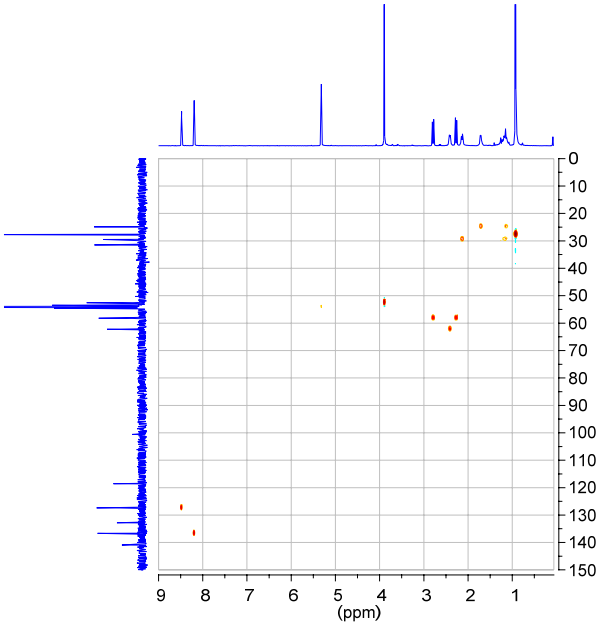

HSQC (CD_2Cl_2, 400 MHz, 298 K).

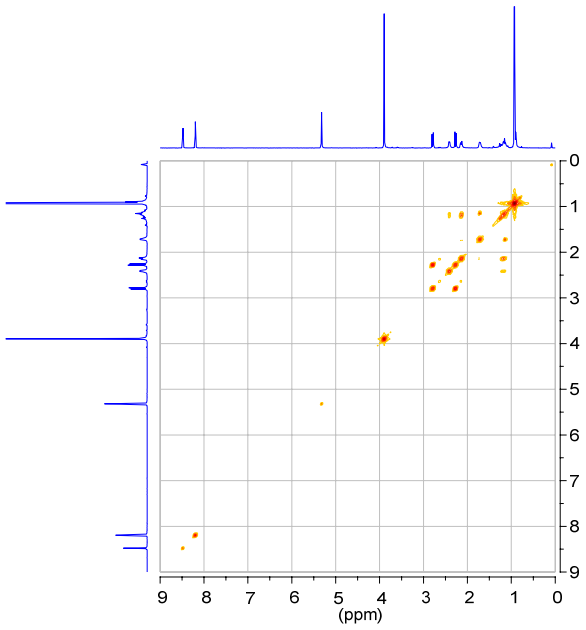

COSY (CD_2Cl_2, 500 MHz, 298 K).

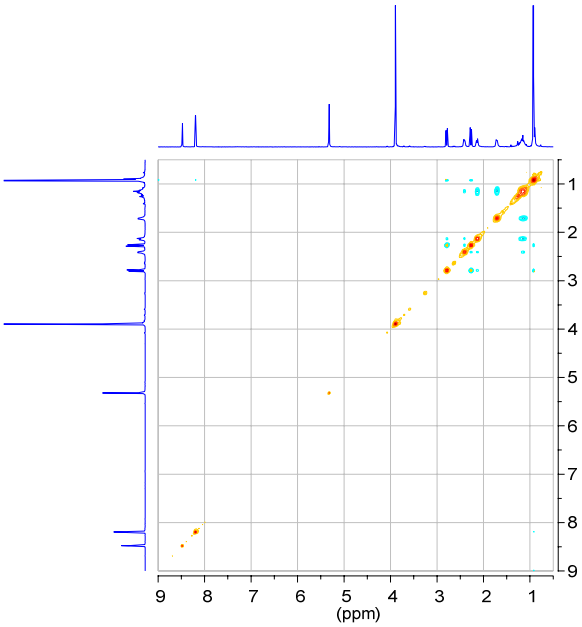

NOESY (CD_2Cl_2, 400 MHz, 298 K).

NMR data of the zinc(II) complex a*R*-**115**.

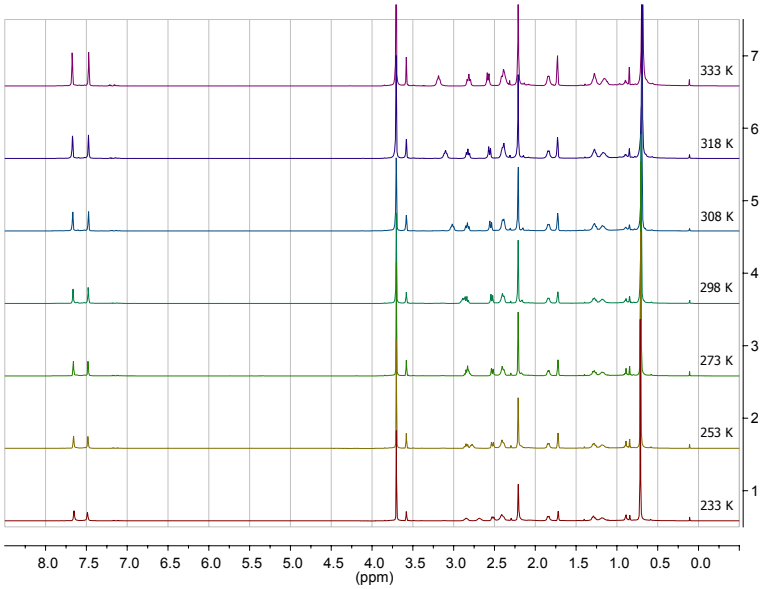

Temperature-dependent 1H NMR spectra (THF-d_8, 500 MHz).

Appendix

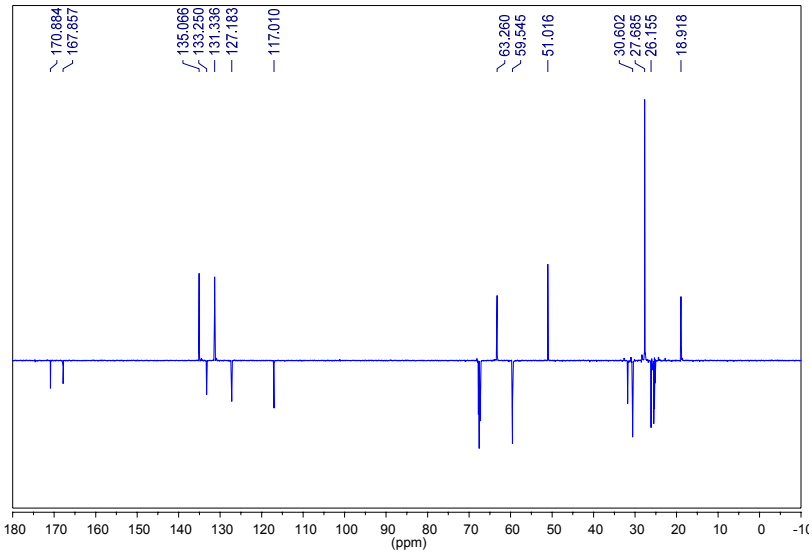

DEPTQ 135 (THF-d_8, 125 MHz, 298 K).

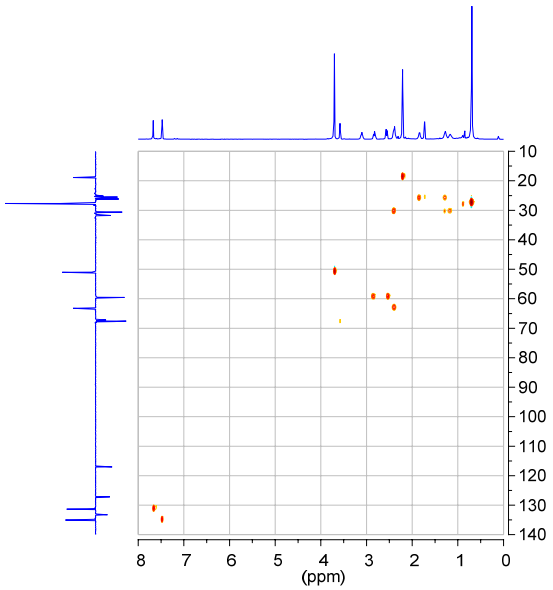

HSQC (THF-d_8, 500 MHz, 298 K).

Single crystal structures

Crystal packing of **44b** crystallised by slow diffusion of *n*-hexane into CH_2Cl_2 (view along the b-axis).

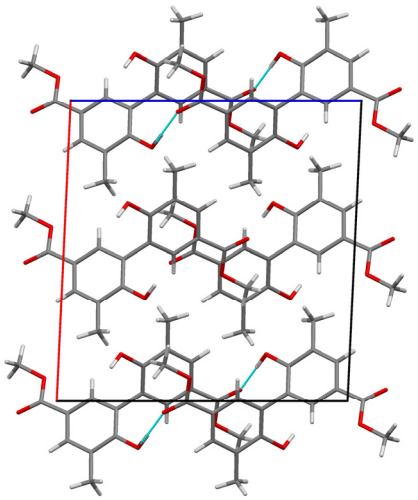

Crystal data and structure refinement for **44b**.

Identification code	**44b**	
Empirical formula	$C_{18}H_{18}O_6$	
Formula weight	330.32	
Temperature	100(2) K	
Wavelength	0.71073 Å	
Crystal system	Monoclinic	
Space group	C2/c	
Unit cell dimensions	a = 14.4823(7) Å	α = 90.00 °
	b = 7.5869(4) Å	β = 92.664(2) °
	c = 14.0067(7) Å	γ = 90.00 °
Volume	1537.33(13) $Å^3$	
Z	4	
Density (calculated)	1.427 mg/m^3	
Absorption coefficient	0.108 mm^{-1}	
F(000)	696	
Crystal size	0.40 x 0.20 x 0.20 mm^3	
Theta range for data collection	2.91 to 36.45 °	

Appendix

Index ranges	-24 <= h <= 24 ,0 <= k <= 12, 0 <= l <= 23
Reflections collected	6517
Independent reflections	5801 [R(int) = 0.0000]
Completeness to theta = 36.45 °	0.945%
Absorption correction	Empirical
Max. and min. transmission	0.9788 and 0.9583
Refinement method	Full-matrix least-squares on F^2
Data / restraints / parameters	6517 / 0 /113
Goodness-of-fit on F^2	1.045
Final R indices [I>2sigma(I)]	R1 = 0.0382, wR2 = 0.1097
R indices (all data)	R1 = 0.0429, wR2 = 0.1136
Largest diff. peak and hole	0.674 and -0.259 e.$Å^{-3}$

Detail of the crystal structure of compound **44a** crystallised from CH_2Cl_2/pentane with hydrogen bonding network.

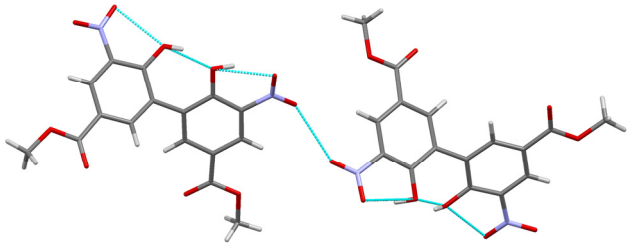

Crystal data and structure refinement for **44a**.

Identification code	**44a**	
Empirical formula	$C_{18}H_{22}N_4O_6$	
Formula weight	390.40	
Temperature	100(2) K	
Wavelength	0.71073 Å	
Crystal system	Monoclinic	
Space group	C2/c	
Unit cell dimensions	a = 25.924(2) Å	α= 90.00 °
	b = 7.2493(9) Å	β = 101.914(5) °
	c = 19.4631(16) Å	γ = 90.00 °
Volume	3578.9(6) $Å^3$	
Z	6	
Density (calculated)	1.087 mg/m^3	

Absorption coefficient	0.083 mm^{-1}
F(000)	1236
Crystal size	0.10 x 0.03 x 0.01 mm^3
Theta range for data collection	2.93 to 35.00 °
Index ranges	-41 <= h <= 41, -11 <= k <= 4, -31 <= l <= 31
Reflections collected	22998
Independent reflections	7704 [R(int) = 0.0678]
Completeness to theta = 35.00 °	0.976%
Absorption correction	Empirical
Max. and min. transmission	0.9992 and 0.9918
Refinement method	Full-matrix least-squares on F^2
Data / restraints / parameters	7704 /8 /295
Goodness-of-fit on F^2	1.313
Final R indices [I>2sigma(I)]	R1 = 0.1154, wR2 = 0.3449
R indices (all data)	R1 = 0.1860, wR2 = 0.4033
Largest diff. peak and hole	1.695 and -0.714 e.$Å^{-3}$

Detail of the crystal structure of compound a*R*-**114** crystallised from CH_2Cl_2/*n*-hexane with hydrogen bonding network.

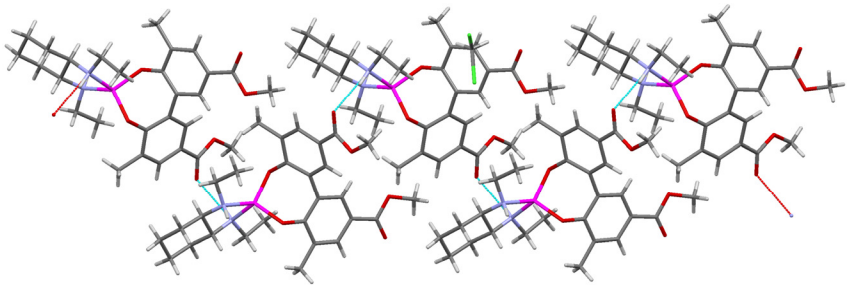

Crystal data and structure refinement for a*R*-**114**.

Identification code	a*R*-**114**
Empirical formula	C28.50H39ClN2O6Zn (includes ½ CH_2Cl_2)
Formula weight	606.44
Temperature	293(2) K
Wavelength	0.71073 Å
Crystal system	Orthorhombic
Space group	C222(1)
Unit cell dimensions	a = 13.323 Å α= 90.00 °

Appendix

	b = 29.906 Å	β = 90.00 °
	c = 14.640 Å	γ = 90.00 °
Volume	5833.1 $Å^3$	
Z	8	
Density (calculated)	1.381 mg/m^3	
Absorption coefficient	0.977 mm^{-1}	
F(000)	2552	
Crystal size	0.20 x 0.10 x 0.01 mm^3	
Theta range for data collection	1.36 to 29.63 °	
Index ranges	-16 <= h <= 18 ,-41 <= k <= 41 ,-20 <= l<= 20	
Reflections collected	7808	
Independent reflections	6065 [R(int) = 0.0707]	
Completeness to theta = 29.63 °	0.969%	
Absorption correction	Empirical	
Max. and min. transmission	0.98 and 0.81	
Refinement method	Full-matrix least-squares on F^2	
Data / restraints / parameters	7808 /0 / 354	
Goodness-of-fit on F^2	1.017	
Final R indices [I>2sigma(I)]	R1 = 0.0434, wR2 = 0.0939	
R indices (all data)	R1 = 0.0686, wR2 = 0.1036	
Absolute Structure Flack parameter	x =0.006(10)	
Largest diff. peak and hole	0.755 and -0.420 $e.Å^{-3}$	

Crystal structure of compound a*S*-**114** crystallised from CH_2Cl_2/*n*-hexane (with co-crystallised solvent).

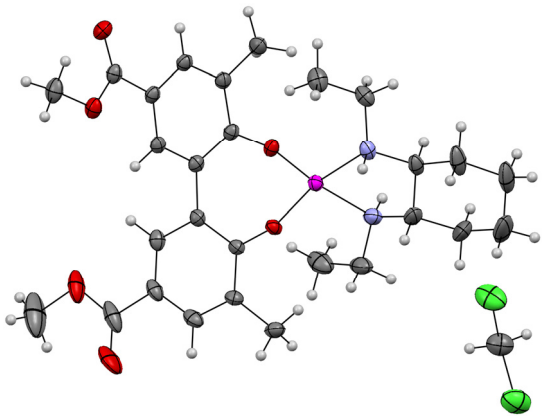

Crystal data and structure refinement for a*S*-**114**.

Identification code	a*S*-**114**	
Empirical formula	$C_{28.50}H_{39}ClN_2O_6Zn$ (includes ½ CH_2Cl_2)	
Formula weight	606.44	
Temperature	100(2) K	
Wavelength	0.71073 Å	
Crystal system	Orthorhombic	
Space group	C222(1)	
Unit cell dimensions	a = 13.2743(7) Å	α= 90.00 °
	b = 29.7684(14) Å	β = 90.00 °
	c = 14.6565(7) Å	γ = 90.00 °
Volume	5791.6(5) $Å^3$	
Z	8	
Density (calculated)	1.391 mg/m^3	
Absorption coefficient	0.984 mm^{-1}	
F(000)	2552	
Crystal size	0.20 x 0.10 x 0.10 mm^3	
Theta range for data collection	1.68 to 35.93 °	
Index ranges	-21 <= h <= 9, -49 <= k <= 41, -22 <= l <= 9	
Reflections collected	12231	
Independent reflections	10313 [R(int) = 0.0251]	
Completeness to theta =35.93 °	0.926%	
Absorption correction	Empirical	
Max. and min. transmission	0.9080 and 0.8275	
Refinement method	Full-matrix least-squares on F^2	
Data / restraints / parameters	12231 / 0 / 362	
Goodness-of-fit on F^2	1.080	
Final R indices [I>2sigma(I)]	R1 = 0.0391, wR2 = 0.0967	
R indices (all data)	R1 = 0.0522, wR2 = 0.1036	
Absolute Structure Flack parameter	x =-0.037(6)	
Largest diff. peak and hole	1.006 and -0.416 e.$Å^{-3}$	

Appendix

Detail of the crystal structure of compound a*R*-**115** crystallised from CH_2Cl_2/*n*-hexane with hydrogen bonding network.

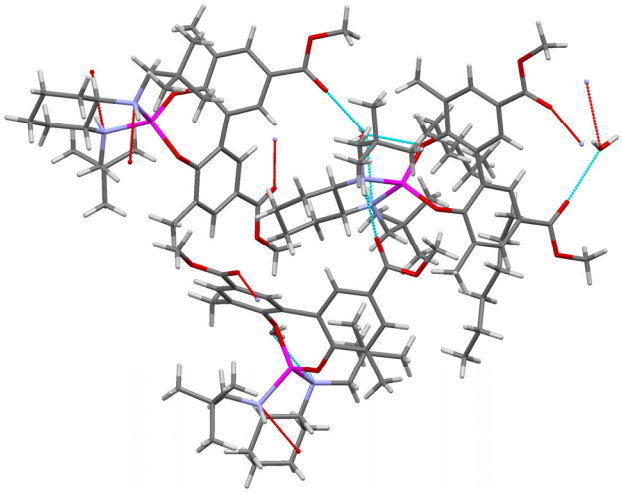

Crystal data and structure refinement for a*R*-**115**.

Identification code	a*R*-**115**	
Empirical formula	C36H56N2O6.67Zn (includes co-crystallised *n*-pentane and H_2O)	
Formula weight	688.86	
Temperature	100(2) K	
Wavelength	0.71073 Å	
Crystal system	Orthorhombic	
Space group	P2(1)2(1)2(1)	
Unit cell dimensions	a = 16.1449(13) Å	α= 90.00 °
	b = 24.1265(18) Å	β = 90.00 °
	c = 30.798(2) Å	γ = 90.00 °
Volume	11996.4(16) $Å^3$	
Z	12	
Density (calculated)	1.144 mg/m^3	
Absorption coefficient	0.657 mm^{-1}	
F(000)	4432	
Crystal size	0.05 x 0.05 x 0.03 mm^3	
Theta range for data collection	1.07 to 25.35 °	
Index ranges	-12 <= h <= 19, -29 <= k <= 28, -37 <= l <= 37	

Reflections collected	83795
Independent reflections	21313 [R(int) = 0.1871]
Completeness to theta = 25.35°	0.983%
Absorption correction	Empirical
Max. and min. transmission	0.9806 and 0.9679
Refinement method	Full-matrix least-squares on F^2
Data / restraints / parameters	21313 / 417 / 1346
Goodness-of-fit on F^2	1.030
Final R indices [I>2sigma(I)]	R1 = 0.0782, wR2 = 0.1715
R indices (all data)	R1 = 0.1668, wR2 = 0.2106
Absolute Structure Flack parameter	x =0.00(4)
Largest diff. peak and hole	0.752 and -0.568 e.Å^{-3}

Crystal structure of compound **118** crystallised from THF/*n*-hexane (with co-crystallised solvent).

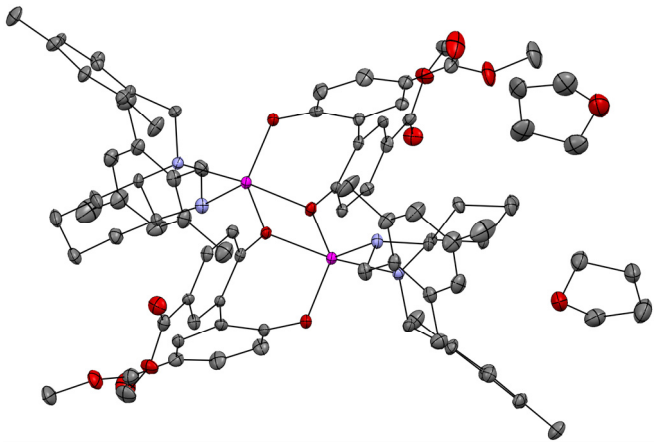

Crystal data and structure refinement for **118**.

Identification code	**118**	
Empirical formula	C92H116N4O14Zn2 (includes 2 THF)	
Formula weight	1632.63	
Temperature	100(2) K	
Wavelength	0.71073 Å	
Crystal system	Triclinic	
Space group	P1	
Unit cell dimensions	a = 11.8749(4) Å	α = 106.696(2) °

Appendix

	b = 12.7931(5) Å	β = 97.038(2) °
	c = 14.4674(6) Å	γ = 100.631(2) °
Volume	2032.77(13) $Å^3$	
Z	1	
Density (calculated)	1.334 mg/m^3	
Absorption coefficient	0.658 mm^{-1}	
F(000)	868	
Crystal size	0.08 x 0.03 x 0.02 mm^3	
Theta range for data collection	1.50 to 33.32 °	
Index ranges	-18 <= h <= 18,-19 <= k <= 18,-22 <= l <= 22	
Reflections collected	24610	
Independent reflections	19129 [R(int) = 0.0504]	
Completeness to theta = 33.32 °	0.930%	
Absorption correction	Empirical	
Max. and min. transmission	0.9870 and 0.9492	
Refinement method	Full-matrix least-squares on F^2	
Data/restraints/parameters	24610 / 13 / 1053	
Goodness-of-fit on F^2	0.987	
Final R indices [I>2sigma(I)]	R1 = 0.0461, wR2 = 0.1010	
R indices (all data)	R1 = 0.0686, wR2 = 0.1109	
Absolute Structure Flack parameter	x =0.002	
Largest diff. peak and hole	0.701 and -0.360 $e.Å^{-3}$	

Crystal packing of [$ZnCl_2$((1*R*,2*R*)-**45a**)] crystallised from toluene (view along the a-axis).

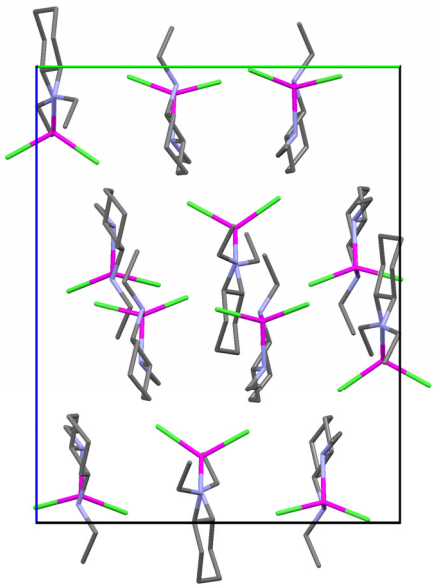

Crystal data and structure refinement for [$ZnCl_2$((1*R*,2*R*)-**45a**)].

Identification code	[$ZnCl_2$((1*R*,2*R*)-**45a**)]	
Empirical formula	C10H22Cl2N2Zn	
Formula weight	306.57	
Temperature	100(2) K	
Wavelength	0.71073 Å	
Crystal system	Orthorhombic	
Space group	P2(1)2(1)2(1)	
Unit cell dimensions	a = 14.7185(8) Å	α = 90.00 °
	b = 15.5078(8) Å	β = 90.00 °
	c = 19.5475(9) Å	γ = 90.00 °
Volume	4461.7(4) $Å^3$	
Z	12	
Density (calculated)	1.369 mg/m^3	
Absorption coefficient	1.986 mm^{-1}	
F(000)	1920	
Crystal size	0.20 x 0.04 x 0.02 mm^3	

Appendix

Theta range for data collection	2.50 to 31.06 °
Index ranges	-16 <= h <= 21, -13 <= k <= 22, -27 <= l <= 25
Reflections collected	28135
Independent reflections	12559 [R(int) = 0.0489]
Completeness to theta = 31.06 °	0.919%
Absorption correction	Empirical
Max. and min. transmission	0.9614 and 0.6921
Refinement method	Full-matrix least-squares on F^2
Data/restraints/parameters	12559 / 0 / 412
Goodness-of-fit on F^2	1.038
Final R indices [I>2sigma(I)]	R1 = 0.0450, wR2 = 0.1056
R indices (all data)	R1 = 0.0594, wR2 = 0.1135
Absolute Structure Flack parameter	x =0.013(9)
Largest diff. peak and hole	2.092 and -0.611 e.Å^{-3}

Crystal packing of [$ZnCl_2$((1*R*,2*R*)-**45c**)] crystallised from toluene (view along the a-axis).

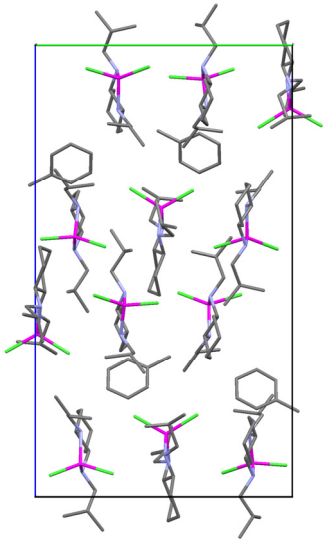

Crystal data and structure refinement for [$ZnCl_2$((1*R*,2*R*)-**45c**)]

Identification code	[$ZnCl_2$((1*R*,2*R*)-**45c**)]	
Empirical formula	C49H98Cl6N6Zn3	
Formula weight	1180.14	
Temperature	100(2) K	
Wavelength	0.71073 Å	
Crystal system	Orthorhombic	
Space group	P2(1)2(1)2(1)	
Unit cell dimensions	a = 13.6344(12) Å	α= 90.00 °
	b = 15.8291(16) Å	β = 90.00 °
	c = 27.859(3) Å	γ = 90.00 °
Volume	6012.5(10) $Å^3$	
Z	4	
Density (calculated)	1.304 mg/m^3	
Absorption coefficient	1.490 mm^{-1}	
F(000)	2504	
Crystal size	0.10 x 0.01 x 0.005 mm^3	
Theta range for data collection	2.54 to 25.48 °	
Index ranges	-16 <= h <= 15, -18 <= k <= 14, -32 <= l <= 33	
Reflections collected	10668	
Independent reflections	5304 [R(int) = 0.2372]	
Completeness to theta = 25.48 °	0.969%	
Absorption correction	Empirical	
Max. and min. transmission	0.9926 and 0.8653	
Refinement method	Full-matrix least-squares on F^2	
Data / restraints / parameters	10668 / 107 / 590	
Goodness-of-fit on F^2	0.976	
Final R indices [I>2sigma(I)]	R1 = 0.0872, wR2 = 0.1703	
R indices (all data)	R1 = 0.1997, wR2 = 0.2204	
Absolute Structure Flack parameter	x = -0.02	
Largest diff. peak and hole	1.029 and -1.285 e.$Å^{-3}$	

Appendix

Crystal packing of [$ZnCl_2$((1*R*,2*R*)-**45h**)] crystallised from toluene (view along the a-axis).

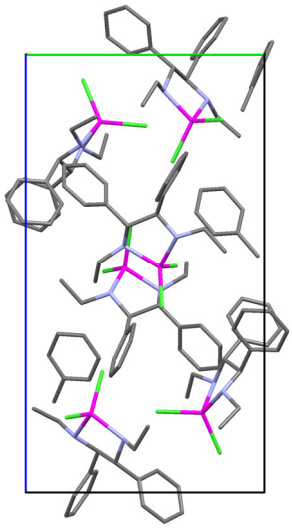

Crystal data and structure refinement for [$ZnCl_2$((1*R*,2*R*)-**45h**)].

Identification code	[$ZnCl_2$((1*R*,2*R*)-**45h**)]	
Empirical formula	$C_{43}H_{60}Cl_4N_4O_2Zn_2$	
Formula weight	937.49	
Temperature	100(2) K	
Wavelength	0.71073 Å	
Crystal system	Trigonal	
Space group	P3(2)	
Unit cell dimensions	a = 13.5191(4) Å	α = 90.00 °
	b = 13.5191(4) Å	β = 90.00 °
	c = 21.6134(9) Å	γ = 120.00 °
Volume	3421.0(2) $Å^3$	
Z	3	
Density (calculated)	1.365 mg/m^3	
Absorption coefficient	1.325 mm^{-1}	
F(000)	1470	
Crystal size	0.1 x 0.1 x 0.05 mm^3	
Theta range for data collection	1.74 to 30.63 °	
Index ranges	-15 <= h <= 19, -16 <= k <= 19, -13 <= l <= 30	
Reflections collected	9876	
Independent reflections	9591 [R(int) = 0.0196]	

Completeness to theta = 30.63 °	0.995%
Absorption correction	Empirical
Max. and min. transmission	? and ?
Refinement method	Full-matrix least-squares on F^2
Data/restraints/parameters	9876 / 7 / 513
Goodness-of-fit on F^2	1.090
Final R indices [I>2sigma(I)]	R1 = 0.0215, wR2 = 0.0573
R indices (all data)	R1 = 0.0225, wR2 = 0.0577
Absolute Structure Flack parameter	x = 0.010
Largest diff. peak and hole	0.690 and -0.298 e.Å^{-3}

Crystal packing of [Cu(BIPOLate)$_2$((1*R*,2*R*)-DACH)$_2$] crystallised from methanol (view along the b-axis).

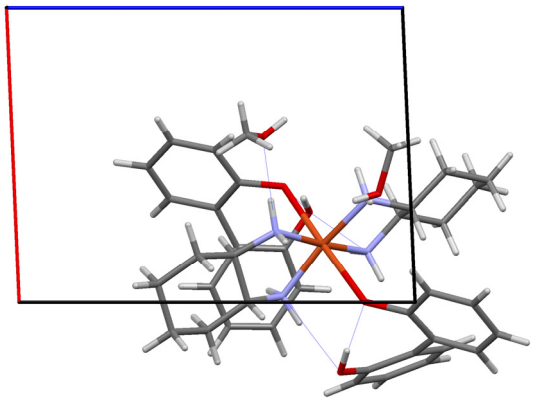

Crystal data and structure refinement for [Cu(BIPOLate)$_2$((1*R*,2*R*)-DACH)$_2$].

Identification code	*R*,*R*,a*R*-**121**	
Empirical formula	$C_{38}H_{54}CuN_4O_6$	
Formula weight	726.39	
Temperature	100(2) K	
Wavelength	0.71073 Å	
Crystal system	Triclinic	
Space group	P1	
Unit cell dimensions	a = 8.8910(6) Å	α= 73.314(3) °
	b = 8.9127(7) Å	β = 85.193(4) °
	c = 12.3096(8) Å	γ = 81.330(4) °
Volume	922.85(11) Å^3	
Z	1	

Appendix

Density (calculated)	1.307 mg/m^3
Absorption coefficient	0.642 mm^{-1}
F(000)	387
Crystal size	0.30 x 0.30 x 0.10 mm^3
Theta range for data collection	2.32 to 33.81 °
Index ranges	-13 <= h <= 13, -13 <= k <= 13, -19 <= l <= 19
Reflections collected	11485
Independent reflections	10892 [R(int) = 0.0309]
Completeness to theta = 33.81 °	0.936%
Absorption correction	Empirical
Max. and min. transmission	0.9386 and 0.8307
Refinement method	Full-matrix least-squares on F^2
Data / restraints / parameters	11485 / 231 / 405
Goodness-of-fit on F^2	1.028
Final R indices [I>2sigma(I)]	R1 = 0.0611, wR2 = 0.1559
R indices (all data)	R1 = 0.0643, wR2 = 0.1597
Absolute Structure Flack parameter	x =0.021(8)
Largest diff. peak and hole	4.416 and -0.882 e.Å^{-3}

Asymmetric unit of [{Cu(μ-BIPOLate)((1*R*,2*R*)-DACH)}$_2$] crystallised from 1,4-dioxane.

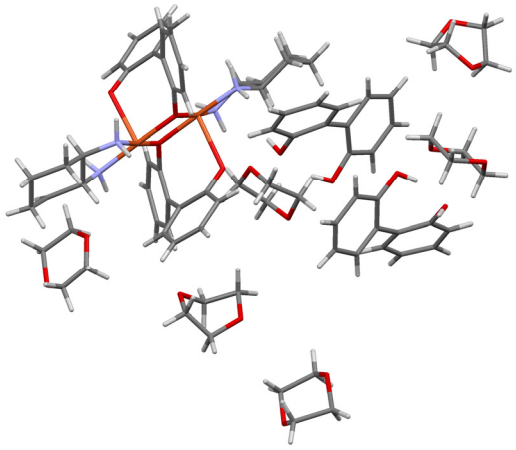

Crystal data and structure refinement for [{Cu(μ-BIPOLate)((1*R*,2*R*)-DACH)}$_2$].

Identification code	**122**	
Empirical formula	C76H95Cu2N4O16	
Formula weight	1447.64	
Temperature	100(2) K	
Wavelength	0.71073 Å	
Crystal system	Monoclinic	
Space group	C2	
Unit cell dimensions	a = 30.212(8) Å	α= 90.00 °
	b = 14.544(3) Å	β = 117.215(8) °
	c = 19.125(4) Å	γ = 90.00 °
Volume	7473(3) Å^3	
Z	4	
Density (calculated)	1.287 mg/m^3	
Absorption coefficient	0.636 mm^{-1}	
F(000)	3060	
Crystal size	0.10 x 0.10 x 0.02 mm^3	
Theta range for data collection	2.67 to 26.53 °	
Index ranges	-37 <= h<=37, -17 <= k <= 18, -23 <= l <= 20	
Reflections collected	12060	
Independent reflections	7304 [R(int) = 0.1322]	
Completeness to theta = 26.53 °	0.971%	
Absorption correction	Empirical	
Max. and min. transmission	0.9874 and 0.9391	
Refinement method	Full-matrix least-squares on F^2	
Data / restraints / parameters	12060 / 157 / 884	
Goodness-of-fit on F^2	1.046	
Final R indices [I>2sigma(I)]	R1 = 0.0988, wR2 = 0.2511	
R indices (all data)	R1 = 0.1628, wR2 = 0.3060	
Absolute Structure Flack parameter	x = 0.01(3)	
Largest diff. peak and hole	1.965 and -1.003 e.Å^{-3}	

Acknowledgements

At this point I would like to thank all the people who have accompanied me during the years of my PhD research project. First I would like to thank Prof. Anton Vidal who has accepted me as a PhD student in his group back in 2006 for offering me the opportunity to work on this interesting field. Furthermore, I would like to thank all present and past group members who have worked with me during that time, in particular Dr. Pablo Etayo Pérez and Dr. Héctor Fernández Pérez for proofreading this thesis, Sílvia Serres Prades, Dr. Juan Etxebarria, and Dr. Anne-Sophie Felten, who were included in the Supramolecular Catalysis project during some time. Naturally, working on such a project would not be possible without proper technical support and thus I would like to express my gratitude to all technical services at ICIQ, in particular the X-ray diffraction unit, the NMR unit, and the MS and Spectroscopy units. My special thanks go also to Pisa to Prof. Lorenzo Di Bari and Dr. Rino Pescitelli, from whom I have learned a lot during my research stay at the University of Pisa. I would also like to thank the many friends that I have found here in Spain, Amparo Forneli, Stephan Röser, John Clifford, Carmela Molinaro, Josep Albero, Núria Huguet, Eduardo Escudero, Laura Hernández, Virginia Valderrey, Inma Pintre, Moira Ciardi, Lydia Vaquer, Esther Alza, and many more to whom I apologise for not being named here.

Last but not least I would like to thank my parents and my family for their never ceasing support and encouragement not only during my time here in Tarragona but also during my whole studying career.